Emergent Transport in Ion Exchange Membranes

by

Jung Min Kim

A dissertation submitted to the Graduate Faculty of
Auburn University
in partial fulfillment of the
requirements for the Degree of
Doctor of Philosophy

Auburn, Alabama
December 11, 2021

Keywords: Membrane science, Polymer chemistry, Ion exchange membranes,
Multi-solute transport, Charge screening, Crosslinked membranes

Approved by

Bryan S. Beckingham, Chair, Assistant Professor of Chemical Engineering, Auburn University
Xinyu Zhang, Professor of Chemical Engineering, Auburn University
Allan E. David, Associate Professor of Chemical Engineering, Auburn University
Tae-Sik Oh, Assistant Professor of Chemical Engineering, Auburn University
Daniel J. Miller, Materials Staff Scientist, Lawrence Berkeley Nation Laboratory
Shiqiang Zou, Reader, Assistant Professor of Civil Engineering, Auburn University

Abstract

The ion exchange membrane (IEM) is a crucial part of various applications from water purification (i.e. electrodialysis) to energy conversion (i.e. photoelectrochemical CO_2 reduction cells (PEC-CRC) and direct urea fuel cells (DUFC)). Theoretically, these approaches are more profitable and eco-friendly than their alternatives, such as distillation and fossil fuels. However, a major drawback of these applications is the selectivity of existing IEMs not being adequate (i.e. crossover of undesired solutes). Moreover, each application requires a different membrane specification. For instance, membranes for PEC-CRCs should be minimizing the crossover of CO_2 reduction products (i.e. methanol (MeOH), ethanol (EtOH), formate (OFm^-), acetate (OAc^-)), while allowing the permeation of electrolytes (i.e. bicarbonate (HCO_3^-)). In the case of DUFC, membranes should minimize the crossover of urea to avoid catalyst sweeping effect. To design target-specific membranes, we took three series of investigations, which are (1) understanding alcohol-carboxylate co-transport behavior in IEMs, (2) analyzing the impact of charge-neutral comonomers in cation exchange membranes (CEM), and (3) introducing a new class of IEMs. From the first series, we conjectured a charge screening behavior based on the carboxylate diffusivity of CEMs being increased and that of anion exchange membranes (AEM) being decreased in co-diffusion with an alcohol. From the second series, we conjectured the interaction between different two dissimilar pendant groups on polymer network can offset the charge screening behavior in CEMs, where the carboxylate diffusivity in CEMs with sulfopropyl groups and poly(ethylene glycol) phenyl ether (PEGPE) groups being consistent in co-diffusion with alcohol. From the third series, we introduced a new class of crosslinked IEMs with phenyl acrylate (hydrophobic monomer). More findings from each series of investigations will be discussed in corresponding sections.

Acknowledgments

I would like to thank Bryan for taking me as a Ph.D. student and giving me all the opportunities to train me to become a scientist. I would like to thank Dan for being such as great mentor. I would like to thank Yihung for allowing me to be his mentor, which was a great learning experience for me. I would like to thank Vinita for her being the life of the party. I would like to thank Elaine, Georgetta, Emma, Brian, and Dr. Eden for them being so thoughtful. I would like to thank Dr. Enick for taking me as an undergraduate researcher at University of Pittsburgh and teaching me how to do polymerization. I would like to thank Geoff for encouraging me and giving me an opportunity to work with him as a post-doctoral research associate at University of Virginia.

I would like to thank my God for allowing me to enjoy this exciting moment. I would like to thank Pastor Lim for his continuous support. I would like to thank Youngsoo and Hanjoo for them being great mentors and friends. I must thank my friends, Beomjun, Eungjin, Munsik, Noori, Jihe, Jonghyun, and Anthony. Thank you all for your support! I would like to give a shout-out to my new friends Kevin, Zach, Nima, Tom, Pravin, Sarah, Tina, Ehsan, Fanqi, Chidera, Amod, Yeseul, Yaeji, Ashraf, Andy, Mackenzie, Jazmine, Loyal, Matthew, and David. I wish the best for all of you and I hope to keep in touch. Lastly, I would like to thank my mom and my family for their support and encouragement.

Table of Contents

List of Tables

List of Figures

List of Abbreviations

1-BuOH	1-Butanol
1-OBu^-	Ethyl $butyrate^-$
2-BuOH	2-Butanol
2-OBu^-	2-$Methylpropanoate^-$
2-PrOH	2-Propanol
AA	Acrylic acid
AEM	Anion exchange membranes
$AgNO_3$	Silver nitrate
AIBN	2,2′-Azobis(2-methylpropionitrile)
AMPS, A	2-Acrylamido-2-methylpropanesulfonic acid
AMVN	Selemion® AMVN
APTA	(3-Acrylamidopropyl) trimethylammonium chloride
ATR-FTIR	Attenuated total reflectance-fourier transform infrared
CEM	Cation exchange membrane
-COOH	Carboxyl
CV	Coefficient of variation
DEFC	Direct ethanol fuel cells
DFT	Density functional theory
DI	Deionized
DMA	Dynamic mechanical analysis
DMSO	Dimethyl sulfoxide
DSC	Differential scanning calorimetry
DUFC	Direct urea fuel cells

EDS	Energy-dispersive X-ray spectroscopy
EGPE	Ethylene glycol phenyl ether
EIS	Electrochemical impedance spectroscopy
EtOH	Ethanol
FAA	Fumasep FAA-3-50
H_2O	Water
HCl	Hydrochloric acid
HCO_3^-	Bicarbonate
HCPK	1-Hydroxyl-cyclohexyl phenyl ketone
HEMA	2-Hydroxylethyl methacrylate
HPLC	High-performance liquid chromatography
IEC	Ion exchange capacity
IEM	Ion exchange membrane
ImPPO	Imidazolium-functionalized poly(phenylene oxide)
IPN	Interpenetrating polymer network
K_2CrO_4	Potassium chromate
KCl	Potassium chloride
$KHCO_3$	Potassium bicarbonate
KOAc	Potassium acetate
KOFm	Potassium formate
KOH	Potassium hydroxide
MACC, M	Methacroylcholine chloride
MeOH	Methanol
NaCl	Sodium chloride
NaOAc	Sodium acetate

NaOFm	Sodium formate
NaOH	Sodium hydroxide
$NiCl_2$	Nickel chloride
n-PrOH	n-Propanol (1-PrOH, 1-propanol)
OAc^-	Acetate
OCV	Open circuit voltage
OFm^-	Formate
-OH	Hydroxyl
OPr^-	$Propionate^-$
PA	Phenyl acrylate
PALS	Positron annihilation lifetime spectroscopy
PEA, PE	Phenoxyethyl acrylate
PEC-CRC	Photoelectrochemical CO_2 reduction cells
PEGDA	Poly(ethylene glycol) diacrylate
PEGMA	Poly(ethylene glycol) methacrylate
PEGPE	Poly(ethylene glycol) phenyl ether
PEGPEA, PG	Poly(ethylene glycol) phenyl ether acrylate
PEMA, PM	Phenoxyethyl methacrylate
PEO	Poly(ethylene oxide)
PF	Perfluorinated
PFSA	Perfluorosulfonic acid
PMA	Phenyl methacrylate
PS-DVB	Polystyrene-divinylbenzene
QA	Quaternary ammonium
RO	Reverse osmosis

SO_3^-	Sulfonate
SPMAK	3-Sulfopropyl methacrylate potassium
UV	Ultraviolet

Chapter 1

Introduction

1.1 Objectives

1.1.1. Methanol-Acetate co-permeation in CEMs

Multi-solute transport in hydrated dense membranes is utilized in many applications, including photoelectrochemical CO_2 reduction cells (PEC-CRC). One of the main challenges in such devices is to design ion exchange membranes (IEM) that minimizes crossover of CO_2 reduction products, such as methanol (MeOH) and acetate (OAc^-), while maintaining sufficient ionic conductivity. Previously, the transport behavior of a sulfonated cation exchange membrane (CEM), Nafion® 117, to MeOH and sodium acetate (NaOAc) was investigated and an increase in permeability to NaOAc was noticed in co-permeation with MeOH. To further investigate this transport behavior, a charge-neutral membrane (PEGDA) and a series of sulfonated CEMs (PEGDA-AMPS) were prepared by varying the poly(ethylene glycol) diacrylate (PEGDA) to 2-acrylamido-2-methylpropanesulfonic acid (AMPS) ratio. A distinct increase in permeability to NaOAc in co-permeation with MeOH is observed in co-permeation experiments compared to single solute permeation experiments. We attribute this transport behavior to the shielding of electrostatic repulsion, in which MeOH interferes with electrostatic repulsion between OAc^- and membrane-bound sulfonate anions.

1.1.2. Alcohol-Carboxylate co-transport in CEMs

Understanding multi-solute transport behavior through IEMs is of interest for PEC-CRC as one role of the IEM in these devices is to minimize the permeation of these CO_2 reduction products [alcohols (MeOH and EtOH) and carboxylates (OFm^- and OAc^-)] to the anolyte as they often oxidize back to CO_2. CEMs are promising candidates for such devices as they act to minimize the permeation of mobile anions (carboxylates). However, the design of new CEMs is necessary as the permeation of carboxylates often increases in co-permeation with alcohols. Here, we investigate the transport behavior of alcohols and carboxylates in two types of CEMs (1) a crosslinked CEM was prepared by free-radical copolymerization of a sulfonated monomer (AMPS) with a crosslinker (PEGDA), and (2) Nafion® 117. We observe an increase in both PEGDA-AMPS and Nafion® 117 diffusivities to carboxylates in co-diffusion with alcohols. We attribute this behavior to charge screening by co-diffusing alcohol that reduces the electrostatic repulsion between bound sulfonates and mobile carboxylates.

1.1.3. Alcohol-Carboxylate co-transport in AEMs

Anion exchange membranes (AEM) have been employed in PEC-CRCs as they act to facilitate the transport of common electrolytes (i.e. bicarbonates). However, as they act to facilitate the transport of carboxylates as well, thereby reducing overall performance, the design of new AEMs is necessary to improve device performance through selective transport of the desired ion(s) or electrolyte(s). Here, we investigate the transport behavior of OFm^- and OAc^- (CO_2 reduction products) and their co-transport with EtOH (CO_2 reduction product) in two types of AEMs (1) a crosslinked AEM prepared by free-radical copolymerization of a monomer with a quaternary

ammonium (QA) group and a crosslinker, and (2) Selemion® AMVN. We observe a decrease in diffusivities to carboxylates in co-diffusion. We attribute this behavior to charge screening by the co-diffusing alcohol that reduces the electrostatic attraction between QAs and carboxylates.

1.1.4. Effect of Hydroxyl-comonomers on co-permeation in CEMs

We investigated the transport behavior of Nafion® 117 and crosslinked CEMs prepared with poly(ethylene glycol) diacrylate (PEGDA, crosslinker) and 2-acrylamido-2-methyl-1-propanesulfonic acid (AMPS, sulfonated comonomer) to MeOH and NaOAc in 1.1.1., where distinct changes in permeabilities of these membranes to NaOAc was observed in co-permeation with MeOH. To further investigate this co-permeation behavior, we modify the PEGDA-AMPS structure by varying the negatively-charged AMPS content with three different comonomers, acrylic acid (AA, $n = 0$, where n is the number of ethylene oxide repeat units), 2-hydroxylethyl methacrylate (HEMA, $n = 1$), and poly(ethylene glycol) methacrylate (PEGMA, $n = 5$), where n represents the number of ethylene oxide repeat units in each comonomer. While the observed permeability to NaOAc in co-permeation with MeOH was increased for membranes with comonomers with short pendant groups (PEGDA-AMPS/AA and PEGDA-AMPS/HEMA), it remained relatively consistent for PEGDA-AMPS/PEGMA membranes. While the underlying causes of this type of behavior remains unresolved, we propose a combination of assisted transport by MeOH and disruption of electrostatic interactions by pendant ethylene oxide repeat units based on our experiments. Overall, such differences in transport behavior underscore the need for increased understanding of emergent co-permeation behavior in hydrated, dense polymer membranes.

1.1.5. Effect of PEGMA on co-transport in CEMs

We investigated the co-transport behavior of MeOH and OAc^- in membranes with various pendant groups, such as sulfonate ($-SO_3^-$), carboxyl (-COOH), ethylene oxide ($-CH_2CH_2OH$), and poly(ethylene oxide) ($-(CH_2CH_2O)_5H$, PEO), where permeabilities to OAc^- was suppressed in PEO-containing films in co-permeation with MeOH. Here, we further examine this co-transport behavior in pendant PEO-containing films by preparing three chemically different crosslinked films with a constant crosslinker (PEGDA) content and varied the remaining between a PEO-containing comonomer (PEGMA) and a sulfonate-containing comonomer (AMPS) (i.e. PEGDA-PEGMA, PEGDA-AMPS/PEGMA, and PEGDA-AMPS). For each chemistry, three structurally distinct films are prepared by varying pre-polymerization water content, leading to differences in water volume fraction (and thereby free volume). We observe the diffusivities of PEGMA-free films (PEGDA-AMPS) to OAc^- are increased in co-diffusion, while those of PEGMA-containing films (PEGDA-PEGMA and PEGDA-AMPS/PEGMA) to OAc^- are decreased. These results suggest the strategic addition of a charge-neutral pendant group in a charged IEMs is a valid approach to suppress the crossover of undesired molecules.

1.1.6. Effect of Phenyl-comonomers on co-transport in CEM

We reported acetate diffusivities are increased in co-diffusion with methanol in sulfonated CEMs. To rationalize this behavior, we conjectured charge screening of the electrostatic repulsion between sulfonate anion and acetate anion by co-diffusing methanol plays a role. Further, we reported this behavior can be suppressed by a pendant PEO ($n = 5$) group. Here, we investigate the effect of two additional pendant groups, phenoxyethyl acrylate (PEA, $n = 1$) or poly(ethylene

glycol) phenyl ether acrylate (PEGPEA, n = 3), to further identify potential pendant groups that can suppress this concerning behavior. 12 chemically dissimilar crosslinked films are prepared with a crosslinker (PEGDA), a sulfonate-containing comonomer, 3-sulfopropyl methacrylate potassium (SPMAK), and a phenyl-containing comonomer either PEA or PEGPEA. Interestingly, we observe acetate diffusivities of PEGDA-SPMAK based CEMs are noticeably decreased with the inclusion of PEGPEA pendent groups (PEGDA-SPMAK/PEGPEA). To rationalize this behavior, we conjecture a reduction in polymer segmental dynamics due to a steric effect between SPMAK and PEGPEA.

1.1.7. New class of IEMs for DUFCs

IEMs are crucial for various direct fuel cells, such as direct methanol fuel cells and direct urea fuel cells (DUFC). A major role of IEM in such devices is to permit counterions (i.e. hydroxides for AEMs) and suppress co-ions (i.e. cations for AEMs). While various commercially available CEMs and AEMs (i.e. FAA-3-50) show decent power density in both direct fuel cells, they often experience considerable MeOH or urea crossover, which reduces the overall device performance. Therefore, the design of an IEM that can suppress fuel crossover is of interest for various fuel cells. Unfortunately, the majority of IEMs are linear copolymers with a hydrophobic monomer and a hydrophilic monomer with a charged functional group (i.e. sulfonates for CEMs and quaternary ammoniums for AEMs), which often requires a non-woven backing and difficult to introduce a pendant functional group to suppress the crossover effect. Here, we prepare a class of stand-alone crosslinked IEM (methylenebisacrylamide, MBAA, as the crosslinker), with high mechanical toughness utilizing a hydrophobic monomer (either phenyl acrylate, PA, or phenyl methacrylate) and a charged monomer (either AMPS, or methacroylcholine chloride, MACC), where AMPS is

a negatively-charged monomer with a sulfonate group for CEM and MACC is a positively-charged monomer with a quaternary ammonium group for AEM. To validate these membranes in a fuel cell application, we selected an AEM (PA/MACC) and performed DUFC experiments, where we observed good power density compared to that achieved with FAA-3-50. Permeabilities of both membranes to urea are measured by a diffusion cell with an in-situ ATR-FTIR to understand the relative urea crossover.

1.2. Organization

In Chapter 2, the background of the governing transport model and theory of molecular transport through dense polymeric membranes will be described. Moreover, hydrogel-based membranes and IEMs will be visited. Lastly, two target applications (photoelectrochemical CO_2 reduction cells and direct urea fuel cells) will be briefly introduced. Crucial experimental methods will be discussed, which include membrane synthesis, characterization, and transport properties in Chapter 3. The systematic approaches on understanding the alcohol-carboxylate multi-solute transport behavior in IEMs and strategic approaches to suppress the solute transport will be discussed in Chapter 4 to 9. A new class of crosslinked IEMs will be introduced in Chapter 10. Lastly, the conclusion and potential research directions will be discussed in Chapter 11.

Chapter 2

Background

Ion exchange membranes (IEM) can be prepared in various materials (i.e. polymer [1,2] and ceramic [3]) and each has benefits and constraints, where this work is focused on polymeric IEMs. As a hydrated dense membrane, the solute transport in IEM will be governed by the solution-diffusion model (Yasuda's model [4,5] and free volume theory [6,7]). As a charged medium, the solute transport in IEM will encounter electrostatic interactions (Donnan exclusion [8] and counterion condensation theory [9,10]) from polymer-bound charge groups. In the case of multi-solute transport (i.e. simultaneous transport of alcohol and carboxylate [11,12]), the transport of a solute (i.e. carboxylate) will be influenced by the other solute (i.e. alcohol) (flux coupling [13] and competitive sorption [14]). This chapter intends to review some of these well-studied topics in membrane science. Lastly, two energy devices, photoelectrochemical CO_2 reduction cells (PEC-CRC [15]) and direct urea fuel cells (DUFC [16]), will be discussed.

2.1. Transport in Dense Polymer Membranes

Dense polymer membranes find use as selective membranes or permselective membrane layers for ionic and molecular separations (Fig. 2.1) due to their ability to selectively transport small molecules (and exclude large molecules). For instance, dense polymer membranes are used for reverse osmosis (RO), which is a water purification process that removes metal ions and unwanted

molecules with a semipermeable membrane, which has a small pore size (1~5 Å) to allow the transport of water while excluding metal ions or aqueous salts (2~12 Å); see Fig. 2.1 [17].

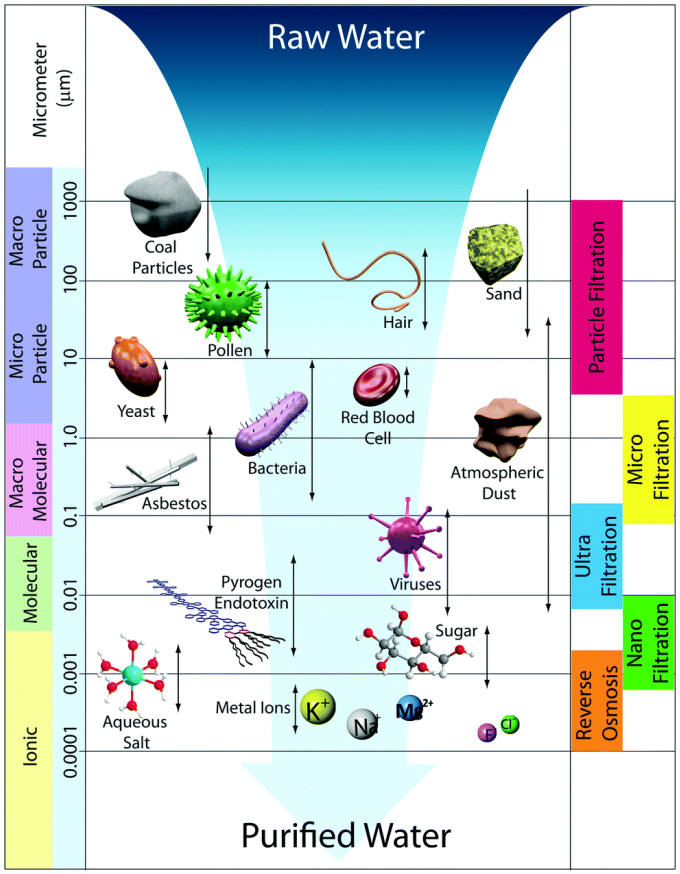

Figure 2.1. Schematic depiction of membrane filtration spectrum. Reverse osmosis membranes have very dense pores that they are considered as non-porous membranes. (0.0001 μm = 1 Å).

The size of the solute is closely related to the diffusion portion of the solution-diffusion model, which states the solute transport in the dense polymeric membrane is governed by the affinity between the polymer and the solute (solubility) and diffusion of the solute in these polymer networks (diffusivity). More on the solution-diffusion model will be stated in 2.1.2.

2.1.1. Free Volume Theory of Diffusion

Solute transport through hydrated dense membranes occurs through dynamic diffusion pathways resulting from polymer segmental dynamics; shown schematically in Fig. 2.2.

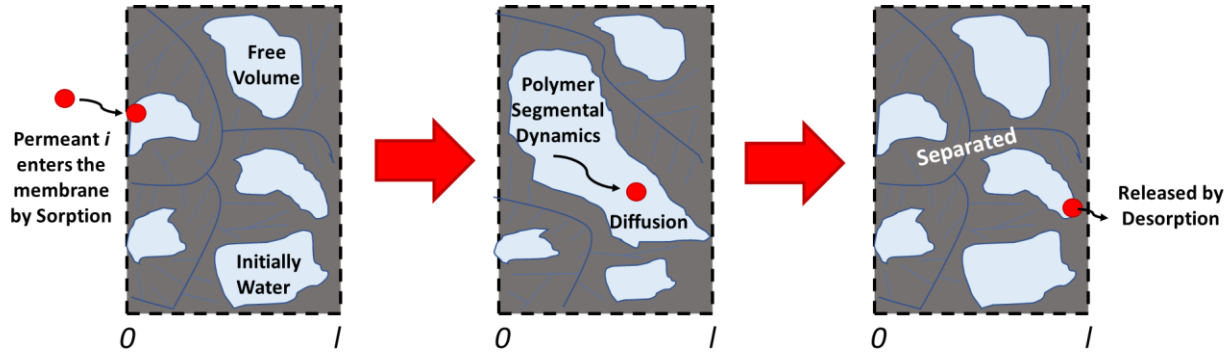

Figure 2.2. Schematic depiction of solute diffusion in a hydrated dense membrane.

These free volume elements are initially occupied with water during the initial equilibrium hydration of the membrane. For transport, a solute, such as methanol of interest here, absorb into the membrane and occupies a free volume element. Next, due to polymer segmental motion, free volume elements evolve within the membrane opening pathways for solute diffusion toward the permeate side due to the concentration gradient. After successive diffusion, the solute reaches the permeate side of the membrane and is released (desorbed) into the permeate chamber [18].

The importance of fractional free volume has led many groups to attempt to measure free volume using Positron Annihilation Lifetime Spectroscopy (PALS), which uses positrons to probe free volume at the sub-nano scale [18–25], as shown schematically in Fig. 2.3. While this is the only technique for attempting to directly measure free volume in a dense polymer membrane, it has a limitation. For instance, positrons can interact with ion exchange functional groups, changing their lifetime and ultimately the impacting the subsequent calculation of free volume [26].

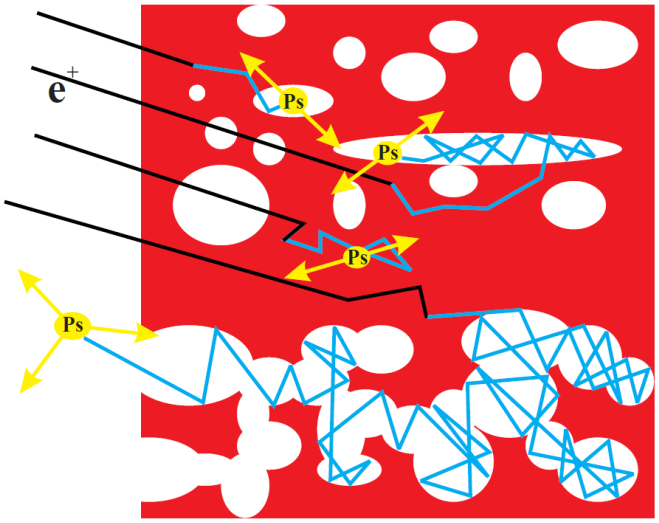

Figure 2.3. Schematic depiction of positrons forming inside the polymer [27].

Water uptake is the most commonly used technique to approximate the free volume within a dense membrane by comparing the quantity of water a membrane will sorb to fill its free volume. It can be measured gravimetrically as

$$\omega_w = \frac{W_s - W_d}{W_d} \tag{2.1}$$

where ω_w is the water uptake, W_s is the mass of a swollen membrane, and W_d is the mass of a dry membrane. Water uptake can be represented in volume fraction, ϕ_w, by using densities of water and the polymer.

$$\phi_w = \frac{(W_s - W_d)/\rho_w}{(W_s - W_d)/\rho_w + W_d/\rho_p} \tag{2.2}$$

where ρ_w is the density of water and ρ_p is the density of the polymer.

2.1.2 Solution-Diffusion Model

Liquid permeant transport through dense membranes is usually described by the solution-diffusion model, while permeant transport through porous membranes is described by the pore-flow model [7]. The proposition for both models start from thermodynamics as the overall driving force for both is a chemical potential gradient (i.e. concentration and pressure) such that the flux of a permeant *i* can be described as

$$J_i = -L_i \frac{d\mu_i}{dx} \tag{2.3}$$

where J_i is the flux of permeant *i*, $\frac{d\mu_i}{dx}$ is the chemical potential gradient, and L_i is the proportional coefficient. By assuming the gradient is dominated by concentration and pressure, the chemical potential can be written as

$$d\mu_i = RTd(ln(\gamma_i c_i)) + \nu_i dp \tag{2.4}$$

where *R* is the gas constant, *T* is the temperature, γ_i is the activity coefficient linking the concentration of permeant *i*, c_i is the molar concentration, ν_i is the molar volume, and *p* is the pressure. Since the volume of an incompressible liquid does not change with pressure this equation becomes

$$\mu_i = \mu_i^o + RTln(\gamma_i c_i) + \nu_i(p - p_i^o) \tag{2.5}$$

where μ_i^o is the chemical potential of permeant *i* at a reference pressure p_i^o. Here, the theory for dense and porous membranes diverges. The pore-flow model assumes the pressure gradient is the only chemical potential gradient, whereas the solution-diffusion model assumes the concentration gradient to be the only chemical potential gradient. Thus, for dense polymer membranes the flux becomes

$$J_i = -\frac{RTL_i}{c_i} \cdot \frac{dc_i}{dx} \tag{2.6}$$

and Fick's first law is derived after replacing the $\frac{RTL_i}{c_i}$ with the diffusivity D_i:

$$J_i = -D_i \frac{dc_i}{dx} \tag{2.7}$$

By integrating the equation over the thickness of the membrane the equation becomes

$$J_i = -D_i \frac{c_{io(m)} - c_{il(m)}}{l} \tag{2.8}$$

where $c_{io(m)}$ is the concentration of permeant i on the feed side of the membrane and $c_{il(m)}$ is the concentration on the permeate side of the membrane. Eq. 2.8 is one of the most general forms of the solution-diffusion model.

To describe simple concentration-driven applications, such as dialysis and our diffusion cell, the solute concentration for both the feed, c_{io}, and the permeate solution, c_{il}, is typically higher than the solute concentration of the feed and the permeate membrane interfaces, $c_{io(m)}$ and $c_{il(m)}$; shown schematically in Fig. 2.4.

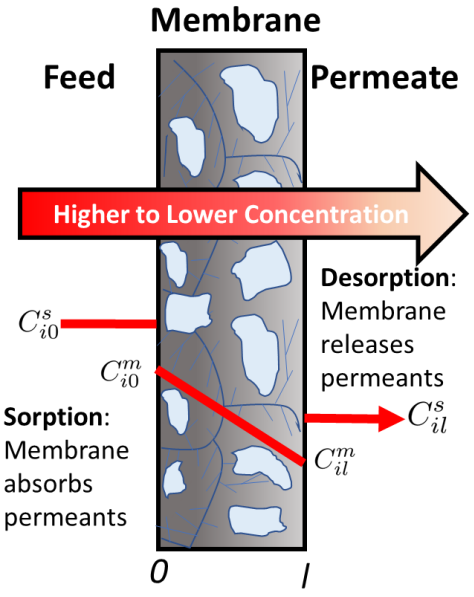

Figure 2.4. Schematic description of the solution-diffusion model.

As our experimental approaches to solute transport experiments are based on the ability to set or measure solute concentration in the solutions (not the membrane), a transport equation using these measurable variables is desired. First, the chemical potentials of the feed and the feed side of the membrane are equated as

$$\mu_{io} = \mu_{io(m)} \tag{2.9}$$

and by substituting Eq. 2.5 in both chemical potential one receives

$$\mu_i^o + RTln(\gamma_{io}c_{io}) + \nu_i(p_o - p_{i_{sat}}) = \mu_i^o + RTln(\gamma_{io(m)}c_{io(m)}) + \nu_i(p_o - p_{i_{sat}}) \tag{2.10}$$

which upon simplification yields

$$\gamma_{io}c_{io} = \gamma_{io(m)}c_{io(m)} \tag{2.11}$$

and therefore

$$c_{io(m)} = \frac{\gamma_{io}}{\gamma_{io(m)}} \cdot c_{io} \tag{2.12}$$

The ratio between two activity coefficients, $\gamma_{io}/\gamma_{io(m)}$, is then replaced by the solubility, K_i

$$c_{io(m)} = K_i \cdot c_{io} \tag{2.13}$$

and this procedure is repeated analogously on the permeate side of the membrane, see Eq. 2.14.

$$c_{il(m)} = K_i \cdot c_{il} \tag{2.14}$$

By substituting Eq. 2.13 and 2.14 into Eq. 2.8, one receives

$$J_i = D_i K_i \frac{(c_{io} - c_{il})}{l} \tag{2.15}$$

where l is the thickness of the membrane. The resulting Eq. 2.15 now contains measurable variables and desired membrane characteristics. The product of the diffusivity and solubility can also be replaced with the permeability, P_i, (Eq. 2.16).

$$J_i = P_i \frac{(c_{io} - c_{il})}{l} \tag{2.16}$$

The permeability, P_i $[\frac{cm^2}{s}]$, is a measure of membrane productivity, which can be explained by two terms: the solubility, K_i, which is a thermodynamic term that measures how well the solutes absorb to or desorb from the membrane interfaces and the diffusivity, D_i $[\frac{cm^2}{s}]$, which is a kinetic term that describes the rate of the solutes moves through the membrane [28].

2.1.3. Yasuda's Model

Permeability is a metric to investigate the structure-property relationship between the solute and the membrane. To determine the solute permeability, one often uses a temperature-controlled diffusion cell [11,29,30]; see Fig. 2.5. In a typical diffusion cell, a membrane is placed in between two chambers, the feed and the receiver cell. These chambers are identical in volume and are temperature-jacketed to minimize the chemical potential gradient from the presence of a temperature gradient.

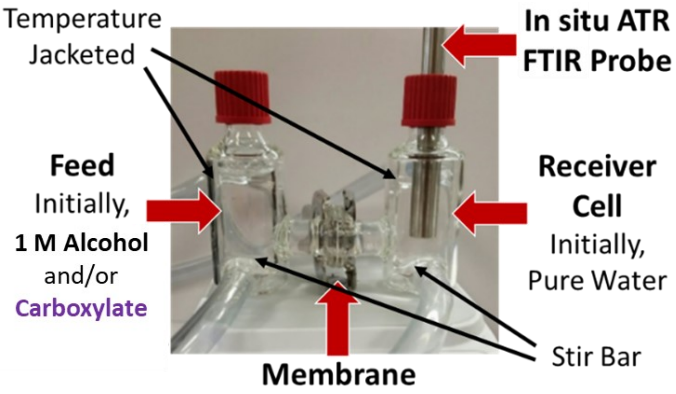

Figure 2.5. Photo of a custom-built diffusion cell.

Diffusion of small molecules (sodium chloride, NaCl) in a dense polymer is commonly described by free volume theory. Yasuda et al. [4,5] described the free volume in hydrated

polymers as proportional to the volume fraction of water in the polymers and the solute diffusivity in the water-swollen polymer, D_i, is dependent on the free volume, ν_f, as

$$D_i \propto exp\left(- \frac{\nu^*}{\nu_f} \right) \tag{2.17}$$

where ν^* is the minimum size of a free volume element to diffuse a solute. As membrane free volume is proportional to the volume fraction of water, ϕ_w, Eq. 2.17 can be expressed as

$$D_i = D_{o,i} \exp\left(- A\left(\frac{1}{\phi_w} - 1 \right) \right) \tag{2.18}$$

where $D_{o,i}$ is the solute diffusivity in water, and A is an empirical constant. However, diffusivity is typically calculated from permeability and solubility values due to difficulty of obtaining these parameters. Permeability using Yasuda's approximation on hydrated membranes can be derived by equating Eq. 2.16 with a molar flux of the solute *i* as

$$J_i = P_i \frac{(c_{io}(t) - c_{il}(t))}{l} = \frac{1}{A} \frac{dn_i(t)}{dt} \tag{2.19}$$

where A is the effective surface area of the membrane and n_i is the number of the solute *i* in a chamber. Since one typically chooses to measure the change in concentration in the permeate chamber, we may rewrite the equation in terms of change in concentration of solute *i* inside the permeate chamber, c_{il}.

$$J_i = P_i \frac{(c_{io}(t) - c_{il}(t))}{l} = \frac{V}{A} \frac{dc_{il}(t)}{dt} \tag{2.20}$$

where V is the volume of the chamber. Assuming all solutes transport from the feed to the permeate chamber as

$$c_{io}(t) = c_{io,0} - c_{il}(t) \tag{2.21}$$

where $c_{io,0}$ is the initial solute concentration in the feed chamber, Eq. 2.20 becomes:

$$P_i \frac{(c_{io,0} - 2c_{il}(t))}{l} = \frac{V}{A}\frac{dc_{il}(t)}{dt} \tag{2.22}$$

By using two boundary conditions (1) the initial concentration of the solute in the permeate chamber is 0, and (2) the solute concentration in the permeate chamber at time equals *t* is $c_{il,t}$ (Eq. 2.23), Eq. 2.22 becomes

$$at\ t = 0,\ c_{il} = 0\ \ and\ at\ t = t,\ c_{il} = c_{il,t} \tag{2.23}$$

$$\frac{P_i \cdot A}{l \cdot V}\int_0^t dt = \int_0^{c_{il,t}} \frac{1}{c_{io,0} - 2c_{il}(t)} dc_{il}(t) \tag{2.24}$$

Solving this differential equation yields Eq. 2.25,

$$\frac{P_i \cdot A}{l \cdot V} t = \frac{1}{2}\ln(c_{io,0}) - \frac{1}{2}\ln(c_{io,0} - 2c_{il,t}) \tag{2.25}$$

and finally, the permeability of the solute *i* can be measured by

$$P_i\left(\frac{-2 \cdot A \cdot t}{l \cdot V}\right) = ln\left(\frac{c_{io,0} - 2c_{il,t}}{c_{io,0}}\right) \tag{2.26}$$

where $c_{io,0}$ can be measured by the mass of the solute before the experiment, *l* can be measured by a caliper before and after each experiment, and $c_{il,t}$ can be measured by a probe, such as a pH, a conductivity, and an in-situ ATR-FTIR probe [11,29,30].

Yasuda's approximation on the transport of small molecules in hydrated dense membranes has been utilized to characterize transport of various aqueous salts, (i.e. NaCl [4], sodium formate (NaOFm) [11], sodium acetate (NaOAc) [11], potassium formate (KOFm), and potassium acetate (KOAc)) and alcohols (i.e. methanol (MeOH) [31], ethanol (EtOH) [29], n-propanol (n-PrOH)) [29]. Here, Yasuda's model will be used to characterize the transport of MeOH, EtOH, NaOFm, NaOAc, KOFm, and KOAc in a series of IEMs.

2.1.4. In-situ ATR-FTIR Spectroscopy

Traditionally, permeability to a solute has been measured in diffusion cells with the downstream concentration monitored by the pH or the conductivity of the solution [22,31]. However, one of the limitations of these measurable attributes is that they are not suitable for examining the transport of more than one solute through a membrane simultaneously. To solve this problem, Beckingham, Lynd, and Miller devised an approach to measure the permeability of multiple solutes using in-situ Attenuated Total Reflectance-Fourier Transform Infrared (ATR-FTIR) Spectroscopy [11].

As the first step, calibration of each solute of interest is conducted from 0.025 to 0.25 M to extract the effective extinction coefficients at wavelengths with distinctive IR peaks using the Beer-Lambert Law (Eq. 2.27)

$$A_\lambda = log(\frac{I_o}{I}) = E_\lambda lc \tag{2.27}$$

where A_λ and E_λ is the measured absorbance and the molar absorptivity of the solute at the wavelength λ, I_o and I are the incident and transmitted intensity of light, l is the path length of the incident light travels through the solution. As the path length is essentially identical, we may combine E_λ and l as

$$E_\lambda l = \epsilon_\lambda \tag{2.28}$$

where ε_λ is the effective molar absorptivity and the Eq. 2.28 becomes

$$A_\lambda = \epsilon_\lambda c \tag{2.29}$$

where the concentration of a single solute can be calculated. In terms of multiple solutes, the contributions from co-solutes at that wavelength must be considered and so Eq. 2.29 becomes

$$A_\lambda = \sum_{i=1}^{n} \epsilon_{\lambda,i} c_i \tag{2.30}$$

where $\varepsilon_{\lambda,i}$ is the effective molar absorptivity of solute i at λ, c_i is the concentration of solute i of interest in our work is the co-transport of MeOH and NaOAc. For these two solutes, distinctive peaks for methanol and acetate can be found at 1018 and 1414 cm^{-1}, respectively, shown in Fig. 2.6.

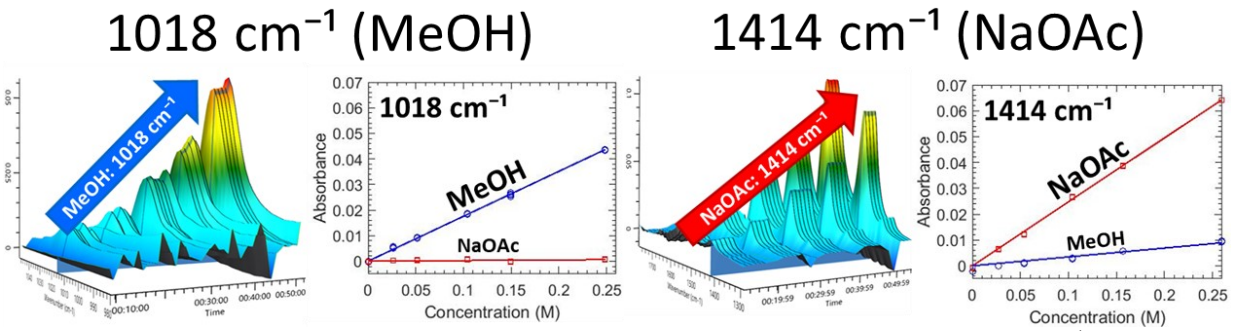

Figure 2.6. ATR-FTIR spectra at increasing concentrations (left) MeOH, 1018 cm^{-1}, and (right) NaOAc, 1414 cm^{-1}. Spectra are zoomed for clarity.

For these two solutes, one can calculate the effective molar absorptivity of MeOH and NaOAc at each wavenumber through calibration. Then the expression becomes.

$$A_{1018} = \epsilon_{1018,m} c_m + \epsilon_{1018,a} c_a$$

$$A_{1414} = \epsilon_{1414,a} c_a + \epsilon_{1414,m} c_m \tag{2.31}$$

where A_{1018} and A_{1414} are the measured absorbance at the distinctive wavelength for MeOH and NaOAc, $\varepsilon_{1018,m}$ and $\varepsilon_{1018,a}$ are the effective molar absorptivity for MeOH and NaOAc at the distinctive wavelength for MeOH, $\varepsilon_{1414,a}$ and $\varepsilon_{1414,m}$ are the effective molar absorptivity for NaOAc and MeOH at the distinctive wavelength for acetate, and c_m and c_a are the concentration of MeOH and NaOAc, respectively. After rearrangement, the concentration of MeOH and NaOAc can be calculated from two absorbances (A_{1018} and A_{1414}) as

$$c_m = \frac{A_{1018} - \frac{\epsilon_{1018,a} A_{1414}}{\epsilon_{1414,a}}}{\epsilon_{1018,m} - \frac{\epsilon_{1018,a}\epsilon_{1414,m}}{\epsilon_{1414,a}}} \qquad c_a = \frac{A_{1414} - \frac{\epsilon_{1414,m} A_{1018}}{\epsilon_{1018,m}}}{\epsilon_{1414,a} - \frac{\epsilon_{1414,m}\epsilon_{1018,a}}{\epsilon_{1018,m}}} \tag{2.32}$$

and a similar procedure can be taken to calculate multiple solutes. ATR-FTIR spectroscopy has also been used to capture diffusivities of solvents in swollen polymers [32–34]. However, directly measuring the concentration of solutes after they permeated through the membrane is our approach to measure transport through polymeric material [11,29,30]; more on this method will further be stated in the experimental section (3.9).

2.2. Hydrogel-based membranes

Synthetic hydrogels are crosslinked polymer networks produced by reaction of one or more monomers, which can hold water due to their hydrophilic structure. Properties of hydrogels, such as crosslink density, biodegradation, and mechanical strength, can be controlled upon designing and polymer synthesis [35].

Hydrogels can be classified by polymeric composition. Some of the most popular classes are homopolymeric and copolymeric hydrogels. Homopolymeric hydrogels are polymer network derived from a single component (i.e. pure PEGDA) [36,37]. Copolymeric hydrogels are derived from more than two monomers, where at least one component is hydrophilic (i.e. PEGDA-AMPS [38], MBAA-PA/MACC, etc.) [35]. Hydrogels can also be classified into three groups on presence of ion exchange functional groups on the crosslink chains, which are (1) nonionic (PEGDA and PEGDA-PEGA), (2) ionic (PEGDA-AMPS), and (3) zwitterionic (containing both cationic and anionic groups) hydrogels [35].

The network structure of a hydrogel membrane is a metric for comparing membrane behavior among different membranes and predicting the diffusive behavior of a solute through the

membrane using relationships between this structure and transport behavior. To investigate solute-polymer interactions, the structural properties of hydrogels, such as the degree of crosslinking and the mesh size can be adjusted. The degree of crosslinking is the density of junctions linking the chains. A higher degree of crosslinking tends to reduce the rate of diffusion but increases mechanical strength. Mesh size is the linear distance between two crosslink junctions [39] that are used to estimate the diffusional space available to transfer molecules through the polymer matrix (Figure 2.7).

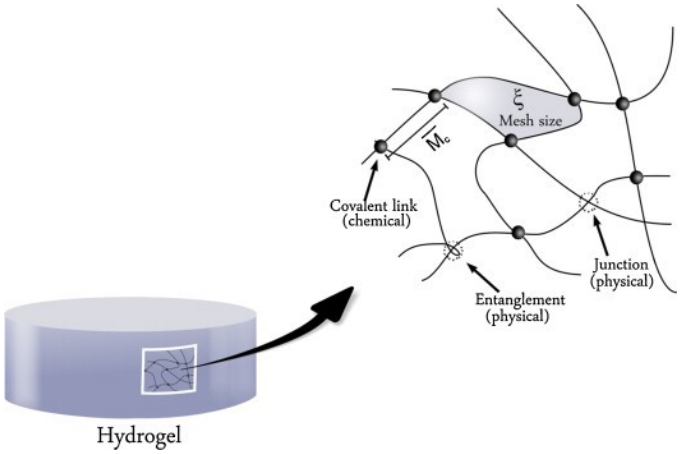

Figure 2.7. Schematic depiction of a typical hydrogel [40], where ξ is the mesh size, and $\overline{M_c}$ is the average molecular weight between crosslinks.

In hydrogels, such as the crosslinked poly(ethylene glycol) diacrylate (PEGDA) based membranes of interest here, the effective mesh size can be calculated by conducting water-swelling experiments and using the Peppas-Merrill equation [27] shown in Eq. 2.33.

$$\frac{1}{\overline{M_c}} = \frac{2}{\overline{M_n}} - \frac{\frac{\bar{\nu}}{V_w}[\ln(1-\nu_{2,s}) + \nu_{2,s} + \chi\nu_{2,s}^2]}{\nu_{2,r}[(\frac{\nu_{2,s}}{\nu_{2,r}})^{1/3} - \frac{1}{2}(\frac{\nu_{2,s}}{\nu_{2,r}})]} \tag{2.33}$$

where $\overline{M_c}$ is the molecular weight between crosslinks, $\overline{M_n}$ is the average molecular weight of PEGDA before photopolymerization, $\bar{\nu}$ is the specific volume of PEG (0.893 $\mathrm{cm^3/g}$) [41], V_w is the molar volume of water (18 $\mathrm{cm^3/mol}$), $\nu_{2,s}$ is the equilibrium volume fraction of a swollen

hydrogel, χ is the Flory-Huggins interaction parameter for PEG and water (0.426) [41–43], and $\nu_{2,r}$ is the equilibrium volume fraction of the crosslinked PEGDA before swelling in water [44].

Using $\overline{M_c}$, we can calculate the effective mesh size, ξ, as

$$\xi = l\left(3\frac{\overline{M_c}}{M_r}\right)^{1/2}\nu_{2,s}^{-1/3}C_n \tag{2.34}$$

where l is the average bond length (1.50 Å [45]), M_r is the molar mass of the PEG repeating unit (44 g/mol), and C_n is the characteristic ratio for the PEG (3.8) [27,36,41,44–46]. Previously, Ju et al. prepared a series of crosslinked PEGDA (n = 13, also utilized in this work Ch. 4–9) at varied prepolymerization water content (0 – 80 wt.%) and measured the mesh size using this approach, where the range was 12 – 30 Å [36]. Therefore, we assume the average mesh size of crosslinked PEGDA-based films to be within this range.

2.3. Ion Exchange Membranes

IEMs are a type of dense membrane that incorporate ion exchange functional groups within in the structure. Ion permselectivity between counterion and co-ion is an essential property in IEM [47], enabling transport of counterions (i.e. protons in cation exchange membranes (CEMs)) and impeding transport of co-ions (i.e. hydroxides or acetates in CEMs) or other neutral molecules (i.e. MeOH); see Fig. 2.8 [38]. IEMs have been developed for a wide range of applications from energy conversion (i.e. photoelectrochemical CO_2 reduction cells (PEC-CRC) and direct urea fuel cells (DUFC) to water purification (i.e. electrodialysis). Among the desired properties, high ion permselectivity is one of the most desired and elusive properties; Fig. 2.9 [47].

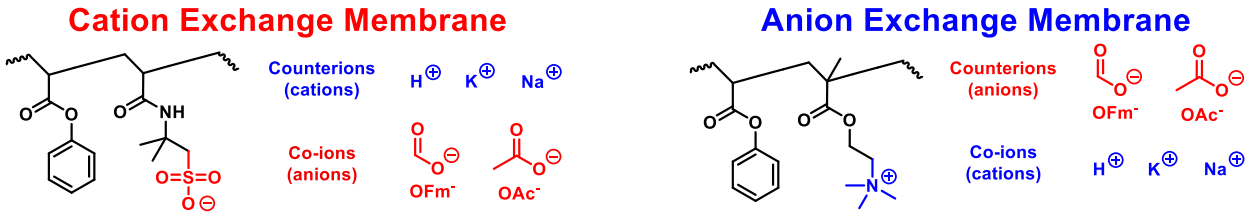

Figure 2.8. Counterions and co-ions of CEMs and AEMs, where cations are counterions in CEMs and anions are co-ions in AEMs. Similarly, anions are co-ions in AEMs and counterions in CEMs.

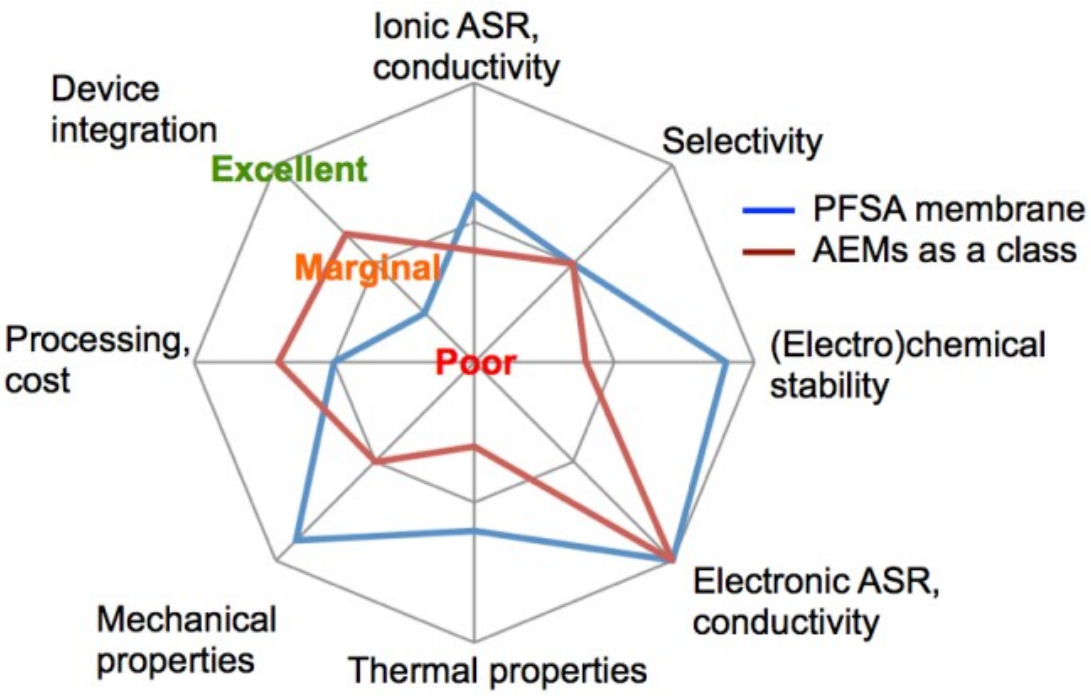

Figure 2.9. Properties of two hydrated polymer IEM for fuel cell applications, where a perfluorosulfonic acid (PFSA) membrane (type of CEM) is shown blue is and AEM is shown in red [48].

Nafion® 117 is a widely studied commercial CEM that enables transport of mobile proton counterions, H^+, through diffusing across negatively-charged sulfonate groups bound to the membrane. Likewise, Selemion® AMVN is a prospective anion exchange membrane (AEM) that enables the transport of hydroxide ions counterion, OH^-, through positively-charged quaternary ammonium groups. The structure of both Nafion® 117 and Selemion® AMVN are shown in Fig 2.10.

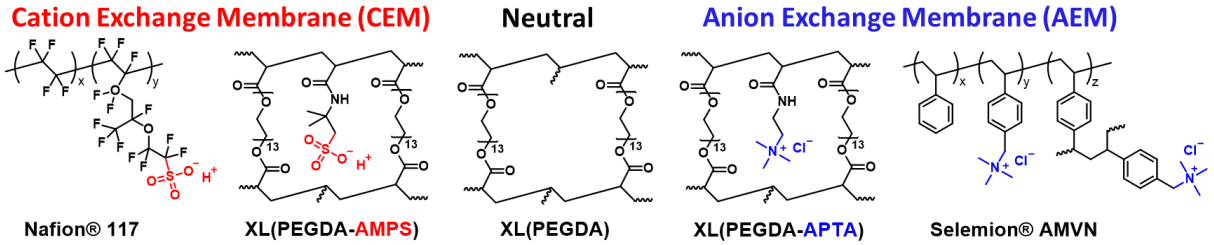

Figure 2.10. Chemical structures of Nafion® 117, PEGDA-AMPS, PEGDA, PEGDA-APTA, and Selemion® AMVN.

In our investigation, these commercial IEMs will be utilized as membranes of interest and importance for studying molecular/ionic transport behavior in CEMs and AEMs in conjunction with model membrane systems to investigate the root structure-property relationships underlying their behavior.

2.4. Photoelectrochemical CO_2 reduction cells

The photoelectrochemical CO_2 reduction cell (PEC-CRC) is an innovative approach devised to target (1) reduction of CO_2 (greenhouse gas) and (2) produce valuable CO_2 reduction products (alcohols and carboxylates) [15]; see Fig. 2.11 for schematic diagram.

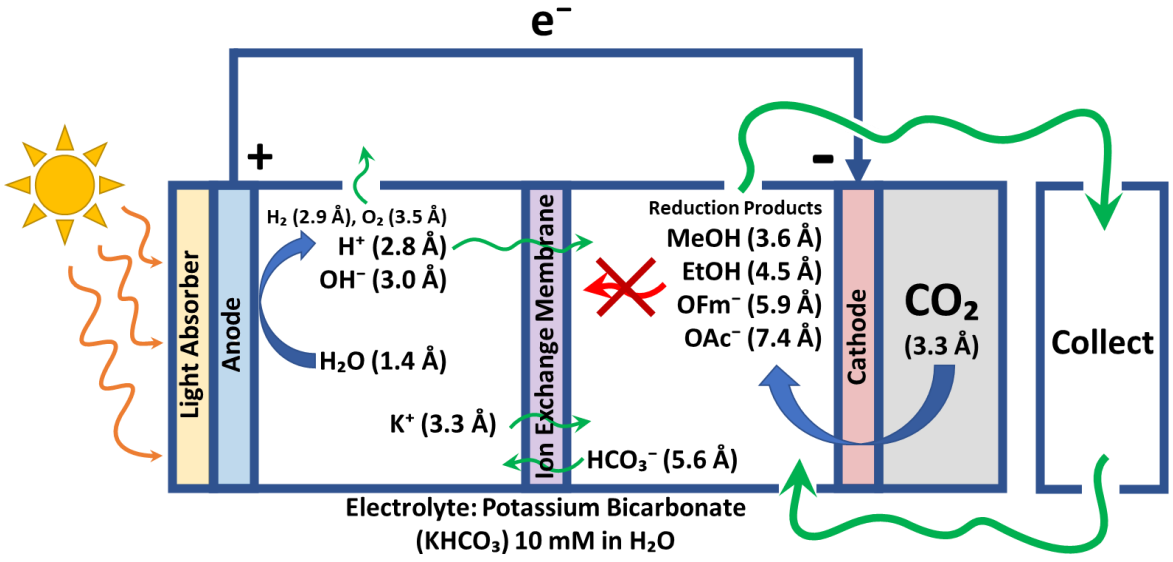

Figure 2.11. Schematic diagram of a photoelectrochemical CO_2 reduction cell.

Two of the current challenges on CO_2 reduction cells are (1) to increase the catalyst specificity to produce the most desirable chemicals (often times alcohol as a fuel) and (2) to suppress the crossover of CO_2 reduction products simultaneously to prevent the chemicals from oxidize back to CO_2 and by-products on the anode [15,49]. This work (Chapter 4–9) is focused on the second challenge, which is to design better IEMs that can suppress the crossover of all CO_2 reduction products and allows the transport of electrolytes (i.e. bicarbonates) and either hydroxides (OH, when an AEM is selected [50,51]) or protons (H, when a CEM is selected).

2.5. Direct urea fuel cells (DUFC)

The direct urea fuel cell (DUFC) is an emerging type of direct fuel cells, which converts urea (from industrial wastewater and urine) to electrical power [52] with a relatively high energy density and a low operating temperature [53–55]; see Fig. 2.12 for schematic diagram.

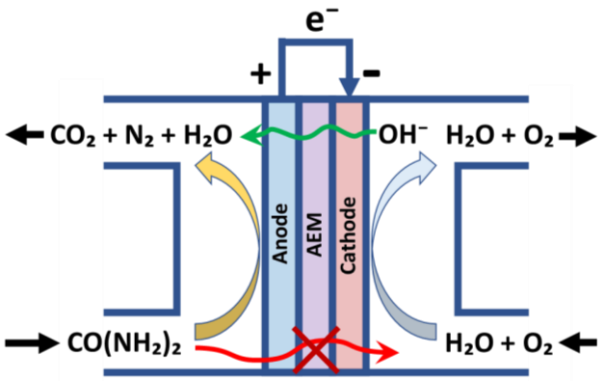

Figure 2.12. Schematic diagram of a direct urea fuel cell.

One of the challenges on this device is a lack of IEMs (either CEM [56] or AEM [57]) that minimize the crossover of urea to the cathode side of the cell, especially at higher concentrations. The outcome of this crossover can suppress the overall reaction (i.e. sweeping effect). This work (Chapter 10) is focused on introducing a new class of IEM that shows a competitive performance.

2.6. References

[1] M.A. Hickner, A.M. Herring, E.B. Coughlin, Anion exchange membranes: Current status and moving forward, J Polym Sci Part B Polym Phys. 51 (2013) 1727–1735. https://doi.org/10.1002/polb.23395.

[2] A. Kusoglu, A.Z. Weber, New Insights into Perfluorinated Sulfonic-Acid Ionomers, Chem Rev. 117 (2017) 987–1104. https://doi.org/10.1021/acs.chemrev.6b00159.

[3] Yu.S. Dzyazko, A. Mahmoud, F. Lapicque, V.N. Belyakov, Cr(VI) transport through ceramic ion-exchange membranes for treatment of industrial wastewaters, J Appl Electrochem. 37 (2007) 209–217. https://doi.org/10.1007/s10800-006-9243-7.

[4] H. Yasuda, C.E. Lamaze, L.D. Ikenberry, Permeability of solutes through hydrated polymer membranes. Part I. Diffusion of sodium chloride, Die Makromolekulare Chemie. 118 (1968) 19–35. https://doi.org/10.1002/macp.1968.021180102.

[5] H. Yasuda, A. Peterlin, C.K. Colton, K.A. Smith, E.W. Merrill, Permeability of solutes through hydrated polymer membranes. Part III. Theoretical background for the selectivity of dialysis membranes, Die Makromolekulare Chemie. 126 (1969) 177–186. https://doi.org/10.1002/macp.1969.021260120.

[6] R.W. Baker, Membrane Technology and Applications, (2018). https://doi.org/10.1002/9781118359686.

[7] J.G. Wijmans, R.W. Baker, The solution-diffusion model: a review, J Membrane Sci. 107 (1995) 1–21. https://doi.org/10.1016/0376-7388(95)00102-i.

[8] F.G. Helfferich, Ion Exchange, Dover, 1995.

[9] J. Kamcev, D.R. Paul, B.D. Freeman, Ion Activity Coefficients in Ion Exchange Polymers: Applicability of Manning's Counterion Condensation Theory, Macromolecules. 48 (2015) 8011–8024. https://doi.org/10.1021/acs.macromol.5b01654.

[10] J. Kamcev, D.R. Paul, G.S. Manning, B.D. Freeman, Ion Diffusion Coefficients in Ion Exchange Membranes: Significance of Counterion Condensation, Macromolecules. 51 (2018) 5519–5529. https://doi.org/10.1021/acs.macromol.8b00645.

[11] B.S. Beckingham, N.A. Lynd, D.J. Miller, Monitoring multicomponent transport using in situ ATR FTIR spectroscopy, J Membrane Sci. 550 (2018). https://doi.org/10.1016/j.memsci.2017.12.072.

[12] J.M. Kim, Y. Lin, B. Hunter, B.S. Beckingham, Transport and Co-Transport of Carboxylate Ions and Ethanol in Anion Exchange Membranes, Polymers-Basel. 13 (2021) 2885. https://doi.org/10.3390/polym13172885.

[13] K.A. Thompson, R. Mathias, D. Kim, J. Kim, N. Rangnekar, J.R. Johnson, S.J. Hoy, I. Bechis, A. Tarzia, K.E. Jelfs, B.A. McCool, A.G. Livingston, R.P. Lively, M.G. Finn, N-Aryl-linked spirocyclic polymers for membrane separations of complex hydrocarbon mixtures., Sci New York N Y. 369 (2020) 310–315. https://doi.org/10.1126/science.aba9806.

[14] R.T. Chern, W.J. Koros, B. Yui, H.B. Hopfenberg, V.T. Stannett, Selective permeation of CO2 and CH4 through kapton polyimide: Effects of penetrant competition and gas-phase nonideality, J Polym Sci Polym Phys Ed. 22 (1984) 1061–1084. https://doi.org/10.1002/pol.1984.180220610.

[15] M.R. Singh, A.T. Bell, Design of an artificial photosynthetic system for production of alcohols in high concentration from CO 2, Energ Environ Sci. 9 (2015) 193–199. https://doi.org/10.1039/c5ee02783g.

[16] R. Lan, S. Tao, J.T.S. Irvine, A direct urea fuel cell – power from fertiliser and waste, Energ Environ Sci. 3 (2010) 438–441. https://doi.org/10.1039/b924786f.

[17] A. Lee, J.W. Elam, S.B. Darling, Membrane materials for water purification: design, development, and application, Environ Sci Water Res Technology. 2 (2015) 17–42. https://doi.org/10.1039/c5ew00159e.

[18] P.N. Patil, D. Roilo, R.S. Brusa, A. Miotello, S. Aghion, R. Ferragut, R. Checchetto, Free volumes and gas transport in polymers: amine-modified epoxy resins as a case study, Phys Chem Chem Phys. 18 (2016) 3817–3824. https://doi.org/10.1039/c5cp07149f.

[19] X. Li, M. Wang, S. Wang, Y. Li, Z. Jiang, R. Guo, H. Wu, X. Cao, J. Yang, B. Wang, Constructing CO2 transport passageways in Matrimid® membranes using nanohydrogels for efficient carbon capture, J Membrane Sci. 474 (2015) 156–166. https://doi.org/10.1016/j.memsci.2014.10.003.

[20] G.Q. Chen, C.A. Scholes, C.M. Doherty, A.J. Hill, G.G. Qiao, S.E. Kentish, Modeling of the sorption and transport properties of water vapor in polyimide membranes, J Membrane Sci. 409 (2012) 96–104. https://doi.org/10.1016/j.memsci.2012.03.047.

[21] Q. Song, S.K. Nataraj, M.V. Roussenova, J.C. Tan, D.J. Hughes, W. Li, P. Bourgoin, M.A. Alam, A.K. Cheetham, S.A. Al-Muhtaseb, E. Sivaniah, Zeolitic imidazolate framework (ZIF-8) based polymer nanocomposite membranes for gas separation, Energ Environ Sci. 5 (2012) 8359–8369. https://doi.org/10.1039/c2ee21996d.

[22] H. Ju, A.C. Sagle, B.D. Freeman, J.I. Mardel, A.J. Hill, Characterization of sodium chloride and water transport in crosslinked poly(ethylene oxide) hydrogels, J Membrane Sci. 358 (2010) 131–141. https://doi.org/10.1016/j.memsci.2010.04.035.

[23] H.B. Park, C.H. Jung, Y.M. Lee, A.J. Hill, S.J. Pas, S.T. Mudie, E.V. Wagner, B.D. Freeman, D.J. Cookson, Polymers with Cavities Tuned for Fast Selective Transport of Small Molecules and Ions, Science. 318 (2007) 254–258. https://doi.org/10.1126/science.1146744.

[24] D.W. Gidley, H.-G. Peng, R.S. Vallery, Positron Annihilation as a method to characterize porous materials, Annu Rev Mater Res. 36 (2006) 49–79. https://doi.org/10.1146/annurev.matsci.36.111904.135144.

[25] M.M. Gomaa, C. Hugenschmidt, M. Dickmann, E.E. Abdel-Hady, H.F.M. Mohamed, M.O. Abdel-Hamed, Crosslinked PVA/SSA proton exchange membranes: correlation between physiochemical properties and free volume determined by positron annihilation spectroscopy, Phys Chem Chem Phys. 20 (2018) 28287–28299. https://doi.org/10.1039/c8cp05301d.

[26] H.F.M. Mohamed, Y. Kobayashi, S. Kuroda, A. Ohira, Positron trapping and possible presence of SO3H clusters in dry fluorinated polymer electrolyte membranes, Chem Phys Lett. 544 (2012) 49–52. https://doi.org/10.1016/j.cplett.2012.06.060.

[27] N.A. Peppas, E.W. Merrill, Crosslinked poly(vinyl alcohol) hydrogels as swollen elastic networks, J Appl Polym Sci. 21 (1977) 1763–1770. https://doi.org/10.1002/app.1977.070210704.

[28] G.M. Geise, H. Lee, D.J. Miller, B.D. Freeman, J.E. McGrath, D.R. Paul, Water purification by membranes: The role of polymer science, J Polym Sci Part B Polym Phys. 48 (2010) 1685–1718. https://doi.org/10.1002/polb.22037.

[29] B.M. Carter, B.M. Dobyns, B.S. Beckingham, D.J. Miller, Multicomponent transport of alcohols in an anion exchange membrane measured by in-situ ATR FTIR spectroscopy, Polymer. 123 (2017). https://doi.org/10.1016/j.polymer.2017.06.070.

[30] B.M. Carter, L. Keller, M. Wessling, D.J. Miller, Preparation and characterization of crosslinked poly(vinylimidazolium) anion exchange membranes for artificial photosynthesis, J Mater Chem A. (2019). https://doi.org/10.1039/c9ta00498j.

[31] M. Galizia, D.R. Paul, B.D. Freeman, Liquid methanol sorption, diffusion and permeation in charged and uncharged polymers, Polymer. 102 (2016) 281–291. https://doi.org/10.1016/j.polymer.2016.09.010.

[32] M. Karimi, A.A. Tashvigh, F. Asadi, F.Z. Ashtiani, Determination of concentration-dependent diffusion coefficient of seven solvents in polystyrene systems using FTIR-ATR technique: experimental and mathematical studies, Rsc Adv. 6 (2016) 9013–9022. https://doi.org/10.1039/c5ra25244j.

[33] P. Wu, H.W. Siesler, Water diffusion into epoxy resin: a 2D correlation ATR-FTIR investigation, Chem Phys Lett. 374 (2003) 74–78. https://doi.org/10.1016/s0009-2614(03)00691-2.

[34] A.F. Breen, C. Breen, F. Clegg, L.-M. Döppers, Khairuddin, M. Labet, C. Sammon, J. Yarwood, FTIR-ATR studies of the sorption and diffusion of acetone:water mixtures in poly(vinyl alcohol)-clay nanocomposites, Polymer. 53 (2012) 4420–4428. https://doi.org/10.1016/j.polymer.2012.07.057.

[35] E.M. Ahmed, Hydrogel: Preparation, characterization, and applications: A review, J Adv Res. 6 (2015) 105–121. https://doi.org/10.1016/j.jare.2013.07.006.

[36] H. Ju, B.D. McCloskey, A.C. Sagle, V.A. Kusuma, B.D. Freeman, Preparation and characterization of crosslinked poly(ethylene glycol) diacrylate hydrogels as fouling-resistant membrane coating materials, J Membrane Sci. 330 (2009) 180–188. https://doi.org/10.1016/j.memsci.2008.12.054.

[37] B.M. Dobyns, J.M. Kim, B.S. Beckingham, Multicomponent transport of methanol and sodium acetate in poly(ethylene glycol) diacrylate membranes of varied fractional free volume, Eur Polym J. 134 (2020) 109809. https://doi.org/10.1016/j.eurpolymj.2020.109809.

[38] D. Stigter, Donnan membrane equilibrium, sedimentation equilibrium, and coil expansion of DNA in salt solutions, Cell Biophys. 11 (1987) 139–158. https://doi.org/10.1007/bf02797120.

[39] N.A. Peppas, P. Bures, W. Leobandung, H. Ichikawa, Hydrogels in pharmaceutical formulations, Eur J Pharm Biopharm. 50 (2000) 27–46. https://doi.org/10.1016/s0939-6411(00)00090-4.

[40] D. Buenger, F. Topuz, J. Groll, Hydrogels in sensing applications, Prog Polym Sci. 37 (2012) 1678–1719. https://doi.org/10.1016/j.progpolymsci.2012.09.001.

[41] G.M. Cruise, D.S. Scharp, J.A. Hubbell, Characterization of permeability and network structure of interfacially photopolymerized poly(ethylene glycol) diacrylate hydrogels, Biomaterials. 19 (1998) 1287–1294. https://doi.org/10.1016/s0142-9612(98)00025-8.

[42] R.J. Russell, A.C. Axel, K.L. Shields, M.V. Pishko, Mass transfer in rapidly photopolymerized poly(ethylene glycol) hydrogels used for chemical sensing, Polymer. 42 (2001) 4893–4901. https://doi.org/10.1016/s0032-3861(00)00851-x.

[43] E.W. Merrill, K.A. Dennison, C. Sung, Partitioning and diffusion of solutes in hydrogels of poly(ethylene oxide), Biomaterials. 14 (1993) 1117–1126. https://doi.org/10.1016/0142-9612(93)90154-t.

[44] C. Echeverria, N.A. Peppas, C. Mijangos, Novel strategy for the determination of UCST-like microgels network structure: effect on swelling behavior and rheology, Soft Matter. 8 (2011) 337–346. https://doi.org/10.1039/c1sm06489d.

[45] M.B. Mellott, K. Searcy, M.V. Pishko, Release of protein from highly cross-linked hydrogels of poly(ethylene glycol) diacrylate fabricated by UV polymerization, Biomaterials. 22 (2001) 929–941. https://doi.org/10.1016/s0142-9612(00)00258-1.

[46] J.L. Stringer, N.A. Peppas, Diffusion of small molecular weight drugs in radiation-crosslinked poly(ethylene oxide) hydrogels, J Control Release. 42 (1996) 195–202. https://doi.org/10.1016/0168-3659(96)01457-5.

[47] T. Luo, S. Abdu, M. Wessling, Selectivity of Ion Exchange Membranes: A Review, J Membrane Sci. 555 (2018) 429–454. https://doi.org/10.1016/j.memsci.2018.03.051.

[48] S. Jeong, H. Sohn, S.W. Kang, Highly permeable PEBAX-1657 membranes to have long-term stability for facilitated olefin transport, Chemical Engineering Journal. (2018). https://doi.org/10.1016/j.cej.2017.09.125.

[49] D.J. Miller, F.A. Houle, Energy and Environment Series, (2018) 341–385. https://doi.org/10.1039/9781788010313-00341.

[50] A. Amel, N. Gavish, L. Zhu, D.R. Dekel, M.A. Hickner, Y. Ein-Eli, Bicarbonate and chloride anion transport in anion exchange membranes, J Membrane Sci. 514 (2016) 125–134. https://doi.org/10.1016/j.memsci.2016.04.027.

[51] S.M. Dischinger, S. Gupta, B.M. Carter, D.J. Miller, Transport of Neutral and Charged Solutes in Imidazolium-Functionalized Poly(phenylene oxide) Membranes for Artificial Photosynthesis, Ind Eng Chem Res. 59 (2019) 5257–5266. https://doi.org/10.1021/acs.iecr.9b05628.

[52] N. Senthilkumar, G.G. kumar, A. Manthiram, 3D Hierarchical Core–Shell Nanostructured Arrays on Carbon Fibers as Catalysts for Direct Urea Fuel Cells, Adv Energy Mater. 8 (2018) 1702207. https://doi.org/10.1002/aenm.201702207.

[53] N. Kakati, G. Li, P.-Y.A. Chuang, Insights into the Ni/C-Based Thin-Film Catalyst Layer Design for Urea Oxidation Reaction in a Three-Electrode System, Acs Appl Energy Mater. 4 (2021) 4224–4233. https://doi.org/10.1021/acsaem.1c00607.

[54] A. Modak, R. Mohan, K. Rajavelu, R. Cahan, T. Bendikov, A. Schechter, Metal–Organic Polymer-Derived Interconnected Fe–Ni Alloy by Carbon Nanotubes as an Advanced Design of Urea Oxidation Catalysts, Acs Appl Mater Inter. 13 (2021) 8461–8473. https://doi.org/10.1021/acsami.0c22148.

[55] D. Yang, L. Yang, L. Zhong, X. Yu, L. Feng, Urea electro-oxidation efficiently catalyzed by nickel-molybdenum oxide nanorods, Electrochim Acta. 295 (2019) 524–531. https://doi.org/10.1016/j.electacta.2018.10.190.

[56] F. Guo, K. Cheng, K. Ye, G. Wang, D. Cao, Preparation of nickel-cobalt nanowire arrays anode electro-catalyst and its application in direct urea/hydrogen peroxide fuel cell, Electrochim Acta. 199 (2016) 290–296. https://doi.org/10.1016/j.electacta.2016.01.215.

[57] J. Yoon, D. Lee, Y.N. Lee, Y.S. Yoon, D.-J. Kim, Solid solution palladium-nickel bimetallic anode catalysts by co-sputtering for direct urea fuel cells (DUFC), J Power Sources. 431 (2019) 259–264. https://doi.org/10.1016/j.jpowsour.2019.05.059.

Chapter 3

Experimental

3.1. Materials

Nafion® 117 (Lot: 2002FS6556) was purchased from Chemours (Wilmington, DE). Selemion® AMVN was purchased from AGC Engineering Co. (Tokyo, Japan). Fumasep FAA-3-50 (FAA) was purchased from FuMA-Tech (St. Ingbert, Germany). Methanol (MeOH, ≥ 99.9 %), ethanol (EtOH, ≥ 99 %), poly(ethylene glycol) diacrylate (PEGDA, n = 13), 2-acrylamido-2-methyl-1-propanesulfonic acid (AMPS, 99 %), (3-acrylamidopropyl) trimethylammonium chloride solution (APTA, 75 wt.% in water), 2-hydroxyethyl methacrylate (HEMA, n = 1), phenoxyethyl methacrylate (PEMA, n = 1), phenoxyethyl acrylate (PEA, n = 1), poly(ethylene glycol) phenyl ether acrylate (PEGPEA, n = 3), 3-sulfopropyl methacrylate potassium salt (SPMAK), hydrochloric acid (HCl), potassium hydroxide (KOH), and 2,2′-azobis(2-methylpropionitrile) (AIBN, 98 %), and ammonium oxalate monohydrate ($(NH_4)_2C_2O_4 \cdot H_2O$) were purchased from Sigma-Aldrich Chemicals (St. Louis, MS). Dimethyl sulfoxide (DMSO, ≥ 99.9 %) was purchased from Macron Fine Chemicals (Radnor, PA). A silver target (Ag, 99.9 %) was purchased from Kurt J. Lesker company (Pittsburgh, PA). Poly(ethylene glycol) methacrylate (PEGMA, n = 5) was purchased from Polysciences Inc. (Warrington, PA). Sodium formate (NaOFm, ≥ 99 %), acrylic acid (AA, n = 0), and nickel chloride hexahydrate ($NiCl_2 \cdot 6\ H_2O$) were purchased from Alfa Aesar

(Haverhill, MA). Phenyl acrylate (PA, 97 %) was purchased from Ambeed (Arlington Heights, IL). Phenyl methacrylate (PMA, > 97 %), methacroylcholine chloride (MACC, ca. 80 % in water), N,N'-methylenebisacrylamide (MBAA, > 98 %), and 1-Hydroxyl-cyclohexyl phenyl ketone (HCPK) were purchased from TCI (Tokyo, Japan). Sodium acetate (NaOAc, ≥ 99 %) was purchased from ACS Chemical Inc. (Point Pleasant, NJ). Potassium formate (KOFm, ≥ 98%) was purchased BeanTown Chemical (Hudson, NH). Sodium chloride (NaCl), sodium hydroxide beads (NaOH), potassium acetate (KOAc, ≥ 99.0%), potassium chromate (K_2CrO_4, 5 % (w/v)), and silver nitrate ($AgNO_3$, 1 M) were purchased from British Drug Houses (Poole, UK). Type-1 deionized water; produced by a Waterpro BT Purification System from Labconco® (18.2 mΩ·cm at 25 °C, 1.2 ppb TOC) (Kansas City, MO).

3.2. Free radical polymerization (Film synthesis)

3.2.1. UV photopolymerization (Chapter 4 – 9)

A total of 37 compositionally dissimilar membranes were prepared by free radical UV photocrosslinking of prepolymerization mixtures (solutions of water, monomer, and photoinitiator (HCPK)); corresponding compositions can be found in corresponding chapters. Each prepolymerization mixture was sonicated for 30 minutes to achieve a homogeneous solution and placed in between two quartz plates (5 x 5 x 1/4") separated by two spacers (305 μm). This setup was then placed inside a UV crosslinking oven, Spectrolinker™ XL-1500 from Spectroline (Westbury, NY), under 254 nm for 3 min at 3.0 mW/cm^2. All films with the thickness of the spacers were carefully recovered and immersed in 1 L of water for 2 days before further use. Essentially complete conversion has been achieved as the mass of polymer network-forming monomers in the

prepolymerization mixtures accords with the mass of the films after vacuum drying at 50 °C following 5 days of swelling in DI water within ~99 % [4–7].

3.2.2. Thermal polymerization (Chapter 10)

3.2.2.1. Cation exchange membrane formation: PA/A and PMA/A

A total of 8 crosslinked CEM organogels were prepared by thermal copolymerization of prepolymerization mixtures, corresponding compositions can be found in Capture 10. A series of crosslinked PA-AMPS films (PA/A) and crosslinked PMA-AMPS films (PMA/A) were prepared. Both PA/A and PMA/A contain 70 mol% of either PA or PMA (a hydrophobic comonomer) and 30 mol% of AMPS (a sulfonated comonomer, hydrophilic). Each film contains from 5 to 30 mol% of MBAA (a crosslinker) and 0.1 wt.% of AIBN (thermal initiator), where both mol% and wt.% are to the sum of a hydrophobic comonomer (either PA or PMA) and the sulfonated comonomer (AMPS). Each pre-polymerization mixture was prepared with 50 wt.% of DMSO (solvent) content. The solutions were sonicated for approximately 15 min to produce homogenous mixtures and purged with nitrogen gas for 10 min to remove dissolved oxygen. The prepolymerization mixture was placed in between two glass plates (5×5×1/4”) separated by two spacers (356 μm) and placed inside a vacuum oven at 60 °C for 8 hours. The solid organogels with the thickness of the spacers were obtained and immersed in 1 L of DI water for 2 days to exchange DMSO with water, where water was replaced daily. The inclusion of AMPS repeat units in the polymer network has been verified by ATR-FTIR spectroscopy.

3.2.2.2. Anion exchange membrane formation: PA/M and PMA/M

A total of 7 crosslinked AEM organogels (PA-MACC (PA/M) and PMA-MACC (PMA/M)) were prepared by thermal copolymerization of prepolymerization mixtures, corresponding compositions can be found in Chapter 10. Both PA/M and PMA/M contain 70 mol% of either PA or PMA and 30 mol% of MACC (a quaternary ammonium (QA^+)-containing comonomer). PA/M films contain from 5 to 30 mol% of MBAA and PMA/M films contain from 5 to 20 mol% of MBAA, where the mol% is the sum of a hydrophobic comonomer (either PA or PMA) and the QA^+-containing comonomer (MACC). We note that phase separation was observed in the prepolymerization mixture prepared analogously for PMA/M-30, such that a homogeneous crosslinked film could not be prepared. All films contain 0.1 wt.% of AIBN, where the wt.% is based on the sum of the two comonomers. Each pre-polymerization mixture was prepared with 50 wt.% of solvent content, where the solvent is composed of water (~8 wt.%) from the MACC solution and the remaining DMSO (~92 wt.%). Each solution was sonicated for 15 min to produce a homogenous mixture and purged with nitrogen gas for 10 min to remove dissolved oxygen. The prepolymerization mixture was placed in between two glass plates separated by two spacers and placed inside a vacuum oven at 60 °C for 8 hours. The solid organogels with the thickness of the spacers were obtained and immersed in 1 L of DI water for 2 days to exchange solvent with water, where the water was replaced daily. The inclusion of MACC repeat units in the polymer network has been verified by ATR-FTIR.

3.3. Water uptake, dry polymer density, water volume fraction

Water uptake was measured gravimetrically. A 0.75-inch diameter hole punch was used to cut each hydrated film. The mass of the hydrated films, W_s, was measured after quickly blotting them with tissue paper. The films were then dried under a vacuum at 50 °C for 24 hours and the mass of the dried films, W_d, measured [10]. The water uptake, ω_w, was calculated as follows:

$$\omega_w = \frac{W_s - W_d}{W_d} \cdot 100\% \tag{3.1}$$

where W_s is the mass of the swollen film and W_d is the mass of the dried film.

Film density was measured by buoyancy method with a density kit (ML-DNY-43, Mettler Toledo) coupled with a scale (ML204T, Mettler Toledo) [11]. The density, ρ_p, was calculated as follows:

$$\rho_p = (\rho_L - \rho_0)\left(\frac{W_0}{W_0 - W_L}\right) + \rho_0 \tag{3.2}$$

where ρ_L is the density of water (997.8 kg/m^3 at 22 °C), ρ_0 is the density of air (1.225 kg/m^3), W_0 is the weight of the dried film in air, and W_L is the weight of the film in water.

Water volume fraction, ϕ_w, was then calculated as follows:

$$\phi_w = \frac{(W_s - W_d)/\rho_L}{(W_s - W_d)/\rho_L + W_d/\rho_p} \tag{3.3}$$

3.4. Counterion exchange in AEMs (Chapter 6 and 10)

The chloride (Cl^-) counterion in AEMs (PEGDA-APTA8, PEGDA-APTA12, and Selemion® AMVN) was exchanged to bicarbonate (HCO_3^-); see Chapter 6. 0.75-inch and 1-inch hole-punches (General Tools 1271 Arch Punches) were used to cut each AEM into 0.75-inch films for sorption-desorption experiments and 1-inch films for diffusion cell experiments. All films were then placed

in 1 M sodium bicarbonate ($NaHCO_3$) for 2 days, where the solution was replaced daily and gently stirred [16]. Next, all films were washed with DI water and placed in DI water for 2 days to remove excess Cl^- and NaHCO3, where the solution was gently stirred, and water was replaced daily. A conductivity meter was used to confirm the conductivity of the solution is the same as DI water (≤ 18.2 mΩ·cm at 25 °C). The degree of conversion for all films from Cl^- to HCO_3^- was measured by elemental analysis using a scanning electron microscope (Zeiss EVO 50 SEM) coupled with energy dispersive spectroscopy (INCA EDS). Similarly, the chloride (Cl^-) counterion in PA/MACC-30 and the bromide (Br^-) counterions in Fumasep® FAA-3-50 were exchanged to hydroxide (OH^-) with 1 M KOH); see Chapter 10.

3.5. Ion exchange capacity (IEC)

Ion exchange capacity (IEC, mmol/g) was measured using a titration method [12–14] for CEMs and Mohr method [15–17] for AEMs. Briefly, all hydrated membranes were dried in a vacuum oven at 50 °C for 24 hours. The mass of the dried films (~1.5 g), W_d, were measured. For CEMs, each dried film was placed in 1 M NaCl solution (~50 mL) for more than 2 days (to exchange H^+ with Na^+) and 3 to 5 drops of phenolphthalein indicator were added to each solution. Lastly, 0.1 M NaOH solution was added dropwise until the color of the solution remains pink. The IEC was calculated as follows:

$$IEC = \frac{V_{NaOH} \times C_{NaOH}}{W_d} \tag{3.4}$$

where V_{NaOH} is the volume of NaOH solution added, C_{NaOH} is the concentration of the NaOH solution (0.1 M), and W_d is the mass of the dried films.

For AEMs, each film was placed in 1 M KOH (~50 mL) for more than 2 days (to exchange Cl^- with OH^-). Each solution was then poured in a beaker filled with ~150 mL of DI water and ~5 mL of the K_2CrO_4 solution. Lastly, 0.1 M $AgNO_3$ solution was added dropwise until the color of the solution remained red-brown. The IEC was calculated as follows:

$$IEC = \frac{V_{AgNO_3} \times C_{AgNO_3}}{W_d} \tag{3.4}$$

where V_{AgNO_3} is the volume of $AgNO_3$ solution added, C_{AgNO_3} is the concentration of the $AgNO_3$ solution (0.1 M), and W_d is the mass of the dried films.

3.6. Ionic conductivity

In-plane conductivity of all films was measured at 25 °C using a four-point conductivity cell (BekkTech BT-110) employed with a Gamry Interface 1000 potentiostat [5]. A rectangular section of the film (length: >1.0 cm, width (W): 0.5 cm) was cut and placed in the conductivity cell. The cell was then placed in DI water (500 mL), and electrochemical impedance spectroscopy (EIS) was performed after stabilization of the open circuit potential (frequency: 10 Hz-1 MHz, AC voltage: 10 mV). The EIS data was analyzed in Gamry Echem Analyst software and the resistance, R (Ω), obtained from the Nyquist plot. The ionic conductivity, σ, was calculated as follows:

$$\sigma = \frac{L}{RWT} \tag{3.5}$$

where L, W, and T are the distance between two electrodes (0.5 cm), the width, and the thickness of the film, respectively.

3.7. Storage modulus (Crosslink density, Chapter 8 – 10)

The storage moduli (E') of films were measured to estimate the crosslink densities [18,19]. 1 mm spacers were used to prepare the all the films. The films were then hydrated in a DI water for at least 5 days and the freeze-dried for 24 hours. The dried films were then cut into a rectangular shape (10×20×1 mm). The storage modulus of all films was measured by dynamic mechanical analysis (DMA, Dynamic Mechanical Analyzer TA Instruments RSA III) at a heating rate of 1 ˚C/min from 23 to 30 ˚C (rubbery plateau) at a test frequency of 1 Hz. Lastly, the crosslink density, ν_e (mmol/cm^3), was estimated from Flory's rubber elasticity relationship [20]:

$$\nu_e = \frac{E'}{3RT} \tag{3.6}$$

where E' is the storage modulus (Pa), R is the gas constant (8314 cm^3 Pa/K mmol), and T is the temperature (298.15 K).

3.8. Tensile test (Stress-strain curve, Chapter 10)

Three hydrated rectangular films (30×10×0.35 mm) were prepared for each composition. Tensile tests (ASTM-D882-18) were performed using a dynamic mechanical analyzer (TA Instruments RSA III), where all samples were tested based on rectangular tensile geometry using a 10 mm gauge length at the crosshead speed of 0.05 mm/s. Young's moduli were calculated based on the initial slope of stress-strain curves.

3.9. Permeability measurement (Diffusion cell experiment)

A more detailed experimental method is discussed in section 2.1.4. Briefly, permeabilities of films to alcohols (MeOH and EtOH) and carboxylates (OFm^- and OAc^-) were measured using a temperature jacketed custom-built diffusion cell coupled with an in-situ ATR-FTIR probe (Mettler-Toledo ReactIR™ 15 with a shallow tip 9.5 mm DSun AgX DiComp probe) to detect the evolving solute concentration in the receiver cell.

To calibrate the probe, a distinct wavenumber (λ, cm^{-1}) for each solute, MeOH (1018 cm^{-1}), EtOH (1044 cm^{-1}), OFm^- (1350 cm^{-1}), and OAc^- (1414 cm^{-1}), was selected from a sample absorbance spectra (0.05 M of each solute in DI water) in order to maximize both separation between peaks and peak sensitivity to changes in concentration ($d[A_\lambda]/d[C]$). Next, we prepared a series of solutions at dissimilar concentrations for each solute (i.e. MeOH) and measured the height of the absorbance at the distinct wavenumber (i.e. 1018 cm^{-1}) for each solution as shown in Fig. 3.1. To account for the effect of co-solutes (i.e. OFm^- or OAc^-) on the absorbance of each solute (e.g. MeOH), the absorbances at the distinct wavenumbers for the co-solutes (i.e. 1350 and 1414 cm^{-1}) were also measured for each solution. The molar absorptivity, $\varepsilon_{i,\lambda}$, for each solute i (i.e. MeOH) at each distinct wavenumber (i.e. 1018, 1350, and 1414 cm^{-1}) is then calculated using the Beer-Lambert law [23]:

$$A_\lambda = \sum_{i=1}^{n} \varepsilon_{i,\lambda} c_i \tag{3.7}$$

where A_λ is the height of the absorbance at the distinct wavenumber (λ), $\varepsilon_{i,\lambda}$ is the molar absorptivity of solute i at the distinct wavenumber, and c_i is the concentration of the solute i. Therefore, three molar absorptivities, $\varepsilon_{i,\lambda}$, were obtained from each solute. For instance, the three molar absorptivities from MeOH calibration are $\varepsilon_{MeOH,1018}$, $\varepsilon_{MeOH,1350}$, and $\varepsilon_{MeOH,1414}$; see Fig. 3.1(A).

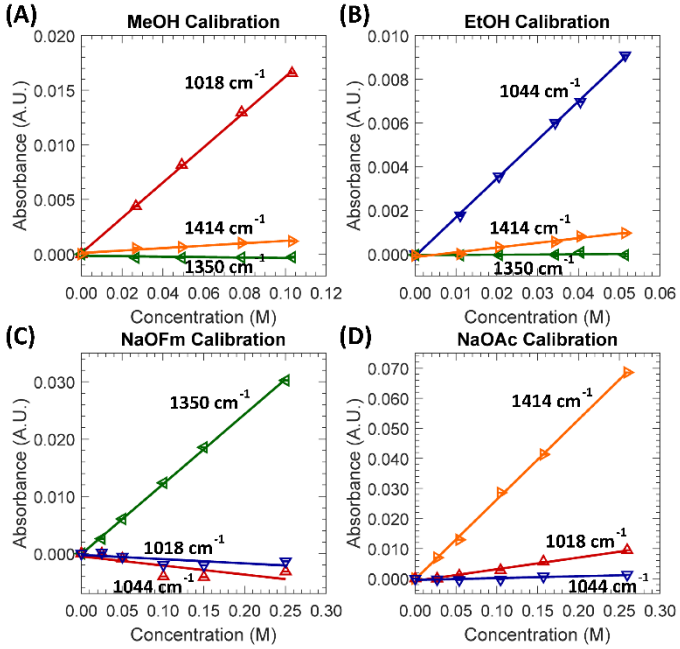

Figure 3.1. ATR-FTIR absorbance as a function of (A) MeOH, (B) EtOH, (C) OFm^-, and (D) OAc^- concentration (M) in DI water at wavenumbers, 1018 cm^{-1} (△, red), 1044 cm^{-1} (▽, blue), 1350 cm^{-1} (◁, green), and 1414 cm^{-1} (▷, yellow). Lines are linear best-fits to absorbance data.

To measure the permeability of each membrane, the feed cell was initially filled with either 1 M unary mixture (i.e. MeOH) or a binary mixture consisting of 1 M alcohol and 1 M carboxylate (i.e. MeOH-OFm^-), while the receiver cell was initially filled with DI water. The time-resolved absorbances, A_λ, were acquired from the solution in the receiver cell and converted to the concentration using the molar absorptivities, $\varepsilon_{i,\lambda}$. For instance, the time-resolved MeOH concentration, c_{MeOH}, during a one-component permeability measurement was calculated by:

$$A_{1018} = \varepsilon_{MeOH,1018} c_{MeOH} \tag{3.8}$$

where A_{1018} is the height of the absorbance at 1018 cm^{-1} and $\varepsilon_{MeOH,1018}$ is the molar absorptivity of MeOH at 1018 cm^{-1}. Moreover, the time-resolved MeOH concentration during a two-component permeability measurement with OFm^- was calculated by:

$$A_{1018} = \varepsilon_{MeOH,1018} c_{MeOH} + \varepsilon_{NaOFm,1018} c_{NaOFm} \tag{3.9}$$

where $\varepsilon_{NaOFm,1018}$ is the molar absorptivity of OFm^- at 1018 cm^{-1} and c_{NaOFm} is the time-resolved NaOFm concentration during a two-component permeability measurement with MeOH. The permeabilities, P_i, were then measured by the Yasuda's model (Eq. 2.26) [24,25]:

$$P_i = ln\left(1 - \frac{2c_{i,l}(t)}{c_{i,0}}\right)\left(\frac{-lV}{2At}\right) \tag{3.10}$$

where $c_{i,l}(t)$ is the time-resolved concentration of solute i in the receiver cell, l is the thickness of the membrane after the measurement, $c_{i,0}$ is the initial concentration in the feed cell (1 M), V is the volume of the half-cell (25 mL), A is the area of the orifice of the half-cell (1.1423 cm^2), and t is the time. The osmotic diffusion of water from the receiver cell to the feed cell is neglected in this study as the difference due to osmotic diffusion was within the experimental error for identical solutions in Nafion® 117 [10]. Similarly, urea permeabilities of phenyl-based crosslinked IEMs were measured (Chapter 10).

3.10. Solubility measurement (Sorption-desorption)

Solubilities of all films to alcohols (MeOH and EtOH) and carboxylates (OFm^- and OAc^-) were measured by a sorption-desorption technique in one- and two-component solutions [5,10,21,22,26]. A 0.75-inch diameter hole punch was used to cut films from each membrane. Each film was then quickly blotted with tissue paper and immersed in a solution vial (15 mL). All vials consisting of either a 1 M unary mixture (MeOH, EtOH, OFm^- and OAc^-) or a binary mixture consisting of 1 M alcohol and 1 M carboxylate (MeOH-OFm^-, MeOH-OAc^-, EtOH-OFm^-, and EtOH-OAc^-), each mixture was prepared in triplicate. All films were placed in the solution vials for 3 days and the solution was replaced daily. A digital caliper (±1 μm) was used to measure the film thickness by finding an average of five random locations and ImageJ software (National Institutes of Health,

MD) was used to calculate the area of the films from digital photographs. Each film was then quickly blotted dry and immersed in a vial of DI water (10 g) for 3 days. The solution from each vial was then transferred to a high-performance liquid chromatography (HPLC) employed with a refractive index detector, Aminex HPX-87H column (Bio-Rad, CA) to determine the solute concentration in each desorption solution. The solubility, K_i of each solute in the film was calculated as:

$$K_i = \frac{C_i^m}{C_i^s} \tag{3.11}$$

where C_i^s is the concentration of the solute *i* in the external solution (1 M) and C_i^m is the concentration of the solute *i* in the film, which is the product of the concentration of the solute *i* of the desorption solution and the volume of the desorption solution (10 mL) divided by the volume of solution-soaked films.

Total volume of the solution in films after sorption was calculated by subtracting the dry volume of the films (dry polymer mass/dry polymer density, ρ_p) from the swollen volume of the films. Volume of each solute *i* in swollen films, V_i, were calculated as:

$$V_i = \frac{n_i \times M_i}{\rho_i} \tag{3.12}$$

where n_i is the mol of solute *i* (from the desorption solution), M_i is the molecular mass of solute *i*, and ρ_i is the density of solute *i*.

3.11. References

[1] H. Ju, A.C. Sagle, B.D. Freeman, J.I. Mardel, A.J. Hill, Characterization of sodium chloride and water transport in crosslinked poly(ethylene oxide) hydrogels, J Membrane Sci. 358 (2010) 131–141. https://doi.org/10.1016/j.memsci.2010.04.035.

[2] H. Ju, B.D. McCloskey, A.C. Sagle, V.A. Kusuma, B.D. Freeman, Preparation and characterization of crosslinked poly(ethylene glycol) diacrylate hydrogels as fouling-resistant membrane coating materials, J Membrane Sci. 330 (2009) 180–188. https://doi.org/10.1016/j.memsci.2008.12.054.

[3] M. Galizia, D.R. Paul, B.D. Freeman, Liquid methanol sorption, diffusion and permeation in charged and uncharged polymers, Polymer. 102 (2016) 281–291. https://doi.org/10.1016/j.polymer.2016.09.010.

[4] N. Yan, D.R. Paul, B.D. Freeman, Water and ion sorption in a series of cross-linked AMPS/PEGDA hydrogel membranes, Polymer. 146 (2018) 196–208. https://doi.org/10.1016/j.polymer.2018.05.021.

[5] J.M. Kim, B.M. Dobyns, R. Zhao, B.S. Beckingham, Multicomponent transport of methanol and acetate in a series of crosslinked PEGDA-AMPS cation exchange membranes, J Membrane Sci. (2020) 118486. https://doi.org/10.1016/j.memsci.2020.118486.

[6] H. Lin, E.V. Wagner, J.S. Swinnea, B.D. Freeman, S.J. Pas, A.J. Hill, S. Kalakkunnath, D.S. Kalika, Transport and structural characteristics of crosslinked poly(ethylene oxide) rubbers, J Membrane Sci. 276 (2006) 145–161. https://doi.org/10.1016/j.memsci.2005.09.040.

[7] A.C. Sagle, H. Ju, B.D. Freeman, M.M. Sharma, PEG-based hydrogel membrane coatings, Polymer. 50 (2009) 756–766. https://doi.org/10.1016/j.polymer.2008.12.019.

[8] J.M. Kim, B.S. Beckingham, Comonomer effects on co-permeation of methanol and acetate in cation exchange membranes, Eur Polym J. (2021) 110307. https://doi.org/10.1016/j.eurpolymj.2021.110307.

[9] Md.T.I. Mredha, S.K. Pathak, V.T. Tran, J. Cui, I. Jeon, Hydrogels with Superior Mechanical Properties from the Synergistic Effect in Hydrophobic–Hydrophilic Copolymers, Chem Eng J. 362 (2018) 325–338. https://doi.org/10.1016/j.cej.2018.12.023.

[10] B.S. Beckingham, N.A. Lynd, D.J. Miller, Monitoring multicomponent transport using in situ ATR FTIR spectroscopy, J Membrane Sci. 550 (2018). https://doi.org/10.1016/j.memsci.2017.12.072.

[11] B.M. Dobyns, J.M. Kim, B.S. Beckingham, Multicomponent transport of methanol and sodium acetate in poly(ethylene glycol) diacrylate membranes of varied fractional free volume, Eur Polym J. 134 (2020) 109809. https://doi.org/10.1016/j.eurpolymj.2020.109809.

[12] T.M. Lim, M. Ulaganathan, Q. Yan, Advances in Batteries for Medium and Large-Scale Energy Storage, Part Four Des Issues Appl. (2015) 477–507. https://doi.org/10.1016/b978-1-78242-013-2.00014-5.

[13] G.M. Geise, B.D. Freeman, D.R. Paul, Characterization of a sulfonated pentablock copolymer for desalination applications, Polymer. 51 (2010) 5815–5822. https://doi.org/10.1016/j.polymer.2010.09.072.

[14] X.C. Chen, J.B. Kortright, N.P. Balsara, Water Uptake and Proton Conductivity in Porous Block Copolymer Electrolyte Membranes, Macromolecules. 48 (2015) 5648–5655. https://doi.org/10.1021/acs.macromol.5b00950.

[15] F. Karas, J. Hnát, M. Paidar, J. Schauer, K. Bouzek, Determination of the ion-exchange capacity of anion-selective membranes, Int J Hydrogen Energ. 39 (2014) 5054–5062. https://doi.org/10.1016/j.ijhydene.2014.01.074.

[16] T. Xua, Z. Liub, b Yanga Weihua, Fundamental studies of a new series of anion exchange membranes: membrane prepared from poly(2,6-dimethyl-1,4-phenylene oxide) (PPO) and triethylamine, J Membrane Sci. 249 (2005) 183–191. https://doi.org/10.1016/j.memsci.2004.10.010.

[17] F. Mohr, Lehrbuch der chemisch-analytischen Titrirmethode: Nach eigenen versuchen und systematisch dargestellt, Volumes 1-2, 4th ed., F. Vieweg und Sohn, 1855.

[18] E.-S. Jang, J. Kamcev, K. Kobayashi, N. Yan, R. Sujanani, T.J. Dilenschneider, H.B. Park, D.R. Paul, B.D. Freeman, Influence of water content on alkali metal chloride transport in cross-linked Poly(ethylene glycol) Diacrylate.1. Ion sorption, Polymer. 178 (2019) 121554. https://doi.org/10.1016/j.polymer.2019.121554.

[19] S. Kalakkunnath, D.S. Kalika, H. Lin, B.D. Freeman, Segmental Relaxation Characteristics of Cross-Linked Poly(ethylene oxide) Copolymer Networks, Macromolecules. 38 (2005) 9679–9687. https://doi.org/10.1021/ma051741t.

[20] P.J. Flory, Principles of Polymer Chemistry, Cornell University Press, 1953.

[21] B.M. Carter, B.M. Dobyns, B.S. Beckingham, D.J. Miller, Multicomponent transport of alcohols in an anion exchange membrane measured by in-situ ATR FTIR spectroscopy, Polymer. 123 (2017). https://doi.org/10.1016/j.polymer.2017.06.070.

[22] B.M. Dobyns, J.M. Kim, J. Li, Z. Jiang, B.S. Beckingham, Multicomponent transport of alcohols in Nafion 117 measured by in situ ATR FTIR spectroscopy, Polymer. (2020) 123046. https://doi.org/10.1016/j.polymer.2020.123046.

[23] Beer, Bestimmung der Absorption des rothen Lichts in farbigen Flüssigkeiten, Ann Phys-Berlin. 162 (1852) 78–88. https://doi.org/10.1002/andp.18521620505.

[24] H. Yasuda, C.E. Lamaze, L.D. Ikenberry, Permeability of solutes through hydrated polymer membranes. Part I. Diffusion of sodium chloride, Die Makromolekulare Chemie. 118 (1968) 19–35. https://doi.org/10.1002/macp.1968.021180102.

[25] H. Yasuda, A. Peterlin, C.K. Colton, K.A. Smith, E.W. Merrill, Permeability of solutes through hydrated polymer membranes. Part III. Theoretical background for the selectivity of dialysis membranes, Die Makromolekulare Chemie. 126 (1969) 177–186. https://doi.org/10.1002/macp.1969.021260120.

[26] G.M. Geise, L.P. Falcon, B.D. Freeman, D.R. Paul, Sodium chloride sorption in sulfonated polymers for membrane applications, J Membrane Sci. 423 (2012) 195–208. https://doi.org/10.1016/j.memsci.2012.08.014.

Chapter 4

Methanol-Acetate co-permeation in CEMs

Reproduced from: J.M. Kim, B.M. Dobyns, R. Zhao, B.S. Beckingham, Multicomponent transport of methanol and acetate in a series of crosslinked PEGDA-AMPS cation exchange membranes, J Membrane Sci. (2020) 118486. https://doi.org/10.1016/j.memsci.2020.118486.

4.1. Introduction

Artificial photosynthesis is a promising technology that utilizes ion exchange membranes (IEM) coupled with reduction of CO_2 via photoelectrochemical CO_2 reduction cells (PEC-CRC) to produce higher-value chemicals, including neutral molecules (i.e. methanol, MeOH) and negatively charged ions, (i.e. acetate, OAc^-). A suitable membrane for PEC-CRCs should have a sufficient ionic conductivity to transport either proton or hydroxide ions and low permeability to CO_2 reduction products, such as MeOH and OAc^-, as these molecules tend reduce the lifespan of the catalyst as CO_2 reduction product oxidize to CO_2 [1]. Therefore, understanding the transport behavior of CO_2 reduction products in IEMs can be a valuable information upon designing new membranes.

Transport of small molecules (or ions) through hydrated polymeric membranes is often described by the solution-diffusion model [2]; see section 2.1.2. Additionally, the transport behavior of IEMs to charged ions (i.e. Na^+ and Cl^-) is governed by electrostatic interactions between membrane-bound charge groups (e.g. SO_3^- for a cation exchange membrane, CEM) and diffusing charged ions [3–5]. On the other hand, the transport behavior to charge-neutral solutes (i.e. MeOH) is typically dominated by the concentration gradient [6,7]. In multi-solute transport,

the membrane diffusivity and solubility to a solute is often affected by other solutes through changes in the solvation and electrostatic interactions [8–10]. While multicomponent experiments have traditionally required aliquotic sampling and spectroscopic analysis of the receiver cell solution over time, we have recently adopted fiber-optic probe based attenuated total reflectance-Fourier transform infrared (ATR-FTIR) spectroscopy to acquire time-resolved concentration data for each permeant in situ [8,11]. Previously, this technique was leveraged in Nafion® 117, a commercial CEM, and an interesting transport behavior was observed that the permeability to sodium acetate (NaOAc) was increased in co-permeation with MeOH presumably due to decrease in electrostatic repulsion (Donnan exclusion [12]) [8].

Herein, we further investigate this electrostatic interaction by measuring permeability of model CEMs to MeOH and NaOAc in co-permeation. As model membranes, we prepared a series of crosslinked poly(ethylene glycol) diacrylate (PEGDA, n = 13) and 2-acrylamido-2-methylpropane sulfonic acid (AMPS) by UV-photopolymerization, where PEGDA is a crosslinker with a chain of hydrophilic ether groups and AMPS is a sulfonated comonomer [3]. We investigate the water uptake and in-plane conductivity of these membranes across the accessible compositional range and investigate the impact of charge content on co-transport behavior by measuring permeabilities to MeOH and NaOAc [3].

4.2. Results and Discussion

A series of PEGDA and PEGDA-AMPS membranes were prepared with constant water content in the prepolymerization mixture; see Fig. 4.1 for the scheme and Table 4.1 for the prepolymerization composition. The variation in PEGDA to AMPS ratio (i.e. 0, 33, 44, and 49 mol% AMPS) changes the ethylene oxide content and the sulfonate content in the resulting polymer networks influencing

membrane properties such as ion exchange capacity (IEC), ionic conductivity, water uptake, water volume fraction, crosslink density, and ionic clustering. For instance, at a given prepolymerization water content, varying the PEGDA to AMPS ratio in the prepolymerization mixture changes the water uptake, as previously reported [3]. This variation in water uptake is linked to both the inclusion of hydrophilic ionic groups and a decreasing crosslinking density of PEGDA-AMPS with varying PEGDA (i.e. crosslinker) to AMPS (i.e. comonomer) composition as previously reported by Yan et al. [3].

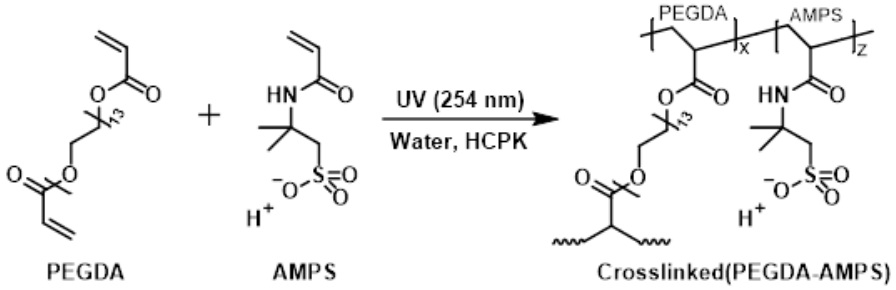

Figure 4.1. Synthetic scheme of crosslinked PEGDA-AMPS membranes.

Table 4.1. Membrane properties from pre-polymerization mixtures

AMPS[a] (mol%)	IEC[b] (meq/g dry polymer)	PEGDA (g)	AMPS (g)	Water (g)	HCPK (g)
0	0.00	8.00	0.00	2.00	0.008
33	0.60	7.00	1.00	2.00	0.008
44	0.90	6.50	1.50	2.00	0.008
49	1.06	6.25	1.75	2.00	0.008

[a]AMPS = mols of AMPS/(mols of PEGDA + mols of AMPS) × 100 %
[b]IEC = mmols of AMPS/(g of PEGDA + g of AMPS)

4.2.1. Water uptake and volume fraction

Water uptakes and water volume fractions were measured in triplicate for each film composition as shown in Fig. 4.2 and Table 4.2. Both water uptake and water volume fraction were increased with increasing AMPS content in the polymer network (decreasing PEGDA content) [3].

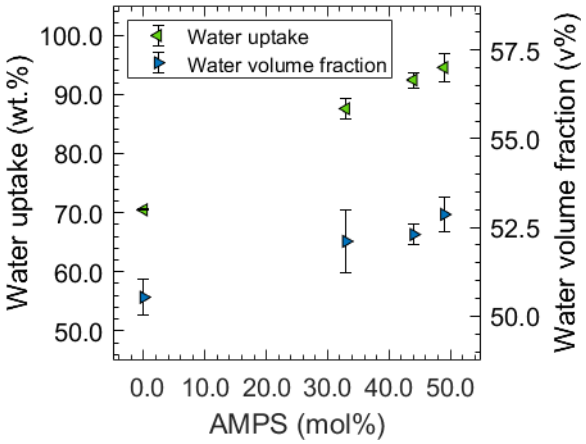

Figure 4.2. Water uptake, ◄, and water volume fraction, ►, of PEGDA and PEGDA-AMPS membranes. Each data point is the average of 3 membranes with error bars corresponding to the standard deviation.

Table 4.2. Properties of membranes considered in this work

AMPS (mol%)	Water uptake (ω_w, g H_2O /g dry membrane ·100%)	Water volume fraction (υ_w, v%)	Conductivity (σ, mS/cm)
0	70 ± 0	50.5 ± 0.5	0 ± 0
33	88 ± 2	52.1 ± 0.9	20 ± 0
44	92 ± 1	52.3 ± 0.3	35 ± 0
49	95 ± 2	52.9 ± 0.5	42 ± 0
Nafion® 117[a]	16 ± 0	25.1 ± 0.2	78 ± 1

[a]Sample was dried under vacuum at 80 °C for 3 hours before immersing in the water at 25 °C.

The measured water uptake for these PEGDA-AMPS were over a factor of 5 higher than the reported water uptake of Nafion® 117. This difference is mainly due to the different polymer backbones, as shown in Fig. 4.3. While both PEGDA-AMPS and Nafion® 117 comprise hydrophilic sulfonate groups, Nafion® 117 contains hydrophobic perfluorinated backbone, while PEGDA-AMPS contains hydrophilic polyether backbones. In Nafion® 117, the majority of water molecules are held by the sulfonate groups and the morphological structure of hydrated sulfonated membranes has been investigated and modeled by several groups [13–15]. Ionic clustering [16,17] has been one of the most studied models for perfluorosulfonic acid-based cation exchange membranes, such as Nafion® 117, where the sulfonate bound anions form clusters to minimize

the free energy. In this study, this model was used to describe a potential internal structure of PEGDA-AMPS bearing analogous sulfonate moieties.

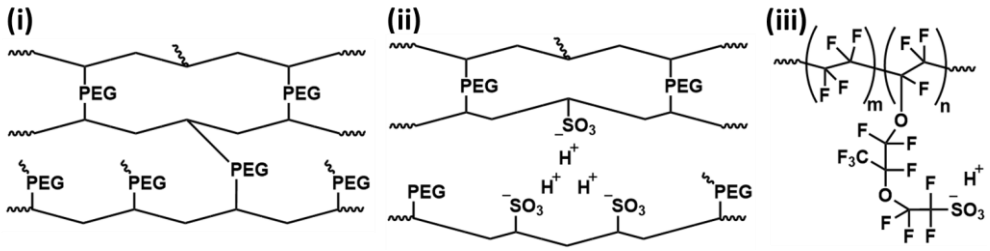

Figure 4.3. Schematics of (i) PEGDA, (ii) PEGDA-AMPS, and (iii) Nafion® 117, where hydrogen counterions formed a cluster to minimize the free energy.

4.2.2. Relative swelling of membranes to solutions

The swollen volume of membranes equilibrated in 1 M MeOH, 1 M NaOAc, and 1 M of each MeOH and NaOAc solutions were measured, as shown in Fig. 4.4; see Fig. 4.5 for photos. Table 4.3 shows the volume of membranes after sorption relative to the hydrated volume of membranes.

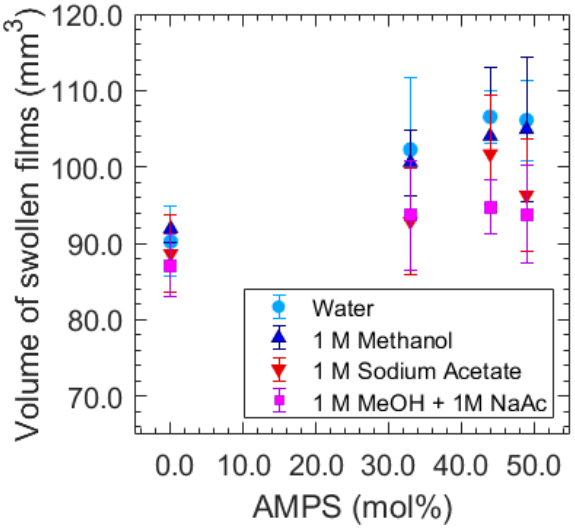

Figure 4.4. Swollen volumes of PEGDA and PEGDA-AMPS membranes (33, 44, and 49 mol% AMPS) immersed in water, ●, 1 M MeOH, ▲, 1 M NaOAc, ▼, and the binary mixture of 1 M MeOH and 1 M NaOAc, ■. Each data point is the average of 3 membranes with error bars corresponding to the standard deviation.

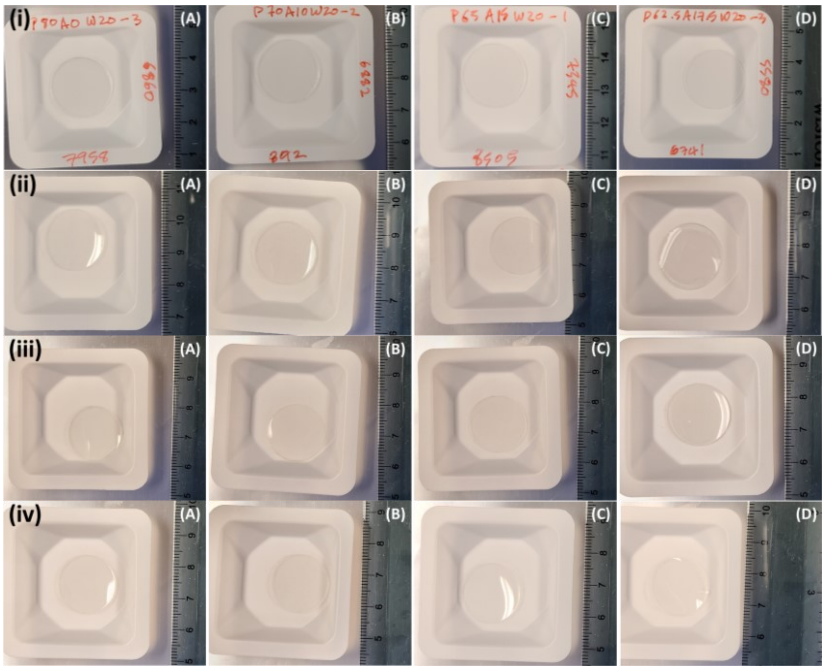

Figure 4.5. Swollen membranes in (i) water, (ii) 1 M MeOH, (iii) 1 M NaOAc, and (iv) binary mixture of 1 M MeOH and 1 M NaOAc, where (A), (B), (C), and (D) are PEGDA-AMPS membranes with 0, 33, 44, and 49 mol% of AMPS, respectively.

Table 4.3. Normalized film volume to hydrated membranes after swelling experiments.

AMPS (mol%)	Water	1 M MeOH	1 M NaOAc	1 M each
0	1.00 ± 0.05	1.02 ± 0.03	0.98 ± 0.06	0.97 ± 0.05
33	1.00 ± 0.09	0.98 ± 0.04	0.91 ± 0.07	0.92 ± 0.08
44	1.00 ± 0.03	0.98 ± 0.09	0.95 ± 0.07	0.89 ± 0.04
49	1.00 ± 0.05	0.99 ± 0.09	0.91 ± 0.08	0.88 ± 0.07
Nafion® 117 [8]	1.00 ± 0.05	1.01 ± 0.04	0.90 ± 0.03	0.92 ± 0.04

Equilibration of all membranes against 1 M MeOH solution induced a negligible change in volume. This result is consistent with a previous work by Galizia and coworkers where both PEGDA and CR61, a commercial cation exchange membrane, did not de-swell significantly in 1 M MeOH solutions [6]. However, both NaOAc and the two-solute solution induced an appreciable decrease in volume of the membrane due to osmotic de-swelling [18–23]. Similar behavior was also observed by Yan and coworkers where water uptake decreased in a series of PEGDA-AMPS membranes as NaCl concentration was increased [3].

4.2.3. Ionic conductivity of membranes

The varied AMPS content corresponds to an equivalent variation in membrane ionic conductivity. Ionic conductivity measurements were performed on membranes; Table 2 and Fig. 4.6. As shown in Fig. 4.6(i), ionic conductivity generally increased with increasing AMPS content and water uptake. Conductivities and water uptakes of PEGDA-AMPS were used to compare to other CEMs using a Robeson's upper bound for CEMs (Fig. 6(ii) [26–91].

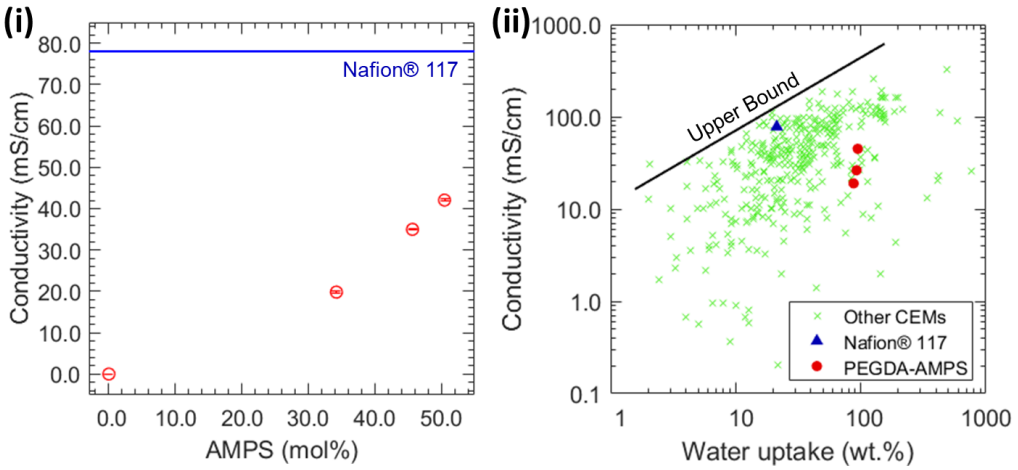

Figure 4.6. (i) Ionic conductivity of PEGDA, PEGDA-AMPS (33, 44, and 49 mol%), ○, and Nafion® 117, a straight line. (ii) Comparing PEGDA-AMPS, ○, and Nafion® 117, ▲, to other cation exchange membranes, ×, used in Robeson's upper bound 2007 [91].

Robeson et al. considered water uptake as a strong function of proton conductivity, assuming the proton transport through the membrane is a function of the concentration-driven water diffusivity [91]. The PEGDA-AMPS membranes synthesized here were all under this upper bound, but they are comparable in water uptake to other CEMs and can access a broad range of conductivity (> factor of 10).

4.2.4. Single and Multi-solute Permeability

The permeability of CO_2 reduction products (i.e. MeOH and OAc^-) is important for solar fuels devices (PEC-CRC) as transport of these species can lead to reductions in device performance

[1,92–95]. To investigate the transport and co-transport behavior of MeOH and OAc^- in these model CEMs of varied ion content, a series of diffusion cell experiments were conducted leveraging in situ ATR-FTIR spectroscopy to monitor the receiver cell solute concentrations [7–9]. Permeabilities of PEGDA and PEGDA-AMPS membranes to MeOH and NaOAc in both single and double components were measured in triplicate, as shown in Table 4.4.

Table 4.4. Diffusive permeabilities of PEGDA and PEGDA-AMPS membranes to MeOH and NaOAc in single and two-solute measurements.

	Single solute in feed cell		Both solutes in feed cell	
AMPS (mol%)	MeOH ($\times 10^{-7}$ cm^2/s)	NaOAc ($\times 10^{-7}$ cm^2/s)	MeOH ($\times 10^{-7}$ cm^2/s)	NaOAc ($\times 10^{-7}$ cm^2/s)
0	10.3 ± 0.2	1.2 ± 0.0	9.5 ± 0.1	1.3 ± 0.2
33	15.1 ± 0.7	1.6 ± 0.4	14.5 ± 0.7	2.0 ± 0.3
43	16.3 ± 0.7	1.8 ± 0.2	14.8 ± 0.7	2.4 ± 0.1
49	19.2 ± 0.4	2.7 ± 0.5	17.1 ± 0.2	3.5 ± 0.2
Nafion® 117 [8]	15.6 ± 0.9	0.5 ± 0.0	11.0 ± 1.0	0.6 ± 0.1

Generally, membrane permeability to both solutes was increased as AMPS (mol%) content increased within the membrane. This trend is consistent with the increase in water volume fraction as AMPS (mol%) content increases. Higher water volume fraction in hydrogels often indicates additional membrane free volume available for species to perform diffusional jumps down the concentration gradient [3,6,96]. The permeability to MeOH was an order of magnitude higher than that to NaOAc. In co-permeation, the difference was reduced for all membranes as MeOH permeability was decreased and NaOAc permeability was increased. This was consistent with the transport behavior observed in Nafion® 117 [8]. In this study, the osmotic flow of water from receiver cell to donor cell was neglected as the difference was within the experimental error for identical solutions in Nafion® 117 [8].

PEGDA, PEGDA-AMPS, and Nafion® 117 permeability to MeOH in both single and co-permeation with NaOAc were very similar, while PEGDA and PEGDA-AMPS permeability to

NaOAc was more than a factor of 2 to 5 higher than that of Nafion® 117. A negligible or slight decrease in permeability to MeOH in co-permeation is observed, such that NaOAc has a small impact on the combined membrane solubility and diffusivity to MeOH; 8, 4, 9, and 11 % decrease for PEGDA and PEGDA-AMPS with 33, 44, 49 mol% of AMPS, respectively [8,9]. However, a distinct change in transport behavior between PEGDA and PEGDA-AMPS permeabilities to NaOAc in co-permeation with MeOH is observed, as shown in Fig. 4.7.

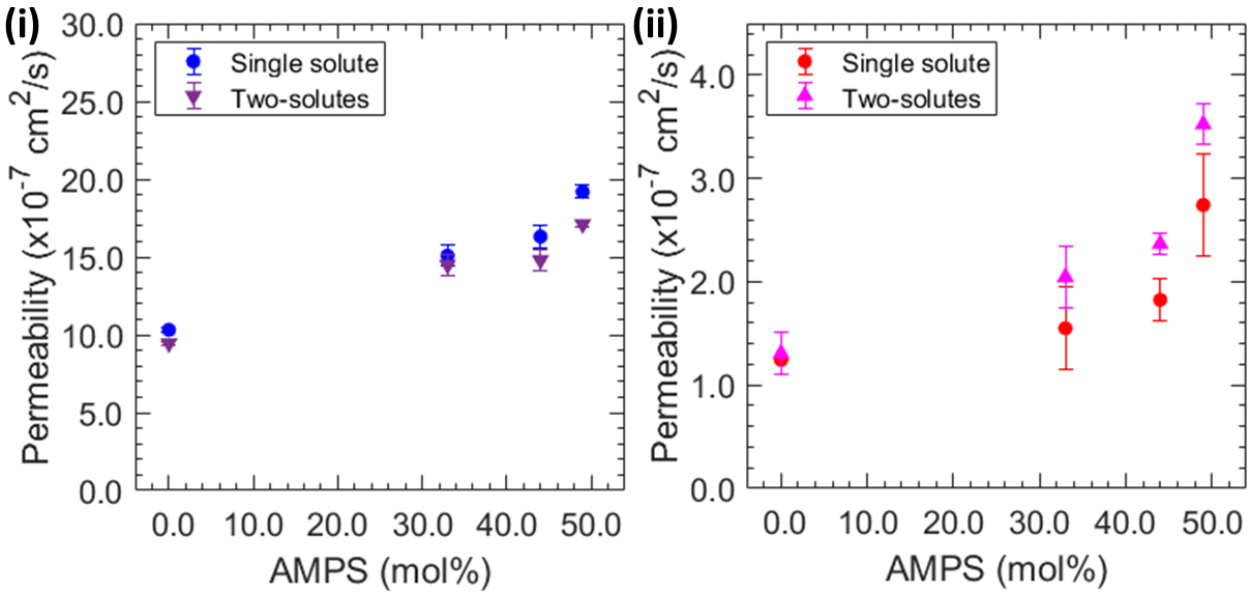

Figure 4.7. PEGDA and PEGDA-AMPS (33, 44, 49 mol%) permeability to (i) MeOH and (ii) NaOAc in single, ●, and two-solute, ▼ and ▲ for MeOH and NaOAc, respectively.

The increase in PEGDA permeability to NaOAc in co-permeation was negligible as MeOH presumably has a negligible effect on the membrane. However, the increase in all PEGDA-AMPS permeability to NaOAc in co-permeation was significant; 32, 30, and 29 % increase for PEGDA-AMPS with 33, 44, 49 mol% of AMPS, respectively. Similarly, in Nafion® 117, permeability to NaOAc was increased by 20 %. The swelling effect of the membrane during permeability measurements was considered by measuring membrane thickness before and after

the experiment. Table 4.5 records normalized film thickness after permeability and swelling experiments to the film thickness before.

Table 4.5. Normalized film thickness to hydrated membrane after permeability measurements and swelling experiments.

AMPS (mol%)		0	33	44	49
Water		1.00 ± 0.01	1.00 ± 0.02	1.00 ± 0.01	1.00 ± 0.01
MeOH	Permeation	0.99 ± 0.03	1.00 ± 0.01	0.98 ± 0.01	1.05 ± 0.01
	Sorption	1.01 ± 0.00	0.99 ± 0.00	1.00 ± 0.02	1.00 ± 0.00
NaOAc	Permeation	0.93 ± 0.00	0.99 ± 0.01	0.98 ± 0.01	1.08 ± 0.01
	Sorption	0.98 ± 0.00	0.97 ± 0.01	0.98 ± 0.00	0.98 ± 0.00
Both	Permeation	0.97 ± 0.01	1.01 ± 0.01	0.98 ± 0.01	1.04 ± 0.01
	Sorption	0.97 ± 0.00	0.96 ± 0.00	0.96 ± 0.00	0.98 ± 0.00

The difference in film thickness for all membranes was negligible as solution concentrations used in this study were relatively low; the largest difference was an 8 % increase after measuring the permeability of PEGDA-AMPS (49 mol%) to 1 M NaOAc in the feed. As we have previously conjectured, this type of emergent transport behavior is likely due to a charge screening behavior that charge-neutral, diffusing MeOH is interfering with the electrostatic repulsion (Donnan exclusion [97–100]) between mobile OAc^- and bound sulfonate anions. As a result, the membrane affinity to OAc^- increases leading to higher permeability to NaOAc; as shown in Fig. 4.8.

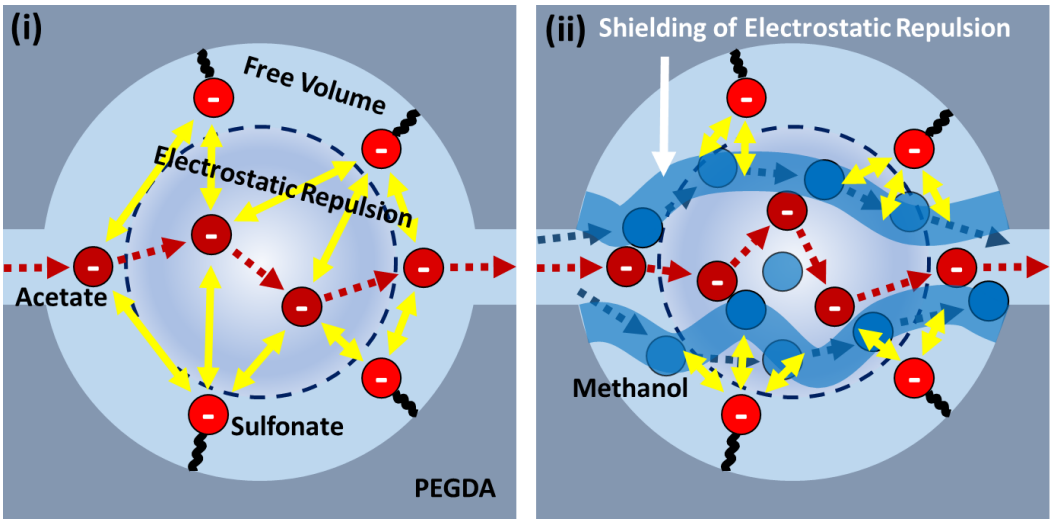

Figure 4.8. Schematic depiction of the shielding of electrostatic repulsion (charge screening). (i) OAc^- is exposed to strong electrostatic repulsion during single component permeability experiment. (ii) OAc^- is exposed to less electrostatic repulsion in co-permeation with MeOH as MeOH interferes the electrostatic repulsion.

This consistent behavior in permeability behavior between these model membranes and Nafion® 117 requires additional investigation to other solutes and cation exchange membranes and should be considered when designing new polymer membranes for applications with complex mixtures of transporting solutes.

4.3. Conclusion

A series of PEGDA-AMPS membranes with varied AMPS content was prepared. Water volume fraction and ionic conductivity were measured to understand membrane transport behavior. Diffusive permeability to MeOH and NaOAc was measured in both single and co-permeation. Interesting transport behavior in permeability to NaOAc was observed in co-permeation with MeOH. We conjecture this behavior as the shielding of electrostatic repulsion (charge screening). Understanding multi-solute transport behavior in the CEMs can open opportunities for potential membrane applications.

4.4. References

[1] M.R. Singh, A.T. Bell, Design of an artificial photosynthetic system for production of alcohols in high concentration from CO 2, Energ Environ Sci. 9 (2015) 193–199. https://doi.org/10.1039/c5ee02783g.

[2] J.G. Wijmans, R.W. Baker, The solution-diffusion model: a review, J Membrane Sci. 107 (1995) 1–21. https://doi.org/10.1016/0376-7388(95)00102-i.

[3] N. Yan, D.R. Paul, B.D. Freeman, Water and ion sorption in a series of cross-linked AMPS/PEGDA hydrogel membranes, Polymer. 146 (2018) 196–208. https://doi.org/10.1016/j.polymer.2018.05.021.

[4] J. Kamcev, E.-S. Jang, N. Yan, D.R. Paul, B.D. Freeman, Effect of ambient carbon dioxide on salt permeability and sorption measurements in ion-exchange membranes, J Membrane Sci. 479 (2015) 55–66. https://doi.org/10.1016/j.memsci.2014.12.031.

[5] G.M. Geise, D.R. Paul, B.D. Freeman, Fundamental water and salt transport properties of polymeric materials, Prog Polym Sci. 39 (2014) 1–42. https://doi.org/10.1016/j.progpolymsci.2013.07.001.

[6] M. Galizia, D.R. Paul, B.D. Freeman, Liquid methanol sorption, diffusion and permeation in charged and uncharged polymers, Polymer. 102 (2016) 281–291. https://doi.org/10.1016/j.polymer.2016.09.010.

[7] B.M. Carter, L. Keller, M. Wessling, D.J. Miller, Preparation and characterization of crosslinked poly(vinylimidazolium) anion exchange membranes for artificial photosynthesis, J Mater Chem A. (2019). https://doi.org/10.1039/c9ta00498j.

[8] B.S. Beckingham, N.A. Lynd, D.J. Miller, Monitoring multicomponent transport using in situ ATR FTIR spectroscopy, J Membrane Sci. 550 (2018). https://doi.org/10.1016/j.memsci.2017.12.072.

[9] B.M. Carter, B.M. Dobyns, B.S. Beckingham, D.J. Miller, Multicomponent transport of alcohols in an anion exchange membrane measured by in-situ ATR FTIR spectroscopy, Polymer. 123 (2017). https://doi.org/10.1016/j.polymer.2017.06.070.

[10] M. Soltanieh, S. Sahebdelfar, Interaction effects in multicomponent separation by reverse osmosis, J Membrane Sci. 183 (2001) 15–27. https://doi.org/10.1016/s0376-7388(00)00554-8.

[11] J.M. Kim, S.B. Chakrapani, B.S. Beckingham, Tuning Compositional Drift in the Anionic Copolymerization of Styrene and Isoprene, Macromolecules. (2020). https://doi.org/10.1021/acs.macromol.0c00526.

[12] F.G. Helfferich, Ion Exchange, Dover, 1995.

[13] H.-G. Haubold, T. Vad, H. Jungbluth, P. Hiller, Nano structure of NAFION: a SAXS study, Electrochim Acta. 46 (2001) 1559–1563. https://doi.org/10.1016/s0013-4686(00)00753-2.

[14] K. Schmidt-Rohr, Q. Chen, Parallel cylindrical water nanochannels in Nafion fuel-cell membranes, Nat Mater. 7 (2007) 75–83. https://doi.org/10.1038/nmat2074.

[15] J.A. Elliott, D. Wu, S.J. Paddison, R.B. Moore, A unified morphological description of Nafion membranes from SAXS and mesoscale simulations, Soft Matter. 7 (2011) 6820. https://doi.org/10.1039/c1sm00002k.

[16] W.Y. Hsu, T.D. Gierke, Ion transport and clustering in nafion perfluorinated membranes, J Membrane Sci. 13 (1983) 307–326. https://doi.org/10.1016/s0376-7388(00)81563-x.

[17] W.Y. Hsu, T.D. Gierke, Elastic theory for ionic clustering in perfluorinated ionomers, Macromolecules. 15 (1982) 101–105. https://doi.org/10.1021/ma00229a020.

[18] W.C. Bauman, J. Eichhorn, Fundamental Properties of a Synthetic Cation Exchange Resin, J Am Chem Soc. 69 (1947) 2830–2836. https://doi.org/10.1021/ja01203a065.

[19] C.W. Davies, G.D. Yeoman, Swelling equilibria with some cation exchange resins, T Faraday Soc. 49 (1953) 968. https://doi.org/10.1039/tf9534900968.

[20] C. Calmon, Application of Volume Change Characteristics of Sulfonated Low Cross-Linked Styrene Resin, Anal Chem. 24 (1952) 1456–1458. https://doi.org/10.1021/ac60069a020.

[21] C. Calmon, Application of Volume Characteristics of Sulfonated Polystyrene Resins as a Tool in Analytical Chemistry, Anal Chem. 25 (1953) 490–492. https://doi.org/10.1021/ac60075a028.

[22] H.P. Gregor, F. Gutoff, J.I. Bregman, Studies on ion-exchange resins. II. Volumes of various cation-exchange resin particles, J Coll Sci Imp U Tok. 6 (1951) 245–270. https://doi.org/10.1016/0095-8522(51)90043-8.

[23] K.W. Pepper, D. Reichenberg, D.K. Hale, 599. Properties of ion-exchange resins in relation to their structure. Part IV. Swelling and shrinkage of sulphonated polystyrenes of different cross-linking, J Chem Soc Resumed. 0 (1952) 3129. https://doi.org/10.1039/jr9520003129.

[24] Y. Sone, Proton Conductivity of Nafion 117 as Measured by a Four-Electrode AC Impedance Method, J Electrochem Soc. 143 (1996) 1254. https://doi.org/10.1149/1.1836625.

[25] L. Onishi, J. Prausnitz, J. Newman, Water-Nafion equilibria. absence of Schroeder's paradox., J Phys Chem B. 111 (2007) 10166–73. https://doi.org/10.1021/jp073242v.

[26] A. Roy, M.A. Hickner, X. Yu, Y. Li, T.E. Glass, J.E. McGrath, Influence of chemical composition and sequence length on the transport properties of proton exchange membranes, J Polym Sci Part B Polym Phys. 44 (2006) 2226–2239. https://doi.org/10.1002/polb.20859.

[27] M.A. Hickner, H. Ghassemi, Y.S. Kim, B.R. Einsla, J.E. McGrath, Alternative Polymer Systems for Proton Exchange Membranes (PEMs), Chem Rev. 104 (2004) 4587–4612. https://doi.org/10.1021/cr020711a.

[28] J. Kim, B. Kim, B. Jung, Proton conductivities and methanol permeabilities of membranes made from partially sulfonated polystyrene-block-poly(ethylene-ran-butylene)-block-polystyrene copolymers, J Membrane Sci. 207 (2002) 129–137. https://doi.org/10.1016/s0376-7388(02)00138-2.

[29] X. Guo, J. Fang, T. Watari, K. Tanaka, H. Kita, K. Okamoto, Novel Sulfonated Polyimides as Polyelectrolytes for Fuel Cell Application. 2. Synthesis and Proton Conductivity of Polyimides from 9,9-Bis(4-aminophenyl)fluorene-2,7-disulfonic Acid, Macromolecules. 35 (2002) 6707–6713. https://doi.org/10.1021/ma020260w.

[30] J.M. Serpico, S.G. Ehrenberg, J.J. Fontanella, X. Jiao, D. Perahia, K.A. McGrady, E.H. Sanders, G.E. Kellogg, G.E. Wnek, Transport and Structural Studies of Sulfonated Styrene−Ethylene Copolymer Membranes, Macromolecules. 35 (2002) 5916–5921. https://doi.org/10.1021/ma020251n.

[31] H.R. Allcock, M.A. Hofmann, C.M. Ambler, S.N. Lvov, X.Y. Zhou, E. Chalkova, J. Weston, Phenyl phosphonic acid functionalized poly[aryloxyphosphazenes] as proton-conducting membranes for direct methanol fuel cells, J Membrane Sci. 201 (2002) 47–54. https://doi.org/10.1016/s0376-7388(01)00702-5.

[32] S.D. Mikhailenko, G.P. Robertson, M.D. Guiver, S. Kaliaguine, Properties of PEMs based on cross-linked sulfonated poly(ether ether ketone), J Membrane Sci. 285 (2006) 306–316. https://doi.org/10.1016/j.memsci.2006.08.036.

[33] S. Zhong, C. Liu, Z. Dou, X. Li, C. Zhao, T. Fu, H. Na, Synthesis and properties of sulfonated poly(ether ether ketone ketone) containing tert-butyl groups as proton exchange membrane materials, J Membrane Sci. 285 (2006) 404–411. https://doi.org/10.1016/j.memsci.2006.09.016.

[34] Z. Wang, H. Ni, C. Zhao, X. Li, G. Zhang, K. Shao, H. Na, Influence of the hydroquinone with different pendant groups on physical and electrochemical behaviors of directly polymerized sulfonated poly(ether ether sulfone) copolymers for proton exchange membranes, J Membrane Sci. 285 (2006) 239–248. https://doi.org/10.1016/j.memsci.2006.08.038.

[35] Z. Bai, M. Durstock, T. Dang, Proton conductivity and properties of sulfonated polyarylenethioether sulfones as proton exchange membranes in fuel cells, J Membrane Sci. 281 (2006) 508–516. https://doi.org/10.1016/j.memsci.2006.04.021.

[36] S. Zhong, T. Fu, Z. Dou, C. Zhao, H. Na, Preparation and evaluation of a proton exchange membrane based on crosslinkable sulfonated poly(ether ether ketone)s, J Power Sources. 162 (2006) 51–57. https://doi.org/10.1016/j.jpowsour.2006.06.067.

[37] X. Li, C. Liu, H. Lu, C. Zhao, Z. Wang, W. Xing, H. Na, Preparation and characterization of sulfonated poly(ether ether ketone ketone) proton exchange membranes for fuel cell application, J Membrane Sci. 255 (2005) 149–155. https://doi.org/10.1016/j.memsci.2005.01.046.

[38] X. Li, C. Liu, D. Xu, C. Zhao, Z. Wang, G. Zhang, H. Na, W. Xing, Preparation and properties of sulfonated poly(ether ether ketone)s (SPEEK)/polypyrrole composite membranes for direct methanol fuel cells, J Power Sources. 162 (2006) 1–8. https://doi.org/10.1016/j.jpowsour.2006.06.030.

[39] Y. Gao, G.P. Robertson, M.D. Guiver, S.D. Mikhailenko, X. Li, S. Kaliaguine, Low-swelling proton-conducting copoly(aryl ether nitrile)s containing naphthalene structure with sulfonic acid groups meta to the ether linkage, Polymer. 47 (2006) 808–816. https://doi.org/10.1016/j.polymer.2005.12.015.

[40] Y. Chen, Y. Meng, S. Wang, S. Tian, Y. Chen, A.S. Hay, Sulfonated poly(fluorenyl ether ketone) membrane prepared via direct polymerization for PEM fuel cell application, J Membrane Sci. 280 (2006) 433–441. https://doi.org/10.1016/j.memsci.2006.01.052.

[41] Y. Gao, G. Robertson, M. Guiver, X. Jian, S. Mikhailenko, S. Kaliaguine, Proton exchange membranes based on sulfonated poly(phthalazinone ether ketone)s/aminated polymer blends, Solid State Ionics. 176 (2005) 409–415. https://doi.org/10.1016/j.ssi.2004.08.009.

[42] Y.S. Kim, M.J. Sumner, W.L. Harrison, J.S. Riffle, J.E. McGrath, B.S. Pivovar, Direct Methanol Fuel Cell Performance of Disulfonated Poly(arylene ether benzonitrile) Copolymers, J Electrochem Soc. 151 (2004) A2150. https://doi.org/10.1149/1.1819837.

[43] B. Liu, D.-S. Kim, J. Murphy, G.P. Robertson, M.D. Guiver, S. Mikhailenko, S. Kaliaguine, Y.-M. Sun, Y.-L. Liu, J.-Y. Lai, Fluorenyl-containing sulfonated poly(aryl ether ether ketone ketone)s (SPFEEKK) for fuel cell applications, J Membrane Sci. 280 (2006) 54–64. https://doi.org/10.1016/j.memsci.2006.01.004.

[44] Y.S. Kim, B. Einsla, M. Sankir, W. Harrison, B.S. Pivovar, Structure–property–performance relationships of sulfonated poly(arylene ether sulfone)s as a polymer electrolyte for fuel cell applications, Polymer. 47 (2006) 4026–4035. https://doi.org/10.1016/j.polymer.2006.02.032.

[45] D.S. Kim, K.H. Shin, H.B. Park, Y.S. Chung, S.Y. Nam, Y.M. Lee, Synthesis and characterization of sulfonated poly(arylene ether sulfone) copolymers containing carboxyl groups for direct methanol fuel cells, J Membrane Sci. 278 (2006) 428–436. https://doi.org/10.1016/j.memsci.2005.11.028.

[46] W. Jang, S. Sundar, S. Choi, Y.-G. Shul, H. Han, Acid–base polyimide blends for the application as electrolyte membranes for fuel cells, J Membrane Sci. 280 (2006) 321–329. https://doi.org/10.1016/j.memsci.2006.01.035.

[47] B. Liu, G.P. Robertson, M.D. Guiver, Y.-M. Sun, Y.-L. Liu, J.-Y. Lai, S. Mikhailenko, S. Kaliaguine, Sulfonated poly(aryl ether ether ketone ketone)s containing fluorinated moieties as proton exchange membrane materials, J Polym Sci Part B Polym Phys. 44 (2006) 2299–2310. https://doi.org/10.1002/polb.20867.

[48] Y. Gao, G.P. Robertson, M.D. Guiver, G. Wang, X. Jian, S.D. Mikhailenko, X. Li, S. Kaliaguine, Sulfonated copoly(phthalazinone ether ketone nitrile)s as proton exchange membrane materials, J Membrane Sci. 278 (2006) 26–34. https://doi.org/10.1016/j.memsci.2005.10.041.

[49] M. Gil, X. Ji, X. Li, H. Na, J.E. Hampsey, Y. Lu, Direct synthesis of sulfonated aromatic poly(ether ether ketone) proton exchange membranes for fuel cell applications, J Membrane Sci. 234 (2004) 75–81. https://doi.org/10.1016/j.memsci.2003.12.021.

[50] Y. Shang, X. Xie, H. Jin, J. Guo, Y. Wang, S. Feng, S. Wang, J. Xu, Synthesis and characterization of novel sulfonated naphthalenic polyimides as proton conductive membrane for DMFC applications, Eur Polym J. 42 (2006) 2987–2993. https://doi.org/10.1016/j.eurpolymj.2006.07.010.

[51] K. Okamoto, Y. Yin, O. Yamada, M. Islam, T. Honda, T. Mishima, Y. Suto, K. Tanaka, H. Kita, Methanol permeability and proton conductivity of sulfonated co-polyimide membranes, J Membrane Sci. 258 (2005) 115–122. https://doi.org/10.1016/j.memsci.2005.02.031.

[52] C. Zhao, H. Lin, K. Shao, X. Li, H. Ni, Z. Wang, H. Na, Block sulfonated poly(ether ether ketone)s (SPEEK) ionomers with high ion-exchange capacities for proton exchange membranes, J Power Sources. 162 (2006) 1003–1009. https://doi.org/10.1016/j.jpowsour.2006.07.055.

[53] H. Zhang, J. hui Pang, D. Wang, A. Li, X. Li, Z. Jiang, Sulfonated poly(arylene ether nitrile ketone) and its composite with phosphotungstic acid as materials for proton exchange membranes, J Membrane Sci. 264 (2005) 56–64. https://doi.org/10.1016/j.memsci.2005.04.021.

[54] B. Kim, J. Kim, B. Jung, Morphology and transport properties of protons and methanol through partially sulfonated block copolymers, J Membrane Sci. 250 (2005) 175–182. https://doi.org/10.1016/j.memsci.2004.10.025.

[55] L.E. Karlsson, P. Jannasch, Polysulfone ionomers for proton-conducting fuel cell membranes: sulfoalkylated polysulfones, J Membrane Sci. 230 (2004) 61–70. https://doi.org/10.1016/j.memsci.2003.10.033.

[56] J. Chen, M. Asano, T. Yamaki, M. Yoshida, Preparation of sulfonated crosslinked PTFE--poly(alkyl vinyl ether) membranes for polymer electrolyte membrane fuel cells by radiation processing, J Membrane Sci. 256 (2005) 38–45. https://doi.org/10.1016/j.memsci.2005.02.005.

[57] J. Kerres, C.-M. Tang, C. Graf, Improvement of Properties of Poly(ether ketone) Ionomer Membranes by Blending and Cross-Linking, Ind Eng Chem Res. 43 (2004) 4571–4579. https://doi.org/10.1021/ie030762d.

[58] J. Qiao, T. Okada, Highly Durable, Proton-Conducting Semi-interpenetrating Polymer Networks from PVA/PAMPS Composites by Incorporating Plasticizer Variants, Electrochem Solid-State Lett. 9 (2006) A379. https://doi.org/10.1149/1.2206888.

[59] C.W. Walker, Proton-conducting polymer membrane comprised of a copolymer of 2-acrylamido-2-methylpropanesulfonic acid and 2-hydroxyethyl methacrylate, J Power Sources. 110 (2002) 144–151. https://doi.org/10.1016/s0378-7753(02)00236-7.

[60] J. Qiao, T. Hamaya, T. Okada, New highly proton-conducting membrane poly(vinylpyrrolidone)(PVP) modified poly(vinyl alcohol)/2-acrylamido-2-methyl-1-propanesulfonic acid (PVA–PAMPS) for low temperature direct methanol fuel cells (DMFCs), Polymer. 46 (2005) 10809–10816. https://doi.org/10.1016/j.polymer.2005.09.007.

[61] Y. Gao, G.P. Robertson, M.D. Guiver, S.D. Mikhailenko, X. Li, S. Kaliaguine, Synthesis of Copoly(aryl ether ether nitrile)s Containing Sulfonic Acid Groups for PEM Application †, Macromolecules. 38 (2005) 3237–3245. https://doi.org/10.1021/ma047572e.

[62] P. Xing, G.P. Robertson, M.D. Guiver, S.D. Mikhailenko, S. Kaliaguine, Sulfonated Poly(aryl ether ketone)s Containing the Hexafluoroisopropylidene Diphenyl Moiety Prepared by Direct Copolymerization, as Proton Exchange Membranes for Fuel Cell Application †, Macromolecules. 37 (2004) 7960–7967. https://doi.org/10.1021/ma0494941.

[63] C.H. Fujimoto, M.A. Hickner, C.J. Cornelius, D.A. Loy, Ionomeric Poly(phenylene) Prepared by Diels−Alder Polymerization: Synthesis and Physical Properties of a Novel Polyelectrolyte, Macromolecules. 38 (2005) 5010–5016. https://doi.org/10.1021/ma0482720.

[64] S. Sundar, W. Jang, C. Lee, Y. Shul, H. Han, Crosslinked sulfonated polyimide networks as polymer electrolyte membranes in fuel cells, J Polym Sci Part B Polym Phys. 43 (2005) 2370–2379. https://doi.org/10.1002/polb.20522.

[65] A. Borriello, M. Lavorgna, N. Malagnino, G. Mensitieri, T. Napoletano, L. Nicolais, Polyelectrolyte Membranes Based on Sulfonated Syndiotactic Polystyrene in Its Clathrate Form, Macromol Symp. 169 (2001) 293–302. https://doi.org/10.1002/masy.200451430.

[66] T. Nakano, S. Nagaoka, H. Kawakami, Preparation of novel sulfonated block copolyimides for proton conductivity membranes, Polym Advan Technol. 16 (2005) 753–757. https://doi.org/10.1002/pat.650.

[67] S. Yang, C. Gong, R. Guan, H. Zou, H. Dai, Sulfonated poly(phenylene oxide) membranes as promising materials for new proton exchange membranes, Polym Advan Technol. 17 (2006) 360–365. https://doi.org/10.1002/pat.718.

[68] Y. Yin, S. Hayashi, O. Yamada, H. Kita, K. Okamoto, Branched/Crosslinked Sulfonated Polyimide Membranes for Polymer Electrolyte Fuel Cells, Macromol Rapid Comm. 26 (2005) 696–700. https://doi.org/10.1002/marc.200500014.

[69] K.B. Wiles, F. Wang, J.E. McGrath, Directly copolymerized poly(arylene sulfide sulfone) disulfonated copolymers for PEM-based fuel cell systems. I. Synthesis and characterization, J Polym Sci Part Polym Chem. 43 (2005) 2964–2976. https://doi.org/10.1002/pola.20744.

[70] C.G. Cho, Y.S. Kim, X. Yu, M. Hill, J.E. McGrath, Synthesis and characterization of poly(arylene ether sulfone) copolymers with sulfonimide side groups for a proton-exchange membrane, J Polym Sci Part Polym Chem. 44 (2006) 6007–6014. https://doi.org/10.1002/pola.21565.

[71] C. Lee, S. Sundar, J. Kwon, H. Han, Structure-property correlations of sulfonated polyimides. II. Effect of substituent groups on membrane properties, J Polym Sci Part Polym Chem. 42 (2004) 3621–3630. https://doi.org/10.1002/pola.20215.

[72] B. Kim, B. Jung, Partially Sulfonated Polystyrene and Poly(2,6-dimethyl-1,4-phenylene oxide) Blend Membranes for Fuel Cells, Macromol Rapid Comm. 25 (2004) 1263–1267. https://doi.org/10.1002/marc.200400119.

[73] T. Lehtinen, G. Sundholm, F. Sundholm, Effect of crosslinking on the physicochemical properties of proton conducting PVDF-g-PSSA membranes, J Appl Electrochem. 29 (1999) 679–685. https://doi.org/10.1023/a:1003404005245.

[74] R. Carter, R. Wycisk, H. Yoo, P.N. Pintauro, Blended Polyphosphazene/Polyacrylonitrile Membranes for Direct Methanol Fuel Cells, Electrochem Solid-State Lett. 5 (2002) A195. https://doi.org/10.1149/1.1495916.

[75] S.H. Tian, D. Shu, Y.L. Chen, M. Xiao, Y.Z. Meng, Preparation and properties of novel sulfonated poly(phthalazinone ether ketone) based PEM for PEM fuel cell application, J Power Sources. 158 (2006) 88–93. https://doi.org/10.1016/j.jpowsour.2005.09.027.

[76] S. Zhong, X. Cui, H. Cai, T. Fu, C. Zhao, H. Na, Crosslinked sulfonated poly(ether ether ketone) proton exchange membranes for direct methanol fuel cell applications, J Power Sources. 164 (2007) 65–72. https://doi.org/10.1016/j.jpowsour.2006.10.077.

[77] V. SHAHI, Highly charged proton-exchange membrane: Sulfonated poly(ether sulfone)-silica polyelectrolyte composite membranes for fuel cells, Solid State Ionics. 177 (2007) 3395–3404. https://doi.org/10.1016/j.ssi.2006.10.023.

[78] M.A. Hickner, C.H. Fujimoto, C.J. Cornelius, Transport in sulfonated poly(phenylene)s: Proton conductivity, permeability, and the state of water, Polymer. 47 (2006) 4238–4244. https://doi.org/10.1016/j.polymer.2006.02.034.

[79] P. Xing, G.P. Robertson, M.D. Guiver, S.D. Mikhailenko, S. Kaliaguine, Synthesis and characterization of poly(aryl ether ketone) copolymers containing (hexafluoroisopropylidene)-diphenol moiety as proton exchange membrane materials, Polymer. 46 (2005) 3257–3263. https://doi.org/10.1016/j.polymer.2005.03.003.

[80] M.J. Sumner, W.L. Harrison, R.M. Weyers, Y.S. Kim, J.E. McGrath, J.S. Riffle, A. Brink, M.H. Brink, Novel proton conducting sulfonated poly(arylene ether) copolymers containing aromatic nitriles, J Membrane Sci. 239 (2004) 199–211. https://doi.org/10.1016/j.memsci.2004.03.031.

[81] Y. Woo, S.Y. Oh, Y.S. Kang, B. Jung, Synthesis and characterization of sulfonated polyimide membranes for direct methanol fuel cell, J Membrane Sci. 220 (2003) 31–45. https://doi.org/10.1016/s0376-7388(03)00185-6.

[82] Z. Wang, X. Li, C. Zhao, H. Ni, H. Na, Synthesis and characterization of sulfonated poly(arylene ether ketone ketone sulfone) membranes for application in proton exchange membrane fuel cells, J Power Sources. 160 (2006) 969–976. https://doi.org/10.1016/j.jpowsour.2006.03.029.

[83] Z. Hu, Y. Yin, H. Kita, K. Okamoto, Y. Suto, H. Wang, H. Kawasato, Synthesis and properties of novel sulfonated polyimides bearing sulfophenyl pendant groups for polymer electrolyte fuel cell application, Polymer. 48 (2007) 1962–1971. https://doi.org/10.1016/j.polymer.2007.02.011.

[84] Z. Hu, Y. Yin, S. Chen, O. Yamada, K. Tanaka, H. Kita, K.-I. Okamoto, Synthesis and properties of novel sulfonated (co)polyimides bearing sulfonated aromatic pendant groups for PEFC applications, J Polym Sci Part Polym Chem. 44 (2006) 2862–2872. https://doi.org/10.1002/pola.21374.

[85] X. Li, G. Zhang, D. Xu, C. Zhao, H. Na, Morphology study of sulfonated poly(ether ether ketone ketone)s (SPEEKK) membranes: The relationship between morphology and transport properties of SPEEKK membranes, J Power Sources. 165 (2007) 701–707. https://doi.org/10.1016/j.jpowsour.2006.12.011.

[86] F.C. Ding, S.J. Wang, M. Xiao, Y.Z. Meng, Cross-linked sulfonated poly(phathalazinone ether ketone)s for PEM fuel cell application as proton-exchange membrane, J Power Sources. 164 (2007) 488–495. https://doi.org/10.1016/j.jpowsour.2006.11.028.

[87] Y.G. Devrim, Z. Rzaev, E. Pişkin, Physically and Chemically Cross-Linked Poly{[(maleic anhydride)-alt-styrene]-co-(2-acrylamido-2-methyl-1-propanesulfonic acid)}/Poly(ethylene

glycol) Proton-Exchange Membranes, Macromol Chem Physic. 208 (2007) 175–187. https://doi.org/10.1002/macp.200600331.

[88] X. Yu, A. Roy, S. Dunn, J. Yang, J.E. McGrath, Synthesis and Characterization of Sulfonated- Fluorinated, Hydrophilic-Hydrophobic Multiblock Copolymers for Proton Exchange Membranes, Macromol Symp. 245–246 (2006) 439–449. https://doi.org/10.1002/masy.200651363.

[89] Y. Gao, G.P. Robertson, D.-S. Kim, M.D. Guiver, S.D. Mikhailenko, X. Li, S. Kaliaguine, Comparison of PEM Properties of Copoly(aryl ether ether nitrile)s Containing Sulfonic Acid Bonded to Naphthalene in Structurally Different Ways †, Macromolecules. 40 (2007) 1512–1520. https://doi.org/10.1021/ma0623542.

[90] D. Poppe, H. Frey, K.D. Kreuer, A. Heinzel, R. Mülhaupt, Carboxylated and Sulfonated Poly(arylene- co -arylene sulfone)s: Thermostable Polyelectrolytes for Fuel Cell Applications, Macromolecules. 35 (2002) 7936–7941. https://doi.org/10.1021/ma012198t.

[91] L.M. Robeson, H.H. Hwu, J.E. McGrath, Upper bound relationship for proton exchange membranes: Empirical relationship and relevance of phase separated blends, J Membrane Sci. 302 (2007) 70–77. https://doi.org/10.1016/j.memsci.2007.06.029.

[92] H. Yang, J.J. Kaczur, S.D. Sajjad, R.I. Masel, Electrochemical conversion of CO2 to formic acid utilizing Sustainion^{TM} membranes, J Co2 Util. 20 (2017) 208–217. https://doi.org/10.1016/j.jcou.2017.04.011.

[93] A. Berger, R.A. Segalman, J. Newman, Material requirements for membrane separators in a water-splitting photoelectrochemical cell, Energy & Environmental Science. (2014). https://doi.org/10.1039/C3EE43807D.

[94] Y. Chen, N.S. Lewis, C. Xiang, Operational constraints and strategies for systems to effect the sustainable, solar-driven reduction of atmospheric CO 2, Energ Environ Sci. 8 (2015) 3663–3674. https://doi.org/10.1039/c5ee02908b.

[95] M. Krödel, B.M. Carter, D. Rall, J. Lohaus, M. Wessling, D.J. Miller, Rational Design of Ion Exchange Membrane Material Properties Limits the Crossover of CO 2 Reduction Products in Artificial Photosynthesis Devices, Acs Appl Mater Inter. 12 (2020) 12030–12042. https://doi.org/10.1021/acsami.9b21415.

[96] H. Ju, A.C. Sagle, B.D. Freeman, J.I. Mardel, A.J. Hill, Characterization of sodium chloride and water transport in crosslinked poly(ethylene oxide) hydrogels, J Membrane Sci. 358 (2010) 131–141. https://doi.org/10.1016/j.memsci.2010.04.035.

[97] J. Kamcev, M. Galizia, F.M. Benedetti, E.-S. Jang, D.R. Paul, B.D. Freeman, G.S. Manning, Partitioning of mobile ions between ion exchange polymers and aqueous salt solutions:

importance of counter-ion condensation, Phys Chem Chem Phys. 18 (2016) 6021–6031. https://doi.org/10.1039/c5cp06747b.

[98] J. Kamcev, B.D. Freeman, Charged Polymer Membranes for Environmental/Energy Applications, Annu Rev Chem Biomol. 7 (2015) 1–23. https://doi.org/10.1146/annurev-chembioeng-080615-033533.

[99] D. Stigter, Donnan membrane equilibrium, sedimentation equilibrium, and coil expansion of DNA in salt solutions, Cell Biophys. 11 (1987) 139–158. https://doi.org/10.1007/bf02797120.

[100] G.M. Geise, L.P. Falcon, B.D. Freeman, D.R. Paul, Sodium chloride sorption in sulfonated polymers for membrane applications, J Membrane Sci. 423 (2012) 195–208. https://doi.org/10.1016/j.memsci.2012.08.014.

Chapter 5

Alcohol-Carboxylate co-transport in CEMs

Reproduced from: J.M. Kim, B.S. Beckingham, Transport and co-transport of carboxylate ions and alcohols in cation exchange membranes, J Polym Sci. (2021). https://doi.org/10.1002/pol.20210383.

5.1. Introduction

Ion exchange membranes (IEM) are a crucial part of various energy devices that require highly selective transport of charged ions [1–4]. Photoelectrochemical CO_2 reduction cells (PEC-CRC [5,6]) are on type of these devices, which utilize solar power to reduce CO_2 to various chemicals [7,8], such as methanol (MeOH), ethanol (EtOH), formate (OFm^-), and acetate (OAc^-). Major roles of the IEM in such devices are to provide a preferential ion transport (i.e. proton (H^+) for cation exchange membranes (CEMs) with membrane-bound charged functional groups (i.e. sulfonate for CEMs) and to minimize the permeation of these CO_2 reduction products to anode chamber, as they readily oxidize back to CO_2 and by-products [5,6]. Traditionally, IEM design for PEC-CRC has been focused on anion exchange membranes (AEM [9–12]) as they show higher diffusibility for negatively-charged electrolytes, such as bicarbonates. However, CEMs [13–16]) can be advantageous as they can minimize the permeation of negatively-charged CO_2 reduction products, such as OFm^- and OAc^-.

Previously, our group has performed a series of investigations to gain a fundamental understanding of the co-transport behavior of an alcohol (MeOH) and a carboxylate anion (either OFm^- or OAc^-) in CEMs (with bound sulfonate). In Nafion® 117 [13,15,17], we observed

increases in both OFm^- and OAc^- permeability in co-permeation with MeOH, where we conjectured that electrostatic repulsions between bound sulfonate and mobile carboxylate ions might be interfered with by the co-permeating MeOH molecules [13]. Next, we prepared a series of charge-neutral crosslinked poly(ethylene glycol) diacrylate (PEGDA, *n=13*, where *n* represents the number of ethylene oxide repeating units [18–23]) films at varied fractional free volume (FFV), where we observed OAc^- permeability increases in co-permeation with MeOH and that the differences between permeability in single solute and co-permeation increased with increasing FFV [18]. We then prepared a series of PEGDA-based CEMs by incorporating 2-acrylamido-2-methyl-1-propanesulfonic acid (AMPS, sulfonated monomer [14,16,24,25]) units into the structure, where we observed OAc^- permeability to be significantly increased in co-permeation with MeOH [16]; see Chapter 4. A pictorial description of how the presence of co-permeating alcohols could be interfering with the electrostatic repulsion between membrane-bound sulfonates and mobile carboxylate anion is shown in Fig. 5.1. In Fig. 5.1(A,B), the permeation of a carboxylate anion by itself is depicted, where the mobile carboxylate anion experiences electrostatic repulsion from bound sulfonate in CEMs (ion-polymer interaction, Fig. 5.1(B)). In Fig. 5.1(C,D), the permeation of carboxylates is assisted by co-permeating alcohols (ion-alcohol interaction, flux coupling [26]), where the electrostatic repulsion between bound sulfonate anion and mobile carboxylate anion is screened by co-permeating alcohol (alcohol-polymer interaction, charge screening [13,16,27,28], Fig. 5.1(D)).

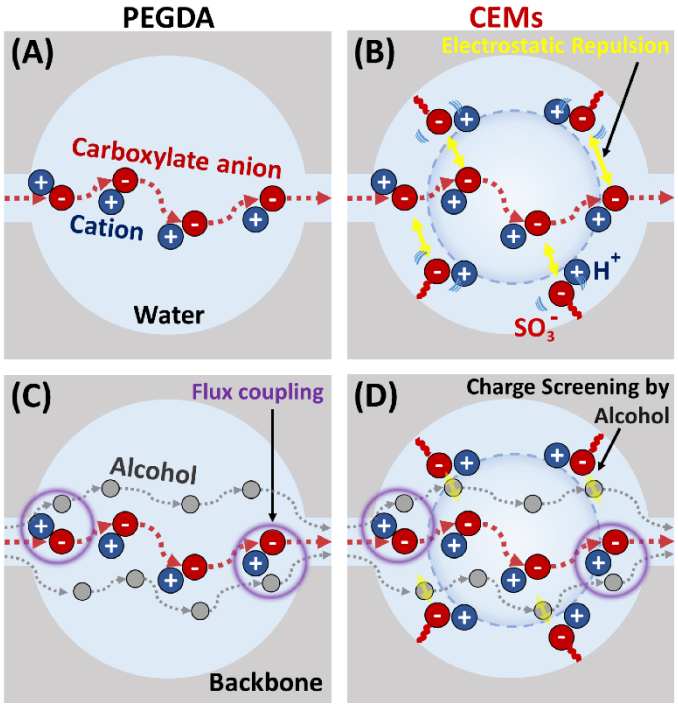

Figure 5.1. Schematic depiction of carboxylate ion permeation in (A,C) PEGDA and (B,D) CEMs in (A,B) single and (C,D) co-permeation with alcohol. Figures are reprinted from [14,16,29–31] with permission from Elsevier, Wiley, and MDPI.

To build upon this previous work here, we expand upon the solutes of interest to include EtOH (alcohol) and OFm^- (carboxylate anion) along with MeOH and OAc^- to further investigate the co-transport behavior of carboxylate anions with alcohols in PEGDA-AMPS and Nafion® 117 films. We determine all components of the solution-diffusion model, assuming the pressure in the membrane is uniform, such that the chemical potential gradient is expressed as a concentration gradient [32]. The model (Eq. 1) describes the overall solute permeation which is dependent on solute sorption [33–38] into the membrane and diffusion (Fickian) [35,39–42] through the fractional free volume [18–20,43] within the polymer matrix:

$$P_i = D_i K_i \tag{5.1}$$

where P_i is the permeability to solute *i*, D_i is the diffusivity to solute *i*, and K_i is the solubility to solute *i,* for an alcohol (MeOH [17,35,37,39,44] or EtOH [10,15]) or a carboxylate anion (OFm^-

or OAc^- [13,45,46]) in single and co-transport between an alcohol and a carboxylate (MeOH-OFm, MeOH-OAc, EtOH-OFm, and EtOH-OAc). Permeabilities are measured by diffusion cell experiments coupled with in-situ attenuated total reflectance–Fourier transform infrared (ATR-FTIR) spectroscopy [13], solubilities are measured by sorption-desorption experiments coupled with a high-performance liquid chromatography (HPLC) [36], and diffusivities by calculation using the Eq (1).

5.2. Results and Discussion

A crosslinked PEGDA and PEGDA-AMPS (CEM) were prepared by UV photopolymerization, where the compositions are shown in the Table 5.1; see 3.2.1. for synthesis. A commercial CEM, Nafion® 117, was purchased. Chemical structures of all three films are shown in Fig. 5.2. The molecular structure of selected alcohols and carboxylate anions are shown in Fig. 5.3. While MeOH contains a methyl group ($-CH_3$), EtOH contains an ethyl group ($-CH_2CH_3$) and, therefore, the kinetic diameter of EtOH is larger (4.5 Å) than that of MeOH (3.6 Å) [47]. Similarly, the hydrated diameter of OAc^- (7.4 Å) is larger than that of OFm^- (5.9 Å) with an additional $-CH_3$ group [45].

Table 5.1. Membrane properties from pre-polymerization mixtures.

	AMPS[a] (mol%)	PEGDA (g)	AMPS (g)	Water (g)	HCPK (g)
PEGDA	0	8.00	0.00	2.00	0.008
PEGDA-AMPS	32	7.02	0.98	2.00	0.008

[a]AMPS = mol of AMPS/(mol of PEGDA + mol of AMPS) × 100 %

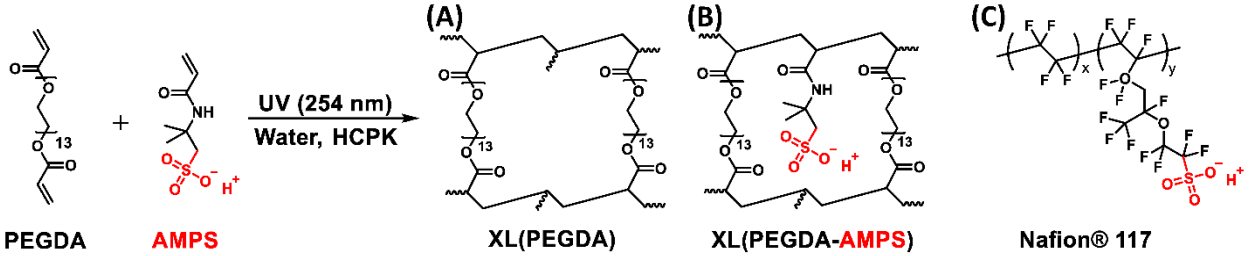

Figure 5.2. (A,B) Synthetic scheme of (A) crosslinked PEGDA and (B) crosslinked PEGDA-AMPS. (C) Schematic of Nafion® 117.

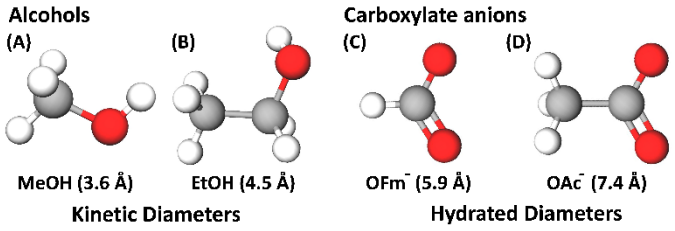

Figure 5.3. Molecular structure of alcohols, (A) MeOH and (B) EtOH, and carboxylate anions, (C) OFm^- and (D) OAc^-. Kinetic diameters were stated for alcohols and hydrated diameters of carboxylate anions were stated for carboxylate anion.

5.2.1. Water uptake, Conductivity, and IEC

Water uptakes of films were measured gravimetrically with results shown in Table 5.2. The water uptake of PEGDA-AMPS was higher than the water uptake of PEGDA by 1.7 times. This behavior is due to both increasing hydrophilic ionogenic sulfonate content and decreasing crosslink density (with decreasing crosslinker, PEGDA). The crosslink densities of analogous films were investigated by Yan et al.[25], where the authors prepared a series of PEGDA-AMPS films at different PEGDA-to-AMPS ratios. They observed a similar result on water uptake, where water uptakes of PEGDA-AMPS were higher than PEGDA. Moreover, they reported the crosslink densities of PEGDA-AMPS were less than PEGDA [25]. Water uptake of PEGDA-AMPS was higher than that of Nafion® 117 by 7.8 times. This is due to the difference in polymer backbones, as shown in Fig. 5.2. While Nafion® 117 contains a hydrophobic (tetrafluoroethylene) backbone,

PEGDA-AMPS contains a hydrophilic (ethylene oxide) backbone. The ionic conductivity and the ion exchange capacity (IEC) of PEGDA-AMPS were measured yielding the results shown in Table 5.2. The ionic conductivity of Nafion® 117 was higher than that of PEGDA-AMPS by a factor of 4 and the IEC of Nafion® 117 was approximately 50 % higher than that of PEGDA-AMPS.

Table 5.2. Water uptake, water volume fraction, dry polymer density, ionic conductivity, and ion exchange capacity of all films.

	Swollen thickness (μm)	Water uptake (g H_2O/g dry membrane ·100%)	Water volume fraction	Conductivity (σ, mS/cm)	IEC (meq /g dry polymer)
PEGDA	328 ± 1	71 ± 1	0.43 ± 0.02	0 ± 0	0.00 ± 0.00
PEGDA-AMPS	343 ± 1	124 ± 2	0.60 ± 0.00	18 ± 0	0.60 ± 0.01
Nafion® 117	198 ± 1[a]	16 ± 0[a]	0.25 ± 0.05[a]	78 ± 1[a]	≥ 0.90[c]

[a]Literature [16]
[b]Literature [48]
[c]Reported by manufacturer

5.2.2. Single and Multi-solute Permeability

Permeabilities to all permeants were measured by diffusion cell experiments, where permeabilities to alcohols (MeOH and EtOH) and carboxylate salts (NaOFm and NaOAc) in single (black, solid line) and co-permeation (colored, dashed) are shown in Fig. 5.4 and Table 5.3. Generally, the thickness of all films was essentially the same after permeation, where that of Nafion® 117 was slightly decreased after permeation in carboxylate salt solutions; see Table 5.4. Generally, alcohol permeabilities were 6 times higher than salt permeabilities, on average, in all films. These results are consistent with our previous studies [13,16], where we measured MeOH and NaOAc permeabilities of crosslinked PEGDA (10.3×10^{-7} cm^2/s and 1.2×10^{-7} cm^2/s, respectively); see Table 4.4 [16], MeOH and NaOAc permeabilities of PEGDA-AMPS (15.1×10^{-7} cm^2/s and 1.6×10^{-7} cm^2/s, respectively) [16], and MeOH, NaOFm, and NaOAc permeabilities in Nafion® 117, (15.6×10^{-7} cm^2/s, 0.94×10^{-7} cm^2/s, and 0.5×10^{-7} cm^2/s, respectively) [13]. These differences

between alcohol and carboxylate anion permeabilities are, of course, coupled to their respective changes in solubility and diffusivity as discussed in detail below. For instance, alcohol solubilities were higher than carboxylate solubilities in all membranes; see Table 5.5 and Fig. 5.5 for solubilities. Moreover, the kinetic diameters of the alcohols (MeOH, 3.6 Å, and EtOH, 4.5 Å [47]) are smaller than the hydrated diameters of carboxylate anions (OFm^-, 5.9 Å, and OAc^-, 7.4 Å [45]), and, therefore, expected to display higher diffusivities as diffusion will be easier [49]; see Table 5.9, Fig. 5.6 and 5.7 for diffusivities.

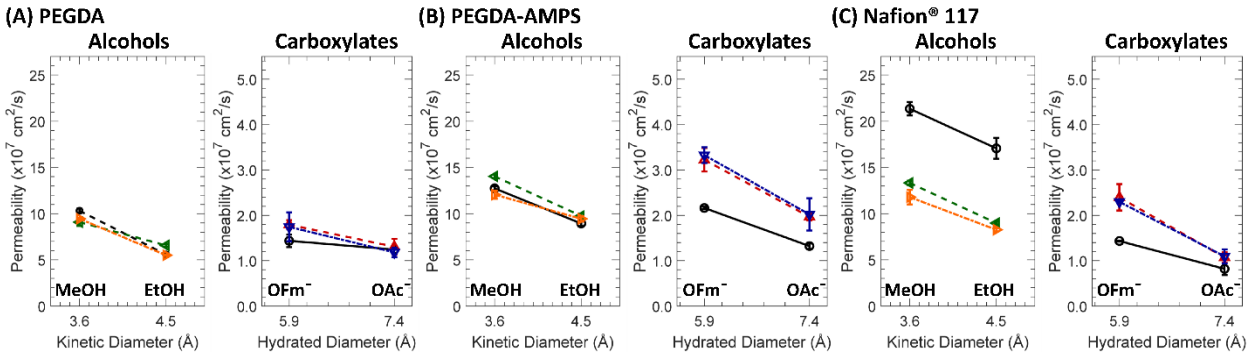

Figure 5.4. Permeability of (A) PEGDA, (B) PEGDA-AMPS, and (C) Nafion® 117 to (left) alcohols, MeOH (3.6 Å), EtOH (4.5 Å), and (right) carboxylate salts, NaOFm (5.9 Å) and NaOAc (7.4 Å), in single (○, black, solid line) and in co-permeation. Each alcohol was co-permeated with NaOFm (◁, green, dashed) and NaOAc (▷, yellow, dot-dashed) and each carboxylic ion was co-permeated with MeOH (△, red, dashed) and EtOH (▽, blue, dot-dashed).

Table 5.3. Diffusive permeabilities ($\times 10^7$ cm^2/s) of PEGDA, PEGDA-AMPS, and Nafion® 117 membranes to alcohols (MeOH and EtOH) and carboxylate salts (NaOFm and NaOAc) in single and ion-alcohol mixture.

PEGDA	MeOH	EtOH		NaOFm	NaOAc
Single	10.3 ± 0.2	5.6 ± 0.3	Single	1.4 ± 0.1	1.2 ± 0.0
w/ NaOFm	9.1 ± 0.4	6.6 ± 0.1	w/ MeOH	1.8 ± 0.1	1.3 ± 0.2
w/ NaOAc	9.5 ± 0.1	5.5 ± 0.1	w/ EtOH	1.7 ± 0.3	1.2 ± 0.1
PEGDA-AMPS	MeOH	EtOH		NaOFm	NaOAc
Single	12.7 ± 0.2	8.9 ± 0.3	Single	2.2 ± 0.0	1.3 ± 0.1
w/ NaOFm	14.0 ± 0.2	9.8 ± 0.2	w/ MeOH	3.2 ± 0.3	2.0 ± 0.1
w/ NaOAc	12.1 ± 0.4	9.4 ± 0.3	w/ EtOH	3.3 ± 0.2	2.0 ± 0.4
Nafion® 117	MeOH	EtOH		NaOFm	NaOAc
Single	21.4 ± 0.7	17.1 ± 1.1	Single	1.4 ± 0.0	0.8 ± 0.1
w/ NaOFm	13.3 ± 0.2	9.0 ± 0.1	w/ MeOH	2.4 ± 0.3	1.1 ± 0.1
w/ NaOAc	11.8 ± 0.8	8.3 ± 0.2	w/ EtOH	2.3 ± 0.0	1.1 ± 0.2

Table 5.4. Normalized film thickness to hydrated membrane after permeability measurements.

	PEGDA	PEGDA-AMPS	Nafion® 117
Hydrated	1.00 ± 0.01	1.00 ± 0.00	1.00 ± 0.02
1. MeOH	1.00 ± 0.00	0.97 ± 0.00	1.00 ± 0.01
2. EtOH	0.99 ± 0.01	1.00 ± 0.01	1.02 ± 0.02
3. NaOFm	0.98 ± 0.01	0.98 ± 0.00	0.96 ± 0.01
4. NaOAc	0.99 ± 0.00	0.97 ± 0.01	0.96 ± 0.02
5. M/F	1.00 ± 0.01	0.98 ± 0.00	0.93 ± 0.02
6. E/F	0.99 ± 0.01	0.99 ± 0.01	0.95 ± 0.02
7. M/A	0.99 ± 0.01	0.97 ± 0.00	0.96 ± 0.03
8. E/A	0.99 ± 0.01	0.97 ± 0.00	0.96 ± 0.03

In co-permeation, sulfonate-free PEGDA permeabilities to MeOH and EtOH were essentially the same. Likewise, NaOAc permeabilities were essentially the same in co-permeation. However, NaOFm permeabilities were increased by 23 %, on average. This is partially due to sorption (Fig. 5.5), where NaOFm solubilities were increased to a similar degree (19 %) when NaOAc solubilities were essentially the same in co-sorption. Similarly, permeabilities of sulfonate-containing PEGDA-AMPS to alcohols (MeOH and EtOH) in co-permeation were essentially the same. However, permeabilities to carboxylate salts (NaOFm and NaOAc) were significantly increased by 51 %, on average [14,16]. One possible cause of this behavior is flux coupling [26] between fast-diffusing alcohol and slow-diffusing carboxylate salts. Nonetheless, we observed this behavior being particularly apparent in sulfonate-containing polymers, where we conjecture the reduction of electrostatic repulsion that describes the electrostatic repulsion (i.e. Donnan exclusion [50–52]) between bound sulfonate anions and mobile carboxylate anions is reduced by co-transporting MeOH [13,16]. This behavior is discussed further in the diffusivity section (5.2.4).

In co-permeation, sulfonate-containing Nafion® 117 permeabilities to alcohols were significantly decreased by 45 %, on average. This behavior is presumably due to the competitive sorption [13,53] and competitive diffusion. In terms of competitive sorption, alcohol solubilities

were decreased by 14 %, on average, in co-sorption due to competition with carboxylates (Fig. 5.5). The competitive diffusion in hydrated, dense membranes is an emergent co-transport behavior, which requires more investigations. For instance, MeOH diffusivities in various membranes were decreased in co-diffusion. Carter et al. measured MeOH diffusivities through Selemion AMV (a commercial anion exchange membrane) in co-diffusion with EtOH and with n-propanol (n-PrOH) and it was decreased by 20 % in both cases [10]. Our group measured MeOH diffusivities through Nafion® 117 in co-diffusion with EtOH and with n-PrOH and it was increased in co-diffusion with EtOH and slightly decreased in co-diffusion with n-PrOH. We then measured MeOH diffusivities of various PEGDA-based films in co-diffusion with OAc^- and they were generally decreased [14]. Clearly, these results are complex as disparate changes are observed based on membrane and solute chemistries, suggesting there are certain types of permeants/membranes systems that are more likely to show the competitive diffusion. However, more studies are needed to fully capture and address the complex multi-component interactions (permeant-permeant-water-polymer interactions) in order to better understand and ultimately predict behavior. Analogous to carboxylate permeabilities being increased in PEGDA-AMPS in co-permeation, Nafion® 117 permeabilities to carboxylates in co-permeation were significantly increased by 52 %, on average. Again, this behavior is presumably due to the reduction in electrostatic repulsion by co-transporting alcohol [13,16], which will be further discussed in the following section.

5.2.3. Hydration, Swelling, and Single and Multicomponent Solubility

Solubilities of all films were determined from sorption-desorption experiments; see 3.10 for experimental details. Solubilities to alcohols (MeOH and EtOH) and carboxylate salts (NaOFm

and NaOAc) in single (black, solid line) and co-sorption (colored, dashed) are shown in Fig. 5.5 and Table 5.5. Generally, the volume of all films after sorption in alcohol solutions was essentially the same and slightly decreased after sorption in carboxylate salt solutions; see Table 5.6. The polymer-solution volume fraction after sorption was calculated assuming the dry polymer volume being consistent, where the fraction for solution decreases after sorption in carboxylate salt solutions; see Table 5.7.

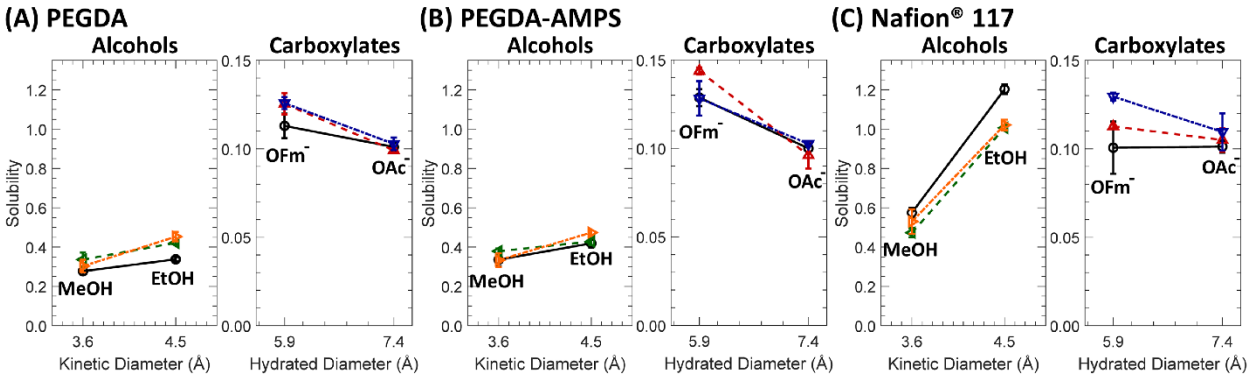

Figure 5.5. Solubility of (A) PEGDA, (B) PEGDA-AMPS, and (C) Nafion® 117 to (left) alcohols, MeOH (3.6 Å), EtOH (4.5 Å), and (right) carboxylate salts, NaOFm (5.9 Å) and NaOAc (7.4 Å), in single (○, black, solid line) and in co-sorption. Each alcohol was co-sorbed with NaOFm (◁, green, dashed) and NaOAc (▷, yellow, dot-dashed) and each carboxylic ion was co-sorbed with MeOH (△, red, dashed) and EtOH (▽, blue, dot-dashed).

Table 5.5. Solubilities of PEGDA, PEGDA-AMPS, and Nafion® 117 membranes to alcohols (MeOH and EtOH) and carboxylate salts (NaOFm and NaOAc) in single and co-sorption.

PEGDA	MeOH	EtOH		NaOFM	NaOAc
Single	0.28 ± 0.02	0.34 ± 0.01	Single	0.11 ± 0.01	0.10 ± 0.00
w/ NaOFm	0.34 ± 0.04	0.42 ± 0.01	w/ MeOH	0.13 ± 0.01	0.10 ± 0.00
w/ NaOAc	0.30 ± 0.03	0.45 ± 0.02	w/ EtOH	0.13 ± 0.00	0.10 ± 0.00
PEGDA-AMPS	MeOH	EtOH		NaOFm	NaOAc
Single	0.34 ± 0.03	0.42 ± 0.02	Single	0.13 ± 0.00	0.10 ± 0.00
w/ NaOFm	0.38 ± 0.01	0.43 ± 0.02	w/ MeOH	0.14 ± 0.00	0.10 ± 0.01
w/ NaOAc	0.33 ± 0.03	0.47 ± 0.01	w/ EtOH	0.13 ± 0.01	0.10 ± 0.00
Nafion® 117	MeOH	EtOH		NaOFm	NaOAc
Single	0.58 ± 0.03	1.20 ± 0.02	Single	0.10 ± 0.01	0.10 ± 0.00
w/ NaOFm	0.47 ± 0.02	1.01 ± 0.01	w/ MeOH	0.11 ± 0.00	0.10 ± 0.01
w/ NaOAc	0.53 ± 0.06	1.02 ± 0.03	w/ EtOH	0.13 ± 0.00	0.11 ± 0.01

Table 5.6. Volume of hydrated films and volume of swollen films (mm^3) after sorption experiments measured from photographs and a digital caliper.

	PEGDA (mm^3)	PEGDA-AMPS (mm^3)	Nafion® 117 (mm^3)
Hydrated	97 ± 1	108 ± 1	33 ± 1
MeOH	96 ± 1	104 ± 1	33 ± 1
EtOH	96 ± 1	109 ± 2	35 ± 1
NaOFm	94 ± 2	106 ± 1	29 ± 0
NaOAc	90 ± 1	94 ± 1	27 ± 0
MeOH/NaOFm	92 ± 0	106 ± 1	29 ± 1
EtOH/NaOFm	90 ± 1	106 ± 0	31 ± 1
MeOH/NaOAc	91 ± 1	94 ± 1	28 ± 0
EtOH/NaOAc	92 ± 2	105 ± 1	30 ± 1

Table 5.7. Water volume fractions (ϕ_w) and solution volume fractions (ϕ_s) of films after sorption experiments, where the remaining is the polymer volume fraction (ϕ_p) from the dry polymer density.

	PEGDA, ϕ_s	PEGDA-AMPS, ϕ_s	Nafion® 117, ϕ_s
Water volume fraction, ϕ_w	0.434	0.603	0.251
MeOH	0.437	0.586	0.271
EtOH	0.439	0.605	0.308
NaOFm	0.426	0.594	0.178
NaOAc	0.403	0.545	0.118
MeOH/NaOFm	0.414	0.593	0.176
EtOH/NaOFm	0.400	0.594	0.222
MeOH/NaOAc	0.409	0.542	0.137
EtOH/NaOAc	0.412	0.590	0.205

Generally, alcohol solubilities of PEGDA-based films and Nafion® 117 were higher than carboxylate salt solubilities by 3 and 7 times, on average, respectively. This indicates alcohol uptake is more preferred in these films over carboxylate salts. For instance, alcohol concentrations in Nafion® 117 after equilibration with sorption solutions (1 M MeOH or 1 M EtOH) were higher than 1 M. This indicates alcohol is more preferred in Nafion® 117 over the external solution; see Table 5.8 for values.

Table 5.8. Volume fraction among the solution, water (ϕ_w)-alcohol (ϕ_a)-carboxylate (ϕ_c), inside the membranes after sorption experiments, where $1\text{-}\phi_a\text{-}\phi_c = \phi_w$.

	External, 1 M		PEGDA		PEGDA-AMPS		Nafion® 117	
	ϕ_a	ϕ_c	ϕ_a	ϕ_c	ϕ_a	ϕ_c	ϕ_a	ϕ_c
MeOH	0.040	-	0.024	-	0.030	-	0.046	-
EtOH	0.058	-	0.043	-	0.051	-	0.131	-
NaOFm	-	0.035	-	0.009	-	0.010	-	0.008
NaOAc	-	0.063	-	0.015	-	0.016	-	0.016
MeOH/NaOFm	0.040	0.035	0.031	0.010	0.033	0.011	0.043	0.009
EtOH/NaOFm	0.058	0.035	0.058	0.011	0.054	0.010	0.123	0.010
MeOH/NaOAc	0.040	0.063	0.028	0.014	0.034	0.015	0.051	0.016
EtOH/NaOAc	0.058	0.063	0.061	0.015	0.060	0.014	0.128	0.015

We observed similar behavior in our previous investigations on Nafion® 117 [13,15], where the alcohol concentrations in Nafion® 117 after sorption in the external solution (1 M of either MeOH, EtOH, or n-PrOH) was higher than those in the external solution. Moreover, we observed EtOH solubilities being higher than MeOH solubilities. A possible cause of these transport behaviors is the difference in relative polarities of alcohols and transporting media. For instance, EtOH can be more favored in polymeric media (less polar) over aqueous media (more polar) than MeOH as the ethyl group of EtOH is more hydrophobic than the methyl group of MeOH (Fig. 5.3 for structures) [35,54]. On the other hand, the solubility of NaOFm were higher than that of NaOAc, when OAc^- is less polar than OFm^- with the additional methyl group (Fig. 5.3) [46]. A possible cause of this difference between the solubilities of alcohols and carboxylate salts are the effect of molecular size, where the larger OAc^- (7.4 Å) would experience more steric hindrance from the polymer structure than smaller OFm^- (5.9 Å) [34,45,54]. However, other factors like molecular structure, concentration, and the degree of ionization may affect the solubilities as well [55,56].

In co-sorption, alcohol solubilities of both PEGDA-based films (PEGDA and PEGDA-AMPS) were increased by 15 %, on average, while those of Nafion® 117 were decreased by 14

%, on average. This behavior in Nafion® 117 is consistent with our previous report [13], where MeOH solubilities were decreased by 24 %, on average, in co-sorption with NaOFm and NaOAc. The likeliest cause of this difference between PEGDA-based films and Nafion® 117 is the polymer backbone chemistry. Nafion® 117 contains a hydrophobic perfluorinated backbone whereas PEGDA is hydrophilic, such that the water uptake of Nafion® 117 is significantly less than that of PEGDA-based films (Table 5.2). Moreover, the volumetric ratio between the bulk region and the bound region for Nafion® 117 is presumably less than that of PEGDA-based films as the majority of the free volume elements in perfluorosulfonic acid polymers (PFSA) is located near sulfonic acid regions [1], while that in poly(ethylene glycol) (PEG)-based polymers is also dispersed along the relatively hydrophilic PEG chains [19,25,57]. Therefore, alcohol in Nafion® 117 might be experiencing more competition (i.e. competitive sorption [13,53]) for the free volume element in co-sorption with carboxylates, which would preferentially reside in the bulk region due to the electrostatic repulsion (i.e. Donnan exclusion [50–52]).

In co-sorption, NaOFm solubilities of all films were increased by 19 %, on average, while NaOAc solubilities were essentially the same. One factor influencing this behavior is the increases in the solution volume fraction, ϕ_s [35]:

$$\phi_s = \frac{V_s - (W_d/\rho_L)}{V_s} \tag{5.2}$$

where W_d is the mass of the dried film, ρ_L is the density of water, and V_s is the volume of the swollen film after sorption. To determine V_s, the film surface area was extracted from digital photographs and the thickness was measured using a digital caliper; see Table 5.7 for values. As the solution volume fraction was higher in co-sorption with an alcohol, the polymer-ion interaction can be decreased. For PEGDA-based film, the attractive interaction between Na^+ and ethylene

oxide is well studied [34]. As such attractive interactions decrease, more salts will be exposed to the bulk water region (away from the polymer chains) and surrounded by more water molecules which leads to an overall increase in ion hydration. While the change in hydration numbers, λ, for both Na^+ (λ: 4-8 [58,59]) and OAc^- (λ: 6-13 [46]) often varies to a great degree (i.e. ionic strength [34]), the change in hydration number for OFm^- is more consistent (λ: 4-6 [46]). Although the increasing solution volume fraction increases the probability that a given salt can find an accessible free volume element within the film, this effect can be more apparent for NaOFm as the increase of OFm^- ion hydration will be negligible compared to that of OAc^- ion hydration.

5.2.4. Single and Multi-solute Diffusivity

Diffusivities to all permeants were calculated using the solution-diffusion relationship (Eq. 5.1), dividing permeabilities (Table 5.3) by solubilities (Table 5.5), where diffusivities to alcohols (MeOH and EtOH) and carboxylate salts (NaOFm and NaOAc) in single (black, solid line) and co-sorption (colored, dashed) are shown in Table 5.9 and Fig. 5.6 and 5.7. Generally, diffusivities were inversely proportional to permeant size (MeOH (3.6 Å) > EtOH (4.5 Å) > OFm^- (5.9 Å) > OAc^- (7.4 Å)) [45,47])[28]. Based on this result, hydrated diameters seem to be a reasonable parameter to explain the one-component diffusion of carboxylate anions. According to free volume theory, the diffusivity, D_i, of solute i in a dense membrane is directly related to the diameter of solute i, b_i [28,60–63]:

$$D_i = a_i \, exp\left(\frac{-b_i}{v_f}\right) \tag{5.3}$$

where a_i is the geometric factor, b_i is the Lennard-Jones diameter of solute i, and v_f is the fractional free volume of the membrane [6]. Therefore, the diffusivity of a solute is often decreased with

increasing solute diameter. Nonetheless, the relative effect of kinetic diameter and hydrated diameter in ion diffusion through hydrated, dense membranes requires more investigation to be fully understood [40]. Moreover, the diffusivity of a solute is often increased with increasing fractional free volume, v_f, of the membrane. Mackie and Meares proposed a model that estimates the solute diffusivity in a hydrated polymer, which assumes (1) the polymer-diffusant interactions are negligible, (2) polymer chains are acting as impenetrable obstacles, (3) the solute diffusivity in these films is the same as in pure water, excluding the polymer volume fraction (ϕ_p) [49]. The Mackie-Meares model states:

$$D_i = D_{o,i}\left(\frac{\phi_w}{2-\phi_w}\right)^2 \tag{5.4}$$

where D_i is the diffusivity of a membrane to a solute i, ϕ_w is the water volume fraction (1-ϕ_p), and $D_{0,i}$ is the solute diffusivity in pure water. For alcohol diffusivities in water, we utilized the reported diffusivities, 1.49×10^{-5} and 1.23×10^{-5} cm^2/s for MeOH and EtOH, respectively [64]. To calculate the diffusivities of salts in water ($D_{0,i}$), we assume the diffusivities of a salt consists of monovalent ions (i.e. Na^+ and Cl^- for NaCl) and that the salt diffusivity is close to the average diffusivities of the two ions. For instance, using the reported diffusivities of Na^+ and Cl^- in water (1.33×10^{-5} and 2.03×10^{-5} cm^2/s, respectively [65]), the estimated diffusivity of NaCl in water is 1.68×10^{-5}, and this is close to the reported diffusivity for NaCl, 1.61×10^{-5} [66]. Here, using the reported diffusivities of Na^+, OFm^-, and OAc^- in water, 1.33×10^{-5}, 1.45×10^{-5}, and 1.09×10^{-5} cm^2/s [65,67], respectively, we estimate the diffusivities of NaOFm and NaOAc in water as 1.39×10^{-5} and 1.21×10^{-5} cm^2/s, respectively (mobility-weighted average diffusivity [68]). The diffusivities of each solute with a Mackie-Meares' fit are shown in Fig. 5.7. The model tends to fit better with the diffusivities of PEGDA and PEGDA-AMPS films (ϕ_w: 0.43 and 0.60) than those with the

diffusivities of Nafion® 117 (ϕ_w: 0.25). We ascribe this discrepancy for Nafion® 117 to the inherent drawback of the model at lower water volume fraction, as the solute diffusion behavior deviates from that in pure water as the water volume fraction decreases. Moreover, the model tends to fit better in co-diffusion, where a possible contribution is the polymer-diffusant interactions being decreased in co-diffusion.

Table 5.9. Diffusivities ($\times 10^7$ cm^2/s) of PEGDA, PEGDA-AMPS, and Nafion® 117 membranes to alcohols (MeOH and EtOH) and carboxylate salts (NaOFm and NaOAc) in single and ion-alcohol mixture.

PEGDA	MeOH	EtOH		NaOFm	NaOAc
Single	37.2	16.5	Single	12.7	12.3
w/ NaOFm	27.0	15.6	w/ MeOH	14.3	13.2
w/ NaOAc	31.2	12.1	w/ EtOH	13.9	11.5

PEGDA-AMPS	MeOH	EtOH		NaOFm	NaOAc
Single	38.0	21.3	Single	16.8	13.2
w/ NaOFm	37.0	22.8	w/ MeOH	22.4	20.5
w/ NaOAc	36.2	19.9	w/ EtOH	25.9	19.7

Nafion® 117	MeOH	EtOH		NaOFm	NaOAc
Single	37.1	14.2	Single	14.2	8.1
w/ NaOFm	28.2	8.9	w/ MeOH	21.3	10.2
w/ NaOAc	22.3	8.1	w/ EtOH	17.8	10.0

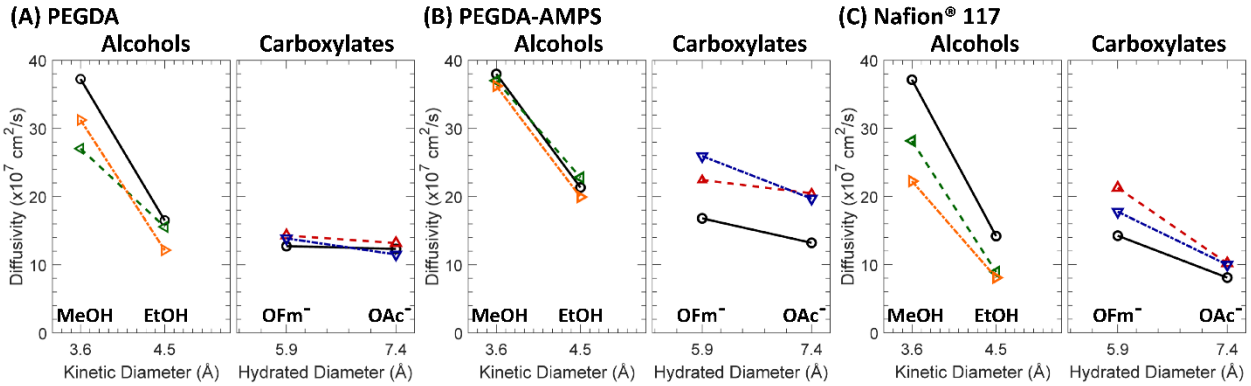

Figure 5.6. Diffusivity of (A) PEGDA, (B) PEGDA-AMPS, and (C) Nafion® 117 to (left) alcohols, MeOH (3.6 Å), EtOH (4.5 Å), and (right) carboxylate salts, NaOFm (5.9 Å) and NaOAc (7.4 Å), in single (○, black, solid line) and in co-diffusion. Each alcohol was co-diffused with NaOFm (◁, green, dashed) and NaOAc (▷, yellow, dot-dashed) and each carboxylic ion was co-diffused with MeOH (△, red, dashed) and EtOH (▽, blue, dot-dashed).

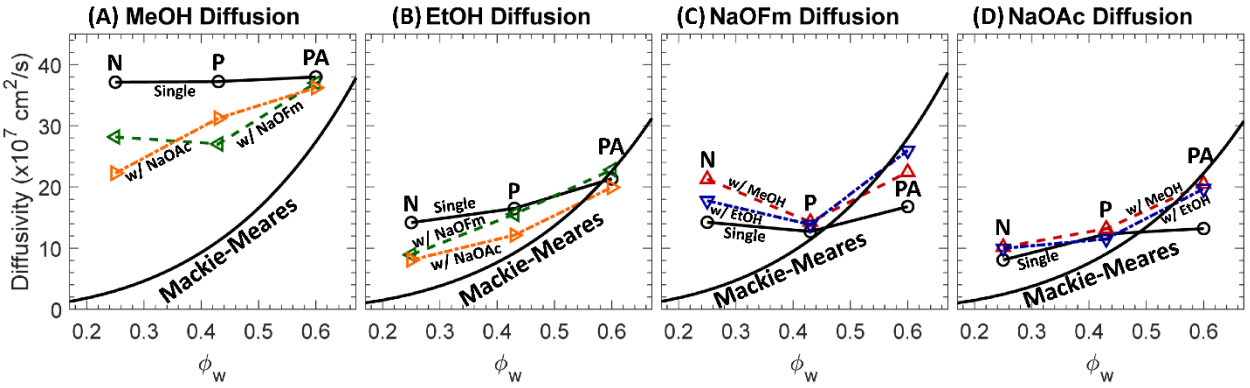

Figure 5.7. Diffusivity of Nafion® 117 (N), PEGDA (P), and PEGDA-AMPS (PA) to (A) MeOH, (B) EtOH, (C) NaOFm, and (D) NaOAc in single (○, black, solid line) and in co-diffusion. Each alcohol was co-diffused with NaOFm (◁, green, dashed) and NaOAc (▷, yellow, dot-dashed) and each carboxylic ion was co-diffused with MeOH (△, red, dashed) and EtOH (▽, blue, dot-dashed).

In co-diffusion, alcohol diffusivities of all films (PEGDA, PEGDA-AMPS, and Nafion® 117) were generally decreased by 20, 2, and 34 %, on average, respectively. As discussed in the permeability section, a possible cause of this behavior is the competitive diffusion. We conjecture the diffusional path of a diffusant (alcohol) is interfered with by a co-diffusant (carboxylate) due to a potential repulsive interaction between two diffusants. For instance, the solubility of a carboxylate in water is significantly higher than that in alcohol, which indicates the carboxylate-alcohol interaction can be repulsive relative to the carboxylate-water interaction and, therefore, both carboxylate and alcohol might consider each other as an obstacle. Therefore, fast-diffusing alcohol, would have to bypass the slow-diffusing carboxylate when moving between a free volume elements. Nevertheless, more investigations [10,13,15] are in need, as this apparent behavior can be affected by numerous factors, such as shapes, length, number of charge-groups, and solute-solvent interaction.

While diffusivities of sulfonate-free PEGDA to carboxylates were essentially the same in co-diffusion, diffusivities of both CEMs (PEGDA-AMPS and Nafion® 117) to carboxylate anions were significantly increased by 47 and 33 %, on average, respectively. This behavior can be

explained through partial charge screening by a co-diffusing alcohol [13,16] such that the electrostatic repulsion between bound sulfonate anions and permeating carboxylate anions (co-ions in CEM) is diminished and, therefore, the overall salt diffusivity is increased (Fig. 5.1). Another example of a charge screening has been obversed in sulfonated reverse osmosis membranes [27,28], where the diffusivities to salts with a divalent cation ($MgCl_2$ and $CaCl_2$) were higher than those to salts with a monovalent cation (NaCl and KCl) presumably due to divalent cations (i.e. Mg^{2+} and Ca^{2+}) partially neutralizing the bound sulfonate charges with relatively high binding affinity. Overall, these changes in interactions suggest that differences in diffusion behavior from the above-described interactions are a primary driver of changes in membrane diffusivities to carboxylate salts in single and co-diffusion with alcohols.

5.3. Conclusion

A sulfonate-free PEGDA, a sulfonate-containing PEGDA-AMPS, and a sulfonate-containing Nafion® 117 were investigated for their transport and co-transport behavior when challenged with carboxylate ions, alcohols, and mixtures of carboxylate ions and alcohols. Permeabilities and solubilities to an alcohol (either MeOH or EtOH) or carboxylate salt (either NaOFm or NaOAc) were measured both by themselves and in co-transport. Solute diffusivities for each case were then calculated using the solution-diffusion model where, generally, alcohols exhibited higher solubility and diffusivity than the carboxylate salts in all films. Two co-diffusive behaviors are conjectured based on the observed co-transport behavior, competitive diffusion and charge screening. Alcohol diffusivities in Nafion® 117 are decreased in co-diffusion with a carboxylate salt, presumably due to higher competition for the free volume element (competitive diffusion).

Concurrently, the carboxylate salt diffusivities of PEGDA-AMPS and Nafion® 117 CEMs are increased in co-diffusion with an alcohol (MeOH or EtOH) which we ascribe to the screening of electrostatic repulsion by the co-diffusing alcohol (charge screening). Nonetheless, the increase in the diffusivity of carboxylates in CEMs is a concerning behavior for CO_2 reduction cells, which should be suppressed via target-specific membrane design. Overall, multi-component transport in IEMs is highly complex system as various mobile components (i.e. cation, carboxylate anion, alcohol, and bulk water) are permeating in various fixed components (i.e. sulfonate anion, polymer backbone, and bound water) and the array of interactions between solutes and between solutes and the membrane are dynamic and complicated. Therefore, while this investigation extends our understanding of transport and co-transport behavior of select solutes (carboxylate ions and alcohols), more fundamental investigations are needed to further develop our understanding of the transport behavior of complex mixtures in polymer membranes.

5.4. References

[1] A. Kusoglu, A.Z. Weber, New Insights into Perfluorinated Sulfonic-Acid Ionomers, Chem Rev. 117 (2017) 987–1104. https://doi.org/10.1021/acs.chemrev.6b00159.

[2] J. Kamcev, B.D. Freeman, Charged Polymer Membranes for Environmental/Energy Applications, Annu Rev Chem Biomol. 7 (2015) 1–23. https://doi.org/10.1146/annurev-chembioeng-080615-033533.

[3] G. Geise, M. Hickner, B. Logan, Ionic resistance and permselectivity tradeoffs in anion exchange membranes., Acs Appl Mater Inter. 5 (2013) 10294–301. https://doi.org/10.1021/am403207w.

[4] M.A. Hickner, Ion-containing polymers: new energy & clean water, Mater Today. 13 (2010) 34–41. https://doi.org/10.1016/s1369-7021(10)70082-1.

[5] M.R. Singh, A.T. Bell, Design of an artificial photosynthetic system for production of alcohols in high concentration from CO 2, Energ Environ Sci. 9 (2015) 193–199. https://doi.org/10.1039/c5ee02783g.

[6] D.J. Miller, F.A. Houle, Energy and Environment Series, (2018) 341–385. https://doi.org/10.1039/9781788010313-00341.

[7] A.J. Garza, A.T. Bell, M. Head-Gordon, Mechanism of CO 2 Reduction at Copper Surfaces: Pathways to C 2 Products, Acs Catal. 8 (2018) 1490–1499. https://doi.org/10.1021/acscatal.7b03477.

[8] L.-C. Weng, A.T. Bell, A.Z. Weber, Towards membrane-electrode assembly systems for CO 2 reduction: a modeling study, Energ Environ Sci. 12 (2019) 1950–1968. https://doi.org/10.1039/c9ee00909d.

[9] B.M. Carter, L. Keller, M. Wessling, D.J. Miller, Preparation and characterization of crosslinked poly(vinylimidazolium) anion exchange membranes for artificial photosynthesis, J Mater Chem A. (2019). https://doi.org/10.1039/c9ta00498j.

[10] B.M. Carter, B.M. Dobyns, B.S. Beckingham, D.J. Miller, Multicomponent transport of alcohols in an anion exchange membrane measured by in-situ ATR FTIR spectroscopy, Polymer. 123 (2017). https://doi.org/10.1016/j.polymer.2017.06.070.

[11] M. Krödel, B.M. Carter, D. Rall, J. Lohaus, M. Wessling, D.J. Miller, Rational Design of Ion Exchange Membrane Material Properties Limits the Crossover of CO 2 Reduction Products in Artificial Photosynthesis Devices, Acs Appl Mater Inter. 12 (2020) 12030–12042. https://doi.org/10.1021/acsami.9b21415.

[12] S.M. Dischinger, S. Gupta, B.M. Carter, D.J. Miller, Transport of Neutral and Charged Solutes in Imidazolium-Functionalized Poly(phenylene oxide) Membranes for Artificial Photosynthesis, Ind Eng Chem Res. 59 (2019) 5257–5266. https://doi.org/10.1021/acs.iecr.9b05628.

[13] B.S. Beckingham, N.A. Lynd, D.J. Miller, Monitoring multicomponent transport using in situ ATR FTIR spectroscopy, J Membrane Sci. 550 (2018). https://doi.org/10.1016/j.memsci.2017.12.072.

[14] J.M. Kim, B.S. Beckingham, Comonomer effects on co-permeation of methanol and acetate in cation exchange membranes, Eur Polym J. (2021) 110307. https://doi.org/10.1016/j.eurpolymj.2021.110307.

[15] B.M. Dobyns, J.M. Kim, J. Li, Z. Jiang, B.S. Beckingham, Multicomponent transport of alcohols in Nafion 117 measured by in situ ATR FTIR spectroscopy, Polymer. (2020) 123046. https://doi.org/10.1016/j.polymer.2020.123046.

[16] J.M. Kim, B.M. Dobyns, R. Zhao, B.S. Beckingham, Multicomponent transport of methanol and acetate in a series of crosslinked PEGDA-AMPS cation exchange membranes, J Membrane Sci. (2020) 118486. https://doi.org/10.1016/j.memsci.2020.118486.

[17] M. Soniat, S.M. Dischinger, L. Weng, H.M. Beltran, A.Z. Weber, D.J. Miller, F.A. Houle, Toward predictive permeabilities: Experimental measurements and multiscale simulation of methanol transport in Nafion, J Polym Sci. (2021). https://doi.org/10.1002/pol.20200771.

[18] B.M. Dobyns, J.M. Kim, B.S. Beckingham, Multicomponent transport of methanol and sodium acetate in poly(ethylene glycol) diacrylate membranes of varied fractional free volume, Eur Polym J. 134 (2020) 109809. https://doi.org/10.1016/j.eurpolymj.2020.109809.

[19] H. Ju, A.C. Sagle, B.D. Freeman, J.I. Mardel, A.J. Hill, Characterization of sodium chloride and water transport in crosslinked poly(ethylene oxide) hydrogels, J Membrane Sci. 358 (2010) 131–141. https://doi.org/10.1016/j.memsci.2010.04.035.

[20] H. Lin, B.D. Freeman, S. Kalakkunnath, D.S. Kalika, Effect of copolymer composition, temperature, and carbon dioxide fugacity on pure- and mixed-gas permeability in poly(ethylene glycol)-based materials: Free volume interpretation, J Membrane Sci. 291 (2007) 131–139. https://doi.org/10.1016/j.memsci.2007.01.001.

[21] A.C. Sagle, H. Ju, B.D. Freeman, M.M. Sharma, PEG-based hydrogel membrane coatings, Polymer. 50 (2009) 756–766. https://doi.org/10.1016/j.polymer.2008.12.019.

[22] S. Kalakkunnath, D.S. Kalika, H. Lin, B.D. Freeman, Segmental Relaxation Characteristics of Cross-Linked Poly(ethylene oxide) Copolymer Networks, Macromolecules. 38 (2005) 9679–9687. https://doi.org/10.1021/ma051741t.

[23] H. Lin, E.V. Wagner, J.S. Swinnea, B.D. Freeman, S.J. Pas, A.J. Hill, S. Kalakkunnath, D.S. Kalika, Transport and structural characteristics of crosslinked poly(ethylene oxide) rubbers, J Membrane Sci. 276 (2006) 145–161. https://doi.org/10.1016/j.memsci.2005.09.040.

[24] Y. Yu, N. Yan, B.D. Freeman, C.-C. Chen, Mobile ion partitioning in ion exchange membranes immersed in saline solutions, J Membrane Sci. 620 (2020) 118760. https://doi.org/10.1016/j.memsci.2020.118760.

[25] N. Yan, D.R. Paul, B.D. Freeman, Water and ion sorption in a series of cross-linked AMPS/PEGDA hydrogel membranes, Polymer. 146 (2018) 196–208. https://doi.org/10.1016/j.polymer.2018.05.021.

[26] K.A. Thompson, R. Mathias, D. Kim, J. Kim, N. Rangnekar, J.R. Johnson, S.J. Hoy, I. Bechis, A. Tarzia, K.E. Jelfs, B.A. McCool, A.G. Livingston, R.P. Lively, M.G. Finn, N-Aryl-linked spirocyclic polymers for membrane separations of complex hydrocarbon mixtures., Sci New York N Y. 369 (2020) 310–315. https://doi.org/10.1126/science.aba9806.

[27] P. Parise, A.A. Jr, B. Parekh, Reverse osmosis: chlorine-resistant polysulfone reverse osmosis membrane and module, Ultrapure Water. (1987).

[28] G.M. Geise, D.R. Paul, B.D. Freeman, Fundamental water and salt transport properties of polymeric materials, Prog Polym Sci. 39 (2014) 1–42. https://doi.org/10.1016/j.progpolymsci.2013.07.001.

[29] J.M. Kim, B.S. Beckingham, Transport and co-transport of carboxylate ions and alcohols in cation exchange membranes, J Polym Sci. (2021). https://doi.org/10.1002/pol.20210383.

[30] J.M. Kim, Y. Lin, B. Hunter, B.S. Beckingham, Transport and Co-Transport of Carboxylate Ions and Ethanol in Anion Exchange Membranes, Polymers-Basel. 13 (2021) 2885. https://doi.org/10.3390/polym13172885.

[31] J.M. Kim, A. Mazumder, J. Li, Z. Jiang, B.S. Beckingham, Impact of PEGMA on transport and co-transport of methanol and acetate in PEGDA-AMPS cation exchange membranes, J Membrane Sci. (2021) 119950. https://doi.org/10.1016/j.memsci.2021.119950.

[32] J.G. Wijmans, R.W. Baker, The solution-diffusion model: a review, J Membrane Sci. 107 (1995) 1–21. https://doi.org/10.1016/0376-7388(95)00102-i.

[33] G.M. Geise, B.D. Freeman, D.R. Paul, Characterization of a sulfonated pentablock copolymer for desalination applications, Polymer. 51 (2010) 5815–5822. https://doi.org/10.1016/j.polymer.2010.09.072.

[34] E.-S. Jang, J. Kamcev, K. Kobayashi, N. Yan, R. Sujanani, T.J. Dilenschneider, H.B. Park, D.R. Paul, B.D. Freeman, Influence of water content on alkali metal chloride transport in cross-

linked Poly(ethylene glycol) Diacrylate.1. Ion sorption, Polymer. 178 (2019) 121554. https://doi.org/10.1016/j.polymer.2019.121554.

[35] M. Galizia, D.R. Paul, B.D. Freeman, Liquid methanol sorption, diffusion and permeation in charged and uncharged polymers, Polymer. 102 (2016) 281–291. https://doi.org/10.1016/j.polymer.2016.09.010.

[36] G.M. Geise, L.P. Falcon, B.D. Freeman, D.R. Paul, Sodium chloride sorption in sulfonated polymers for membrane applications, J Membrane Sci. 423 (2012) 195–208. https://doi.org/10.1016/j.memsci.2012.08.014.

[37] M. Soniat, F.A. Houle, Swelling and Diffusion during Methanol Sorption into Hydrated Nafion, J Phys Chem B. (2018). https://doi.org/10.1021/acs.jpcb.8b03169.

[38] K. Chang, H. Luo, G.M. Geise, Water content, relative permittivity, and ion sorption properties of polymers for membrane desalination, J Membrane Sci. 574 (2019) 24–32. https://doi.org/10.1016/j.memsci.2018.12.048.

[39] D.T. Hallinan, Y.A. Elabd, Diffusion and Sorption of Methanol and Water in Nafion Using Time-Resolved Fourier Transform Infrared−Attenuated Total Reflectance Spectroscopy, J Phys Chem B. 111 (2007) 13221–13230. https://doi.org/10.1021/jp075178n.

[40] E.-S. Jang, J. Kamcev, K. Kobayashi, N. Yan, R. Sujanani, T.J. Dilenschneider, H.B. Park, D.R. Paul, B.D. Freeman, Influence of water content on alkali metal chloride transport in cross-linked Poly(ethylene glycol) diacrylate.2. Ion diffusion, Polymer. 192 (2020) 122316. https://doi.org/10.1016/j.polymer.2020.122316.

[41] J. Kamcev, D.R. Paul, G.S. Manning, B.D. Freeman, Ion Diffusion Coefficients in Ion Exchange Membranes: Significance of Counterion Condensation, Macromolecules. 51 (2018) 5519–5529. https://doi.org/10.1021/acs.macromol.8b00645.

[42] G.S. Manning, Limiting Laws and Counterion Condensation in Polyelectrolyte Solutions II. Self-Diffusion of the Small Ions, J Chem Phys. 51 (1969) 934–938. https://doi.org/10.1063/1.1672158.

[43] W.J. Horne, M.S. Shannon, J.E. Bara, Correlating fractional free volume to CO2 selectivity in [Rmim][Tf2N] ionic liquids, J Chem Thermodyn. 77 (2014) 190–196. https://doi.org/10.1016/j.jct.2014.03.012.

[44] N.W. DeLuca, Y.A. Elabd, Polymer electrolyte membranes for the direct methanol fuel cell: A review, J Polym Sci Part B Polym Phys. 44 (2006) 2201–2225. https://doi.org/10.1002/polb.20861.

[45] R. Caminiti, P. Cucca, M. Monduzzi, G. Saba, G. Crisponi, Divalent metal–acetate complexes in concentrated aqueous solutions. An x-ray diffraction and NMR spectroscopy study, J Chem Phys. 81 (1984) 543–551. https://doi.org/10.1063/1.447336.

[46] H.M.A. Rahman, G. Hefter, R. Buchner, Hydration of Formate and Acetate Ions by Dielectric Relaxation Spectroscopy, J Phys Chem B. 116 (2011) 314–323. https://doi.org/10.1021/jp207504d.

[47] E.R. Nightingale, Phenomenological Theory of Ion Solvation. Effective Radii of Hydrated Ions, J Phys Chem. 63 (1959) 1381–1387. https://doi.org/10.1021/j150579a011.

[48] K.J. Oberbroeckling, D.C. Dunwoody, S.D. Minteer, J. Leddy, Density of Nafion Exchanged with Transition Metal Complexes and Tetramethyl Ammonium, Ferrous, and Hydrogen Ions: Commercial and Recast Films, Anal Chem. 74 (2002) 4794–4799. https://doi.org/10.1021/ac025586h.

[49] J.S. Mackie, P. Meares, The diffusion of electrolytes in a cation-exchange resin membrane I. Theoretical, Proc Royal Soc Lond Ser Math Phys Sci. 232 (1955) 498–509. https://doi.org/10.1098/rspa.1955.0234.

[50] G.M. Geise, H. Lee, D.J. Miller, B.D. Freeman, J.E. McGrath, D.R. Paul, Water purification by membranes: The role of polymer science, J Polym Sci Part B Polym Phys. 48 (2010) 1685–1718. https://doi.org/10.1002/polb.22037.

[51] F.G. Donnan, The Theory of Membrane Equilibria., Chem Rev. 1 (1924). https://doi.org/10.1021/cr60001a003.

[52] F.G. Helfferich, Ion Exchange, Dover, 1995.

[53] R.T. Chern, W.J. Koros, B. Yui, H.B. Hopfenberg, V.T. Stannett, Selective permeation of CO2 and CH4 through kapton polyimide: Effects of penetrant competition and gas-phase nonideality, J Polym Sci Polym Phys Ed. 22 (1984) 1061–1084. https://doi.org/10.1002/pol.1984.180220610.

[54] P.J. Flory, Principles of Polymer Chemistry, Cornell University Press, 1953.

[55] P.J. Moon, S.J. Parulekar, S.-P. Tsai, Competitive anion transport in desalting of mixtures of organic acids by batch electrodialysis, J Membrane Sci. 141 (1998) 75–89. https://doi.org/10.1016/s0376-7388(97)00292-5.

[56] J. Liu, J. Liang, X. Feng, W. Cui, H. Deng, Z. Ji, Y. Zhao, X. Guo, J. Yuan, Effects of inorganic ions on the transfer of weak organic acids and their salts in electrodialysis process, J Membrane Sci. 624 (2021) 119109. https://doi.org/10.1016/j.memsci.2021.119109.

[57] H. Ju, B.D. McCloskey, A.C. Sagle, V.A. Kusuma, B.D. Freeman, Preparation and characterization of crosslinked poly(ethylene glycol) diacrylate hydrogels as fouling-resistant membrane coating materials, J Membrane Sci. 330 (2009) 180–188. https://doi.org/10.1016/j.memsci.2008.12.054.

[58] P.R. Smirnov, V.N. Trostin, Structure of the nearest surrounding of the Na+ ion in aqueous solutions of its salts, Russ J Gen Chem. 77 (2007) 844–850. https://doi.org/10.1134/s1070363207050052.

[59] J. Mähler, I. Persson, A Study of the Hydration of the Alkali Metal Ions in Aqueous Solution, Inorg Chem. 51 (2012) 425–438. https://doi.org/10.1021/ic2018693.

[60] D.F. Sanders, Z.P. Smith, R. Guo, L.M. Robeson, J.E. McGrath, D.R. Paul, B.D. Freeman, Energy-efficient polymeric gas separation membranes for a sustainable future: A review, Polymer. 54 (2013) 4729–4761. https://doi.org/10.1016/j.polymer.2013.05.075.

[61] M.H. Cohen, D. Turnbull, Molecular Transport in Liquids and Glasses, J Chem Phys. 31 (1959) 1164–1169. https://doi.org/10.1063/1.1730566.

[62] H. Lin, B.D. Freeman, Gas Permeation and Diffusion in Cross-Linked Poly(ethylene glycol diacrylate), Macromolecules. 39 (2006) 3568–3580. https://doi.org/10.1021/ma051686o.

[63] H. Yasuda, C.E. Lamaze, L.D. Ikenberry, Permeability of solutes through hydrated polymer membranes. Part I. Diffusion of sodium chloride, Die Makromolekulare Chemie. 118 (1968) 19–35. https://doi.org/10.1002/macp.1968.021180102.

[64] L. Hao, D.G. Leaist, Binary Mutual Diffusion Coefficients of Aqueous Alcohols. Methanol to 1-Heptanol, J Chem Eng Data. 41 (1996) 210–213. https://doi.org/10.1021/je950222q.

[65] E.E. Hills, M.H. Abraham, A. Hersey, C.D. Bevan, Diffusion coefficients in ethanol and in water at 298K: Linear free energy relationships, Fluid Phase Equilibr. 303 (2011) 45–55. https://doi.org/10.1016/j.fluid.2011.01.002.

[66] H.S. Harned, C.L. Hildreth, The Differential Diffusion Coefficients of Lithium and Sodium Chlorides in Dilute Aqueous Solution at 25°, J Am Chem Soc. 73 (1951) 650–652. https://doi.org/10.1021/ja01146a043.

[67] P. Vany´sek, Ionic Conductivity and Diffusion at Infinite Dilution, CRC Handbook of Chemistry and Physics, 93rd Edition. (2012).

[68] D.T. Hallinan, N.P. Balsara, Polymer Electrolytes, Annu Rev Mater Res. 43 (2013) 503–525. https://doi.org/10.1146/annurev-matsci-071312-121705.

Chapter 6

Alcohol-Carboxylate co-transport in AEMs

Reproduced from: J.M. Kim, Y. Lin, B. Hunter, B.S. Beckingham, Transport and Co-Transport of Carboxylate Ions and Ethanol in Anion Exchange Membranes, Polymers. 13 (2021) 2885. https://doi.org/10.3390/polym13172885.

6.1. Introduction

Anion exchange membranes (AEM [1,2]) are a crucial part of devices for various applications, including direct ethanol fuel cells [3], direct urea fuel cells [4], water purification [5], water electrolyzers [6], CO_2 electrolyzers [7], and photoelectrochemical CO_2 reduction cells (PEC-CRC) [8–12]. Of particular interest here are PEC-CRCs, which utilize solar power to reduce CO_2 to various chemicals [13,14], such as methanol (MeOH), ethanol (EtOH), formate (OFm^-), and acetate (OAc^-). Major roles of the AEM in such devices are to provide preferential ion transport (i.e. hydroxide (OH^-) and anionic electrolytes (bicarbonates, HCO_3^-) [15,16]) with membrane-bound charged functional groups (i.e. quaternary ammonium (QA^+) for AEMs) and to minimize the permeation of CO_2 reduction products to the anode chamber, as they readily oxidize back to CO_2 and by-products [11,12]. Here, to further investigate multicomponent transport behavior [17] in IEMs, we perform an analogous investigation on a series of AEMs, Selemion® AMVN (AMVN) and PEGDA-APTA (A8 and A12). AMVN is a commercial AEM and PEGDA-APTA is a crosslinked AEM that we prepare by incorporating (3-acrylamidopropyl) trimethylammonium chloride (APTA, QA^+-containing ionomer) with a crosslinker, PEGDA [18–21]; see Fig. 6.1

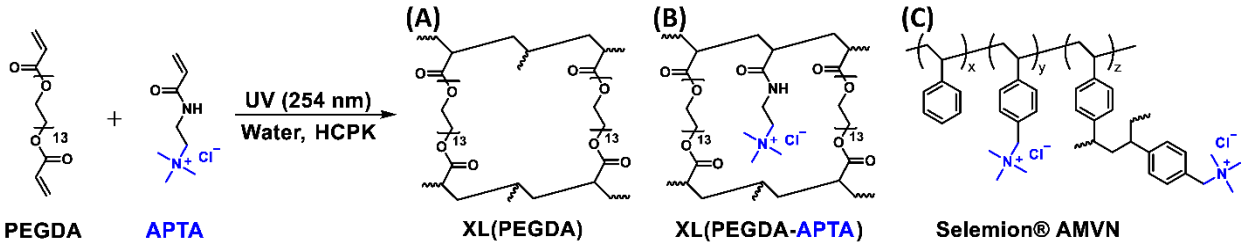

Figure 6.1. (A,B) Synthetic scheme of (A) crosslinked PEGDA, A0, and (B) crosslinked PEGDA-APTA, A8 and A12. (C) Schematic of Selemion AMVN, functionalized polystyrene-divinylbenzene (PS-DVB)-based film.

Moreover, we prepare and characterize a crosslinked PEGDA (A0) as an uncharged analog to exclude the effect of QA^+ from A8 and A12 for comparison. The aim of this work is to examine how the presence of co-permeating EtOH impacts the transport behavior and whether this behavior is consistent with our prior findings for similar systems. Previously, Carter et al. investigated co-transport of alcohols (MeOH, EtOH, and n-PrOH) in Selemion AMV, where they observed a competitive sorption and flux coupling behavior in co-transport [8]. Based on our prior work described above on co-transport of carboxylates and alcohols in CEMs, a pictorial description of how the presence of co-permeating alcohols could be interfering with the electrostatic interactions (repulsion for CEMs and attraction for AEMs [22–24]) between membrane-bound charge groups (sulfonates for CEMs or QA^+ for AEMs) and mobile carboxylate anion is shown in Fig. 6.2. In Fig. 6.2(A-C), the diffusion of carboxylate anion by itself is depicted, where the mobile carboxylate anion experiences electrostatic repulsion from bound sulfonate in CEMs (Fig. 6.2(A)) and electrostatic attraction from bound QA^+ in AEMs (Fig. 6.2(C)) (ion-polymer interaction). In Fig. 6.2(D-F), the diffusion of carboxylates is assisted by co-diffusing alcohols (flux coupling [25]) (ion-alcohol interaction), where the electrostatic interaction between bound charge groups and mobile carboxylate anion is being screened by co-permeating alcohol (alcohol-polymer interaction, charge screening [21,26–28], Fig. 6.2(D,F)).

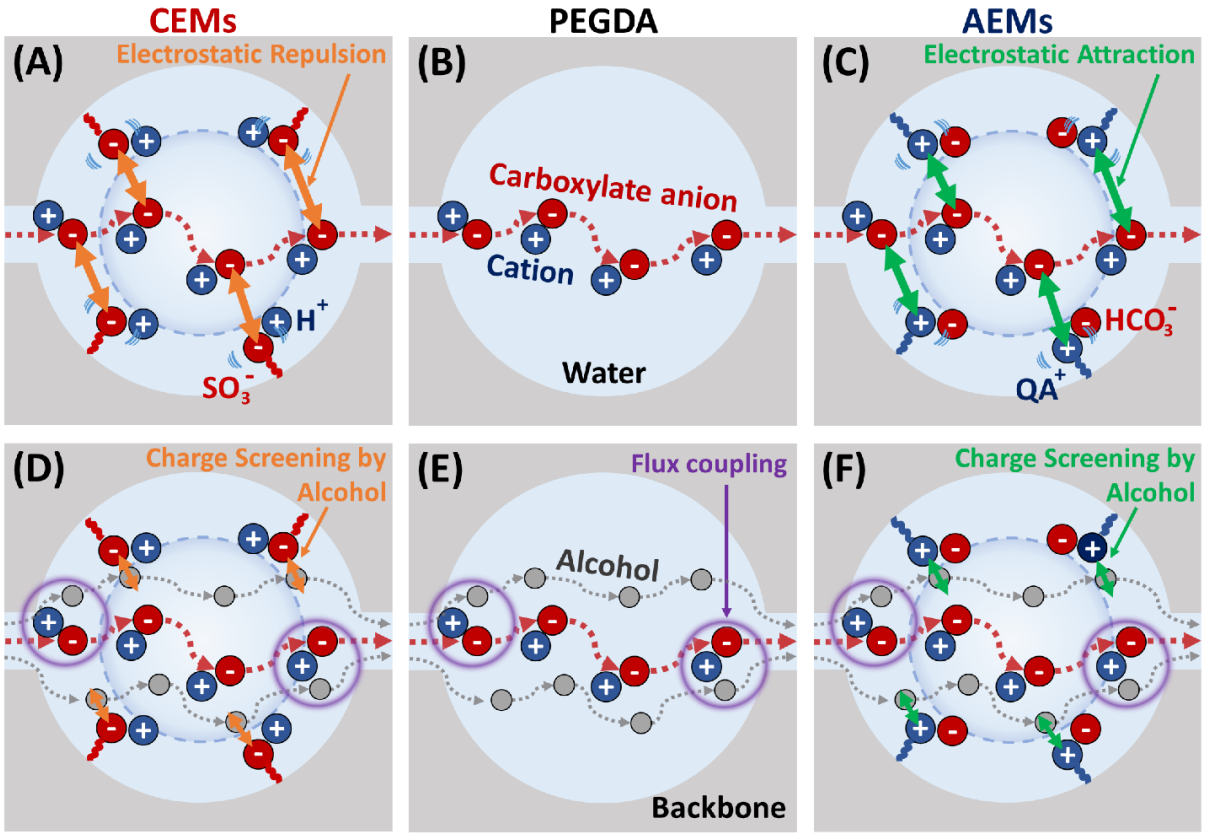

Figure 6.2. Schematic depiction of a carboxylate salt diffusion in (A,D) cation exchange membranes (i.e. PEGDA-AMPS and Nafion® 117), (B,E) crosslinked PEGDA (i.e. A0) and (C,F) anion exchange membranes (i.e. P8, P12, and AMVN) in (A-C) single and (D-F) co-diffusion with an alcohol (MeOH or EtOH). Figures are reprinted from [20,21,29,30] with permission from Elsevier, Wiley, and MDPI.

To probe this behavior in the AEMs of interest here, for each AEM we measure their permeability (P_i) and solubility (K_i) to both K^+ and Na^+ forms of formate (OFm^-) and acetate (OAc^-). Permeabilities are measured by diffusion cell experiments coupled with in-situ attenuated total reflectance–Fourier transform infrared (ATR-FTIR) spectroscopy [26], solubilities are measured by sorption-desorption experiments coupled with a high-performance liquid chromatography (HPLC) [31]. Additionally, we measure carboxylate permeability (in co-diffusion) and solubility (from a mixture) with ethanol (EtOH). We then calculate diffusivities (D_i) to OFm^- and OAc^- in both K^+ and Na^+ forms (KOFm, KOAc, NaOFm, and NaOAc) using the solution-diffusion model

(Eq. 1) [32], that describes the overall solute permeation which is dependent on solute sorption [31,33–36] into the membrane and diffusion [23,35,37,38] through the fractional free volume [39–42] within the polymer matrix,

$$P_i = D_i K_i, \tag{6.1}$$

where P_i is the permeability to solute *i*, D_i is the diffusivity to solute *i*, and K_i is the solubility to solute *i,* for EtOH [8,43] or a carboxylate anion (OFm^- or OAc^- [44,45]) in single and co-transport between EtOH and a carboxylate (EtOH-KOFm, EtOH-KOAc, EtOH-NaOFm, and EtOH-NaOAc. Ultimately, we analyze and discuss the observed multi-solute transport behavior in these AEMs, which will allow more target-specific design of membranes for CO_2 reduction cells.

6.2. Results and Discussion

A charge-neutral film (A0) and three positively-charged AEMs (A8, A12, and AMVN; see Fig. 6.3 for photos) were prepared as shown in the Table 6.1 (see 3.2.1. for synthesis) to investigate the effect of polymer-bound QA^+ on OFm^--containing salts (KOFm and NaOFm) and OAc^--containing salts (KOAc and NaOAc) in single and co-transport with EtOH. To further understand this behavior, EtOH transport of all films in single and co-transport with each salt was also analyzed. Permeabilities, solubilities, and diffusivities of each solute in all films were measured. These values were then analyzed based on three parameters: (1) the charge densities of cations, Na^+ (0.14 mC/cm^2) > K^+ (0.07 mC/cm^2) [46], (2) the hydrated diameters of cations, K^+ (6.6 Å [47]) < Na^+ (7.2 Å [47]), and anions, OFm^- (5.9 Å [44]) < OAc^- (7.4 Å [44]), and the kinetic diameter of EtOH (4.5 Å [47]) (Fig. 6.4), and (3) the in-water diffusivities of cations, K^+ (2.0×10^5 cm^2/s [48]) > Na^+ (1.3×10^5 cm^2/s [48]), anions, OFm^- (1.5×10^5 cm^2/s [49]) > OAc^- (1.1×10^5 cm^2/s

[48,49]), and EtOH (1.23×10^5 cm^2/s [50]). The relative kinetic diameter and hydrated diameters are shown in Fig. 6.4.

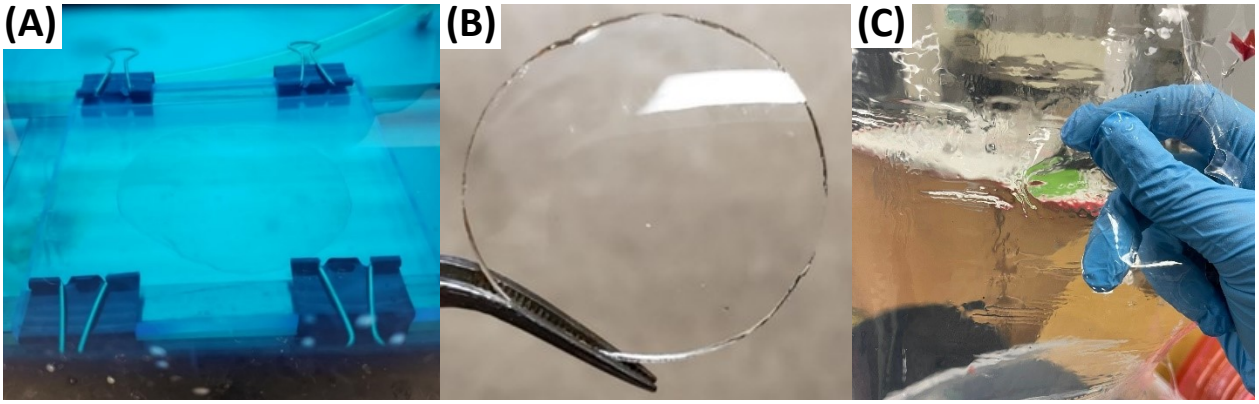

Figure 6.3. (A) Photopolymerization of a prepolymerization mixture. (B) A hydrated crosslinked film. (C) Selemion® AMVN.

Table 6.1. Membrane properties from pre-polymerization mixtures.

	APTA[1] (mol%)	PEGDA (g)	APTA (g)	Water (g)	HCPK (g)
A0	0	8.00	0.00	2.00	0.008
A8	8	7.80	0.20	2.00	0.008
A12	12	7.69	0.31	2.00	0.008

[1]APTA = mol of APTA/(mol of PEGDA + mol of APTA) × 100 %.

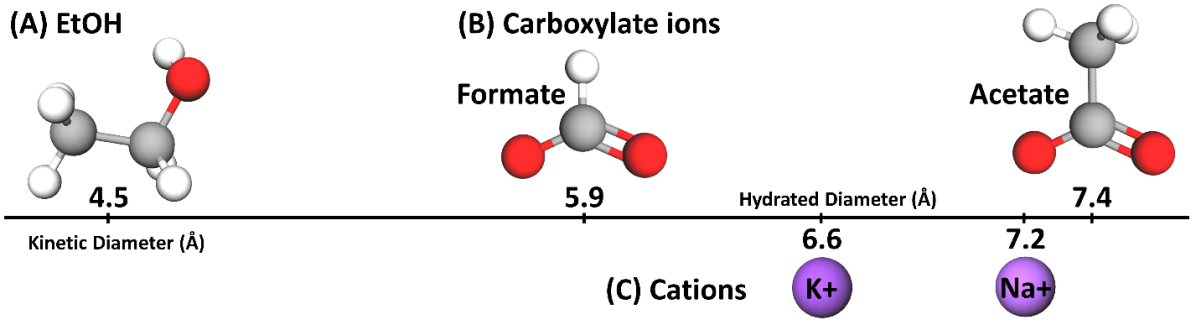

Figure 6.4. Molecular structure of (A) EtOH (4.5 Å), (B) carboxylate ions, OFm^- (5.9 Å) and OAc^- (7.4 Å) and (C) cations, K^+ (6.6 Å) and Na^+ (7.2 Å), where kinetic diameters were stated for EtOH and hydrated diameters were stated for ions. Carbons are shown in grey, oxygens are shown in red, hydrogens are shown in white, K^+ is shown in a darker purple, and Na^+ is shown in a lighter purple.

6.2.1. Water uptake, density, and water volume fraction

Water uptakes, dry polymer densities, and water volume fractions of films were measured gravimetrically with results shown in Table 6.2. Generally, water uptakes of PEGDA-based films (A0, A8, and A12) were higher than that of the PS-DVB-based film (AMVN, see Fig. 6.1 for structure) by 4 times, on average. This is due to the difference in polymer backbones, where PEGDA-based films are consisting of a hydrophilic backbone (PEG) and AMVN is consist of a hydrophobic backbone (PS-DVB). Water uptakes of A8 and A12 were higher than A0 by 3 and 6 %, respectively, for those in Cl^--form and by 13 and 22 %, respectively for those in HCO_3^--form. This is likely due to the increase in the free volume in films with decreasing crosslink density (PEGDA content) and increasing charged QA^+ content (APTA content) [19]. Generally, water uptakes of AEMs (A8, A12, and AMVN) in HCO_3^--form were higher than those in Cl^--form by 15 %, on average, analogous to prior results for QA^+-polysulfone-based AEMs reported elsewhere [15]. Here, hydration number plays a role as the hydration number of HCO_3^- (7-8 [51]) is higher than that of Cl^- (5.1-8.4 [52,53]) and, therefore, the films in HCO_3^- form are more likely to be holding more water molecules over the films in Cl^- form.

Table 6.2. Water uptake, dry polymer density, and water volume fraction of all films.

	Water uptake, ω_w (water g/dry polymer g·100%)		**Dry polymer density, ρ_p (g/mL)**		**Water volume fraction, ϕ_w**	
	Cl^-	HCO_3^-	Cl^-	HCO_3^-	Cl^-	HCO_3^-
A0	68 ± 1		1.22 ± 0.01		0.45	
A8	70 ± 0	77 ± 0	1.24 ± 0.02	1.25 ± 0.05	0.46	0.49
A12	72 ± 2	83 ± 1	1.21 ± 0.00	1.22 ± 0.01	0.46	0.50
AMVN	18 ± 1	27 ± 0	1.01 ± 0.00	1.02 ± 0.01	0.15	0.22

The dry polymer density of A0 (1.22 g/mL) is consistent with previously reported values [19,34,41]. Generally, the densities of the PEGDA-based films are higher than that of PS-DVB-

based AMVN, in part due to the difference in atomic compositions; see Table 6.2 for values. For instance, PEGDA-based films contain of ~35 % of oxygen (16 g/mol) and ~65 % of carbon (12 g/mol), whereas AMVN contains only ~5 % of oxygen and ~94 % of carbon. Moreover, densities of AEMs in HCO_3^--form are slightly higher than those in Cl^--form, which is attributed to the higher density of HCO_3^- compared to Cl^- (i.e. the densities of $KHCO_3$ and KCl are 2.17 and 1.98 g/mL, respectively).

The diffusivity of a solute in a hydrated dense membrane is often described by free volume theory, in which solute diffusion occurs through the vacant and transient space between reptating polymer chains [54,55]. To describe this behavior, Yasuda et al. assumed that all the fractional free volume (FFV) within a hydrated film would be filled with water and proposed the following equation:

$$D_i = D_{0,i} \exp\left[-A\left(\frac{1}{\phi_w} - 1\right)\right] \tag{6.2}$$

where D_i is the diffusivity of a membrane to a solute i, $D_{0,i}$ is the solute diffusivity in pure water, A is the empirical constant for each polymeric material, and ϕ_w is the water volume fraction. Therefore, Equation 6.2 predicts solute diffusivity to rapidly increases with the water volume fraction and gradually equilibriates toward the solute diffusivity in pure water ($\phi_w = 1$). Assuming the empirical constants do not differ drastically, solute diffusivities of PEGDA-based films (A0, A8, and A12) will be higher than those of AMVN due to the differences in water volume fraction; see Table 6.2, a point we will return to in our discussion of solute diffusivities calculated using the solution diffusion equation.

6.2.2. Counterion conversion, ionic conductivity, and IEC

The weight compositions carbon, oxygen, and chloride were measured from EDS elemental analysis on A8, A12, and AMVN before and after the counterion conversion; see Table 6.3 for values. Generally, the carbon and oxygen compositions of both A8 and A12 were closely matched with the theoretical compositions from the prepolymerization mixture. However, chlorine compositions were less than the theoretical values by 3 times, on average. Complete counterion conversions (Cl^- to HCO_3^-) is presumed in all AEMs (A8, A12, and AMVN) as Cl^- was not detected in EDS elemental analysis on all films after the conversion [16]; see Fig. 6.5.

Table 6.3. Weight percent (wt.%) of AEMs (A8, A12, and AMVN) in Cl^- and HCO_3^- forms.

		Measured			Theoretical*		
		C	O	Cl	C	O	Cl
Cl-form	A8	57.8 ± 0.7	41.6 ± 0.6	0.6 ± 0.1	59.9	37.8	2.3
	A12	57.7 ± 0.3	41.1 ± 0.3	1.2 ± 0.1	59.8	36.8	3.4
	AMVN	89.6 ± 0.4	6.2 ± 0.3	4.1 ± 0.1	-	-	-
HCO_3-form	A8	59.5 ± 0.2	40.5 ± 0.2	-	59.7	40.3	-
	A12	58.9 ± 0.5	41.1 ± 0.5	-	59.6	40.4	-
	AMVN	91.3 ± 0.3	8.7 ± 0.3	-	-	-	-

*Theoretical values of A8 and A12 were calculated based on the compositions in prepolymerization mixtures.

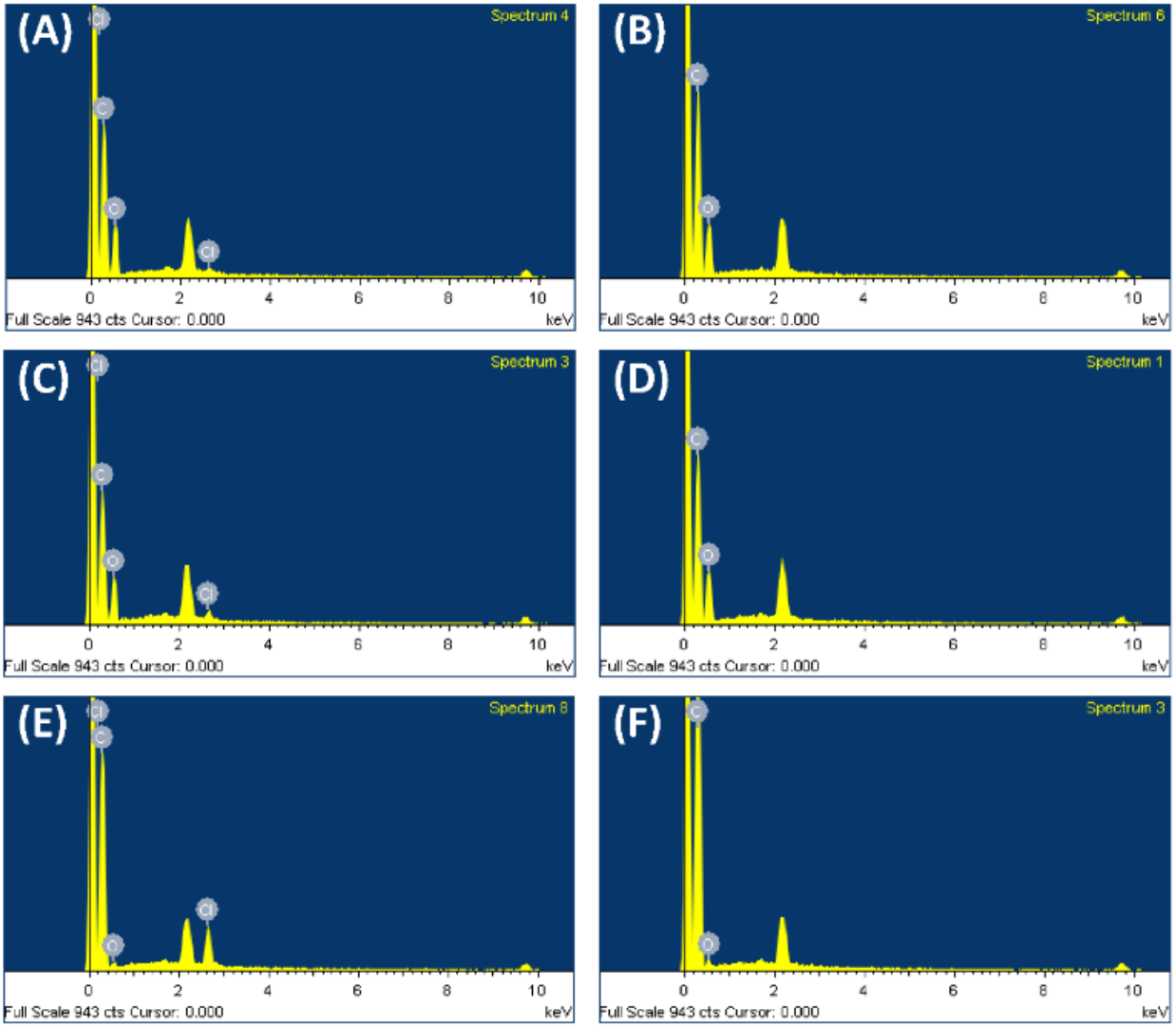

Figure 6.5. Exemplary EDS spectra for AEMs, (A,B) A8, (C,D) A12, (E,F) AMVN, in (A,C,E) Cl^- and (B,D,F) HCO_3^- forms.

The ionic conductivity (σ) and ion exchange capacity (IEC) of each AEM (A8, A12, and AMVN) were determined yielding the results shown in Table 6.4. Generally, the measured IEC for both A8 and A12 are close to that of the theoretical IEC (calculated from the composition of the prepolymerization mixture). This indicates essentially complete conversion from monomers (PEGDA and APTA) to a crosslinked film has been achieved. The IEC of AMVN (1.5 meq/g) was significantly higher than those of PEGDA-based films by an order of magnitude, such that

considerably more interactions between bound QA^+ and mobile species (K^+, Na^+, OFm^-, OAc^-, and EtOH) are expected for AMVN. Consequently, the ionic conductivity of AMVN is also greater than A8 and A12; by 6 times, on average.

Table 6.4. Water uptake, dry polymer density, and water volume fraction of all films.

	Ionic conductivity (σ, mS/cm)		**IEC (meq/g dry polymer)**	
	Cl^-	HCO_3^-	Cl^-	HCO_3^-
A8	1.0 ± 0.0	0.9 ± 0.0	0.121	0.125 ± 0.004
A12	1.2 ± 0.0	0.8 ± 0.0	0.187	0.190 ± 0.001
AMVN	7.0 ± 0.0	4.1 ± 0.0	1.5[1]	-

[1]Reported by the manufacturer

Ionic conductivities of the AEMs in HCO_3^--form were less than those in Cl^--form by 1.4 times, on average [16]. Ionic conductivities of films in both Cl^-- and HCO_3^--form are plotted in a function of inverse water volume in Fig. 6.6 along with the upper bound regression line for a series of Selemion® AMV and ImPPO-χ AEMs [16]. While conductivities of AMVN are within the range of other AEMs (Selemion® AMV and ImPPO-χ [16]), the conductivities of both A8 and A12 are less than their expected conductivity for their respective water volume fractions. This indicates the transport behavior in A8 and A12 is expected to be closer to hydrated dense membranes (i.e. A0) over the state-of-the-art AEMs (i.e. AMVN, Selemion® AMV and ImPPO-χ).

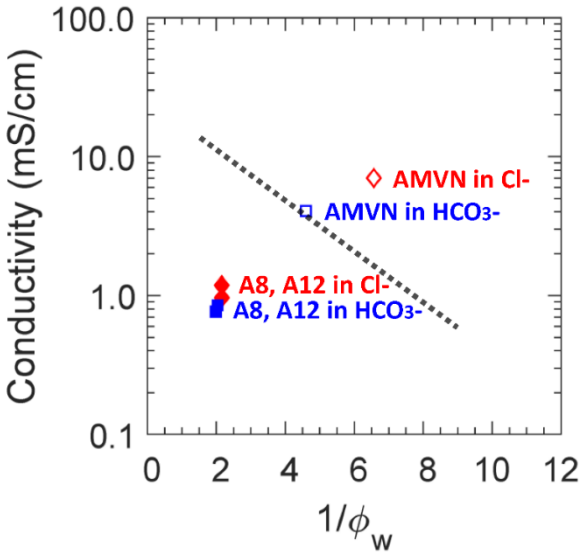

Figure 6.6. Ionic conductivity as a function of inverse water volume fraction for A8, A12 (filled markers) and AMVN (empty markers) in Cl^- (diamonds, ◇) and in HCO_3^- (squares, □). The line is a regression on a series of ImPPO-χ AEMs and Selemion® AMV from a literature [16].

6.2.3. Permeation

One-component permeabilities to EtOH and carboxylate salts (KOFm, NaOFm, KOAc, and NaOAc) of a charge-neutral A0 and positively charged A8, A12, and AMVN films in HCO_3^--forms are shown in Fig. 6.7, where (A) and (B) are scaled differently. Generally, the thickness of AMVN films after permeation was essentially the same (all within 5 %) and those of PEGDA-based films were slightly decreased (7-17 %) with increasing APTA content; see Table 6.5. Permeabilities across all films were increased with increasing water volume fraction, showing similar results to those reported elsewhere [16,21,35,41]. This is primarily due to increased diffusion, where solute diffusivities tend to increase with increasing water volume fraction (i.e. free volume theory [54,55]); will be discussed further in the diffusion section. For all films, salt permeabilities are in the order of KOFm > NaOFm > KOAc > NaOAc indicating the primary discrimination is the size difference between the two carboxylate anions, OFm^- (5.9 Å) < OAc^- (7.4 Å) followed by the difference between the two cations, K^+ (6.6 Å) < Na^+ (7.2 Å), see Fig. 6.4.

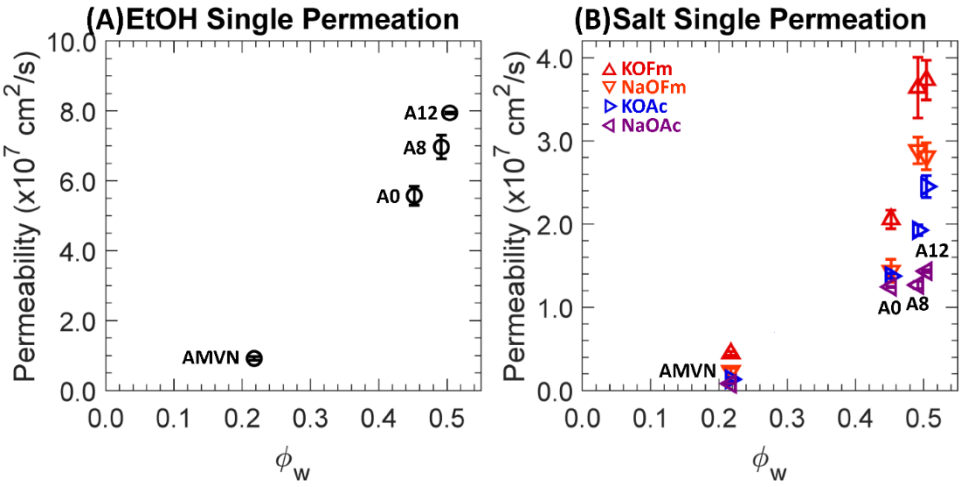

Figure 6.7. (A) Permeabilities to EtOH, ○, in single permeation. (B) Permeabilities to KOFm (△, red), NaOFm (▽, orange), KOAc (▷, blue) and NaOAc (◁, purple) in single permeation. Each data point is the average of 3 experiments with error bars corresponding to the standard deviation.

Table 6.5. Normalized film thickness to hydrated membrane after permeability measurements.

	AMVN	A0	A8	A12
Hydrated	1.00	1.00	1.00	1.00
EtOH	1.05	0.93	0.91	0.85
KOFm	0.99	0.93	0.90	0.83
NaOFm	0.95	0.92	0.88	0.85
KOAc	1.02	0.91	0.90	0.83
NaOAc	1.05	0.93	0.89	0.83
EtOH/KOFm	1.01	0.92	0.91	0.87
EtOH/NaOFm	1.03	0.93	0.90	0.85
EtOH/KOAc	1.03	0.93	0.90	0.84
EtOH/NaOAc	1.03	0.93	0.90	0.84

Two-component permeabilities to EtOH and carboxylate salts (KOFm, NaOFm, KOAc, and NaOAc) of a charge-neutral A0 and positively-charged A8, A12, and AMVN films in HCO_3-forms are shown in Fig. 6.8, where (A) and (B) are scaled differently.

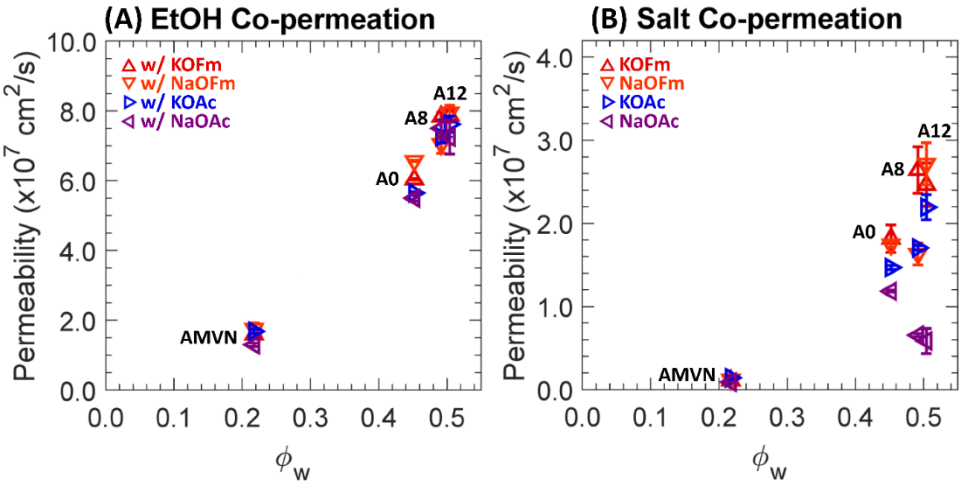

Figure 6.8. (A) Permeabilities to EtOH in co-permeation with KOFm (△, red), NaOFm (▽, orange), KOAc (▷, blue) and NaOAc (◁, purple). (B) Permeabilities to KOFm (△, red), NaOFm (▽, orange), KOAc (▷, blue) and NaOAc (◁, purple) in co-permeation with EtOH. Each data point is the average of 3 experiments with error bars corresponding to the standard deviation.

In co-permeation, permeabilities of AMVN to EtOH are increased by 1.7 times, while those of PEGDA-based films are essentially the same. This is largely due to the differences in sorption which is described below; see Fig. 6.9 and 6.10. Interestingly, QA^+-free A0 permeabilities to NaOAc and KOFm are decreased by 1.1 times, on average, in copermeation while those to NaOFm and KOAc are increased by 1.2 and 1.1 times, respectively, on average. However, QA^+-containing A8 and A12 permeabilities to NaOAc, KOFm, NaOFm, and KOAc all decrease; by 2.2, 1.4, 1.3, and 1.1 times, respectively, on average. To rationalize this behavior, we conjecture the permeation of carboxylate salts to be dependent on the polyatomic carboxylate anions over the cations. Consequently, electrostatic attraction (i.e. counterion condensation [23]) between the bound QA^+ and mobile carboxylate anions (OFm^- and OAc^-) can be suppressed by co-permeation with EtOH (i.e. charge screening [21,26,29]), see Fig. 6.2. As a result, the overall salt permeabilities of QA^+-containing A8 and A12 are decreased in co-permeation with EtOH. Similarly, AMVN permeabilities to OFm^--containing salts (KOFm and NaOFm) are decreased by 3 times, while

those to OAc^--containing salts (KOAc and NaOAc) are similar. More detail over this behavior will be discussed below in the section for diffusion; see section 6.2.5.

6.2.4. Sorption

One-component solubilities to EtOH and carboxylate salts (KOFm, KOAc, NaOFm and NaOAc) of a charge-neutral A0 and positively charged A8, A12, and AMVN films in HCO_3^--forms are shown in Fig. 6.9, where (A) and (B) are scaled differently. Generally, the volumes of AMVN films after sorption in all external solution were slightly increased (6 – 9 %), and the volumes of PEGDA-based films were essentially the same (within 3 %) or slightly increased (up to 9 %) after sorption; see Table 6.6.

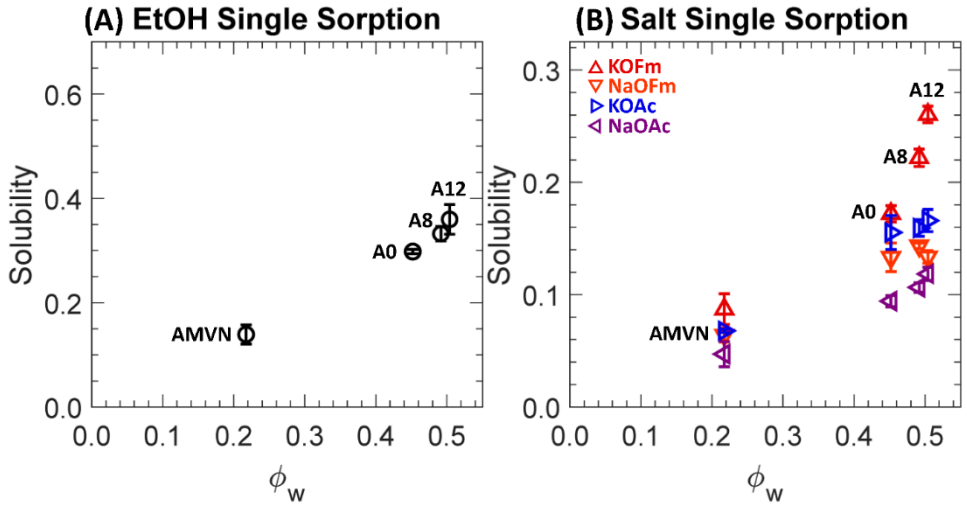

Figure 6.9. (A) Solubilities to EtOH, ○, in single sorption. (B) Solubilities to KOFm (△, red), NaOFm (▽, orange), KOAc (▷, blue) and NaOAc (◁, purple) in single sorption. Each data point is the average of 3 experiments with error bars corresponding to the standard deviation.

Table 6.6. Volume of hydrated films and volume of swollen films (mm^3) after sorption experiments measured from photographs and a digital caliper. Normalized to the volume of the hydrated films.

	A0	A8	A12	AMVN
Hydrated	1.000	1.000	1.000	1.000
EtOH	0.988	0.904	0.899	1.085
KOFm	0.976	0.926	0.926	1.081
NaOFm	0.994	0.885	0.959	1.078
KOAc	0.968	0.885	0.880	1.068
NaOAc	0.946	0.899	0.876	1.084
EtOH/KOFm	1.090	1.016	0.993	1.070
EtOH/NaOFm	1.074	0.975	0.975	1.082
EtOH/KOAc	1.022	0.980	1.005	1.093
EtOH/NaOAc	1.002	0.969	0.984	1.078

Generally, EtOH solubilities are larger than those of salt solubilities by 1.7 times, on average indicating EtOH uptake is more preferred in these films (ϕ_w: 0.2-0.5) over uptake of carboxylate salts. We observed similar behavior in a previous investigations of cation exchange membranes (CEM) [26,29,43], where the alcohol (MeOH and EtOH) solubilities were higher than the carboxylate (NaOFm and NaOAc) solubilities. However, contrary to our previous investigations of CEMs, the EtOH concentrations in the AEMs here (A0, A8, A12, and AMVN) after sorption in the external solution (1 M EtOH) is less than that of the external solution such that EtOH is less preferred in these films over the external solution; see Table 6.7.

Table 6.7. Volume fraction among the solution, EtOH (ϕ_e)-carboxylate salt (ϕ_c), inside the membranes after sorption experiments, where the remaining is the volume fraction of water (ϕ_w) from the solution.

	External, 1 M		AMVN		A0		A8		A12	
	ϕ_e	ϕ_c	ϕ_e	ϕ_c	ϕ_e	ϕ_c	ϕ_e	ϕ_c	ϕ_e	ϕ_c
1. EtOH	0.058	-	0.038	-	0.033	-	0.051	-	0.047	-
2. KOFm	-	0.044	-	0.017	-	0.016	-	0.025	-	0.025
3. NaOFm	-	0.035	-	0.010	-	0.009	-	0.014	-	0.010
4. KOAc	-	0.063	-	0.022	-	0.018	-	0.027	-	0.024
5. NaOAc	-	0.054	-	0.012	-	0.010	-	0.015	-	0.015
6. EtOH/KOFm	0.058	0.044	0.044	0.015	0.076	0.014	0.051	0.019	0.046	0.017
7. EtOH/NaOFm	0.058	0.035	0.045	0.008	0.081	0.010	0.053	0.011	0.047	0.010
8. EtOH/KOAc	0.058	0.063	0.051	0.019	0.070	0.012	0.053	0.024	0.046	0.019
9. EtOH/NaOAc	0.058	0.054	0.052	0.011	0.087	0.013	0.056	0.014	0.047	0.013

For PEGDA-based films (A0, A8, and A12), the carboxylate salt solubilities were in the order of KOFm > KOAc > NaOFm > NaOAc. This result indicates the salts with K^+ (KOFm and KOAc) are more preferred over the salts with Na^+ (NaOFm and NaOAc). A similar result was observed by Jang et al. [34], where potassium chloride (KCl) solubilities of crosslinked PEGDA films were higher than sodium chloride (NaCl) solubilities. They proposed it to be easier for K^+ ions to bind with PEG as they can directly interact with the dipole moment of ether oxygen group with absence of strong bound hydration layer due to a relatively low surface charge density (0.072 mC/cm^2), while it will be more difficult for Na^+ ions to interact with the dipole moment with strong bound hydration layer due to a relatively high surface charge density (0.142 mC/cm^2) [34]. Similarly, Sartori et al. reported the binding constant of K^+ to ethylene oxide to be higher than that of Na^+ to ethylene oxide [56]. This result also suggests the salts with OFm^- (KOFm and NaOFm) are more preferred over the salts with OAc^- (KOAc and NaOAc). A possible cause of this difference between the solubilities of OFm^- and OAc^- are the effect of molecular size, where the larger OAc^- (7.4 Å) would experience more steric hindrance from the polymer structure than smaller OFm^- (5.9 Å) (Fig. 6.3) [29,34,44,57]. For AMVN, the salt solubilities are in the order of KOFm > NaOFm > KOAc > NaOAc; the order between NaOFm and KOAc is changed. This indicates the effect of carboxylates ($OFm^- > OAc^-$) is more apparent over the effect of cations ($K^+ > Na^+$). This is likely due to the polystyrene-divinylbenzene (PS-DVB) backbone in AMVN not containing functional groups with a strong dipole moment like the ether oxygen groups in PEG; see Fig. 6.1.

Two-component solubilities to EtOH and carboxylate salts (KOFm, NaOFm, KOAc, and NaOAc) of a charge-neutral A0 and positively charged A8, A12, and AMVN films in HCO_3-forms are shown in Fig. 6.10, where (A) and (B) are scaled differently.

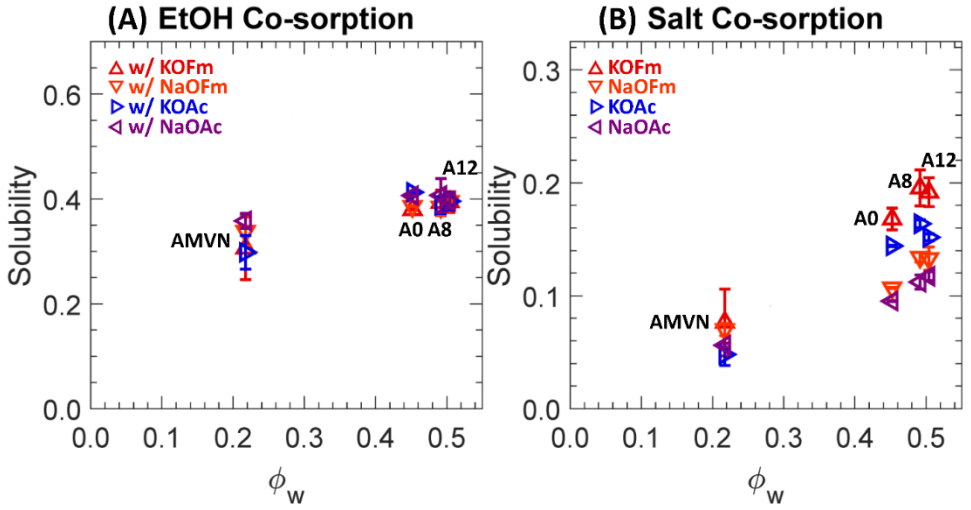

Figure 6.10. (A) Solubilities to EtOH in co-sorption with KOFm (△, red), NaOFm (▽, orange), KOAc (▷, blue) and NaOAc (◁, purple). (B) Solubilities to KOFm (△, red), NaOFm (▽, orange), KOAc (▷, blue) and NaOAc (◁, purple) in co-sorption with EtOH. Each data point is the average of 3 experiments with error bars corresponding to the standard deviation.

In co-sorption, PEGDA-based films (A0, A8, and A12) solubilities to EtOH are increased by 1.3, 1.2, and 1.1 times, on average, respectively, while those to salts are decreased by 1.1 times, on average. Again, EtOH is preferentially sorbed into PEGDA-based films over carboxylate salts in co-sorption. Our group reported similar behavior [29] for a series of crosslinked PEGDA (same as A0) and sulfonate-bearing PEGDA-based CEMs (similar to A8 and A12, but a CEM with negatively-charged sulfonate groups). For those CEMs solubilities to alcohols in co-sorption with a carboxylate salt were increased by 1.2 and 1.1 times, on average, respectively, while those to salts in co-sorption were essentially the same. A possible cause of this behavior is the difference in hydrophobicity [58]. While both EtOH and carboxylate salts are hydrophilic, as they bear an alcohol group (-OH) and charged groups (i.e. a carboxylate$^-$ and either K^+ or Na^+), respectively, the carboxylate salts are relatively more hydrophilic due to the hydration of the charge groups and, therefore, their interaction might be less preferred with a polymer structure (relatively hydrophobic).

In co-sorption, AMVN solubilities to EtOH are increased by 2.1 times, on average, while those to salts are essentially the same. This is contrary to behavior reported for CEMs [29], where solubilities of a commercial perfluorosulfonic acid (PFSA) CEM, Nafion® 117, to alcohols in co-sorption with a carboxylate salt were decreased by 1.1 times, on average. As current state-of-the-art IEMs, AMVN and Nafion® 117 share some common characteristics, such as a hydrophobic backbone (i.e. PS-DVB and PF), similar IEC (i.e. 1.5 and 0.9 meq/g), and similar water volume fraction (i.e. 0.22 and 0.25 [21]). To rationalize this difference in transport behavior between AEM and CEM, we conjecture a potential repulsive interaction between bound QA^+ and mobile EtOH in single sorption (i.e. AEM direct ethanol fuel cells, DEFC [3]), which might be interfered with by mobile carboxylate anions as they are attracted to the bound QA^+ and screen the interaction between the QA^+ and EtOH. Nevertheless, the increase in EtOH sorption in AEM is a concerning behavior for CO_2 reduction cells [8–10,12,16] and, therefore, it can be appropriate to make efforts to suppress this behavior upon design of AEMs for CO_2 reduction [7,20].

6.2.5. Diffusion

One-component diffusivities to EtOH and carboxylate salts (KOFm, KOAc, NaOFm, and NaOAc) of a charge-neutral A0 and positively charged A8, A12, and AMVN films in HCO_3-forms are calculated using the solution-diffusion relationship (Eq. 1) and the results are shown in Fig. 6.11. The Mackie-Meares model [59] was used to correlate the diffusivities with the water volume fraction of each membrane (Eq. 6.3).

$$D_i = D_{0,i}\left(\frac{\phi_w}{2-\phi_w}\right)^2 \tag{6.3}$$

where D_i is the diffusivity of a membrane to a solute i and $D_{0,i}$ is the solute diffusivity in pure water (EtOH [50]: 1.23, OFm^- [49]: 1.454, OAc^- [48,49]: 1.089, K^+ [48]: 1.957, and Na^+ [48]: 1.334 $\times 10^5$ cm^2/s) (mobility-weighted average diffusivity [60]).

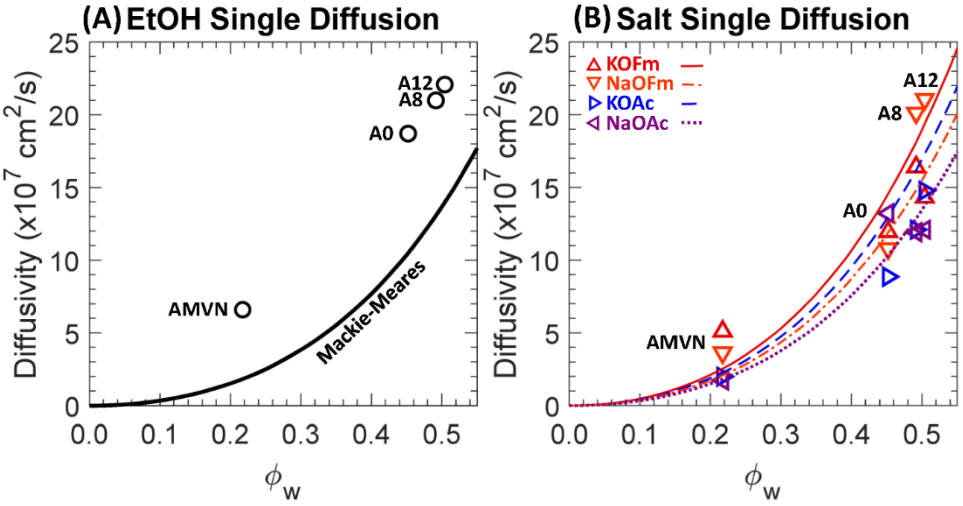

Figure 6.11. (A) Diffusivities to EtOH, ○, in single diffusion. The solid line is the Mackie-Meares' fit. (B) Diffusivities to KOFm (△, red), NaOFm (▽, orange), KOAc (▷, blue) and NaOAc (◁, purple) in single diffusion. The lines are the Mackie-Meares' fits, KOFm (solid line, red), NaOFm (dot-dashed, orange), KOAc (dashed, blue), and NaOAc (dotted, purple).

Calculated EtOH diffusivities are higher than those estimated by the Mackie-Meares model by 2.1 times, on average, showing a similar result to MeOH diffusivities reported elsewhere [35]. This under prediction of alcohol diffusivity has been observed previously and attributed to the Mackie-Meares model being initially devised for ionic species [59]. The relative difference in the calculated and the estimated diffusivities was larger in AMVN. For instance, the calculated EtOH diffusivity of AMVN was 3.6 times higher than the estimated value from the Mackie-Meares model, while those of PEGDA-based films were 1.7 times. A contribution for the significantly low estimation for AMVN is due to the inherent weakness of the model at low water volume fraction. For instance, the model implies the solutes become immobile at zero water volume fraction, which is not true as they can diffuse through the backbone structure [23,59]. Another contribution is the increase in the volume fraction of solution, ϕ_s [35]:

$$\phi_s = \frac{V_s - (W_d/\rho_p)}{V_s} \tag{6.3}$$

where W_d is the mass of the dried film, ρ_p is the density of the dry film, and V_s is the volume of the swollen film after sorption. To determine V_s, the film surface area was extracted from digital photographs and the thickness was measured using a digital caliper; see Table 6.8 for values.

Table 6.8. Water volume fractions (ϕ_w) and solution volume fractions (ϕ_s) of films after sorption experiments, where the remaining is the polymer volume fraction (ϕ_p) from the dry polymer density.

	AMVN, ϕ_s	A0, ϕ_s	A8, ϕ_s	A12, ϕ_s
Water volume fractions, ϕ_w	0.217	0.452	0.492	0.504
1. EtOH	0.245	0.452	0.382	0.446
2. KOFm	0.242	0.445	0.397	0.462
3. NaOFm	0.240	0.455	0.369	0.481
4. KOAc	0.233	0.441	0.369	0.434
5. NaOAc	0.244	0.428	0.380	0.432
6. EtOH/KOFm	0.235	0.503	0.451	0.499
7. EtOH/NaOFm	0.243	0.496	0.427	0.489
8. EtOH/KOAc	0.250	0.470	0.430	0.505
9. EtOH/NaOAc	0.240	0.460	0.424	0.494

As the solution volume fraction was higher than the water volume fraction by 1.1 times, the AMVN diffusivities can be closer to the Mackie-Meares' fit as this would constitute a rightward shift of the values on Fig. 6.11(A). The salt diffusivities are closer to the Mackie-Meares' fits; see Fig. 6.11(B).

Generally, salt diffusivities to AMVN are higher than the estimated diffusivities by 1.4 times, on average, while those to PEGDA-based films are essentially the same. Again, a contribution for the low estimation for AMVN is presumably due to the inherent weakness of the model at low water volume fraction. For AMVN, the calculated diffusivities to K^+-containing salts (KOFm and KOAc) are higher than the estimated diffusivities by 1.5 times, on average, while those to Na^+-containing salts (NaOFm and NaOAc) are higher than the estimated diffusivities by 1.4 times, on

average. The calculated diffusivities of PEGDA-based films to Na^+-containing salts are higher the estimated diffusivities by 1.1 times, on average, while those to K^+-containing salts are less than the estimated diffusivities by 1.3 times, on average.

Two-component diffusivities to EtOH and carboxylate salts (KOFm, NaOFm, KOAc, and NaOAc) of a charge-neutral A0 and positively charged A8, A12, and AMVN films in HCO_3^- forms are shown in Fig. 6.12 along with predicted diffusivities using the Mackie-Meares model.

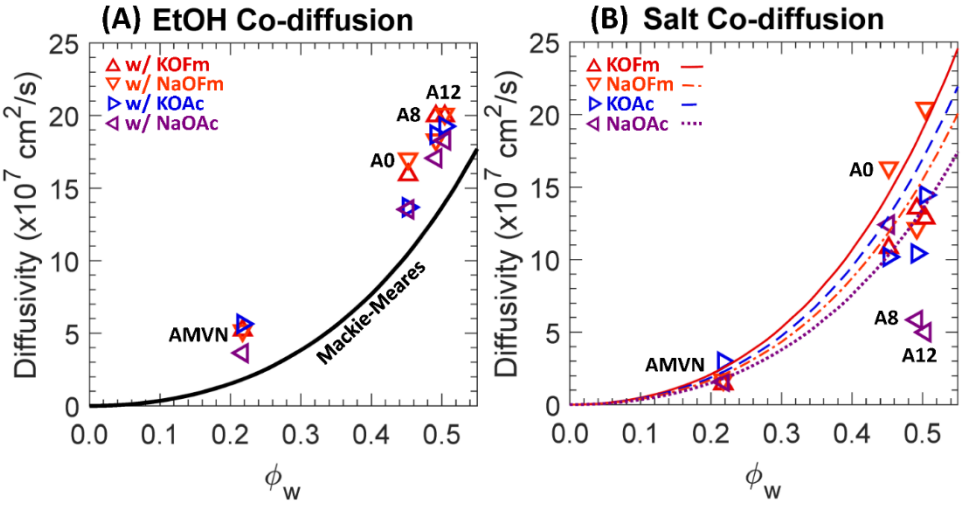

Figure 6.12. (A) Diffusivities to EtOH, ○, in co-diffusion with KOFm (△, red), NaOFm (▽, orange), KOAc (▷, blue) and NaOAc (◁, purple). The solid line is the Mackie-Meares' fit. (B) Diffusivities to KOFm (△, red), NaOFm (▽, orange), KOAc (▷, blue) and NaOAc (◁, purple) in co-diffusion with EtOH. The lines are the Mackie-Meares' fits, KOFm (solid line, red), NaOFm (dot-dashed, orange), KOAc (dashed, blue), and NaOAc (dotted, purple).

In co-diffusion, the EtOH diffusivities are decreased by 1.2 times, on average. Our group reported a similar result for CEMs (PEGDA-AMPS and Nafion® 117) [29], where both MeOH and EtOH diffusivities were decreased in co-diffusion with a carboxylate salt (either NaOFm or NaOAc). To rationalize this behavior, we conjectured there to be competitive diffusion between the co-solutes [29], and that the diffusional path of a fast-diffusing diffusant can be interfered with by a slow-diffusing co-diffusant. A similar diffusant-diffusant interaction if likely of consequence

for the EtOH diffusion with these carboxylate salts in the AEMs being studied here. For PEGDA-based films (A0, A8, and A12), the decrease in EtOH diffusivities were more apparent in co-diffusion with OAc^--containing salts (KOAc and NaOAc). While EtOH diffusivities in co-diffusion with OFm^--containing salts (KOFm and NaOFm) were decreased by 1.11 times, on average, those with OAc^--containing salts were decreased by 1.23 times, on average. The impact from the difference in carboxylate anion (as stated above) was more apparent over the impact from the difference in cation, where EtOH diffusivities in co-diffusion with K^+-containing salts (KOFm and KOAc) and Na^+-containing salts (NaOFm and NaOAc) were decreased by 1.15 and 1.18 times, on average, respectively. A possible cause is the hydrated diameter of OFm^- (5.9 Å) being significantly less than that of OAc^- (7.4 Å) and, therefore, the larger diameter anion correlates to a larger impediment to the fast-diffusing EtOH, while the difference in the hydrated diameters of K^+ (6.6 Å) and Na^+ (7.2 Å) are relatively small (Fig. 6.3). For AMVN, the impact from the difference in cation was more apparent over the impact from the difference in anion. While EtOH diffusivities in co-diffusion with K^+-containing salts were decreased by 1.39 times, on average, those with Na^+-containing salts were increased by 1.07 times, on average. EtOH diffusivities in co-diffusion with OFm^--containing salts and OAc^--containing salts were decreased by 1.13 and 1.10 times on average, respectively. To rationalize the increase of EtOH diffusivity in co-diffusion with Na^+-containing salts, we conjecture the diffusional path of EtOH being less interfered with by the salts with Na^+. As the surface charge density of Na^+ being higher than that of K^+, the electrostatic repulsion from bound QA^+ to Na^+ can be higher than that to K^+. Consequently, more salts with Na^+ might be diffusing away from the bound water region and, therefore, more EtOH can be diffusing near the bound water region that will induce less impediment to the fast-diffusing EtOH.

On the other hand, the diffusional path of EtOH and the salts with K^+ might be overlapping and, therefore, more salts can impede the EtOH diffusion.

In co-diffusion with EtOH, QA^+-free A0 (crosslinked PEGDA) diffusivities to carboxylate salts were slightly increased by 1.1 times, on average, where a similar result was reported elsewhere [29]. This behavior is partially due to flux coupling [12,25] between fast-diffusing EtOH and slow-diffusing carboxylate salts. The diffusivities of QA^+-containing AEMs (A8, A12, and AMVN) to carboxylate salts were decreased by 1.3 times, on average, in co-diffusion with EtOH. We observed an opposing behavior in sulfonate (SO_3^-)-containing CEMs [29], where the diffusivities of SO_3^--containing PEGDA-AMPS (equivalent to A8 and A12, but with SO_3^- group) and Nafion® 117 were increased by 1.4 times, on average. To rationalize this behavior, we conjectured a partial charge screening [27,28] by a co-diffusing alcohol [21,26] such that the electrostatic repulsion (Donnan exclusion [22]) between bound SO_3^- and mobile carboxylate anions (co-ions in CEM) is diminished and, therefore, the overall salt diffusivity is increased. Typically, the salt diffusion in an IEM (while maintaining the charge neutrality) is often limited by the co-ion (electrostatic repulsion) [23] and, therefore, the charge screening between the bound charge and the co-ion was in sound with the traditional understanding of salt diffusion in IEM. If the co-ion (either K^+ or Na^+) of these carboxylate salts shows a significant impact on the diffusion through AEMs, then the charge screening by alcohol might be assisting the overall salt diffusion (rather than suppressing as seen in this investigation). This leads to a conjecture that the impact of K^+ or Na^+ is not apparent and a possible contribution is a difference in the kinetic diameters of cations and carboxylate anions. As polyatomic anions, the kinetic diameters of carboxylate anions are significantly larger than those of K^+ and Na^+. These differences may impact the hydration shells of the cations (unlike those with a smaller monovalent anion, Cl^- [37]). Taken together, the

electrostatic attraction (counterion condensation theory [23,24,61]) between bound QA^+ and mobile carboxylate anions (counterions in AEM) can be dominant over cations and can be diminished through a partial charge screening by the co-diffusing EtOH and, therefore, the overall salt diffusivity is decreased as the diffusivity of condensed counterion [23] is diminished; see Fig. 6.2. Overall, these changes in interactions suggest that differences in diffusion behavior from the above-described interactions are a primary driver of changes in membrane diffusivities to carboxylate salts in single and co-diffusion with alcohols and perhaps for understanding the co-diffusion of other complex mixtures through IEMs.

6.3. Conclusion

A QA^+-free PEGDA (A0), two QA^+-containing PEGDA-APTA (A8 and A12) and Selemion® AMVN (AMVN) were investigated for their transport and co-transport behavior when challenged with carboxylate ions, EtOH, and mixtures of carboxylate ions and EtOH. Permeabilities and solubilities to EtOH or carboxylate salt (either KOFm, KOAc, NaOFm or NaOAc) were measured both by themselves and in co-transport. Solute diffusivities for each case were then calculated using the solution-diffusion model where, generally, EtOH exhibited higher solubility and diffusivity than the carboxylate salts in all films. A charge screening behavior is conjectured based on the assumption that the diffusion of a carboxylate salt is dependent on the polyatomic carboxylate anion over cation. The carboxylate salt diffusivities of AEMs (A8, A12, and AMVN) are decreased in co-diffusion with EtOH which we ascribe to the screening of electrostatic attraction by the co-diffusing EtOH (charge screening). Overall, multi-component transport in ion exchange membranes is highly complex system as various mobile components (i.e. cation, uncondensed carboxylate anions, condensed carboxylate anions, EtOH, and bulk water) are

permeating in various fixed components (i.e. QA^+, polymer backbone, and bound water) and the array of interactions between solutes and between solutes and the membrane are dynamic and complicated. Therefore, while this investigation extends our understanding of transport and co-transport behavior of select solutes (carboxylate ions and EtOH), more fundamental investigations are needed to further develop our understanding of the transport behavior of complex mixtures in polymer membranes.

6.4. References

[1] M.A. Hickner, A.M. Herring, E.B. Coughlin, Anion exchange membranes: Current status and moving forward, J Polym Sci Part B Polym Phys. 51 (2013) 1727–1735. https://doi.org/10.1002/polb.23395.

[2] G. Geise, M. Hickner, B. Logan, Ionic resistance and permselectivity tradeoffs in anion exchange membranes., Acs Appl Mater Inter. 5 (2013) 10294–301. https://doi.org/10.1021/am403207w.

[3] N. Fujiwara, Z. Siroma, S. Yamazaki, T. Ioroi, H. Senoh, K. Yasuda, Direct ethanol fuel cells using an anion exchange membrane, J Power Sources. 185 (2008) 621–626. https://doi.org/10.1016/j.jpowsour.2008.09.024.

[4] J. Yoon, D. Lee, Y.N. Lee, Y.S. Yoon, D.-J. Kim, Solid solution palladium-nickel bimetallic anode catalysts by co-sputtering for direct urea fuel cells (DUFC), J Power Sources. 431 (2019) 259–264. https://doi.org/10.1016/j.jpowsour.2019.05.059.

[5] G.Q. Chen, K. Wei, A. Hassanvand, B.D. Freeman, S.E. Kentish, Single and binary ion sorption equilibria of monovalent and divalent ions in commercial ion exchange membranes, Water Res. 175 (2020) 115681. https://doi.org/10.1016/j.watres.2020.115681.

[6] D. Li, E.J. Park, W. Zhu, Q. Shi, Y. Zhou, H. Tian, Y. Lin, A. Serov, B. Zulevi, E.D. Baca, C. Fujimoto, H.T. Chung, Y.S. Kim, Highly quaternized polystyrene ionomers for high performance anion exchange membrane water electrolysers, Nat Energy. 5 (2020) 378–385. https://doi.org/10.1038/s41560-020-0577-x.

[7] D.A. Salvatore, C.M. Gabardo, A. Reyes, C.P. O'Brien, S. Holdcroft, P. Pintauro, B. Bahar, M. Hickner, C. Bae, D. Sinton, E.H. Sargent, C.P. Berlinguette, Designing anion exchange

membranes for CO2 electrolysers, Nat Energy. (2021) 1–10. https://doi.org/10.1038/s41560-020-00761-x.

[8] B.M. Carter, B.M. Dobyns, B.S. Beckingham, D.J. Miller, Multicomponent transport of alcohols in an anion exchange membrane measured by in-situ ATR FTIR spectroscopy, Polymer. 123 (2017). https://doi.org/10.1016/j.polymer.2017.06.070.

[9] B.M. Carter, L. Keller, M. Wessling, D.J. Miller, Preparation and characterization of crosslinked poly(vinylimidazolium) anion exchange membranes for artificial photosynthesis, J Mater Chem A. (2019). https://doi.org/10.1039/c9ta00498j.

[10] M. Krödel, B.M. Carter, D. Rall, J. Lohaus, M. Wessling, D.J. Miller, Rational Design of Ion Exchange Membrane Material Properties Limits the Crossover of CO 2 Reduction Products in Artificial Photosynthesis Devices, Acs Appl Mater Inter. 12 (2020) 12030–12042. https://doi.org/10.1021/acsami.9b21415.

[11] M.R. Singh, A.T. Bell, Design of an artificial photosynthetic system for production of alcohols in high concentration from CO 2, Energ Environ Sci. 9 (2015) 193–199. https://doi.org/10.1039/c5ee02783g.

[12] D.J. Miller, F.A. Houle, Energy and Environment Series, (2018) 341–385. https://doi.org/10.1039/9781788010313-00341.

[13] A.J. Garza, A.T. Bell, M. Head-Gordon, Mechanism of CO 2 Reduction at Copper Surfaces: Pathways to C 2 Products, Acs Catal. 8 (2018) 1490–1499. https://doi.org/10.1021/acscatal.7b03477.

[14] L.-C. Weng, A.T. Bell, A.Z. Weber, Towards membrane-electrode assembly systems for CO 2 reduction: a modeling study, Energ Environ Sci. 12 (2019) 1950–1968. https://doi.org/10.1039/c9ee00909d.

[15] A. Amel, N. Gavish, L. Zhu, D.R. Dekel, M.A. Hickner, Y. Ein-Eli, Bicarbonate and chloride anion transport in anion exchange membranes, J Membrane Sci. 514 (2016) 125–134. https://doi.org/10.1016/j.memsci.2016.04.027.

[16] S.M. Dischinger, S. Gupta, B.M. Carter, D.J. Miller, Transport of Neutral and Charged Solutes in Imidazolium-Functionalized Poly(phenylene oxide) Membranes for Artificial Photosynthesis, Ind Eng Chem Res. 59 (2019) 5257–5266. https://doi.org/10.1021/acs.iecr.9b05628.

[17] M. Soltanieh, S. Sahebdelfar, Interaction effects in multicomponent separation by reverse osmosis, J Membrane Sci. 183 (2001) 15–27. https://doi.org/10.1016/s0376-7388(00)00554-8.

[18] Y. Yu, N. Yan, B.D. Freeman, C.-C. Chen, Mobile ion partitioning in ion exchange membranes immersed in saline solutions, J Membrane Sci. 620 (2020) 118760. https://doi.org/10.1016/j.memsci.2020.118760.

[19] N. Yan, D.R. Paul, B.D. Freeman, Water and ion sorption in a series of cross-linked AMPS/PEGDA hydrogel membranes, Polymer. 146 (2018) 196–208. https://doi.org/10.1016/j.polymer.2018.05.021.

[20] J.M. Kim, B.S. Beckingham, Comonomer effects on co-permeation of methanol and acetate in cation exchange membranes, Eur Polym J. (2021) 110307. https://doi.org/10.1016/j.eurpolymj.2021.110307.

[21] J.M. Kim, B.M. Dobyns, R. Zhao, B.S. Beckingham, Multicomponent transport of methanol and acetate in a series of crosslinked PEGDA-AMPS cation exchange membranes, J Membrane Sci. (2020) 118486. https://doi.org/10.1016/j.memsci.2020.118486.

[22] F.G. Helfferich, Ion Exchange, Dover, 1995.

[23] J. Kamcev, D.R. Paul, G.S. Manning, B.D. Freeman, Ion Diffusion Coefficients in Ion Exchange Membranes: Significance of Counterion Condensation, Macromolecules. 51 (2018) 5519–5529. https://doi.org/10.1021/acs.macromol.8b00645.

[24] G.S. Manning, Limiting Laws and Counterion Condensation in Polyelectrolyte Solutions I. Colligative Properties, J Chem Phys. 51 (1969) 924–933. https://doi.org/10.1063/1.1672157.

[25] K.A. Thompson, R. Mathias, D. Kim, J. Kim, N. Rangnekar, J.R. Johnson, S.J. Hoy, I. Bechis, A. Tarzia, K.E. Jelfs, B.A. McCool, A.G. Livingston, R.P. Lively, M.G. Finn, N-Aryl-linked spirocyclic polymers for membrane separations of complex hydrocarbon mixtures., Sci New York N Y. 369 (2020) 310–315. https://doi.org/10.1126/science.aba9806.

[26] B.S. Beckingham, N.A. Lynd, D.J. Miller, Monitoring multicomponent transport using in situ ATR FTIR spectroscopy, J Membrane Sci. 550 (2018). https://doi.org/10.1016/j.memsci.2017.12.072.

[27] G.M. Geise, D.R. Paul, B.D. Freeman, Fundamental water and salt transport properties of polymeric materials, Prog Polym Sci. 39 (2014) 1–42. https://doi.org/10.1016/j.progpolymsci.2013.07.001.

[28] A.E. Allegrezza, B.S. Parekh, P.L. Parise, E.J. Swiniarski, J.L. White, Chlorine resistant polysulfone reverse osmosis modules, Desalination. 64 (1987) 285–304. https://doi.org/10.1016/0011-9164(87)90103-2.

[29] J.M. Kim, B.S. Beckingham, Transport and co-transport of carboxylate ions and alcohols in cation exchange membranes, J Polym Sci. (2021). https://doi.org/10.1002/pol.20210383.

[30] J.M. Kim, Y. Lin, B. Hunter, B.S. Beckingham, Transport and Co-Transport of Carboxylate Ions and Ethanol in Anion Exchange Membranes, Polymers-Basel. 13 (2021) 2885. https://doi.org/10.3390/polym13172885.

[31] G.M. Geise, L.P. Falcon, B.D. Freeman, D.R. Paul, Sodium chloride sorption in sulfonated polymers for membrane applications, J Membrane Sci. 423 (2012) 195–208. https://doi.org/10.1016/j.memsci.2012.08.014.

[32] R.W. Baker, Membrane Technology and Applications, (2018). https://doi.org/10.1002/9781118359686.

[33] G.M. Geise, B.D. Freeman, D.R. Paul, Characterization of a sulfonated pentablock copolymer for desalination applications, Polymer. 51 (2010) 5815–5822. https://doi.org/10.1016/j.polymer.2010.09.072.

[34] E.-S. Jang, J. Kamcev, K. Kobayashi, N. Yan, R. Sujanani, T.J. Dilenschneider, H.B. Park, D.R. Paul, B.D. Freeman, Influence of water content on alkali metal chloride transport in cross-linked Poly(ethylene glycol) Diacrylate.1. Ion sorption, Polymer. 178 (2019) 121554. https://doi.org/10.1016/j.polymer.2019.121554.

[35] M. Galizia, D.R. Paul, B.D. Freeman, Liquid methanol sorption, diffusion and permeation in charged and uncharged polymers, Polymer. 102 (2016) 281–291. https://doi.org/10.1016/j.polymer.2016.09.010.

[36] K. Chang, H. Luo, G.M. Geise, Water content, relative permittivity, and ion sorption properties of polymers for membrane desalination, J Membrane Sci. 574 (2019) 24–32. https://doi.org/10.1016/j.memsci.2018.12.048.

[37] E.-S. Jang, J. Kamcev, K. Kobayashi, N. Yan, R. Sujanani, T.J. Dilenschneider, H.B. Park, D.R. Paul, B.D. Freeman, Influence of water content on alkali metal chloride transport in cross-linked Poly(ethylene glycol) diacrylate.2. Ion diffusion, Polymer. 192 (2020) 122316. https://doi.org/10.1016/j.polymer.2020.122316.

[38] G.S. Manning, Limiting Laws and Counterion Condensation in Polyelectrolyte Solutions II. Self-Diffusion of the Small Ions, J Chem Phys. 51 (1969) 934–938. https://doi.org/10.1063/1.1672158.

[39] H. Ju, A.C. Sagle, B.D. Freeman, J.I. Mardel, A.J. Hill, Characterization of sodium chloride and water transport in crosslinked poly(ethylene oxide) hydrogels, J Membrane Sci. 358 (2010) 131–141. https://doi.org/10.1016/j.memsci.2010.04.035.

[40] W.J. Horne, M.S. Shannon, J.E. Bara, Correlating fractional free volume to CO2 selectivity in [Rmim][Tf2N] ionic liquids, J Chem Thermodyn. 77 (2014) 190–196. https://doi.org/10.1016/j.jct.2014.03.012.

[41] B.M. Dobyns, J.M. Kim, B.S. Beckingham, Multicomponent transport of methanol and sodium acetate in poly(ethylene glycol) diacrylate membranes of varied fractional free volume, Eur Polym J. 134 (2020) 109809. https://doi.org/10.1016/j.eurpolymj.2020.109809.

[42] H. Lin, B.D. Freeman, S. Kalakkunnath, D.S. Kalika, Effect of copolymer composition, temperature, and carbon dioxide fugacity on pure- and mixed-gas permeability in poly(ethylene glycol)-based materials: Free volume interpretation, J Membrane Sci. 291 (2007) 131–139. https://doi.org/10.1016/j.memsci.2007.01.001.

[43] B.M. Dobyns, J.M. Kim, J. Li, Z. Jiang, B.S. Beckingham, Multicomponent transport of alcohols in Nafion 117 measured by in situ ATR FTIR spectroscopy, Polymer. (2020) 123046. https://doi.org/10.1016/j.polymer.2020.123046.

[44] R. Caminiti, P. Cucca, M. Monduzzi, G. Saba, G. Crisponi, Divalent metal–acetate complexes in concentrated aqueous solutions. An x-ray diffraction and NMR spectroscopy study, J Chem Phys. 81 (1984) 543–551. https://doi.org/10.1063/1.447336.

[45] H.M.A. Rahman, G. Hefter, R. Buchner, Hydration of Formate and Acetate Ions by Dielectric Relaxation Spectroscopy, J Phys Chem B. 116 (2011) 314–323. https://doi.org/10.1021/jp207504d.

[46] R.A. Robinson, R.H. Stokes, Electrolyte Solutions: Second Revised Edition, 2002.

[47] E.R. Nightingale, Phenomenological Theory of Ion Solvation. Effective Radii of Hydrated Ions, J Phys Chem. 63 (1959) 1381–1387. https://doi.org/10.1021/j150579a011.

[48] E.E. Hills, M.H. Abraham, A. Hersey, C.D. Bevan, Diffusion coefficients in ethanol and in water at 298K: Linear free energy relationships, Fluid Phase Equilibr. 303 (2011) 45–55. https://doi.org/10.1016/j.fluid.2011.01.002.

[49] P. Vany´sek, Ionic Conductivity and Diffusion at Infinite Dilution, CRC Handbook of Chemistry and Physics, 93rd Edition. (2012).

[50] L. Hao, D.G. Leaist, Binary Mutual Diffusion Coefficients of Aqueous Alcohols. Methanol to 1-Heptanol, J Chem Eng Data. 41 (1996) 210–213. https://doi.org/10.1021/je950222q.

[51] J.R. Rustad, S.L. Nelmes, V.E. Jackson, D.A. Dixon, Quantum-Chemical Calculations of Carbon-Isotope Fractionation in CO 2 (g), Aqueous Carbonate Species, and Carbonate Minerals, J Phys Chem. 112 (2008) 542–555. https://doi.org/10.1021/jp076103m.

[52] A. Tongraar, B.M. Rode, The hydration structures of F − and Cl − investigated by ab initio QM/MM molecular dynamics simulations, Phys Chem Chem Phys. 5 (2002) 357–362. https://doi.org/10.1039/b209240a.

[53] A. Tongraar, J. T-Thienprasert, S. Rujirawat, S. Limpijumnong, Structure of the hydrated Ca2+ and Cl − : Combined X-ray absorption measurements and QM / MM MD simulations study, Phys Chem Chem Phys. 12 (2010) 10876–10887. https://doi.org/10.1039/c0cp00136h.

[54] H. Yasuda, C.E. Lamaze, L.D. Ikenberry, Permeability of solutes through hydrated polymer membranes. Part I. Diffusion of sodium chloride, Die Makromolekulare Chemie. 118 (1968) 19–35. https://doi.org/10.1002/macp.1968.021180102.

[55] H. Yasuda, A. Peterlin, C.K. Colton, K.A. Smith, E.W. Merrill, Permeability of solutes through hydrated polymer membranes. Part III. Theoretical background for the selectivity of dialysis membranes, Die Makromolekulare Chemie. 126 (1969) 177–186. https://doi.org/10.1002/macp.1969.021260120.

[56] R. Sartori, L. Sepulveda, F. Quina, E. Lissi, E. Abuin, Binding of electrolytes to poly(ethylene oxide) in aqueous solutions, Macromolecules. 23 (1990) 3878–3881. https://doi.org/10.1021/ma00219a002.

[57] P.J. Flory, Principles of Polymer Chemistry, Cornell University Press, 1953.

[58] C.M. HANSEN, The Three Dimensional Solubility Parameter and Solvent Diffusion Coefficient, DANISH TECHNICAL PRESS, COPENHAGEN, 1967.

[59] J.S. Mackie, P. Meares, The diffusion of electrolytes in a cation-exchange resin membrane I. Theoretical, Proc Royal Soc Lond Ser Math Phys Sci. 232 (1955) 498–509. https://doi.org/10.1098/rspa.1955.0234.

[60] D.T. Hallinan, N.P. Balsara, Polymer Electrolytes, Annu Rev Mater Res. 43 (2013) 503–525. https://doi.org/10.1146/annurev-matsci-071312-121705.

[61] J. Kamcev, D.R. Paul, B.D. Freeman, Ion Activity Coefficients in Ion Exchange Polymers: Applicability of Manning's Counterion Condensation Theory, Macromolecules. 48 (2015) 8011–8024. https://doi.org/10.1021/acs.macromol.5b01654.

Chapter 7

Effect of Hydroxyl-comonomers on co-permeation in CEMs

Reproduced from: J.M. Kim, B.S. Beckingham, Comonomer effects on co-permeation of methanol and acetate in cation exchange membranes, Eur Polym J. (2021) 110307. https://doi.org/10.1016/j.eurpolymj.2021.110307.

7.1. Introduction

Dense polymeric membranes are semipermeable membranes that can promote selective transport of certain small molecules over others, leading to separation based on polymer properties such as internal morphology, hydrophobicity, ion content, etc. [1–3]. Ion exchange membranes (IEM) are a unique type of dense membranes that can provide additional selectivity toward charged ions through repulsive electrostatic interactions with their covalently attached charged moieties [4–6]. With these properties, IEMs are utilized in numerous energy applications, such as direct methanol fuel cells (DMFC [7]), vanadium redox flow battery [8], and solar fuels devices [9]. While a typical goal of IEM research is enhanced ionic conductivity at relatively low swelling [10], requirements of each application are different. For instance, one of the major membrane requirements for DMFC is the minimization of methanol (MeOH) permeation as it reduces overall performance [7,11]. Alternatively, a photoelectrochemical CO_2 reduction cell (PEC-CRC) is a solar fuels device that reduces CO_2 into valuable products, including MeOH and OAc^-, at the cathode [12,13]. A crucial membrane requirement for PEC-CRC is to minimize the permeation of CO_2 reduction products such as these from the complex mixtures of simultaneously produced reduction products [9,13–

15]. Research on CO_2 reduction catalysts for selective CO_2 reduction is an active field of research, which can be found elsewhere [16,17]. Favorably, PEC-CRC does not require membranes with high ionic conductivity as these devices can be operated at relatively low current, which creates an opportunity to trade ionic conductivity for more controlled transport behavior by manipulating the chemistry and morphology of the polymer matrix [9,13,18]. Recently, we observed analogous behavior in isotropic CEMs prepared by free radical UV photocrosslinking of poly(ethylene glycol) diacrylate (PEGDA, n = 13) and 2-acrylamido-2-methylpropane sulfonic acid (AMPS, bound anion) [19]. Previously, to rationalize this observed emergent transport behavior, we proposed a major cause for this transport behavior is the shielding of electrostatic repulsion (charge screening), where co-diffusing MeOH interfere with the electrostatic repulsion between membrane-bound sulfonates and transporting OAc^- molecules [19,20]. Here, we further investigate this multi-solute transport behavior in CEMs by modifying the internal structure of crosslinked PEGDA-AMPS membranes [19,21]. We vary the AMPS content with charge-neutral pendant comonomers of different chain lengths, namely acrylic acid (AA, $n = 0$, where n is the number of ethylene oxide repeat units [22]), 2-hydroxyethyl methacrylate (HEMA, $n = 1$), and poly(ethylene glycol) methacrylate (PEGMA, $n = 5$) [23]. Membranes are characterized for in-plane ionic conductivity and water uptake in addition to investigating the effect of comonomer chains in multi-solute transport of MeOH and OAc^- by measuring diffusive permeabilities of MeOH and OAc^- by themselves and in co-permeation.

7.2. Results and Discussion

A series of PEGDA-Comonomer and PEGDA-AMPS/Comonomer films were prepared using free radical UV photopolymerization (see Table 7.1 for compositions where all prepolymerization

mixtures contain 7.00 g of PEGDA, 2.00 g of water, and 0.01 g HCPK) and used as model membranes to investigate the effect of comonomers on solute and multi-solute transport behavior of CEMs. Water uptake, ionic conductivity, and diffusive permeabilities of PEGDA-AMPS CEMs acquired in a previous study are leveraged towards understanding the transport behavior of the membranes prepared here [19]. Each comonomer has a pendant chain with a terminal alcohol moiety, but a different number of pendant PEG repeating units, AA (carboxyl, n = 0), HEMA (ethylene oxide, n = 1), and PEGMA (poly(ethylene oxide), PEO, n = 5), impacting both the side chain length and the overall PEO content in the resulting polymer network; see Fig. 7.1 for structures. This structural variation is important to note as it influences membrane properties such as water uptake, and the probability of interactions between neighboring and other repeat units (chain-chain interactions) [19,21–23]. Moreover, variation between AMPS-to-comonomer content impacts the overall PEO and membrane-bound sulfonate content, which in turn influences the network structure, ionic conductivity, and water uptake of the membranes. We note here that as the comonomer pendant chain length of AA and HEMA are relatively short, they are less likely to interact with neighboring AMPS chains. In contrast, the considerably longer PEGMA chain is more likely to interact with neighboring AMPS repeat units, and thereby more likely to impact the electrochemical gradient inside the membrane during ionic transport through these films. Ultimately, we believe these differences in side-chain length play a key role in the observed emergent transport behavior, a point we will return to in the discussion. In the context of this varied polymer membrane chemistry and potential structural changes, we evaluate the similarities and differences in transport-related physiochemical properties and transport behavior.

Table 7.1. Membrane properties from pre-polymerization mixtures

	AMPS[a] (mol%)	Comonomer[b] (mol%)	AMPS (g)	Comonomer (g)
PEGDA-AMPS/AA	0	33	0.00	0.35
	16.5	16.5	0.50	0.17
PEGDA-AMPS/HEMA	0	33	0.00	0.63
	16.5	16.5	0.50	0.31
PEGDA-AMPS/PEGMA	0	33	0.00	1.38
	16.5	16.5	0.50	0.69
PEGDA-AMPS*	33	0	1.00	0.00

*Previously reported by Kim et al. [19]
[a]AMPS = mol of AMPS/(mol of PEGDA + mol of AMPS + mol of comonomer) × 100 %
[b]Comonomer = mol of comonomer/(mol of PEGDA + mol of AMPS + mol of comonomer) × 100 %

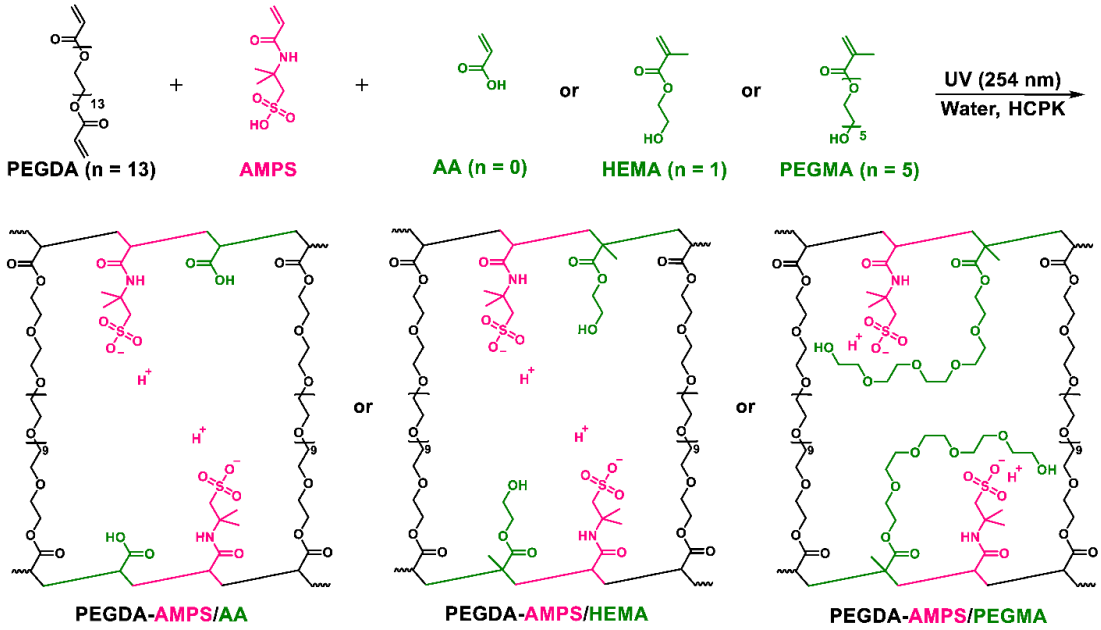

Figure 7.1. Scheme of PEGDA-AMPS/AA, PEGDA-AMPS/HEMA, and PEGDA-AMPS/PEGMA membrane polymerization via by free radical UV photopolymerization.

7.2.1. Water uptake and ionic conductivity of membranes

Membrane water uptake was measured gravimetrically with results shown in Fig. 7.2(A); see Table 7.2. Water uptakes of PEGDA-AA, PEGDA-HEMA, and PEGDA-PEGMA remained relatively constant, 69, 68, and 67 %, respectively. Similar behavior has been observed by Sagle et al., where water uptakes of PEGDA-Comonomer films prepared with different comonomers (AA, 2-

hydroxyethyl acrylate (HEA), and poly(ethylene glycol) acrylate (PEGA)) were consistent for films prepared with less than 40 mol % of comonomer content [23]. Water uptakes of PEGDA-AMPS/Comonomer films were between those of PEGDA-Comonomer and PEGDA-AMPS within the same type of comonomer and PEGDA content. This is consistent with prior work where increasing content of ionogenic groups (and likely thereby the hydrophilicity) leads to increasing water uptake and often water-solubility of the linear (non-crosslinked) polymers [24–27]. The variation among films containing different comonomers were negligible such that the amount of fractional free volume among PEGDA-Comonomer films and among PEGDA-AMPS/Comonomer films are likely similar.

The ionic conductivity of the prepared membranes was measured yielding the results shown in Fig. 7.2(B); see Table 7.2. Ionic conductivities of all PEGDA-Comonomer films which do not contain AMPS were negligible; on the order of 10^{-2} mS/cm for PEGDA-AA and 10^{-3} mS/cm for PEGDA-HEMA and PEGDA-PEGMA. Note, AA contains acidic groups, however the ionic conductivity of PEGDA-AA is negligible due to the weak acidic nature of the pendant carboxylic acid group [28]. All AMPS-containing films displayed ionic conductivities which increased with increasing AMPS content. Additionally, the ionic conductivities of PEGDA-AMPS/Comonomer films were analogous for films with the same AMPS content regardless of the comonomer, e.g. 8, 8, and 7 mS/cm with 16.5 mol% AMPS.

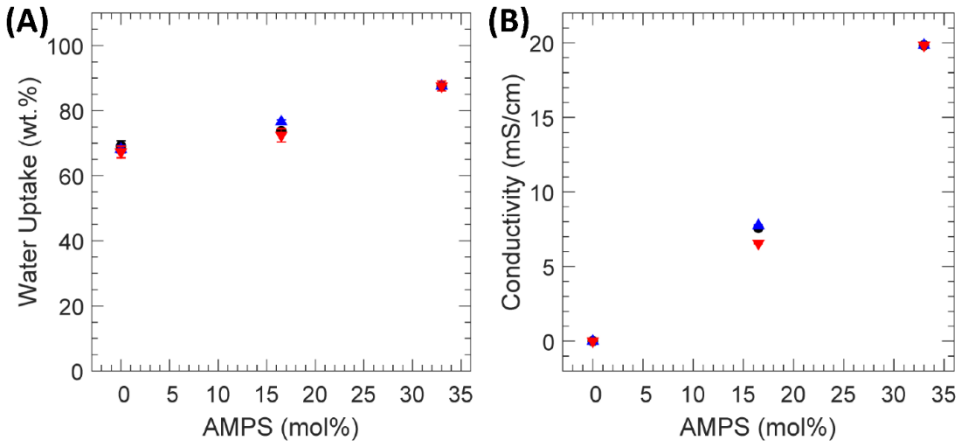

Figure 7.2. (A) Water uptake and (B) ionic conductivity of AA-containing, ●, HEMA-containing, ▲, and PEGMA-containing,▼, films. Each data point is the average of 3 membranes with error bars corresponding to the standard deviation.

Table 7.2. Water uptake and ionic conductivity of all membranes

	AMPS (mol%)	Water uptake (ω_w, g H_2O/g dry membrane ·100%)	Conductivity (σ, mS/cm)
PEGDA-AMPS/AA	0	69 ± 2	0 ± 0
	16.5	74 ± 1	8 ± 0
PEGDA-AMPS/HEMA	0	68 ± 1	0 ± 0
	16.5	77 ± 1	8 ± 0
PEGDA-AMPS/PEGMA	0	67 ± 2	0 ± 0
	16.5	72 ± 2	7 ± 0
PEGDA-AMPS	33*	88 ± 2*	20 ± 0*

*Previously reported by Kim et al.[19]

7.2.2. Single and Multi-solute Permeability

The diffusive permeabilities of all prepared membranes to MeOH and sodium acetate (NaOAc) in single and co-permeation were measured in triplicate. All permeability values are shown in Table 7.3 and Fig. 7.3. Overall, negligible membrane swelling is observed, where 16 out of 21 cases were within 2 % change in normalized film thickness; see Table 7.4. Slight deswelling (4 – 7 % change in normalized film thickness compared to in DI water) was observed for PEGDA-PEGMA films in all cases, and for PEGDA-HEMA films in NaOAc-containing transport experiments.

Table 7.3. Diffusive permeabilities of PEGDA-AMPS/Comonomer membranes to MeOH and NaOAc in single and two-solute measurements.

		Single solute in feed cell		Both solutes in feed cell	
	AMPS (mol%)	MeOH ($\times 10^{-7}$ cm^2/s)	NaOAc ($\times 10^{-7}$ cm^2/s)	MeOH ($\times 10^{-7}$ cm^2/s)	NaOAc ($\times 10^{-7}$ cm^2/s)
PEGDA-AMPS/AA	0	9.9 ± 0.0	1.2 ± 0.0	10.5 ± 0.1	1.7 ± 0.0
	16.5	14.3 ± 0.2	1.4 ± 0.0	12.6 ± 0.7	2.1 ± 0.4
PEGDA-AMPS/HEMA	0	9.8 ± 0.1	1.0 ± 0.0	9.4 ± 0.4	1.6 ± 0.2
	16.5	13.7 ± 0.2	1.2 ± 0.0	12.2 ± 0.8	2.3 ± 0.2
PEGDA-AMPS/PEGMA	0	11.2 ± 0.3	1.4 ± 0.1	11.0 ± 0.1	1.6 ± 0.1
	16.5	13.1 ± 0.5	1.4 ± 0.1	12.7 ± 0.2	1.6 ± 0.2
PEGDA-AMPS	33*	15.1 ± 0.7	1.6 ± 0.4	14.5 ± 0.7	2.0 ± 0.3

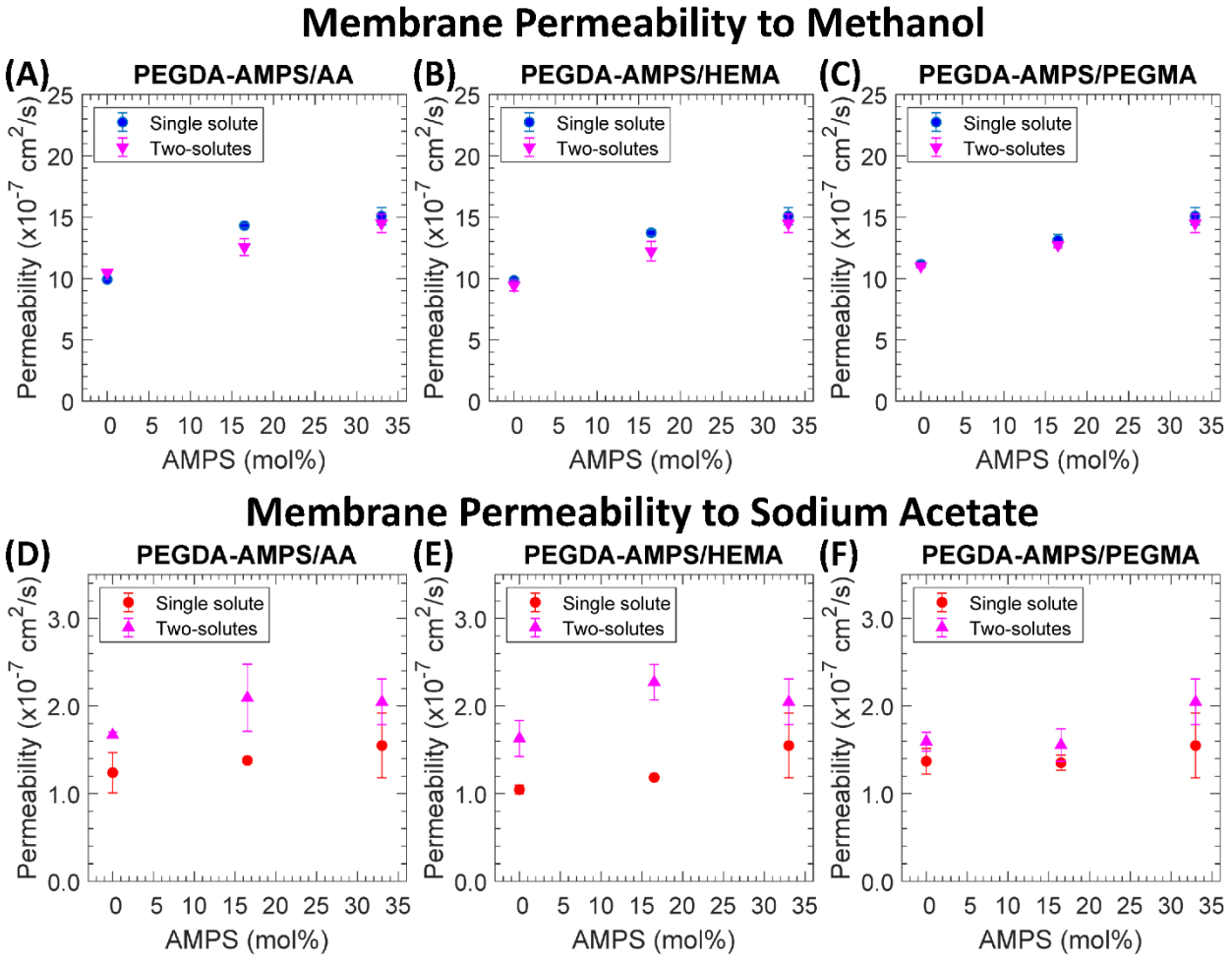

Figure 7.3. (A-C) MeOH and (D-F) NaOAc permeability in (A,D) PEGDA-AMPS/AA, (B,E) PEGDA-AMPS/HEMA, and (C,F) PEGDA-AMPS/PEGMA. Each data point is the average of 3 membranes with error bars corresponding to the standard deviation.

Table 7.4. Normalized film thickness to hydrated membrane after permeability measurements.

	AMPS			NaOAc	
	(mol%)	Water	MeOH		Both
PEGDA-AMPS/AA	0	1.00 ± 0.00	0.98 ± 0.01	1.01 ± 0.00	1.01 ± 0.02
	16.5	1.00 ± 0.00	0.98 ± 0.03	0.98 ± 0.01	0.99 ± 0.01
PEGDA-AMPS/HEMA	0	1.00 ± 0.00	0.98 ± 0.01	0.94 ± 0.01	0.96 ± 0.01
	16.5	1.00 ± 0.01	0.98 ± 0.01	0.98 ± 0.01	0.99 ± 0.01
PEGDA-AMPS/PEGMA	0	1.00 ± 0.00	0.94 ± 0.00	0.94 ± 0.01	0.93 ± 0.00
	16.5	1.00 ± 0.01	0.99 ± 0.00	1.00 ± 0.00	1.01 ± 0.01
PEGDA-AMPS	33	1.00 ± 0.01	1.00 ± 0.01	0.99 ± 0.01	1.01 ± 0.01

Generally, MeOH permeabilities were larger than NaOAc permeabilities by a factor of ~8. This behavior is partially due to diffusivity differences [7] as the kinetic diameter of MeOH (3.6 Å [29]) is smaller than the hydrated diameters of dissociated ions, such as sodium ion (7.16 Å [30]) and acetate ion (7.44 Å [31,32]). In single-component permeation, permeability to MeOH was increased with increasing AMPS content which also correlates to higher free volume within each membrane as indicated from water uptake [7]. Permeability to NaOAc also increased with increasing AMPS content and water uptake. For NaOAc this indicates the impact of increasing electrostatic repulsion between polymer-bound sulfonate anions and transporting OAc^- (which would hinder transport) was minor compared to the increased transport from higher free volume. To examine the effect of free volume on solute permeability more clearly, the coefficient of variation (CV) was calculated for the ratios of water uptake to MeOH permeability and water uptake to OAc^- permeability in single solute transport; see Table 7.5 for values.

Table 7.5. Coefficients of variation for the ratio of water uptake (%) over MeOH and NaOAc permeabilities measured by itself (10^7 cm^2/s).

	AMPS (mol%)	Water uptake (%) /Permeability to MeOH (10^7 cm^2/s)	Water uptake (%) /Permeability to NaOAc (10^7 cm^2/s)
PEGDA-AMPS/AA	0	7.0	56
	16.5	5.2	53
PEGDA-AMPS/HEMA	0	6.9	65
	16.5	5.6	65
PEGDA-AMPS/PEGMA	0	6.0	49
	16.5	5.5	54
PEGDA-AMPS	33	5.8	56
Standard deviation[a]		0.65	5.5
Coefficient of variation[b]		10.8 %	9.7 %

[a]Standard deviation (σ) = $\sqrt{\sum(x-\bar{x})^2/n}$.
[b]Coefficient of variation (%) = $\sigma \div \bar{x} \times 100$ %.

The CVs of both ratios were less than 11 %, which indicates that water uptake is closely linked with the permeation of both solutes in these films. We also examined the effect of different comonomers on solute permeabilities by calculating the CV among PEGDA-Comonomer films and among PEGDA-AMPS/Comonomer films; see Table 7.6 for values. The CV of all single component permeabilities were also small (less than 7 % except for OAc^- in PEGDA-comonomer films which was 11 %) indicating that while differences in permeability were observed based on the membrane chemistry that the overall impact of the different comonomers was generally limited (but most pronounced for the OAc^- in PEGDA-Comonomer films) in the context of deviation from the average single component permeabilities.

In co-permeation, MeOH permeabilities were consistent with single component permeabilities. To examine the relative difference in MeOH permeabilities from all films, the CV of the ratios between two component permeability over single component permeability were calculated; see Table 7.7.

Table 7.6. Coefficients of variation for diffusive permeabilities of PEGDA-Comonomer films to MeOH and NaOAc measured in single component and for PEGDA-AMPS/Comonomer films to MeOH and NaOAc measured in single component.

		Single Component		Two Component	
		MeOH ($\times 10^{-7}$ cm^2/s)	NaOAc ($\times 10^{-7}$ cm^2/s)	MeOH ($\times 10^{-7}$ cm^2/s)	NaOAc ($\times 10^{-7}$ cm^2/s)
PEGDA-Comonomer	AA	9.9 ± 0.0	1.2 ± 0.0	10.5 ± 0.1	1.7 ± 0.0
	HEMA	9.8 ± 0.1	1.0 ± 0.0	9.4 ± 0.4	1.6 ± 0.2
	PEGMA	11.2 ± 0.3	1.4 ± 0.1	11.0 ± 0.1	1.6 ± 0.1
Standard deviations[a]		0.60	0.13	0.66	0.03
Coefficient of variation[b]		5.8 %	10.9 %	6.4 %	1.9 %
PEGDA-AMPS/Comonomer	AA	14.3 ± 0.2	1.4 ± 0.0	12.6 ± 0.7	2.1 ± 0.4
	HEMA	13.7 ± 0.2	1.2 ± 0.0	12.2 ± 0.8	2.3 ± 0.2
	PEGMA	13.1 ± 0.5	1.4 ± 0.1	12.7 ± 0.2	1.6 ± 0.2
Standard deviation[a]		0.48	0.09	0.21	0.30
Coefficient of variation[b]		3.5 %	6.6 %	1.7 %	15.4 %

[a]Standard deviation (σ) = $\sqrt{\sum(x-\bar{x})^2/n}$.
[b]Coefficient of variation (%) = $\sigma \div \bar{x} \times 100$ %.

Table 7.7. Coefficients of variation for the ratios of two component permeability over single component permeability to MeOH and NaOAc.

	AMPS (mol%)	Two/Single Component Permeability to MeOH	Two/Single Component Permeability to NaOAc
PEGDA-AMPS/AA	0	1.06	1.34
	16.5	0.88	1.52
PEGDA-AMPS/HEMA	0	0.96	1.56
	16.5	0.89	1.92
PEGDA-AMPS/PEGMA	0	0.99	1.16
	16.5	0.97	1.15
PEGDA-AMPS	33	0.96	1.32
Standard deviation[a]		0.06	0.25
Coefficient of variation[b]		5.8 %	17.4 %

[a]Standard deviation (σ) = $\sqrt{\sum(x-\bar{x})^2/n}$.
[b]Coefficient of variation (%) = $\sigma \div \bar{x} \times 100$ %.

The CV of the ratios was relatively small (5.8 %), corresponding to a small effect of co-permeating OAc^- on MeOH transport. Particularly, MeOH permeabilities of PEGDA-Comonomer films (PEGDA-AA, PEGDA-HEMA, and PEGDA-PEGMA) were consistent with those measured

in single component permeation; where the differences were 6, 4, and 1 %, respectively. This indicates the presence of co-permeating NaOAc has a small-to-negligible impact on the permeation of MeOH in these AMPS-free films. Alternatively, MeOH permeabilities in PEGDA-AMPS/AA and PEGDA-AMPS/HEMA films were decreased by 14 and 12 % in co-permeation with NaOAc, indicating co-permeating NaOAc has a much larger impact on MeOH permeability in AMPS-containing films. In all cases, one possible cause of this reduced permeability is competitive transport [15,33–35], where the transport of a permeant (MeOH) may be decreased in co-permeation due to competition with other permeants (OAc^-) for the free volume necessary to perform diffusional jumps. We note, that while membrane swelling is a factor this behavior cannot be explained strictly through a swelling argument as PEGDA-AA films experienced slightly higher swelling (based on normalized film thickness, Table 7.4) with both solutes compared to solely MeOH (1.01 vs 0.98), while PEGDA-HEMA films exhibit the opposite behavior (0.96 vs 0.98). On the other hand, the difference between one- and two-component permeability to MeOH was relatively small, ~3 %, in PEGDA-AMPS/PEGMA films, which also exhibited negligible change in swelling (0.94 vs 0.93 normalized film thickness). As we noted above, the difference in co-transport behavior between PEGMA-containing films and other films may be examined and rationalized through the differing chain length of the comonomers and their impact on solutes permeating through the polymer film. The significantly longer ethylene oxide chain in PEGMA-containing films compared to AA- and HEMA-containing films, as shown in Fig. 7.1, may have more interactions with the permeants and thereby interfere with the other permeant-membrane interactions such as between permeants and the sulfonates on the AMPS chain end.

In co-permeation, NaOAc permeabilities to all films were substantially increased (15 to 92 %). To examine the relative difference in NaOAc permeabilities from all films, the CV of the

ratios between two component permeability over single component permeability were calculated; see Table 7.7. The CV of the ratios for OAc^- permeability was relatively large (17.4 %), indicating that co-permeating MeOH has a more significant impact on OAc^- permeation. One possible contribution to this behavior is assisted transport [19,20,34,36], where interactions with a fast-permeating co-permeant (MeOH) facilitates diffusional jumps of the slower permeant (OAc-) thereby increasing its observed permeability. However, this is likely not the only contributing phenomena as many other factors (hydration number of dissociated ions [37,38], feed concentration [20], degree of swelling, charge screening by alcohol [19,20], etc.) likely play a role in this transport behavior. However, we also note again that there is a distinct difference between the behavior based on the comonomer chain length. The increase in NaOAc permeabilities of membranes prepared with shorter comonomers (AA and HEMA) was higher than those of membranes prepared with PEGMA, the longest. In PEGDA-Comonomer films, the increase in NaOAc permeability in co-permeation was relatively large in PEGDA-AA and PEGDA-HEMA, 34 and 56 %, respectively, while it was relatively small in PEGDA-PEGMA, 16 %. This indicates the length of the pendant chain is likely a key factor where, for instance, a long pendant chain (PEGMA) may interfere with the assisted transport by MeOH. Similarly, the increase in NaOAc permeability in co-permeation was large in PEGDA-AMPS/AA and PEGDA-AMPS/HEMA, 52 and 92 %, respectively, while it was relatively small in PEGDA-AMPS/PEGMA, 15 %. A pictorial description of the interactions and transport within these films is shown in Fig. 7.4, where Fig 7.4(1) and Fig 7.4(3) depict OAc^- transport, Fig 7.4(2) and Fig 7.4(4) depict OAc^- and MeOH co-transport. In particular, Fig. 7.4(2) portrays how OAc^- transport could be assisted by co-permeating MeOH in absence of long pendant chains and Fig. 7.4(4) shows the effect of assisted transport being diminished by long pendant chains.

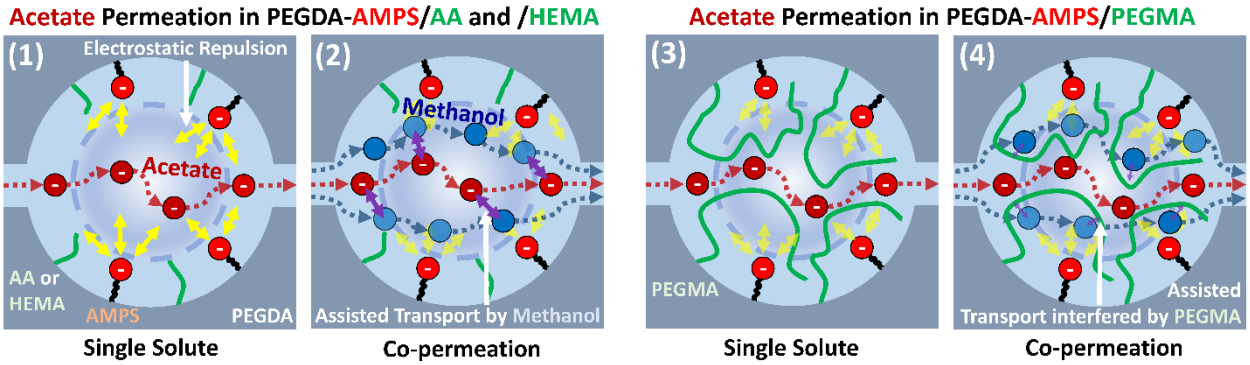

Figure 7.4. A postulated OAc^- permeation in films with (1,2) shorter comonomers, AA and HEMA, and (3,4) a longer comonomer, PEGMA, where (2) co-permeating MeOH assist OAc^- transport and (4) long PEGMA chain interfere the assisted transport.

We also examined the difference in NaOAc permeabilities in co-permeation among PEGDA-Comonomer films and among PEGDA-AMPS/Comonomer films by calculating the CVs; see Table 7.6 for values. The CV of NaOAc permeabilities in co-permeation for PEGDA-Comonomer films was small (1.9 %), while that for PEGDA-AMPS/Comonomer films was large (15.4 %) with the permeability of PEGDA-AMPS/PEGMA film being significantly less than those of PEGDA-AMPS/AA and PEGDA-AMPS/HEMA. This signifies how the effect of different comonomer was most pronounced for OAc^- transport in AMPS-containing films. Focusing on films with shorter comonomers, AA and HEMA, the increases in OAc^- permeabilities in AMPS-containing films, PEGDA-AMPS/AA and PEGDA-AMPS/HEMA, were larger than AMPS-free films, PEGDA-AA and PEGDA-HEMA. Overall, this points to a distinct link between comonomer chain length and transport behavior as the difference in one- and two-component OAc^- permeabilities of films with longer comonomer (PEGMA) are small, while those of films with shorter comonomers (AA and HEMA) are more significant. However, this is just one of many factors in manipulating transport and multicomponent transport in these and analogous films where

more investigations are needed in order to further develop our understanding of these complex transport behaviors.

7.3. Conclusion

A series of PEGDA-Comonomer and PEGDA-AMPS/Comonomer membranes with varied AMPS to comonomer content were prepared. Water uptake and ionic conductivity were measured in addition to diffusive permeabilities to MeOH and NaOAc in both single and co-permeation. Emergent co-transport behavior is observed and conjectured to both competitive and assisted transport effects that result from the combined impacts of membrane structure, species concentrations, ion hydration number, electrostatic repulsion, and swelling. The change in permeation behavior upon introduction of the co-solute was significantly reduced in PEGMA-containing films which we believe is a direct result of the longer pendant PEGMA chain interfering with the interactions between MeOH and NaOAc. While this behavior requires further study, this work highlights the role employing uncharged comonomers in IEMs can play in manipulating co-permeation behavior.

7.4. References

[1] H. Yasuda, C.E. Lamaze, L.D. Ikenberry, Permeability of solutes through hydrated polymer membranes. Part I. Diffusion of sodium chloride, Die Makromolekulare Chemie. 118 (1968) 19–35. https://doi.org/10.1002/macp.1968.021180102.

[2] H. Yasuda, A. Peterlin, C.K. Colton, K.A. Smith, E.W. Merrill, Permeability of solutes through hydrated polymer membranes. Part III. Theoretical background for the selectivity of dialysis membranes, Die Makromolekulare Chemie. 126 (1969) 177–186. https://doi.org/10.1002/macp.1969.021260120.

[3] J.G. Wijmans, R.W. Baker, The solution-diffusion model: a review, J Membrane Sci. 107 (1995) 1–21. https://doi.org/10.1016/0376-7388(95)00102-i.

[4] A. Kusoglu, A.Z. Weber, New insights into perfluorinated sulfonic-acid ionomers, Chem Rev. 117 (2017) 987–1104. https://doi.org/10.1021/acs.chemrev.6b00159.

[5] J. Kamcev, B.D. Freeman, Charged polymer membranes for environmental/energy applications, Annu Rev Chem Biomol. 7 (2015) 1–23. https://doi.org/10.1146/annurev-chembioeng-080615-033533.

[6] G. Geise, M. Hickner, B. Logan, Ionic resistance and permselectivity tradeoffs in anion exchange membranes., Acs Appl Mater Inter. 5 (2013) 10294–301. https://doi.org/10.1021/am403207w.

[7] M. Galizia, D.R. Paul, B.D. Freeman, Liquid methanol sorption, diffusion and permeation in charged and uncharged polymers, Polymer. 102 (2016) 281–291. https://doi.org/10.1016/j.polymer.2016.09.010.

[8] A.R. Crothers, R.M. Darling, D.I. Kushner, M.L. Perry, A.Z. Weber, Theory of multicomponent phenomena in cation-exchange membranes: Part III. Transport in vanadium redox-flow-battery separators, J Electrochem Soc. 167 (2020) 013549. https://doi.org/10.1149/1945-7111/ab6725.

[9] D.J. Miller, F.A. Houle, Energy and Environment Series, (2018) 341–385. https://doi.org/10.1039/9781788010313-00341.

[10] L.M. Robeson, H.H. Hwu, J.E. McGrath, Upper bound relationship for proton exchange membranes: Empirical relationship and relevance of phase separated blends, J Membrane Sci. 302 (2007) 70–77. https://doi.org/10.1016/j.memsci.2007.06.029.

[11] A. Heinzel, V.M. Barragán, A review of the state-of-the-art of the methanol crossover in direct methanol fuel cells, J Power Sources. 84 (1999) 70–74. https://doi.org/10.1016/s0378-7753(99)00302-x.

[12] M.R. Singh, A.T. Bell, Design of an artificial photosynthetic system for production of alcohols in high concentration from CO 2, Energ Environ Sci. 9 (2015) 193–199. https://doi.org/10.1039/c5ee02783g.

[13] A. Berger, R.A. Segalman, J. Newman, Material requirements for membrane separators in a water-splitting photoelectrochemical cell, Energy & Environmental Science. (2014). https://doi.org/10.1039/C3EE43807D.

[14] S.M. Dischinger, S. Gupta, B.M. Carter, D.J. Miller, Transport of neutral and charged solutes in imidazolium-functionalized poly(phenylene oxide) membranes for artificial

photosynthesis, Ind Eng Chem Res. 59 (2019) 5257–5266. https://doi.org/10.1021/acs.iecr.9b05628.

[15] B.M. Carter, B.M. Dobyns, B.S. Beckingham, D.J. Miller, Multicomponent transport of alcohols in an anion exchange membrane measured by in-situ ATR FTIR spectroscopy, Polymer. 123 (2017). https://doi.org/10.1016/j.polymer.2017.06.070.

[16] X. Nie, M.R. Esopi, M.J. Janik, A. Asthagiri, Selectivity of CO(2) reduction on copper electrodes: the role of the kinetics of elementary steps., Angewandte Chemie Int Ed Engl. 52 (2013) 2459–62. https://doi.org/10.1002/anie.201208320.

[17] A. Loiudice, P. Lobaccaro, E.A. Kamali, T. Thao, B.H. Huang, J.W. Ager, R. Buonsanti, Tailoring copper nanocrystals towards C2 Products in electrochemical CO2 reduction, Angewandte Chemie Int Ed. 55 (2016) 5789–5792. https://doi.org/10.1002/anie.201601582.

[18] M. Krödel, B.M. Carter, D. Rall, J. Lohaus, M. Wessling, D.J. Miller, Rational design of ion exchange membrane material properties limits the crossover of CO2 reduction products in artificial photosynthesis devices, Acs Appl Mater Inter. 12 (2020) 12030–12042. https://doi.org/10.1021/acsami.9b21415.

[19] J.M. Kim, B.M. Dobyns, R. Zhao, B.S. Beckingham, Multicomponent transport of methanol and acetate in a series of crosslinked PEGDA-AMPS cation exchange membranes, J Membrane Sci. (2020) 118486. https://doi.org/10.1016/j.memsci.2020.118486.

[20] B.S. Beckingham, N.A. Lynd, D.J. Miller, Monitoring multicomponent transport using in situ ATR FTIR spectroscopy, J Membrane Sci. 550 (2018). https://doi.org/10.1016/j.memsci.2017.12.072.

[21] N. Yan, D.R. Paul, B.D. Freeman, Water and ion sorption in a series of cross-linked AMPS/PEGDA hydrogel membranes, Polymer. 146 (2018) 196–208. https://doi.org/10.1016/j.polymer.2018.05.021.

[22] K. Kabiri, S. Lashani, M.J. Zohuriaan-Mehr, M. Kheirabadi, Super alcohol-absorbent gels of sulfonic acid-contained poly(acrylic acid), J Polym Res. 18 (2010) 449–458. https://doi.org/10.1007/s10965-010-9436-y.

[23] A.C. Sagle, E.M.V. Wagner, H. Ju, B.D. McCloskey, B.D. Freeman, M.M. Sharma, PEG-coated reverse osmosis membranes: Desalination properties and fouling resistance, J Membrane Sci. 340 (2009) 92–108. https://doi.org/10.1016/j.memsci.2009.05.013.

[24] F.G. Helfferich, Ion Exchange, Dover, 1995.

[25] G.M. Geise, B.D. Freeman, D.R. Paul, Characterization of a sulfonated pentablock copolymer for desalination applications, Polymer. 51 (2010) 5815–5822. https://doi.org/10.1016/j.polymer.2010.09.072.

[26] S. Lindenbaum, C.F. Jumper, G.E. Boyd, Selectivity coefficient measurements with variable capacity cation and anion exchangers, J Phys Chem. 63 (1959) 1924–1929. https://doi.org/10.1021/j150581a031.

[27] L.E. Karlsson, P. Jannasch, B. Wesslén, Preparation and solution properties of amphiphilic sulfonated acrylamide copolymers, Macromol Chem Physic. 203 (2002) 686–694. https://doi.org/10.1002/1521-3935(20020301)203:4<686::aid-macp686>3.0.co;2-c.

[28] N.A. Choudhury, A.K. Shukla, S. Sampath, S. Pitchumani, Cross-linked polymer hydrogel electrolytes for electrochemical capacitors, J Electrochem Soc. 153 (2006) A614. https://doi.org/10.1149/1.2164810.

[29] T. Borjigin, F. Sun, J. Zhang, K. Cai, H. Ren, G. Zhu, A microporous metal–organic framework with high stability for GC separation of alcohols from water, Chem Commun. 48 (2012) 7613–7615. https://doi.org/10.1039/c2cc33023g.

[30] E.R. Nightingale, Phenomenological theory of ion solvation. Effective radii of hydrated ions, J Phys Chem. 63 (1959) 1381–1387. https://doi.org/10.1021/j150579a011.

[31] R. Caminiti, P. Cucca, M. Monduzzi, G. Saba, G. Crisponi, Divalent metal–acetate complexes in concentrated aqueous solutions. An x-ray diffraction and NMR spectroscopy study, J Chem Phys. 81 (1984) 543–551. https://doi.org/10.1063/1.447336.

[32] Hitoshi. Ohtaki, Tamas. Radnai, Structure and dynamics of hydrated ions, Chem Rev. 93 (1993) 1157–1204. https://doi.org/10.1021/cr00019a014.

[33] B.M. Dobyns, J.M. Kim, J. Li, Z. Jiang, B.S. Beckingham, Multicomponent transport of alcohols in Nafion 117 measured by in situ ATR FTIR spectroscopy, Polymer. (2020) 123046. https://doi.org/10.1016/j.polymer.2020.123046.

[34] B.M. Dobyns, J.M. Kim, B.S. Beckingham, Multicomponent transport of methanol and sodium acetate in poly(ethylene glycol) diacrylate membranes of varied fractional free volume, Eur Polym J. 134 (2020) 109809. https://doi.org/10.1016/j.eurpolymj.2020.109809.

[35] B. Pan, B. Xing, Competitive and Complementary Adsorption of Bisphenol A and 17α-Ethinyl Estradiol on Carbon Nanomaterials, J Agr Food Chem. 58 (2010) 8338–8343. https://doi.org/10.1021/jf101346e.

[36] K.A. Thompson, R. Mathias, D. Kim, J. Kim, N. Rangnekar, J.R. Johnson, S.J. Hoy, I. Bechis, A. Tarzia, K.E. Jelfs, B.A. McCool, A.G. Livingston, R.P. Lively, M.G. Finn, N-Aryl-linked spirocyclic polymers for membrane separations of complex hydrocarbon mixtures., Sci New York N Y. 369 (2020) 310–315. https://doi.org/10.1126/science.aba9806.

[37] V.N. Afanas'ev, Solvation of electrolytes and nonelectrolytes in aqueous solutions, J Phys Chem B. 115 (2011) 6541–6563. https://doi.org/10.1021/jp1108834.

[38] G.M. Geise, D.R. Paul, B.D. Freeman, Fundamental water and salt transport properties of polymeric materials, Prog Polym Sci. 39 (2014) 1–42. https://doi.org/10.1016/j.progpolymsci.2013.07.001.

Chapter 8

Effect of PEGMA on co-transport in CEMs

Reproduced from: J.M. Kim, A. Mazumder, J. Li, Z. Jiang, B.S. Beckingham, Impact of PEGMA on transport and co-transport of methanol and acetate in PEGDA-AMPS cation exchange membranes, J Membrane Sci. (2021) 119950. https://doi.org/10.1016/j.memsci.2021.119950.

8.1. Introduction

Understanding multi-component transport behavior in ion exchange membranes (IEMs) is of great interest for applications such as wastewater purification (i.e. electrodialysis [1,2]), energy storage devices (i.e. vanadium redox flow batteries [3]) and artificial photosynthesis devices (i.e. photoelectrochemical CO_2 reduction cells (PEC-CRCs) [4,5]). In particular, a major interest of PEC-CRCs is to design an IEM that minimize the crossover of CO_2 reduction products dissolved in catholyte, such as alcohols (e.g. methanol (MeOH) and ethanol) and carboxylate ions (e.g. formate and acetate (OAc^-)) [4,5]. Favorably, typical artificial photosynthesis devices do not require particularly high ionic conductivity [5], which often provides a higher degree-of-freedom upon tailoring the internal structure of the polymer matrix in a way that potentially minimizes the permeation of CO_2 reduction products in multi-component permeation.

Previously, our group observed a significant increase in OAc^- permeability in co-permeation with MeOH in cation exchange membranes (CEMs), Nafion® 117 [6] and UV-crosslinked CEMs synthesized with a sulfonated monomer, 2-acrylamido-2-methylpropane sulfonic acid (AMPS) [7], and a crosslinker, poly(ethylene glycol) diacrylate (PEGDA, n = 13,

where *n* represents the number of ethylene oxide repeat units) (Chapter 4). To rationalize this transport behavior, we proposed that a major contributor to this transport behavior is the charge screening by co-permeating MeOH (Fig. 8.1(F)), where co-diffusing MeOH suppresses the electrostatic repulsion (Donnan exclusion [8]) between bound sulfonate anions and mobile OAc^- anions [6,7,9] (Chapter 5). Furthermore, we varied the AMPS content with charge-neutral comonomers with different chain lengths, acrylic acid (AA, $n = 0$), 2-hydroxyethyl methacrylate (HEMA, $n = 1$), and poly(ethylene glycol) methacrylate (PEGMA, $n = 5$) [10], where we observed increased OAc^- permeability in membranes prepared with shorter comonomers (AA and HEMA), while it was suppressed in films prepared with longer comonomer (PEGMA) (Fig. 8.1(B)) (Chapter 7).

Here, to further investigate this multi-component transport behavior in charged polymer networks, we prepare a series of PEGMA-containing films by varying the PEGMA content with AMPS to understand the effect of this longer pendant chain (PEGMA) on multi-component transport behavior. For a better understanding, we have also varied the free volume [11] at each membrane composition by varying prepolymerization water content [12–14].

A pictorial description of how the presence of pendant PEGMA and co-diffusing MeOH could be suppressing the electrostatic repulsion between bound charge groups (sulfonates, SO_3^-) and mobile OAc^- is shown in Fig. 8.1. In Fig. 8.1(A-C), the diffusion of OAc^- by itself is depicted, where the mobile OAc^- experiences electrostatic repulsion from bound SO_3^- in CEMs (Fig. 8.1(C), ion-polymer interaction) and the interaction is being screened by the pendant PEG group (Fig. 8.1(B), polymer-polymer interaction). In Fig. 8.1(D-F), the diffusion of OAc^- with MeOH is depicted, where the electrostatic repulsion is being screened by co-diffusing MeOH [6,7,9,15–17] and MeOH form a flux coupling [18] with OAc^- (Fig. 8.1(F), alcohol-polymer and ion-alcohol

interactions). Further, the ion-alcohol flux coupling is being suppressed by pendant PEG group (Fig. 8.1(D,E), ion-alcohol-polymer interaction).

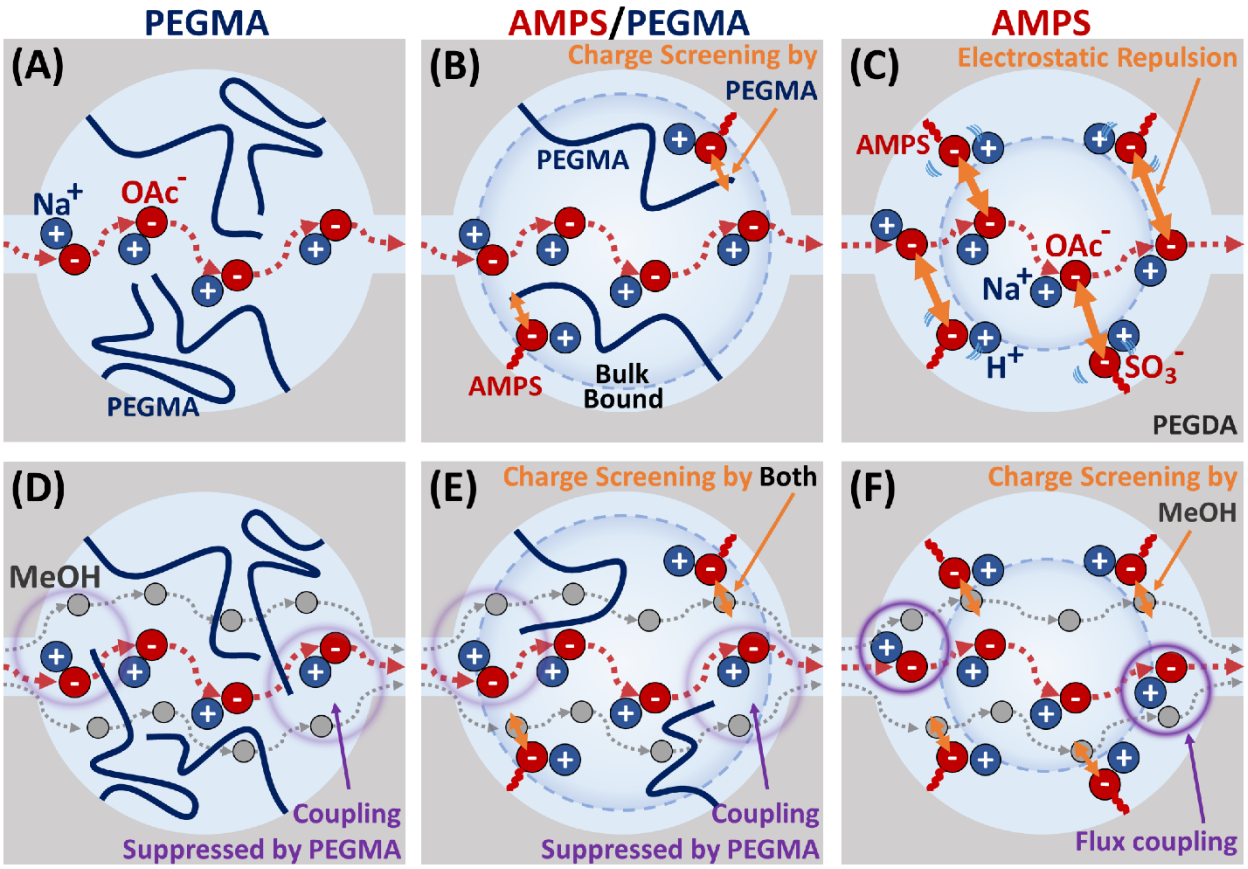

Figure 8.1. Schematic depiction of NaOAc diffusion in (A,D) PEGDA-PEGMA, (B,E) PEGDA-AMPS/PEGMA, and (C,F) PEGDA-AMPS in (A-C) single and (D-F) co-diffusion with MeOH. Figures are reprinted from [7,9,10] with permission from Elsevier.

We measure permeabilities and solubilities of these films to MeOH and NaOAc in one- and two-component experiments and calculate diffusivities based on the solution-diffusion model (Eq. 8.1) to fully capture the transport behavior of this emergent transport behavior. As a dense membrane, molecular transport in IEMs is often described by the solution-diffusion model [19], which describes the overall solute transport is dependent on the sorption into the membrane and diffusion through the fractional free volume within the polymer matrix:

$$P_i = D_i K_i \tag{8.1}$$

where P_i is the permeability to solute i, D_i is the diffusivity to solute i, and K_i is the solubility to solute i. The permeability often changes in multi-solute transport as the presence of co-solutes affect both sorption (i.e. competitive sorption [20]) and diffusion (i.e. ion hydration [21] (free volume theory [11,22]), flux coupling [9,18] and charge screening [9]). Here, the impact of a pendant PEG chain (PEGMA) on the co-transport of two CO_2 reduction products (e.g. OAc^- and MeOH) through a series of sulfonated PEGDA-AMPS-based films is studied.

8.2. Results and Discussion

A series of PEGDA-PEGMA (20, 40, 60-M), PEGDA-AMPS/PEGMA (20, 40, 60-A/M), and PEGDA-AMPS (20, 40, 60-A) films were prepared with varying water content in prepolymerization mixtures, 20, 40, and 60 wt.%, to investigate the effect of uncharged pendant comonomer, PEGMA (M), sulfonated pendant group, AMPS (A), and the free volume on solute and multi-component transport behavior; see Table 8.1 and Fig. 8.2. We evaluate the similarities and the differences in solubilities, permeabilities, and diffusivities of these polymer matrices in one- and two-component transport behavior.

Table 8.1. Membrane properties from pre-polymerization mixtures

	AMPS[a] (mol%)	PEGMA[b] (mol%)	PEGDA (g)	AMPS (g)	PEGMA (g)	Water (g)	HCPK (g)
20-M	0	32	6.71	0.00	1.29	2.00	0.008
20-A/M	16	16	6.86	0.48	0.66	2.00	0.008
20-A	32	0	7.02	0.98	0.00	2.00	0.008
40-M	0	32	5.03	0.00	0.97	4.00	0.006
40-A/M	16	16	5.15	0.36	0.49	4.00	0.006
40-A	32	0	5.27	0.73	0.00	4.00	0.006
60-M	0	32	3.35	0.00	0.65	6.00	0.004
60-A/M	16	16	3.43	0.24	0.33	6.00	0.004
60-A	32	0	3.51	0.49	0.00	6.00	0.004

[a]AMPS = mol of AMPS/(mol of PEGDA + mol of AMPS + mol of PEGMA) × 100 %
[b]PEGMA = mol of PEGMA/(mol of PEGDA + mol of AMPS + mol of PEGMA) × 100 %

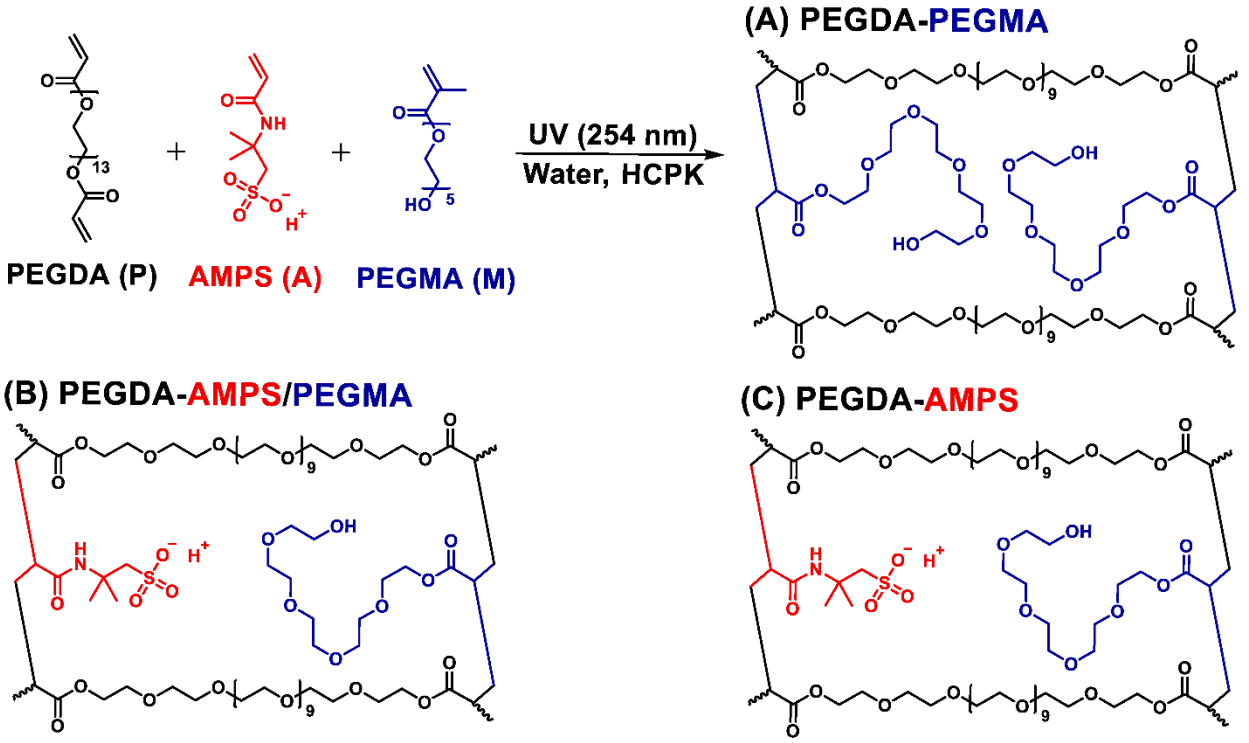

Figure 8.2. Scheme of (A) PEGDA-PEGMA (-M), (B) PEGDA-AMPS/PEGMA (-A/M), and (C) PEGDA-AMPS (-A) films.

8.2.1. Ionic conductivity, IEC, and water volume fraction

The ionic conductivity of the prepared membranes was measured yielding the results shown in Fig. 8.3(A) and Table 8.2. Ionic conductivities of all AMPS-free films (20, 40, 60-M) are zero, indicating they are not ionically conductive, as expected, due to the absence of charged moieties. The ionic conductivity of AMPS-containing films (20, 40, 60-A/M and -A) increases with increasing AMPS content. Similarly, the ion exchange capacity (IEC) of each film increases with increasing AMPS content as more counterions (H^+) are retained within the polymer matrix due to the membrane-bound sulfonates. Notably, the differences between measured and theoretical IEC

of membranes are close, where the largest difference was observed in 40-A by 8 %, as shown in Table 8.2.

The water volume fraction of all films was measured as shown in Fig. 8.3(B) and Table 8.2. Generally, the water volume fraction was increased with increasing AMPS content. This is likely due to the increase in the water content as the hydration number (λ, H_2O/ion) of the sulfonate anion (12-16 [23]) is larger than that of the pendant PEG (n = 5) group (< 10 [24]). Moreover, the water volume fraction increases with increasing prepolymerization water content (from 20 to 60 wt.%). Similar behavior has been observed by Ju et al. [25], where the water volume fraction of crosslinked PEGDA films prepared with 40 and 60 wt.% prepolymerization water content were higher than that of the films prepared with 20 wt.% by 23 and 49 %. This is presumably due to a reduction in crosslink density (as indicated from the storage modulus). Assuming the crosslinker (PEGDA) and the photoinitiator (HCPK) are fully dissolved in solvent (water), the prepolymerization mixture will become an isotropic hydrogel, where the crosslinks will be evenly dispersed through the film and, therefore, free volume elements (initially filled with water) will also be evenly dispersed.

The ionic conductivities increase with increasing water volume fractions; see Fig. 8.3(C). This is partially linked with Robeson's upper bound relationship for CEMs [26], which explains the transport of protons within the negatively-charged CEMs are limited by the amount of water within the polymer network because the free volume element (as represented by the water volume fraction) is the transport medium for protons and the films with less amount of the free volume element will allow less number of protons to transport [12,13,25,27].

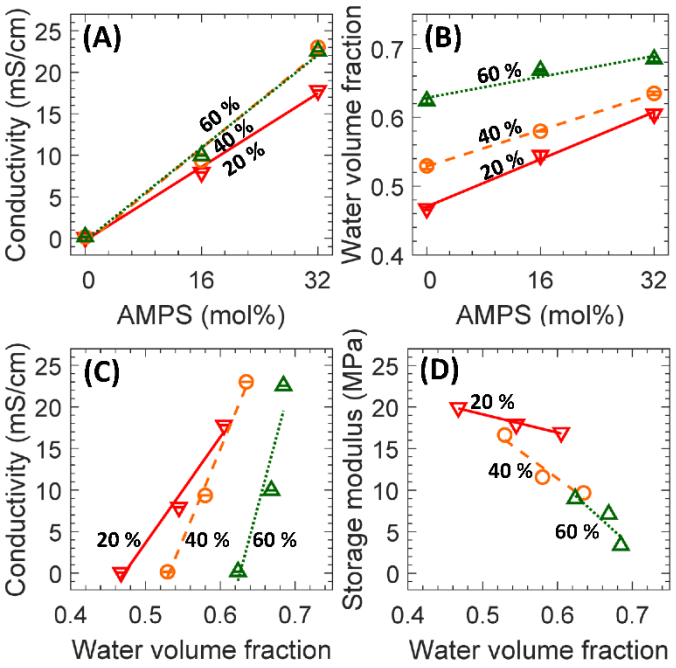

Figure 8.3. (A) Ionic conductivities and (B) water volume fractions of all films, 0 (M), 16 (A/M), and 32 mol% (-A) of AMPS content, prepared with 20 (▽, red, solid line), 40 (○, orange, dashed) and 60 wt.% (△, green, dotted) of prepolymerization water content. (C) Ionic conductivities to water volume fractions. (D) Storage modulus to water volume fractions. Each data point is the average of 3 membranes with error bars corresponding to the standard deviation. Lines are present as a guide to the eye.

Table 8.2. Ionic conductivity, ion exchange capacity, water volume fraction, storage modulus of all films.

	AMPS (mol%)	Conduc-tivity (σ, mS/cm)	Theoretical IEC (meq/g dry polymer)[a]	Measured IEC (meq/g dry polymer)	Water volume fraction	Storage modulus (MPa)
20-M	0	0 ± 0	-	-	0.467 ± 0.002	19.9
20-A/M	16	8 ± 0	0.29	0.32 ± 0.00	0.545 ± 0.006	17.9
20-A	32	18 ± 0	0.59	0.60 ± 0.01	0.605 ± 0.006	16.9
40-M	0	0 ± 0	-	-	0.529 ± 0.005	16.6
40-A/M	16	9 ± 0	0.29	0.32 ± 0.00	0.580 ± 0.000	11.6
40-A	32	23 ± 0	0.59	0.62 ± 0.00	0.635 ± 0.003	9.7
60-M	0	0 ± 0	-	-	0.624 ± 0.004	9.0
60-A/M	16	10 ± 0	0.29	0.34 ± 0.01	0.668 ± 0.002	7.1
60-A	32	23 ± 0	0.59	0.60 ± 0.01	0.685 ± 0.003	3.4

[a]Theoretical IEC = mmol of AMPS/(mass of PEGDA + mass of AMPS + mass of comonomer)

8.2.2. Dynamic mechanical analysis

The storage modulus of all films at the rubbery plateau is shown in Fig. 8.3(D) and Table 8.2. Generally, the storage modulus of the films decreases with increasing the prepolymerization water content. For instance, the storage moduli of the films prepared with 20 wt.% prepolymerization water content are higher than those of with 40 and 60 wt.% prepolymerization water content by 1.4 and 2.8 times, on average. Moreover, the storage modulus of the films decreases with increasing AMPS content. For example, the storage moduli of the films prepared without AMPS (20, 40, 60-M), is higher than those of with 16 and 32 mol% AMPS contents (20, 40, 60-A/M and -A), by 1.2 and 1.5 times, on average.

The storage modulus of a crosslinked film is a proxy to understand the crosslink density (crosslinks per unit volume, mol/cm^3) of the film [28]. For instance, Flory's rubber elasticity relationship is often utilized as a proxy to the crosslink densities, ν_e, of the films [28]:

$$\nu_e = \frac{E'}{3RT} \tag{8.2}$$

where *E'* is the storage modulus (MPa), *R* is the gas constant (8.314 cm^3 MPa/K mol), and *T* is the temperature (298.15 K). This relationship suggests the crosslink density of the films decrease with either increasing prepolymerization water content [13,25,29] or with increasing AMPS content [14,30]. Lastly, as the free volume often increases with a decreasing the crosslink density, the water volume fraction is a reasonable proxy to estimate the free volume within these films [13,25,29]; see Fig. 8.3(D).

8.2.3. Single and Multi-solute Permeability

The diffusive permeabilities of all membranes to MeOH and NaOAc in single and co-permeation were measured via diffusion cell experiments. Extracted permeability values using the Yasuda model [31,32] are shown in Table 8.3 and Fig. 8.4; where Fig. 8.4 (A) and (B) are scaled differently. Negligible membrane swelling was observed during all permeability measurements, as measured by the changes in membrane thickness; see Table 8.4.

Table 8.3. Diffusive permeabilities of PEGDA-PEGMA, PEGDA-AMPS/PEGMA, and PEGDA-AMPS membranes to MeOH and NaOAc in single and two-solute measurements.

		Single solute in feed cell		Both solutes in feed cell	
	AMPS (mol%)	MeOH ($\times 10^7$ cm^2/s)	NaOAc ($\times 10^7$ cm^2/s)	MeOH ($\times 10^7$ cm^2/s)	NaOAc ($\times 10^7$ cm^2/s)
20-M	0	11.0 ± 0.1	1.7 ± 0.0	10.5 ± 0.4	1.1 ± 0.1
20-A/M	16	12.9 ± 0.2	1.4 ± 0.0	12.3 ± 0.4	1.3 ± 0.1
20-A	32	13.6 ± 0.2	1.3 ± 0.1	12.7 ± 0.5	1.5 ± 0.1
40-M	0	17.0 ± 0.2	3.1 ± 0.2	15.6 ± 0.5	2.6 ± 0.3
40-A/M	16	18.9 ± 0.3	3.5 ± 0.1	17.0 ± 0.4	3.1 ± 0.3
40-A	32	20.3 ± 0.2	2.9 ± 0.1	18.5 ± 0.4	3.3 ± 0.1
60-M	0	27.4 ± 0.9	8.4 ± 0.1	24.0 ± 0.5	7.8 ± 0.3
60-A/M	16	30.6 ± 0.9	8.7 ± 0.2	26.8 ± 0.3	8.1 ± 0.2
60-A	32	30.7 ± 0.7	7.7 ± 0.2	27.1 ± 0.6	8.3 ± 0.3

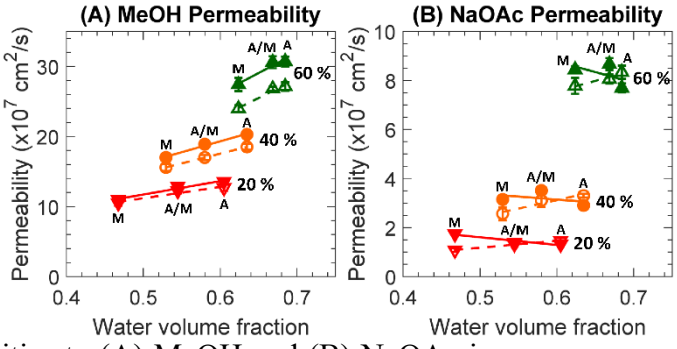

Figure 8.4. Permeabilities to (A) MeOH and (B) NaOAc in one-component, solid lines with ▼ (red), ● (orange), and ▲ (green) for 20, 40, and 60 wt.% of prepolymerization water contents, respectively, and two-component, dashed lines with ▽ (red), ○ (orange), and △ (green) for 20, 40, and 60 wt.% of prepolymerization water content, respectively. M, A/M, and A denote films prepared with 0, 16, and 32 mol% of AMPS contents, respectively. Each data point is the average of 3 experiments with error bars corresponding to the standard deviation. Lines are present as a guide to the eye.

Table 8.4. Normalized film thickness to hydrated membrane after permeability measurements.

	AMPS (mol%)	Water	MeOH	NaOAc	Both
20-M	0	1.00 ± 0.01	1.00 ± 0.00	0.99 ± 0.00	0.99 ± 0.01
20-A/M	16	1.00 ± 0.00	1.00 ± 0.01	1.01 ± 0.01	1.01 ± 0.01
20-A	32	1.00 ± 0.00	1.00 ± 0.00	1.00 ± 0.01	1.00 ± 0.00
40-M	0	1.00 ± 0.00	0.99 ± 0.01	0.97 ± 0.01	0.97 ± 0.01
40-A/M	16	1.00 ± 0.00	0.98 ± 0.00	0.98 ± 0.01	0.97 ± 0.01
40-A	32	1.00 ± 0.00	0.99 ± 0.00	0.99 ± 0.01	0.99 ± 0.00
60-M	0	1.00 ± 0.02	1.04 ± 0.04	0.96 ± 0.01	0.98 ± 0.04
60-A/M	16	1.00 ± 0.00	1.01 ± 0.00	0.99 ± 0.01	0.98 ± 0.01
60-A	32	1.00 ± 0.01	1.00 ± 0.00	0.97 ± 0.00	1.01 ± 0.00

Generally, permeabilities to MeOH were consistent with the relative water volume fraction of the corresponding membrane films [7,10,12,33], suggesting that the permeation of MeOH is strongly dependent on the free volume and less dependent on the type of pendent groups (PEGMA and/or AMPS). In co-permeation with NaOAc, MeOH permeability was decreased in all films. For instance, MeOH permeabilities of films prepared with 20, 40, and 60 wt.% water content in co-permeation were decreased by 1.05, 1.09, and 1.12 times, respectively, on average. To rationalize this behavior, we conjectured a competitive diffusion [9,10,12,17,34–36], which describes the diffusional path of a fast-diffusing solute can be interfered with by a slow-diffusing co-solute and has to move around it. Higher decreases in MeOH permeabilities of films prepared with higher prepolymerization water content (and thereby free volume) could thereby be a result of increased interaction as the permeation of NaOAc increases.

Generally, permeabilities to NaOAc were distinctly increased in films prepared with higher water contents. NaOAc permeabilities of films prepared with 40 and 60 wt.% were higher than those of films prepared with 20 wt.% water content by 1.2 and 2.2 times, respectively, on average. A contribution to these increases in NaOAc permeabilities is due to the difference in NaOAc solubilities, where the solubilities of these films were increased with the increasing

prepolymerization water content and correspondingly the water volume fractions of the film. NaOAc permeabilities were about 5 times smaller than MeOH permeabilities on average. This behavior is partially due to diffusion [33] as the kinetic diameter of MeOH (3.6 Å [37]) is smaller than the hydrated diameters of dissociated ions, such as Na^+ ion (7.16 Å [38]) and OAc^- ion (7.44 Å [39,40]).

In co-permeation, NaOAc permeabilities were increased in PEGMA-free films (20, 40, 60-A) by 1.11 times, on average, while they were decreased in PEGMA-containing films (20, 40, 60-M and -A/M) by 1.15 times on average. This increased permeability in -A films is possibly a result of the flux coupling [6,7,10,12] where the diffusion of NaOAc is facilitated by a fast-diffusing MeOH upon a flux coupling. Another contribution is the charge screening by MeOH [9], which is a conjecture that the electrostatic interaction between bound charge group and mobile ion can be suppressed by co-diffusing alcohol. However, these are likely not the only contributing phenomena as other factors (hydration number of dissociated ions [16,41], feed concentration [6], relative permittivity [42,43], etc.) can also have a role in this emergent behavior. The observed decrease in permeability of PEGMA-containing films (20, 40, 60-M and -A/M) to NaOAc in co-permeation is potentially a consequence of the flux coupling between MeOH and NaOAc being suppressed by the pendant PEO from PEGMA (solute-solute-chain interaction). Similar behavior has been observed in a previous investigation [10] where NaOAc permeabilities of films with long pendant PEO side chains were consistent in co-permeation with MeOH, while those of films with a shorter pendant group (carboxyl or ethylene oxide) were significantly increased in co-permeation. This conjected solute-solute-chain interaction in the co-permeation of NaOAc will further be discussed in the following section.

8.2.4. Single and Multi-solute Solubility

The solubilities of MeOH and NaOAc in all films are shown in Table 8.5 and Fig. 8.5. Membrane volumes were calculated before and after the sorption experiments by measuring the film thickness, the average of 5 random locations measured with a digital caliper (± 1 μm), and the area, a digital photograph coupled with ImageJ software (National Institutes of Health, MD) [30]; see Table 8.6 for values.

Table 8.5. Solubilities of PEGDA-PEGMA, PEGDA-AMPS/PEGMA, and PEGDA-AMPS membranes to MeOH and NaOAc in single and two-solute measurements.

	AMPS	Single solute		Both solutes	
	(mol%)	MeOH	NaOAc	MeOH	NaOAc
20-M	0	0.22 ± 0.05	0.11 ± 0.01	0.25 ± 0.06	0.11 ± 0.00
20-A/M	16	0.27 ± 0.02	0.10 ± 0.01	0.30 ± 0.04	0.10 ± 0.00
20-A	32	0.31 ± 0.02	0.09 ± 0.01	0.30 ± 0.02	0.09 ± 0.00
40-M	0	0.30 ± 0.02	0.19 ± 0.01	0.32 ± 0.05	0.21 ± 0.01
40-A/M	16	0.27 ± 0.04	0.16 ± 0.01	0.32 ± 0.08	0.20 ± 0.05
40-A	32	0.30 ± 0.01	0.15 ± 0.01	0.29 ± 0.00	0.15 ± 0.00
60-M	0	0.33 ± 0.08	0.31 ± 0.02	0.27 ± 0.06	0.31 ± 0.02
60-A/M	16	0.35 ± 0.01	0.31 ± 0.00	0.32 ± 0.06	0.32 ± 0.00
60-A	32	0.34 ± 0.04	0.30 ± 0.01	0.32 ± 0.03	0.30 ± 0.00

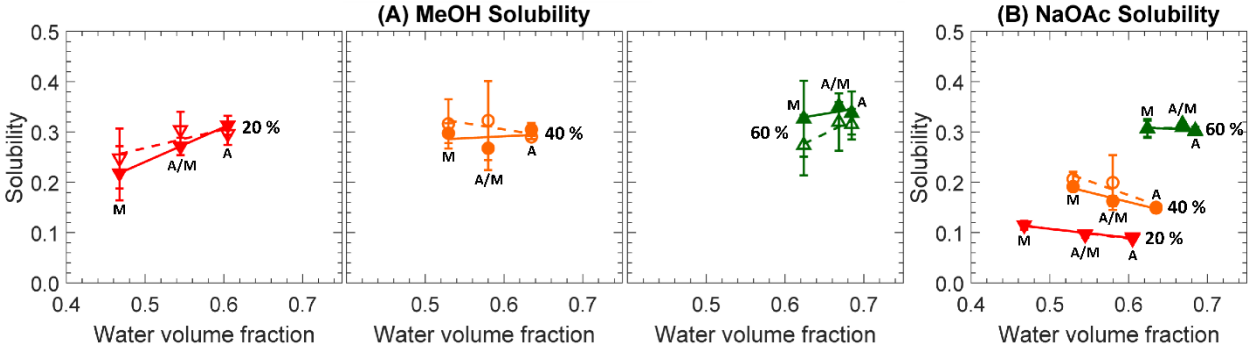

Figure 8.5. Solubilities to (A) MeOH and (B) NaOAc in one-component, solid lines with ▼ (red), ● (orange), and ▲ (green) for 20, 40, and 60 wt.% of prepolymerization water contents, respectively, and two-component, dashed lines with ▽ (red), ○ (orange), and △ (green) for 20, 40, and 60 wt.% of prepolymerization water content, respectively. M, A/M, and A denote films prepared with 0, 16, and 32 mol% of AMPS contents, respectively. Each data point is the average of 3 experiments with error bars corresponding to the standard deviation. Lines are present as a guide to the eye.

Table 8.6. Volume of swollen membranes.

	AMPS (mol%)	Water (mm^3)	1 M MeOH (mm^3)	1 M NaOAc (mm^3)	1 M each (mm^3)
20-M	0	94 ± 1	97 ± 1	89 ± 1	89 ± 0
20-A/M	16	93 ± 0	92 ± 1	82 ± 2	84 ± 0
20-A	32	90 ± 2	87 ± 1	76 ± 1	76 ± 2
40-M	0	95 ± 0	97 ± 2	90 ± 0	90 ± 2
40-A/M	16	94 ± 0	94 ± 1	85 ± 1	83 ± 2
40-A	32	89 ± 0	93 ± 1	77 ± 2	76 ± 1
60-M	0	98 ± 0	104 ± 1	94 ± 1	94 ± 1
60-A/M	16	94 ± 0	96 ± 2	87 ± 2	89 ± 1
60-A	32	88 ± 1	95 ± 1	77 ± 1	77 ± 1

While all films did not experience significant swelling or deswelling during sorption experiments to MeOH [7,33], they experienced slight deswelling during sorption experiments to NaOAc, where the degree of deswelling increases with an increase in AMPS content. For instance, the average volumetric deswelling of PEGDA-PEGMA (20, 40, 60-M), PEGDA-AMPS/PEGMA (20, 40, 60-A/M), and PEGDA-AMPS (20, 40, 60-A) films after sorption in 1 M NaOAc containing solutions were 1.05, 1.11, and 1.16 times, respectively. A possible contribution is an increase in the electrostatic repulsion between bound sulfonate anions and OAc^- with increasing sulfonate contents. For instance, the films will experience a similar osmotic pressure from the external solution (1 M NaOAc) and, therefore, a similar amount of water is expected to desorb into the external solution. However, since less OAc^- will be able to enter the internal polymer structure (electrostatic repulsion), the overall amount of free volume elements will be decreased and, consequently, the overall volume will be decreased [6,44].

In single sorption, MeOH solubilities of films generally increase with increasing water volume fraction, see Fig. 8.5(A). For instance, MeOH solubilities of the films prepared with 20 wt.% of prepolymerization water content are less than those with 40 and 60 wt.% of the prepolymerization water content by 1.08 and 1.26 times, respectively, on average. Moreover,

MeOH solubilities of films prepared without AMPS (20, 40, 60-M) are less than those with 16 (20, 40, 60-A/M) and 32 mol% of AMPS content (20, 40, 60-A) by 1.06 and 1.13 times, respectively, on average. Similar behavior has been reported by Galizia et al., where they observed MeOH solubilities (Sorption solutions: 0.1-12 M) of crosslinked PEGDA films (prepared with 0, 20, and 60 wt.% of prepolymerization water contents) to be increased with increasing water content [33]. This indicates the MeOH-polymer interaction is less favorable than the MeOH-water interaction in sorption.

We observe a different behavior in co-sorption with NaOAc, where MeOH solubilities of the films prepared with 20 wt.% of prepolymerization water content are less than those with 40 and 60 wt.% of prepolymerization water content by 1.09 times and 1.07 times, respectively, on average. Also, MeOH solubilities of the films prepared in absence of AMPS are less than those with 16 and 32 mol% of AMPS content by 1.13 and 1.08 times, respectively, on average. This indicates the MeOH-polymer interaction is less apparent in co-sorption.

In single sorption, NaOAc solubilities of films generally increase with increasing prepolymerization water content, where films prepared with 20 wt.% of prepolymerization water content are less than those with 40 and 60 wt.% prepolymerization water content by 1.67 and 3.04 times, respectively, on average. Similar behavior has been reported by Jang et al. [45], where they observed solubilities (for sorption solutions of 0.01-1 M) of crosslinked PEGDA films (prepared with 0, 20, and 40 wt.% of prepolymerization water contents) to various salts (i.e. NaCl, KCl, and LiCl) to increase with increasing water content. This indicates the NaOAc-polymer interaction is less favorable than the NaOAc-water interaction in sorption. On the other hand, NaOAc solubilities of films are generally decreased with increasing AMPS content, where films prepared without AMPS have higher solubilities than those with 16 and 32 mol% of the AMPS content by 1.08 and

1.13 times, respectively, on average. Similar behavior has been reported by Yan et al, where they observed the solubilities (for sorption solutions of 0.01-1 M) of crosslinked PEGDA-AMPS films (prepared by varying PEGDA to AMPS ratio at a constant prepolymerization water content, 25 wt.%) to NaCl to decrease with increasing AMPS content [30]. This indicates the NaOAc-polymer interaction is significant, as the electrostatic repulsion (Donnan exclusion [8]) between bound sulfonate anions (AMPS) and mobile acetate anions (OAc^-) is considerable. The effect of electrostatic interactions between a negatively-charge ion (chloride) and a charged segment (sulfonate) in crosslinked PEGDA-AMPS membranes has also been investigated by Yu et al. [46], where they found the increasing electrostatic interactions in strongly charged membranes, such as those examined herein, led to decreased chloride solubility. For very strongly charged membranes both the ideal Donnan equilibrium model [8] and Manning's limiting law [47] were able to capture this behavior, while a polyelectrolyte non-random two-liquid (NRTL) model [48], which included both long-range electrostatic interactions (polyion-ion and ion-ion) and short-range interactions [49], was better able to capture the behavior across varied membrane charge content and external solution salt content. The reduced solubility of OAc^- in the AMPS-containing films (20, 40, 60-A and-A/M) is thereby attributable to the analogous electrostatic interactions between the negatively-charged OAc^- and bound sulfonate.

We observe similar behavior in co-sorption with MeOH, where NaOAc solubilities of the films prepared with 20 wt.% of prepolymerization water content are less than those with 40 and 60 wt.% of prepolymerization water content by 1.85 times and 3.07 times, respectively, on average. Also, NaOAc solubilities of the films prepared in absence of AMPS was higher than those with 16 and 32 mol% of AMPS content by 1.02 and 1.17 times, respectively, on average. This is an indication that MeOH has a negligible impact on the NaOAc-polymer interaction in sorption.

8.2.5. Single and Multi-solute Diffusivity

The diffusivities of all prepared membranes to MeOH and NaOAc in single and co-diffusion are calculated using Eq. (8.1), dividing measured permeabilities by measured solubility. Calculated diffusivities are shown in Table 8.7 and Fig. 8.8; where Fig. 8.8(A) and (B) are scaled differently. The Mackie-Meares model [50] was used to estimate the MeOH and NaOAc diffusivities in these films, which states:

$$D_i = D_{o,i}\left(\frac{\phi_w}{2-\phi_w}\right)^2 \tag{8.3}$$

where D_i is the diffusivity of a membrane to solute i, ϕ_w is the water volume fraction, and $D_{0,i}$ is the solute diffusivity in pure water (1.49×10^{-5} cm^2/s for MeOH [51] and 1.21×10^{-5} cm^2/s for NaOAc [9,52,53]). The model tends to better fit data for salts over other small molecules as Mackie and Meares initially devised the model to estimate the salt diffusivities [50]. As a result, the model has better agreement with NaOAc diffusivities over MeOH diffusivities (Fig. 8.8), where similar behaviors were reported elsewhere [9,33,54]. Additionally, this model neglects the solute-polymer interactions and treats polymer chains as impenetrable obstacles [50]. In the case of NaOAc diffusivities, the model tends to fit better with PEGMA-containing films (20, 40, 60-M and -A/M), which we take as an indication that the NaOAc-polymer interaction (solute-polymer) is lessened in these films over PEGMA-free films (20, 40, 60-A); see Fig. 8.8(B).

Table 8.7. Diffusivity of PEGDA-PEGMA, PEGDA-AMPS/PEGMA, and PEGDA-AMPS membranes to MeOH and NaOAc in single and two-solute.

		Single solute		Both solutes	
	AMPS (mol%)	MeOH ($\times 10^7$ cm^2/s)	NaOAc ($\times 10^7$ cm^2/s)	MeOH ($\times 10^7$ cm^2/s)	NaOAc ($\times 10^7$ cm^2/s)
20-M	0	50	15	42	9
20-A/M	16	47	14	40	14
20-A	32	43	14	43	17
40-M	0	57	16	49	12
40-A/M	16	71	22	53	16
40-A	32	67	19	64	22
60-M	0	84	27	88	25
60-A/M	16	87	28	84	26
60-A	32	91	25	86	28

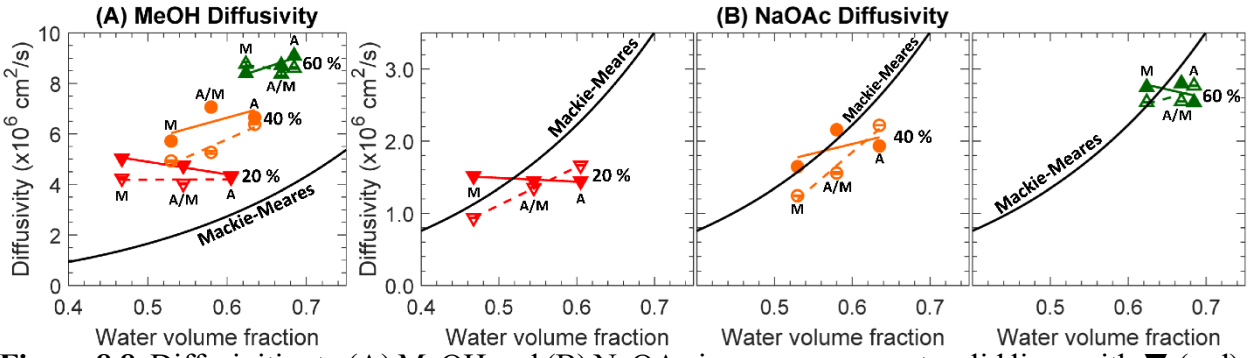

Figure 8.8. Diffusivities to (A) MeOH and (B) NaOAc in one-component, solid lines with ▼ (red), ● (orange), and ▲ (green) for 20, 40, and 60 wt.% of prepolymerization water contents, respectively, and two-component, dashed lines with ▽ (red), ○ (orange), and △ (green) for 20, 40, and 60 wt.% of prepolymerization water content, respectively. M, A/M, and A denote films prepared with 0, 16, and 32 mol% of AMPS contents, respectively. Lines are present as a guide to the eye. Mackie-Meares' fits for each solute are shown in solid lines.

Generally, MeOH diffusivities increase with increasing water volume fractions. For instance, MeOH diffusivities of the films prepared with 20 wt.% prepolymerization water content (20-M, A/M, A) are less than those with 40 and 60 wt.% prepolymerization water content (40- and 60-M, A/M, A) by 1.4 and 1.9 times, respectively, on average, in single diffusion. Similar behavior has been reported by Galizia et al., where they observed MeOH diffusivities (for feed solutions of 0.1-12 M) of crosslinked PEGDA films (prepared with 0, 20, and 60 wt.% of prepolymerization

water contents) to increase with increasing water content [33]. Similar to single solute diffusivities, MeOH diffusivities of 20- films are less than those of 40- and 60- films by 1.3 and 2.0 times, respectively, on average, in co-diffusion with NaOAc. Interestingly, MeOH diffusivities of the films prepared with 20 wt.% of water content decrease with decreasing AMPS content within the films, while those of the films prepared with either 40 or 60 wt.% of water content increase with increasing AMPS content; see Fig.8.8(A). A possible cause is the pendant sulfonate group may act as a bulky obstruction, especially at a low water volume fraction.

In co-diffusion, MeOH diffusivities of the films prepared with 20 and 40 wt.% decrease by 1.12 and 1.17 times, respectively, on average; see Fig. 8.8(A). We reported similar behavior in both CEMs [9] and anion exchange membranes [17]. To rationalize this behavior, we conjectured the diffusional path of fast-diffusing MeOH being obstructed by slow-diffusing NaOAc (Competitive diffusion). Here, we augment this conjecture such that this co-diffusive behavior remains consistent in films with longer, pendant PEO chains. Interestingly, MeOH diffusivities of the films prepared with both PEGMA and AMPS (-A/M) are higher than those with either PEGMA (-M) or AMPS (-A) in single diffusion, but -A/M diffusivities to MeOH are less than -M and -A diffusivities in co-diffusion. One possibility is a steric effect between PEGMA and AMPS (chain-chain interaction) that is in favor of the diffusion of MeOH. However, the impact of chain-chain interactions might be suppressed in co-diffusion as the diffusant-diffusant interaction (competitive diffusion) is more apparent on the diffusion of MeOH. On the other hand, MeOH diffusivities of the films prepared with 60 wt.% in co-diffusion are essentially the same as those in single diffusion. This indicates the competitive diffusion is more apparent in films with less water volume fraction (free volume).

Similar to MeOH diffusivities, NaOAc diffusivities increase with increasing water volume fraction. For instance, NaOAc diffusivities of 20- films are less than those of 40- and 60- films by 1.3 and 1.8 times, respectively, on average, in single diffusion. Similar behavior has been reported by Jang et al., where they observed diffusivities (for feed solutions of 0.01-1 M) of crosslinked PEGDA films (prepared with 0, 20, and 40 wt.% prepolymerization water content) to various salts (i.e. NaCl, KCl, and LiCl) to increase with increasing water content [54]. Again, NaOAc diffusivities of 20- films are less than those of 40- and 60- films by 1.3 and 2.0 times, respectively, on average, in co-diffusion with MeOH. Moreover, NaOAc diffusivities of the films prepared with 20 wt.% of water content decrease with decreasing AMPS content within the films; see Fig.6(B). Again, this is presumably due to the pendant sulfonate group act as a blocking group to suppress the solute diffusion.

For the films prepared with 20 and 40 wt.% prepolymerization water content, NaOAc diffusivities of -M films and -A/M films decrease by 1.4 and 1.2 times, respectively, on average, and those of -A films increase by 1.2 times, on average, in co-diffusion with MeOH; see Fig. 8.8(B). We reported the increase of NaOAc diffusivities in co-diffusion with MeOH in CEMs [6,9]. To rationalize this behavior, we conjectured the electrostatic repulsion (Donnan exclusion [8]) between bound sulfonate anions and mobile OAc^- is screened by co-diffusing MeOH (Charge screening by co-diffusant, [6,9,10,16]); see Fig. 8.1(F). Recently, Katzenberg et al. investigated the water-alcohol interaction in Nafion (commercial CEM), where they suggested alcohols may penetrate between the water and polymer interfaces as the alcohol-polymer affinity is stronger than the water-polymer affinity (non-uniform distribution of water-alcohol in CEM) [55]. This can be a contribution to suppress the electrostatic interaction between OAc^- and polymer ($sulfonate^-$), as the alcohol (less polar)-polymer (less polar) affinity can be stronger than the OAc^-(polar)-polymer

affinity. The decrease of NaOAc diffusivities in co-diffusion with MeOH is an emergent transport behavior. Previously, we reported the NaOAc permeabilities of 20-M and 20-A/M being consistent in co-permeation with MeOH, while those of analogous films prepared with a shorter comonomer (either acrylic acid or hydroxyethyl methacrylate) were significantly increased in co-permeation with MeOH [10]. To rationalize this behavior, we conjectured (1) the electrostatic repulsion between bound sulfonate and OAc^- is screened by long pendant PEO chains even in single permeation (charge screening by chains, Fig. 8.1(B)) and (2) flux coupling with co-permeating MeOH has been suppressed by long pendant PEO chains (Fig. 8.1(D,E)). Here, we augment these conjectures as diffusion-based transport behaviors. Moreover, the results from this investigation validate the addition of a charge-neutral pendant group in a charged IEM as a valid strategic approach to suppress the crossover of undesired molecules (i.e. MeOH and OAc^- in CO_2 reduction cells).

For 60- films, NaOAc diffusivities of -M films and -A/M films decrease by 1.1 and 1.1 times, respectively, on average, and those of -A films increase by 1.1 times, on average, in co-diffusion; see Fig. 8.8(B). This indicates both the electrostatic repulsion (sulfonate-OAc^-) and the flux coupling (MeOH-NaOAc) are more apparent in films with less water volume fraction (free volume). While these new findings may serve as practical tools for designing target-specific membranes, more fundamental investigations (i.e. Maxwell-Stefan [56], dielectric constant [57], internal structure [13,58], etc.) can be valuable to fully capture these complex multicomponent transport behaviors in IEMs.

8.3. Conclusion

A series of PEGDA-PEGMA (-M), PEGDA-AMPS/PEGMA (-A/M), and PEGDA-AMPS (-A) films with varied prepolymerization water contents (20, 40, and 60 wt.%) were prepared. Water volume fractions and ionic conductivities are measured to describe the transport behavior within these AMPS-free dense membranes (-M) and AMPS-containing cation exchange membranes (-A/M and -A). Permeabilities and solubilities to MeOH and NaOAc are measured in one- and two-component diffusion cell experiments and diffusivities are calculated from the solution-diffusion relationship. In one-component transport, both MeOH and NaOAc permeabilities are increased with increasing water volume fractions. However, NaOAc permeabilities of PEGMA-free films (-A) to NaOAc are increased and those of PEGMA-containing films (-M and -A/M) are decreased in co-permeation with MeOH. We postulate that the introduction of both diffusant-diffusant interactions (MeOH-NaOAc) and diffusant-diffusant-chain interactions (MeOH-NaOAc-PEGMA) leads to these changes in permeation behavior and that the presence of the pendant PEGMA side chains is principally responsible for this emergent behavior by suppressing the electrostatic repulsions between bound sulfonate anions and mobile OAc^-. Lastly, for both MeOH and OAc- we find the primary driver in differences in membrane permeability to be through changes in diffusion compared to changes in sorption behavior. Additional insights from computational approaches to simulate these multi-component transport or the development of experimental approaches to probe this behavior are needed. Overall, this investigation advances a preliminary understanding of how varied membrane physiochemical properties lead to differences in emergent transport behavior for charged polymer networks challenged with solutes and complex mixtures of solutes.

8.4. References

[1] M. Grzegorzek, K. Majewska-Nowak, A.E. Ahmed, Removal of fluoride from multicomponent water solutions with the use of monovalent selective ion-exchange membranes, Sci Total Environ. 722 (2020) 137681. https://doi.org/10.1016/j.scitotenv.2020.137681.

[2] T. Benvenuti, M. García-Gabaldón, E.M. Ortega, M.A.S. Rodrigues, A.M. Bernardes, V. Pérez-Herranz, J. Zoppas-Ferreira, Influence of the co-ions on the transport of sulfate through anion exchange membranes, J Membrane Sci. 542 (2017) 320–328. https://doi.org/10.1016/j.memsci.2017.08.021.

[3] A.R. Crothers, R.M. Darling, D.I. Kushner, M.L. Perry, A.Z. Weber, Theory of multicomponent phenomena in cation-exchange membranes: Part III. Transport in vanadium redox-flow-battery separators, J Electrochem Soc. 167 (2020) 013549. https://doi.org/10.1149/1945-7111/ab6725.

[4] M.R. Singh, A.T. Bell, Design of an artificial photosynthetic system for production of alcohols in high concentration from CO2, Energ Environ Sci. 9 (2015) 193–199. https://doi.org/10.1039/c5ee02783g.

[5] M. Krödel, B.M. Carter, D. Rall, J. Lohaus, M. Wessling, D.J. Miller, Rational design of ion exchange membrane material properties limits the crossover of CO2 reduction products in artificial photosynthesis devices, Acs Appl Mater Inter. 12 (2020) 12030–12042. https://doi.org/10.1021/acsami.9b21415.

[6] B.S. Beckingham, N.A. Lynd, D.J. Miller, Monitoring multicomponent transport using in situ ATR FTIR spectroscopy, J Membrane Sci. 550 (2018). https://doi.org/10.1016/j.memsci.2017.12.072.

[7] J.M. Kim, B.M. Dobyns, R. Zhao, B.S. Beckingham, Multicomponent transport of methanol and acetate in a series of crosslinked PEGDA-AMPS cation exchange membranes, J Membrane Sci. (2020) 118486. https://doi.org/10.1016/j.memsci.2020.118486.

[8] F.G. Helfferich, Ion Exchange, Dover, 1995.

[9] J.M. Kim, B.S. Beckingham, Transport and co-transport of carboxylate ions and alcohols in cation exchange membranes, J Polym Sci. (2021). https://doi.org/10.1002/pol.20210383.

[10] J.M. Kim, B.S. Beckingham, Comonomer effects on co-permeation of methanol and acetate in cation exchange membranes, Eur Polym J. (2021) 110307. https://doi.org/10.1016/j.eurpolymj.2021.110307.

[11] R.W. Baker, Membrane Technology and Applications, Wiley, (2012). https://doi.org/10.1002/9781118359686.

[12] B.M. Dobyns, J.M. Kim, B.S. Beckingham, Multicomponent transport of methanol and sodium acetate in poly(ethylene glycol) diacrylate membranes of varied fractional free volume, Eur Polym J. 134 (2020) 109809. https://doi.org/10.1016/j.eurpolymj.2020.109809.

[13] H. Ju, A.C. Sagle, B.D. Freeman, J.I. Mardel, A.J. Hill, Characterization of sodium chloride and water transport in crosslinked poly(ethylene oxide) hydrogels, J Membrane Sci. 358 (2010) 131–141. https://doi.org/10.1016/j.memsci.2010.04.035.

[14] A.C. Sagle, H. Ju, B.D. Freeman, M.M. Sharma, PEG-based hydrogel membrane coatings, Polymer. 50 (2009) 756–766. https://doi.org/10.1016/j.polymer.2008.12.019.

[15] P. Parise, A.A. Jr, B. Parekh, Reverse osmosis: chlorine-resistant polysulfone reverse osmosis membrane and module, Ultrapure Water. (1987).

[16] G.M. Geise, D.R. Paul, B.D. Freeman, Fundamental water and salt transport properties of polymeric materials, Prog Polym Sci. 39 (2014) 1–42. https://doi.org/10.1016/j.progpolymsci.2013.07.001.

[17] J.M. Kim, Y. Lin, B. Hunter, B.S. Beckingham, Transport and Co-Transport of Carboxylate Ions and Ethanol in Anion Exchange Membranes, Polymers-Basel. 13 (2021) 2885. https://doi.org/10.3390/polym13172885.

[18] K.A. Thompson, R. Mathias, D. Kim, J. Kim, N. Rangnekar, J.R. Johnson, S.J. Hoy, I. Bechis, A. Tarzia, K.E. Jelfs, B.A. McCool, A.G. Livingston, R.P. Lively, M.G. Finn, N-Aryl-linked spirocyclic polymers for membrane separations of complex hydrocarbon mixtures., Sci New York N Y. 369 (2020) 310–315. https://doi.org/10.1126/science.aba9806.

[19] J.G. Wijmans, R.W. Baker, The solution-diffusion model: a review, J Membrane Sci. 107 (1995) 1–21. https://doi.org/10.1016/0376-7388(95)00102-i.

[20] R.T. Chern, W.J. Koros, B. Yui, H.B. Hopfenberg, V.T. Stannett, Selective permeation of CO2 and CH4 through kapton polyimide: Effects of penetrant competition and gas-phase nonideality, J Polym Sci Polym Phys Ed. 22 (1984) 1061–1084. https://doi.org/10.1002/pol.1984.180220610.

[21] H.M.A. Rahman, G. Hefter, R. Buchner, Hydration of formate and acetate ions by dielectric relaxation spectroscopy, J Phys Chem B. 116 (2011) 314–323. https://doi.org/10.1021/jp207504d.

[22] M.L. Greenfield, D.N. Theodorou, Geometric analysis of diffusion pathways in glassy and melt atactic polypropylene, Macromolecules. 26 (1993) 5461–5472. https://doi.org/10.1021/ma00072a026.

[23] A. Kusoglu, A.Z. Weber, New insights into perfluorinated sulfonic-acid ionomers, Chem Rev. 117 (2017) 987–1104. https://doi.org/10.1021/acs.chemrev.6b00159.

[24] H. Schott, Extent of Hydration of Ethers in Aqueous Solution., J Chem Eng Data. 11 (1966) 417–418. https://doi.org/10.1021/je60030a039.

[25] H. Ju, B.D. McCloskey, A.C. Sagle, V.A. Kusuma, B.D. Freeman, Preparation and characterization of crosslinked poly(ethylene glycol) diacrylate hydrogels as fouling-resistant membrane coating materials, J Membrane Sci. 330 (2009) 180–188. https://doi.org/10.1016/j.memsci.2008.12.054.

[26] L.M. Robeson, H.H. Hwu, J.E. McGrath, Upper bound relationship for proton exchange membranes: Empirical relationship and relevance of phase separated blends, J Membrane Sci. 302 (2007) 70–77. https://doi.org/10.1016/j.memsci.2007.06.029.

[27] X.C. Chen, J.B. Kortright, N.P. Balsara, Water uptake and proton conductivity in porous block copolymer electrolyte membranes, Macromolecules. 48 (2015) 5648–5655. https://doi.org/10.1021/acs.macromol.5b00950.

[28] P.J. Flory, Principles of Polymer Chemistry, Cornell University Press, 1953.

[29] H. Lin, T. Kai, B.D. Freeman, S. Kalakkunnath, D.S. Kalika, The effect of cross-linking on gas permeability in cross-linked poly(ethylene glycol diacrylate), Macromolecules. 38 (2005) 8381–8393. https://doi.org/10.1021/ma0510136.

[30] N. Yan, D.R. Paul, B.D. Freeman, Water and ion sorption in a series of cross-linked AMPS/PEGDA hydrogel membranes, Polymer. 146 (2018) 196–208. https://doi.org/10.1016/j.polymer.2018.05.021.

[31] H. Yasuda, C.E. Lamaze, L.D. Ikenberry, Permeability of solutes through hydrated polymer membranes. Part I. Diffusion of sodium chloride, Die Makromolekulare Chemie. 118 (1968) 19–35. https://doi.org/10.1002/macp.1968.021180102.

[32] H. Yasuda, A. Peterlin, C.K. Colton, K.A. Smith, E.W. Merrill, Permeability of solutes through hydrated polymer membranes. Part III. Theoretical background for the selectivity of dialysis membranes, Die Makromolekulare Chemie. 126 (1969) 177–186. https://doi.org/10.1002/macp.1969.021260120.

[33] M. Galizia, D.R. Paul, B.D. Freeman, Liquid methanol sorption, diffusion and permeation in charged and uncharged polymers, Polymer. 102 (2016) 281–291. https://doi.org/10.1016/j.polymer.2016.09.010.

[34] B.M. Dobyns, J.M. Kim, J. Li, Z. Jiang, B.S. Beckingham, Multicomponent transport of alcohols in Nafion 117 measured by in situ ATR FTIR spectroscopy, Polymer. (2020) 123046. https://doi.org/10.1016/j.polymer.2020.123046.

[35] B. Pan, B. Xing, Competitive and complementary adsorption of bisphenol A and 17α-ethinyl estradiol on carbon nanomaterials, J Agr Food Chem. 58 (2010) 8338–8343. https://doi.org/10.1021/jf101346e.

[36] B.M. Carter, B.M. Dobyns, B.S. Beckingham, D.J. Miller, Multicomponent transport of alcohols in an anion exchange membrane measured by in-situ ATR FTIR spectroscopy, Polymer. 123 (2017). https://doi.org/10.1016/j.polymer.2017.06.070.

[37] T. Borjigin, F. Sun, J. Zhang, K. Cai, H. Ren, G. Zhu, A microporous metal–organic framework with high stability for GC separation of alcohols from water, Chem Commun. 48 (2012) 7613–7615. https://doi.org/10.1039/c2cc33023g.

[38] E.R. Nightingale, Phenomenological theory of ion solvation. Effective radii of hydrated ions, J Phys Chem. 63 (1959) 1381–1387. https://doi.org/10.1021/j150579a011.

[39] R. Caminiti, P. Cucca, M. Monduzzi, G. Saba, G. Crisponi, Divalent metal–acetate complexes in concentrated aqueous solutions. An x-ray diffraction and NMR spectroscopy study, J Chem Phys. 81 (1984) 543–551. https://doi.org/10.1063/1.447336.

[40] Hitoshi. Ohtaki, Tamas. Radnai, Structure and dynamics of hydrated ions, Chem Rev. 93 (1993) 1157–1204. https://doi.org/10.1021/cr00019a014.

[41] V.N. Afanas'ev, Solvation of electrolytes and nonelectrolytes in aqueous solutions, J Phys Chem B. 115 (2011) 6541–6563. https://doi.org/10.1021/jp1108834.

[42] K. Chang, H. Luo, G.M. Geise, Water content, relative permittivity, and ion sorption properties of polymers for membrane desalination, J Membrane Sci. 574 (2019) 24–32. https://doi.org/10.1016/j.memsci.2018.12.048.

[43] K. Chang, H. Luo, G.M. Geise, Influence of salt concentration on hydrated polymer relative permittivity and state of water properties, Macromolecules. 54 (2021) 637–646. https://doi.org/10.1021/acs.macromol.0c02188.

[44] G.M. Geise, L.P. Falcon, B.D. Freeman, D.R. Paul, Sodium chloride sorption in sulfonated polymers for membrane applications, J Membrane Sci. 423 (2012) 195–208. https://doi.org/10.1016/j.memsci.2012.08.014.

[45] E.-S. Jang, J. Kamcev, K. Kobayashi, N. Yan, R. Sujanani, T.J. Dilenschneider, H.B. Park, D.R. Paul, B.D. Freeman, Influence of water content on alkali metal chloride transport in cross-linked Poly(ethylene glycol) Diacrylate.1. Ion sorption, Polymer. 178 (2019) 121554. https://doi.org/10.1016/j.polymer.2019.121554.

[46] Y. Yu, N. Yan, B.D. Freeman, C.-C. Chen, Mobile ion partitioning in ion exchange membranes immersed in saline solutions, J Membrane Sci. 620 (2020) 118760. https://doi.org/10.1016/j.memsci.2020.118760.

[47] G.S. Manning, Limiting laws and counterion condensation in polyelectrolyte solutions I. Colligative properties, J Chem Phys. 51 (1969) 924–933. https://doi.org/10.1063/1.1672157.

[48] Y. Yu, Y. Li, N. Hossain, C.-C. Chen, Nonrandom two-liquid activity coefficient model for aqueous polyelectrolyte solutions, Fluid Phase Equilibr. 497 (2019) 1–9. https://doi.org/10.1016/j.fluid.2019.05.009.

[49] Y. Song, C.-C. Chen, Symmetric electrolyte nonrandom two-liquid activity coefficient model, Ind Eng Chem Res. 48 (2009) 7788–7797. https://doi.org/10.1021/ie9004578.

[50] J.S. Mackie, P. Meares, The diffusion of electrolytes in a cation-exchange resin membrane I. Theoretical, Proc Royal Soc Lond Ser Math Phys Sci. 232 (1955) 498–509. https://doi.org/10.1098/rspa.1955.0234.

[51] L. Hao, D.G. Leaist, Binary mutual diffusion coefficients of aqueous alcohols. Methanol to 1-heptanol, J Chem Eng Data. 41 (1996) 210–213. https://doi.org/10.1021/je950222q.

[52] E.E. Hills, M.H. Abraham, A. Hersey, C.D. Bevan, Diffusion coefficients in ethanol and in water at 298K: Linear free energy relationships, Fluid Phase Equilibr. 303 (2011) 45–55. https://doi.org/10.1016/j.fluid.2011.01.002.

[53] P. Vany´sek, Ionic Conductivity and Diffusion at Infinite Dilution, CRC Handbook of Chemistry and Physics, 93rd Edition. (2012).

[54] E.-S. Jang, J. Kamcev, K. Kobayashi, N. Yan, R. Sujanani, T.J. Dilenschneider, H.B. Park, D.R. Paul, B.D. Freeman, Influence of water content on alkali metal chloride transport in cross-linked Poly(ethylene glycol) diacrylate.2. Ion diffusion, Polymer. 192 (2020) 122316. https://doi.org/10.1016/j.polymer.2020.122316.

[55] A. Katzenberg, A. Angulo, A. Kusoglu, M.A. Modestino, Impacts of organic sorbates on the ionic conductivity and nanostructure of perfluorinated sulfonic-acid ionomers, Macromolecules. 54 (2021) 5187–5195. https://doi.org/10.1021/acs.macromol.1c00494.

[56] M. Soltanieh, S. Sahebdelfar, Interaction effects in multicomponent separation by reverse osmosis, J Membrane Sci. 183 (2001) 15–27. https://doi.org/10.1016/s0376-7388(00)00554-8.

[57] K. Chang, G.M. Geise, Dielectric permittivity properties of hydrated polymers: Measurement and Connection to Ion Transport Properties, Ind Eng Chem Res. 59 (2019) 5205–5217. https://doi.org/10.1021/acs.iecr.9b03950.

[58] G.M. Geise, C.M. Doherty, A.J. Hill, B.D. Freeman, D.R. Paul, Free volume characterization of sulfonated styrenic pentablock copolymers using positron annihilation lifetime spectroscopy, J Membrane Sci. 453 (2014) 425–434. https://doi.org/10.1016/j.memsci.2013.11.004.

Chapter 9

Effect of Phenyl-comonomers in CEMs

Reproduced from: J.M. Kim, Y-h. Lin, P. PA, B.S. Beckingham, Impact of hydrophobic pendant phenyl groups on transport and co-transport of methanol and acetate in PEGDA-SPMAK cation exchange membranes, J Membrane Sci. (In revision).

9.1. Introduction

Artificial photosynthetic applications (i.e. photoelectrochemical CO_2 reduction cells (PEC-CRCs [1])) are a promising approach for reducing atmospheric CO_2, which is a primary greenhouse gas of concern for climate change. Due to a lack of catalyst specificity, CO_2 is often being reduced to a variety of chemicals within a device [2], including carbon monoxide (CO), methane (CH_4), ethylene (C_2H_4), formate (OFm^-), acetate (OAc^-), methanol (MeOH), and ethanol (EtOH) [3]. PEC-CRCs incorporate either a cation exchange membrane (CEM) [4,5] or an anion exchange membrane (AEM) [6–10] to provide ion-selective transport and an electrolyte (i.e. potassium bicarbonate ($KHCO_3$) [9,11]) to facilitate the CO_2 reduction process. Recently, Singh and Bell devised an advanced PEC-CRC [1], which targets maximizing the recovery of alcohols (MeOH and EtOH) in order to utilize them as carbon-neutral fuels. One of the major challenges of this approach is the current lack of ion exchange membranes that sufficiently minimize the crossover of electrolyte-dissolved CO_2 reduction products (i.e. MeOH [12–17] and OAc^- [17–19]), as they often oxidize back to CO_2 and by-products at the anode. In this context, understanding the transport behavior of CO_2 reduction products is important to design a target-specific membrane.

Several investigations have been performed on understanding single permeant transport behavior in ion exchange membranes and captured valuable interactions between bound charged groups and mobile permeants (such as Donnan exclusion [20], counterion condensation [21,22], volume expansion [14], and charge screening [23–25]). However, relatively few efforts have been made to analyze and understand multi-solute transport behavior [8,15–19,26]. Previously, our group observed the permeabilities, P_i, of CEMs (Nafion® 117 [17] and PEGDA-AMPS (Chapter 5 [18]) to carboxylates (OFm^- and OAc^-) being increased in co-permeation with alcohol (either MeOH or EtOH), where we showed this is mainly due to the change in the diffusivities, D_i, over the solubilities, K_i (solution-diffusion model, $P_i = K_i \times D_i$ [27,28]) [26]. In attempt to identify potential functional groups that suppress this concerning behavior [29], we browsed through a series of pendant groups (carboxyl (n = 0, where n is the number of ethylene oxide repeat units), ethylene oxide (n = 1), and poly(ethylene oxide) (PEO, n = 5)) by incorporating the comonomer (acrylic acid (AA), hydroxyethyl methacrylate (HEMA), and poly(ethylene glycol) methacrylate (PEGMA), respectively) in a model CEM, which we prepared with a crosslinker, poly(ethylene glycol) diacrylate (PEGDA, n = 13, [30–32]), and a negatively-charged comonomer, 2-acrylamido-2-methylpropanesulfonic acid (AMPS [33,34]), namely PEGDA-AMPS/AA, PEGDA-AMPS/HEMA, PEGDA-AMPS/PEGMA; see Chapter 7 [19]. While OAc^- permeabilities of PEGDA-AMPS/AA and PEGDA-AMPS/HEMA were increased in co-permeation with an alcohol (MeOH), those of PEGDA-AMPS/PEGMA in co-permeation was consistent with OAc^- permeabilities by itself [19]. We then focused on PEGDA-AMPS/PEGMA films to investigate the effect of pendant PEO chains (see Chapter 8), where we reported (1) the change in permeabilities is due to the change in diffusivities and (2) the electrostatic repulsion between bound sulfonate

anions and mobile OAc^- might be suppressed by relatively longer pendant groups (PEO, n = 5) and, therefore, the electrostatic repulsion might already be suppressed even in single diffusion [35].

Here, we investigate the effect of two additional pendant chains, phenoxyethyl acrylate (PEA, n = 1) or poly(ethylene glycol) phenyl ether acrylate (PEGPEA, n = 3) on OAc^- diffusion in single and co-diffusion with MeOH through a model CEM, which we prepared with a crosslinker, PEGDA (n = 13) and a negative-charged comonomer, 3-sulfopropyl methacrylate potassium (SPMAK). As in PEGDA-AMPS, we observed OAc^- diffusivities of PEGDA-SPMAK being increased in co-diffusion with MeOH. This is presumably due to the charge screening by MeOH; see Fig. 9.1(A,D).

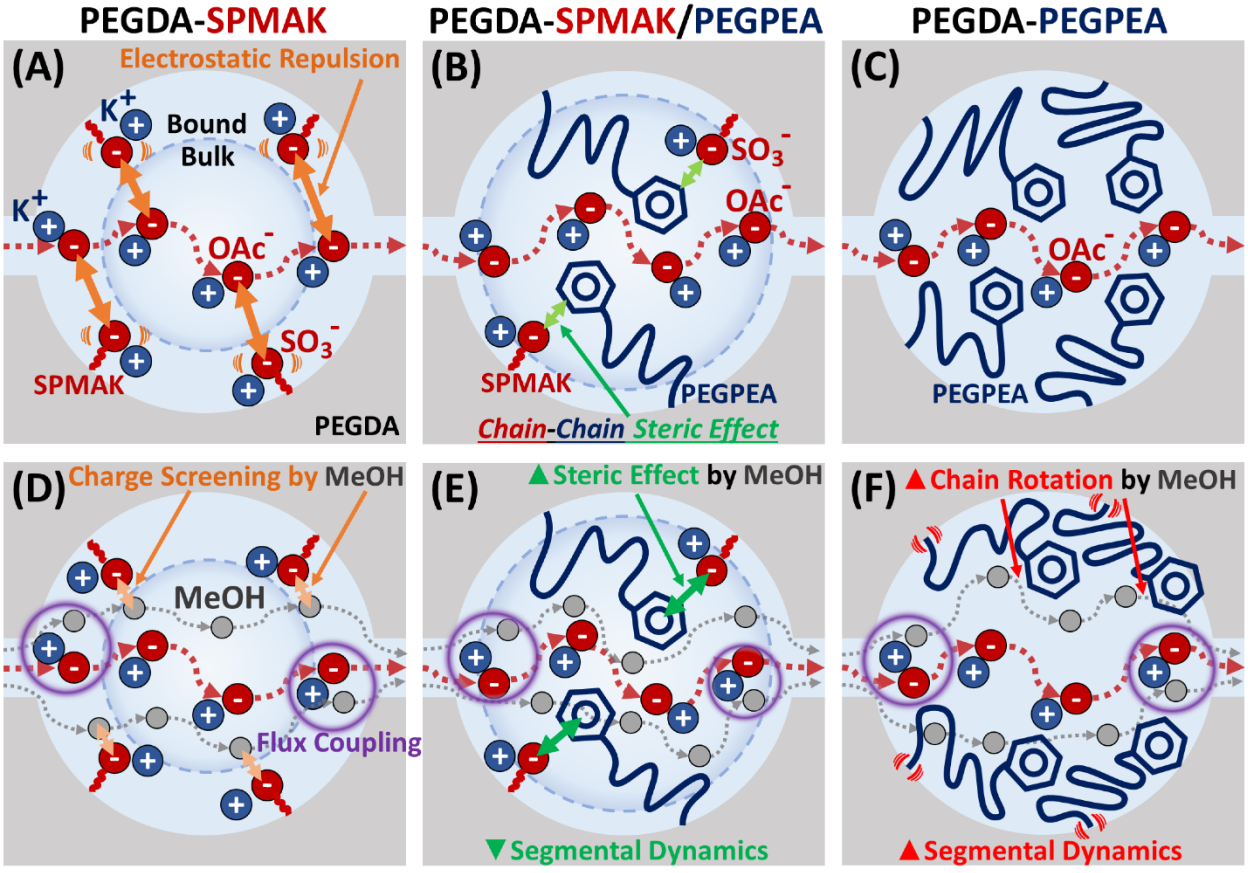

Figure 9.1. Schematic depiction of KOAc diffusion in (A,D) PEGDA-SPMAK, (B,E) PEGDA-SPMAK/PEGPEA, and (C,F) PEGDA-PEGPEA in (A-C) single and (D-F) co-diffusion with MeOH. Figures are reprinted from [8,18,19,26,35] with permission from Elsevier, Wiley, and MDPI.

Conversely, we observed distinct behaviors in PEGPEA-containing films, namely PEGDA-PEGPEA and PEGDA-SPMAK/PEGPEA. OAc^- diffusivities of sulfonate-free PEGDA-PEGPEA films were increased in co-diffusion, which is presumably due to an increase in segmental dynamics as MeOH encounters relatively long (n = 3) and bulky (with phenyl group) PEGPE chains; see Fig. 9.1(C,F). On the other hand, OAc^- diffusivities of PEGDA-SPMAK/PEGPEA films were decreased in co-diffusion, which is presumably due to a decrease in segmental dynamics as SPMAK encounters PEGPEA chains and induces steric effects; see Fig. 9.1(B,E). These empirical-based conjectures will further be discussed in this work.

9.2. Results and Discussion

A series of binary films, PEGDA-SPMAK (P-S), PEGDA-PEA (P-E), and PEGDA-PEGPEA (P-G), and ternary films, PEGDA-SPMAK/PEA (P-S/E) and PEGDA-SPMAK/PEGPEA (P-S/G), were prepared (see Table 9.1 for prepolymerization compositions), to investigate the effect of PEA (n = 1) and PEGPEA (n = 3) chains on the multi-solute transport of MeOH and KOAc in CEMs. Moreover, the interactions between (1) mobile MeOH (partially hydrophobic) and PEGPEA (hydrophobic) chains and (2) SPMAK (hydrophilic) and PEGPEA were conjectured.

Table 9.1. Membrane characteristics from pre-polymerization mixtures

	SPMAK[a] (mol %)	E or G[b] (mol %)	PEGDA (g)	SPMAK (g)	E or G[b] (g)	Water (g)	HCPK (g)
1. P	-	-	8.00	-	-	2.00	0.008
2. P-S16	16	-	7.50	0.50	-	2.00	0.008
3. P-S24	24	-	7.20	0.80	-	2.00	0.008
4. P-S32	32	-	6.86	1.14	-	2.00	0.008
5. P-E16	-	16	7.60	-	0.40	2.00	0.008
6. P-E32	-	32	7.08	-	0.92	2.00	0.008
7. P-G16	-	16	7.35	-	0.65	2.00	0.008
8. P-G32	-	32	6.57	-	1.43	2.00	0.008
9. P-S16/E16	16	16	6.97	0.58	0.45	2.00	0.008
10. P-S24/E8	24	8	6.92	0.86	0.22	2.00	0.008
11. P-S16/G16	16	16	6.71	0.56	0.73	2.00	0.008
12. P-S24/G8	24	8	6.79	0.84	0.37	2.00	0.008

[a]SPMAK = mol of SPMAK/(mol of PEGDA + mol of SPMAK + mol of E or G) × 100 %
[b]E or G = mol of E or G/(mol of PEGDA + mol of SPMAK + mol of E or G) × 100 %

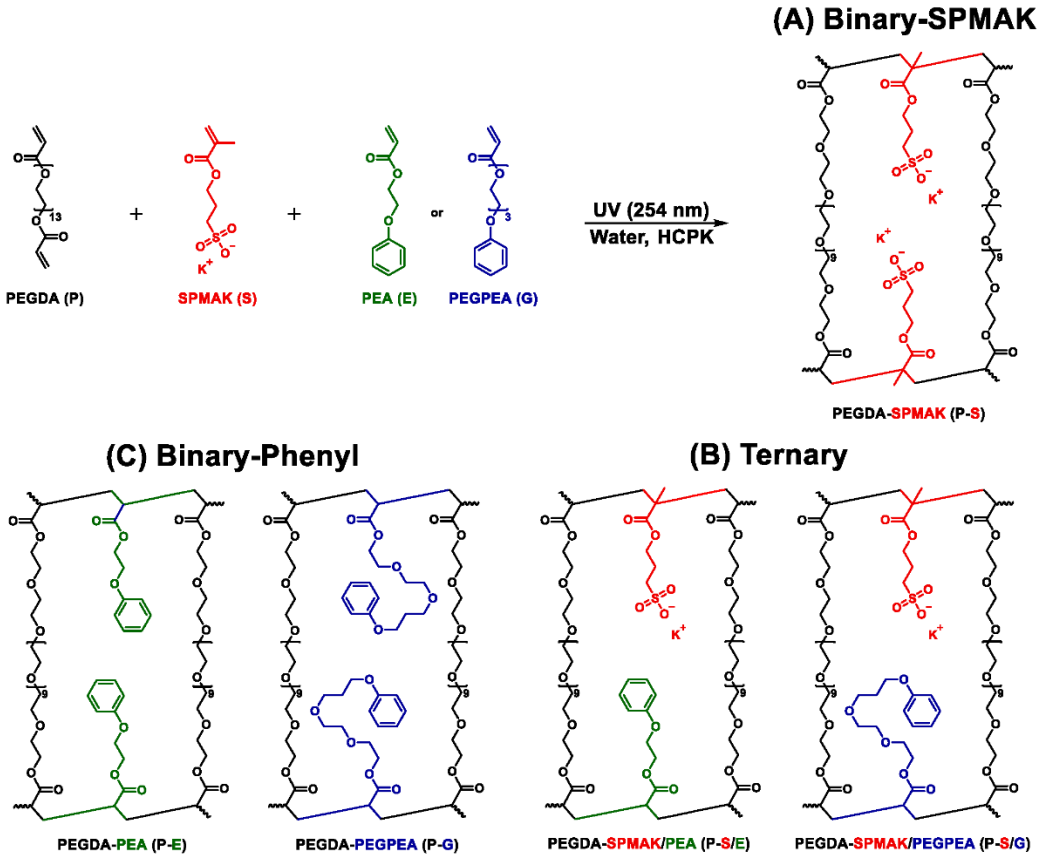

Figure 9.2. Scheme of prepared (A) binary-SPMAK films, P-S, (B) binary-phenyl films, P-E and P-G, and (C) ternary films, P-S/E and P-S/G.

9.2.1. Ionic conductivity and IEC of membranes

The ionic conductivity of SPMAK containing films (P-S, P-S/E, and P-S/G) was measured yielding the results shown in Fig. 9.3 and Table 9.2. Ionic conductivities of SPMAK-free membranes (P, P-E, and P-G) were not measured as they are not ionically conductive due to the absence of charged moieties [19]. As expected, ionic conductivities of SPMAK-containing films were increased with increasing SPMAK content [19,35]. Similarly, the ion exchange capacity (IEC) of each membrane increases with increasing SPMAK content as more counterions are retained within the polymer matrix due to the increase in sulfonate content. Notably, the average difference between measured and theoretical IEC of membranes was close (2 %), as shown in Table 9.2.

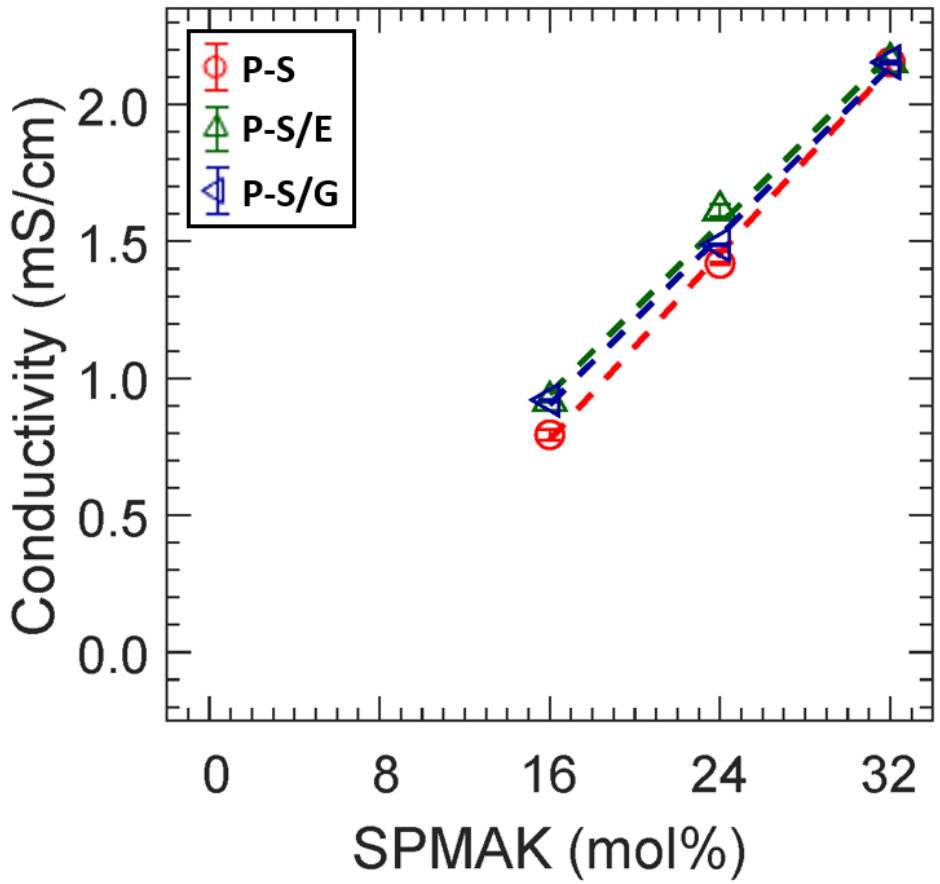

Figure 9.3. Ionic conductivity of (A) binary SPMAK films, P-S, ○, and (B) ternary films, P-S/PM, □, P-S/PE, △, and P-S/PG, ◁. Each data point is the average of 3 membranes with error bars corresponding to the standard deviation. Dotted lines are present as a guide to the eye.

Table 9.2. Ionic conductivity and ion exchange capacity of cation exchange membranes

	PEGDA (mol%)	SPMAK (mol%)	Conductivity (σ, mS/cm)	Theoretical IEC (meq/g dry polymer)[a]	Measured IEC (meq/g dry polymer)
P-S	100	0	-	-	-
	84	16	0.79 ± 0.02	0.26	0.27 ± 0.01
	76	24	1.42 ± 0.00	0.41	0.40 ± 0.01
	68	32	2.15 ± 0.01	0.58	0.57 ± 0.01
P-S/E	68	0	-	-	-
	68	16	0.92 ± 0.00	0.29	0.29 ± 0.00
	68	24	1.61 ± 0.02	0.44	0.43 ± 0.01
	68	32	2.15 ± 0.01	0.58	0.57 ± 0.01
P-S/G	68	0	-	-	-
	68	16	0.92 ± 0.00	0.28	0.28 ± 0.00
	68	24	1.49 ± 0.00	0.43	0.42 ± 0.01
	68	32	2.15 ± 0.01	0.58	0.57 ± 0.01

[a]Theoretical IEC = mmol of SPMAK/(mass of PEGDA + mass of SPMAK + mass of E or G)

9.2.2. Water volume fraction

Membrane water volume fractions were measured with results shown in Fig. 9.4 and Table 9.3. Moreover, water uptakes and dry polymer densities are also shown in Table 9.3. Generally, water volume fractions of P-S films were increased with SPMAK content (decreased with PEGDA content); see Fig. 9.4(A). This is likely due to (1) bound sulfonate anions being hydrophilic and holding more water molecules than PEGDA [4] and (2) crosslink densities of films are decreased as PEGDA content decreases [31]. In the case of P-E and P-G films, water volume fractions were essentially the same; see Fig. 9.4(B,C). This is likely due to the decrease in crosslinking (increase in water volume fraction) being offset by inclusion of the more hydrophobic phenyl-containing pendant groups (PEA and PEGPEA). In ternary films (P-S/E, and P-S/G), water volume fractions increase with SPMAK content (decrease with phenyl content); see Fig. 9.4(D,E). This is due to an increase in the hydrophilic sulfonate group and a decrease in the hydrophobic phenyl group.

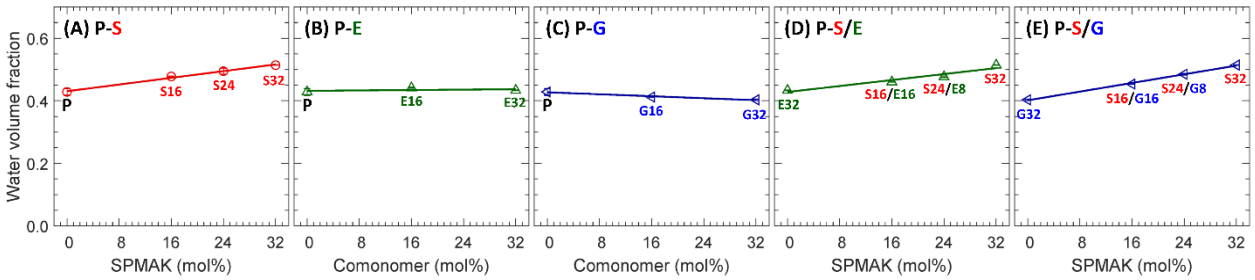

Figure 9.4. Water volume fraction of (A) binary-SPMAK films, P-S, ○, (B-D) binary-comonomer films, P-PM, □, P-PE, △, and P-PG, ◁, and (E-G) ternary films, P-S/PM, □, P-S/PE, △, and P-S/PG, ◁. Each data point is the average of 3 membranes with error bars corresponding to the standard deviation. Lines are present as a guide to the eye.

Table 9.3. Water uptake, dry polymer density, water volume fraction, crosslink density, and glass transition temperature of all membranes

	SPMAK (mol%)	Water uptake (ω_w, g H_2O/g dry membrane ·100%)	Dry polymer density (g/mL)	Water volume fraction	Storage modulus (MPa)	Glass transition (°C)
1. P	-	62 ± 3	1.20 ± 0.00	0.428 ± 0.011	25.6 ± 0.8	-43 ± 1
2. P-S16	16	75 ± 0	1.22 ± 0.00	0.478 ± 0.001	28.2 ± 1.3	-33 ± 3
3. P-S24	24	79 ± 3	1.24 ± 0.01	0.495 ± 0.010	28.3 ± 0.3	-33 ± 2
4. P-S32	32	84 ± 0	1.25 ± 0.01	0.514 ± 0.001	29.1 ± 2.5	-29 ± 2
5. P-E16	-	65 ± 0	1.22 ± 0.01	0.441 ± 0.002	25.8 ± 1.8	-36 ± 2
6. P-E32	-	63 ± 0	1.21 ± 0.00	0.433 ± 0.001	25.4 ± 3.3	-33 ± 2
7. P-G16	-	58 ± 0	1.20 ± 0.00	0.412 ± 0.001	24.3 ± 1.5	-38 ± 1
8. P-G32	-	56 ± 1	1.19 ± 0.01	0.403 ± 0.003	24.9 ± 1.4	-38 ± 0
9. P-S16/E16	16	70 ± 0	1.22 ± 0.00	0.460 ± 0.000	23.2 ± 1.4	-30 ± 2
10. P-S24/E8	24	74 ± 1	1.23 ± 0.00	0.477 ± 0.003	24.2 ± 3.6	-32 ± 2
11. P-S16/G16	16	68 ± 0	1.21 ± 0.00	0.454 ± 0.000	24.3 ± 2.8	-28 ± 3
12. P-S24/G8	24	76 ± 1	1.24 ± 0.01	0.485 ± 0.002	26.8 ± 5.7	-31 ± 2

9.2.3. Storage modulus

The storage modulus of all films at 25 °C (rubbery plateau) is shown in Fig. 9.5 and Table 9.3. Generally, the storage modulus of all films was slightly increased with increasing water volume fraction. This is unexpected behavior because the storage modulus is often decreased with increasing water volume fraction (1) as water volume fraction is a proxy to estimate the amount

free volume within hydrogels and (2) more free volume often coincides with decreased crosslink density (Flory's rubber elasticity relationship, Eq. 9.1 [39]) [33]. This indicates the rubber elasticity relationship may not be suitable to predict the crosslink densities of films with certain pendant functional groups.

$$\nu_e = \frac{E'}{3RT} \tag{9.1}$$

where the crosslink density, ν_e (mmol/cm^3), E' is the storage modulus (Pa), R is the gas constant (8314 cm^3 Pa/K mmol), and T is the temperature (298.15 K). This indicates the rubber elasticity relationship may not be suitable to predict the crosslink densities of films with pendant groups (i.e. PEA and PEGPEA) that are dissimilar from the crosslinker (i.e. PEGDA).

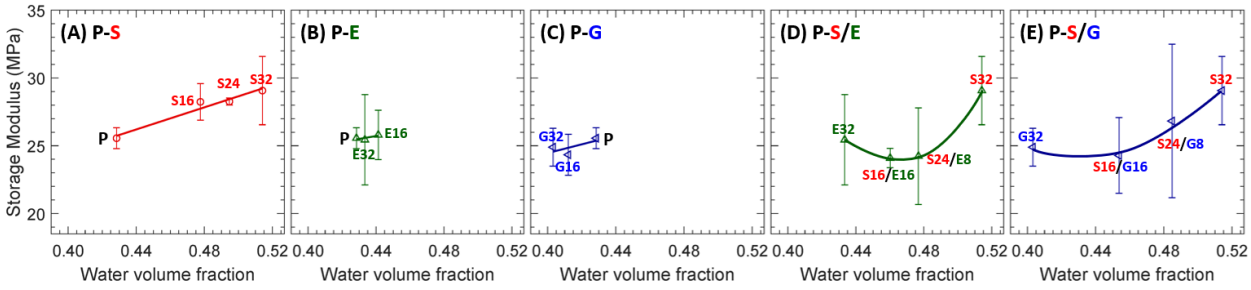

Figure. 9.5. Storage modulus of (A) P-S, ○, (B) P-E, △, (C) P-G, ◁, (D) P-S/E, △, and P-S/G, ◁. Each data point is the average of 3 membranes with error bars corresponding to the standard deviation. Lines are present as a guide to the eye.

The storage modulus of P-S films increases with increasing SPMAK content; see Fig. 9.5(A). A possible cause is the effect of the methyl group in the methacrylate (as opposed to acrylates) of SPMAK, which increases the polymer backbone rigidity (steric effect [46]) and, therefore, store more mechanical energy. Yan et al. conducted similar experiments on analogous films (PEGDA-AMPS, where AMPS is an acrylate (no additional methyl group)), and reported the storage modulus of PEGDA-AMPS films is decreased with increasing AMPS content, presumably due to a reduction with crosslink density as the crosslinker (PEGDA) content is

replaced by the pendent monomer (AMPS) [33]. The difference in these studies suggests various factors may impact the storage modulus of copolymeric hydrogels [47].

While the storage modulus of both P-E (n = 1) and P-G (n = 3) films was essentially the same with increasing phenyl content; see Fig. 9.5(B,C). This indicates two additional ethylene oxide repeat units on PEGPEA have negligible impacts on the storage modulus. In the case of ternary films, the storage modulus was generally increased with increasing SPMAK content; see Fig. 9.5(D,E). This is presumably due to the steric effect between hydrophilic SPMAK and hydrophobic PEA or PEGPEA chains, that decreases the polymer segmental dynamics (reduction in storage modulus).

9.2.4. Single and Multi-solute Permeability

The permeabilities of all films to MeOH and KOAc were measured by diffusion cell experiments. Extracted permeability values using the Yasuda model [44,45] are shown in Fig. 9.6; where Fig. 9.6(A-E) and (F-J) are scaled differently. Additionally, the volume expansion of each membrane was estimated from the thickness of the film before (hydrated) and after permeation, where the thickness was measured by a digital caliper to get the average of 5 random locations; see Table 9.4 for the normalized values. Generally, the thickness of all films did not change significantly. For instance, the thickness of the film after single MeOH permeation was essentially the same (increased by 0.2 %), on average, and those of the film after single KOAc permeation and co-permeation (1 M of each in feed) were slightly decreased by 1.4 and 1.6 %, respectively, on average. A contribution to this slight deswelling in KOAc permeation is the difference in osmotic pressure as the water concentration in the hydrated film is higher than that of the salt solution in the feed cell [17,43].

The permeabilities of all films to MeOH and KOAc were measured by the diffusion cell experiments. Extracted permeability values using the Yasuda model [25,26] are shown in Fig. 9.6; where Fig. 9.6(A-C) and (D-J) are scaled differently. Additionally, the volume expansion of each membrane was estimated from the thickness of the film before (hydrated) and after permeation, where the thickness was measured by a digital caliper to get the average of 5 random locations; see Table 9.4 for the normalized values.

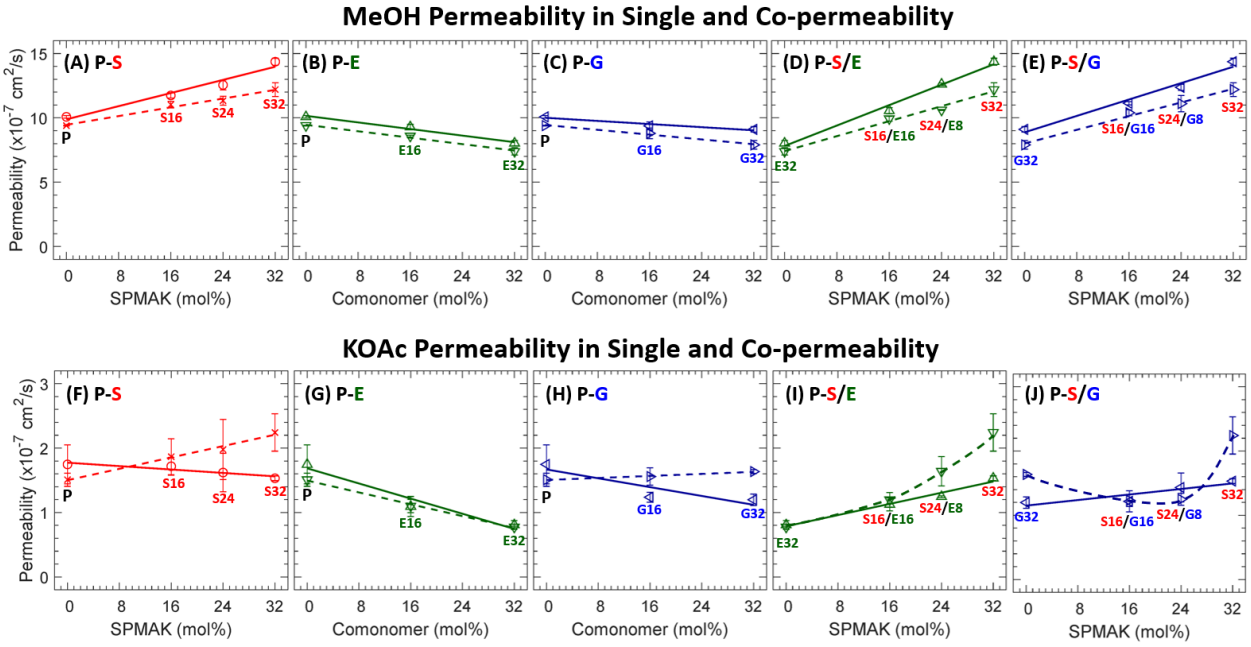

Figure. 9.6. Permeabilities of all films to (A-E) MeOH and (F-J) KOAc measured in one-component (solid line) and two-component (dashed), which consist of (A,F) P-S (red, one: ○ and two: ×), (B,G) P-E (green, one: △ and two: ▽), (C,H) P-G (blue, one: ◁ and two: ▷), (D,I) P-S/E (green, one: △ and two: ▽), and (E,J) P-S/G (blue, one: ◁ and two: ▷) films. Each data point is the average of 3 experiments with error bars corresponding to the standard deviation. Lines are present as a guide to the eye.

Table 9.4. Normalized film thickness to hydrated membrane after permeability measurements.

	SPMAK (mol%)	Water	1 M MeOH	1 M KOAc	1 M MeOH and KOAc
1. P	-	1.00 ± 0.00	0.99 ± 0.01	0.99 ± 0.01	0.99 ± 0.01
2. P-S16	16	1.00 ± 0.01	1.00 ± 0.01	1.00 ± 0.01	0.98 ± 0.01
3. P-S24	24	1.00 ± 0.00	1.02 ± 0.01	0.99 ± 0.01	1.00 ± 0.01
4. P-S32	32	1.00 ± 0.00	1.01 ± 0.00	0.98 ± 0.00	0.99 ± 0.01
5. P-A16	-	1.00 ± 0.00	1.00 ± 0.01	0.98 ± 0.01	0.98 ± 0.00
6. P-A32	-	1.00 ± 0.02	0.99 ± 0.01	0.98 ± 0.00	0.98 ± 0.01
7. P-G16	-	1.00 ± 0.01	1.00 ± 0.00	0.99 ± 0.00	1.00 ± 0.01
8. P-G32	-	1.00 ± 0.02	1.01 ± 0.00	0.99 ± 0.01	0.99 ± 0.01
9. P-S16/E16	16	1.00 ± 0.00	1.01 ± 0.00	1.00 ± 0.00	1.00 ± 0.01
10. P-S24/E8	24	1.00 ± 0.00	1.01 ± 0.01	0.99 ± 0.01	0.99 ± 0.01
11. P-S16/G16	16	1.00 ± 0.02	0.98 ± 0.00	0.96 ± 0.01	0.97 ± 0.00
12. P-S24/G8	24	1.00 ± 0.00	1.00 ± 0.00	0.98 ± 0.01	0.97 ± 0.00
Average		**1.000**	**1.002**	**0.986**	**0.984**

Generally, MeOH permeabilities increase with increasing SPMAK content (Fig. 9.6(A,D,E)) and slightly decrease with increasing phenyl-containing comonomer content (Fig. 9.6(B-E)). These trends are somewhat consistent with those observed in the water volume fraction (Fig. 9.4), where the water volume fractions increase with increasing SPMAK content (Fig. 9.4(A,D,E)) and slightly decrease with increasing phenyl-containing comonomer content (Fig. 9.4(D,E)). In co-permeation with KOAc, MeOH permeabilities decrease slightly. We observed similar behaviors elsewhere [12,17–19,26]. As the permeability, *P*, is a product of solubility, *K*, and diffusivity, *D* (solution-diffusion model), this co-transport behavior will be examined in terms of sorption and diffusion in the following sections. Nevertheless, a reduction in membrane permeability to MeOH is favorable for typical CO_2 reduction cells (minimization of product crossover).

In the case of binary films (P-S, P-E, and P-G), KOAc permeabilities in single permeation decrease with increasing comonomer content (both sulfonate and phenyl contents); see solid lines in Fig. 9.6(F-H). A contribution to the decrease of P-S permeabilities to KOAc is electrostatic

repulsion (Donnan exclusion [20]), where repulsive interactions between bound sulfonate anions and mobile OAc^- increase with increasing IEC (Table 1). A possible contribution to the decrease in KOAc permeabilities in P-E and P-G is the hydrophobicity of the bound phenyl groups and hydrophilicity of the mobile KOAc which together lead to a repulsive interaction. In the case of ternary films (P-S/E and P-S/G), KOAc permeabilities in single permeation increase with increasing SPMAK content; see solid lines in Fig. 9.6(I,J). This is consistent with the behavior in binary films as the permeabilities decrease more rapidly with increasing phenyl content than with increasing SPMAK content.

In the case of co-permeation with MeOH, KOAc permeabilities of P-S films increase. We observed similar behavior in CEMs (Nafion® 117 [17,26] and PEGDA-AMPS [18,26]), where we conjectured the electrostatic repulsion between bound sulfonate anions and mobile carboxylate anions is suppressed by mobile alcohols (charge screening [17,18,24–26]); see Fig. 9.1(A,D). KOAc permeabilities in co-permeation with MeOH for P-E and P-G films are similar and higher, respectively, compared to those measured by itself. To rationalize these differences in co-permeation, we conjecture potential changes in polymer segmental dynamics in the presence of MeOH. As MeOH is more hydrophobic than ionized K^+ and OAc^- in water, MeOH is able to permeate closer to the hydrophobic phenyl groups [48]. This potential steric effect between MeOH and phenyl groups might induce more chain rotation, which then can increase the overall segmental dynamics. Compared to the chain rotation in P-E (n = 1) films, the chain rotation in P-G (n = 3) will be more plausible as PEGPEA chains are more mobile than PEA chains with two additional repeat units. More discussion on these conjectures will be continued in the diffusivity section. For P-S/E films, KOAc permeabilities gradually increase with increasing SPMAK content. Again, this is presumably due to the electrostatic repulsion between bound sulfonates and mobile carboxylates

being screened by mobile MeOH and, therefore, easier to permeate in co-diffusion [26]. While KOAc permeabilities of P-S and P-G films increase in co-permeation with MeOH, those of P-S/G films (P-S16/G16 and P-S24/G8) are essentially the same; see Fig. 9.6(J). We observe a similar trend in the grass transition temperatures (T_g) of the dry polymers, where the T_g of P-G32, P-S16/G16, P-S24/G8, and P-S32 films are -38, -28, -31, and -29 °C, respectively. Generally, more permeation (and diffusion) is expected in polymer films with a lower T_g due to a higher segmental dynamics [49]; see Table 9.3 for T_g values. Combining these two results, we conjecture a potential steric effect between hydrophilic SPMAK chains and hydrophobic PEGPEA chains, which decreases the overall segmental dynamics; see Fig. 9.1(E). More discussion on these conjectures will be continued in the diffusivity section.

9.2.5. Single and Multi-solute Solubility

The solubilities of all films to MeOH and KOAc were measured by sorption-desorption experiments and values are shown in Fig. 9.7; where Fig. 9.7(A-E) and (F-J) are scaled differently. Additionally, the volume expansion of each membrane was calculated from the volumes of the film before (hydrated) and after sorption (solvated) in each solution (1 M MeOH, 1 M KOAc, or 1 M of each). The volume, V, of each membrane was measured by the photograph-caliper method [18,26], where the area, A, was measured from a digital photograph coupled with ImageJ software [33] and the thickness, T, was measured by a digital caliper to get the average of 5 random locations ($V = A \times T$); see Table 9.5 for values. Generally, the volumes of all films did not change significantly. For instance, the volume of the film after sorption in 1 M MeOH was essentially the same and those of the film after sorption in KOAc-containing solutions (1 M KOAc and 1 M of each) were slightly deswelled by 1.07 times, on average. A contribution to this deswelling is the

difference in osmotic pressure, where the concentration of water within the film is higher than that in the external solution [17,43].

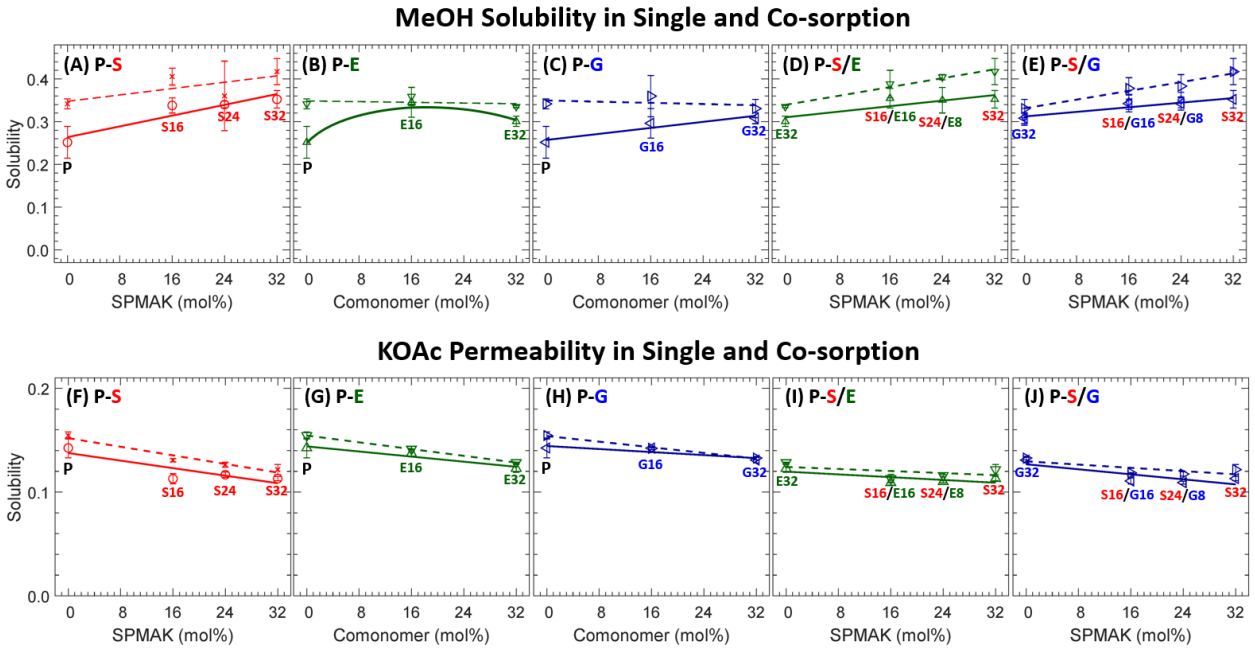

Figure 9.7. Solubilities of all films to (A-E) MeOH and (F-J) KOAc measured in one-component (solid line) and two-component (dashed), which consist of (A,F) P-S (red, one: ○ and two: ×), (B,G) P-E (green, one: △ and two: ▽), (C,H) P-G (blue, one: ◁ and two: ▷), (D,I) P-S/E (green, one: △ and two: ▽), and (E,J) P-S/G (blue, one: ◁ and two: ▷) films. Each data point is the average of 3 experiments with error bars corresponding to the standard deviation. Lines are present as a guide to the eye.

Table 9.5. Volume of swollen membranes.

	SPMAK (mol%)	Water (mm^3)	1 M MeOH (mm^3)	1 M KOAc (mm^3)	1 M MeOH and KOAc (mm^3)
1. P	-	95 ± 0	99 ± 1	94 ± 2	93 ± 1
2. P-S16	16	99 ± 5	101 ± 4	91 ± 4	90 ± 3
3. P-S24	24	95 ± 1	96 ± 1	88 ± 1	87 ± 1
4. P-S32	32	98 ± 0	99 ± 4	88 ± 1	87 ± 3
5. P-E16	-	91 ± 0	94 ± 1	87 ± 1	88 ± 1
6. P-E32	-	92 ± 0	94 ± 2	87 ± 1	89 ± 0
7. P-G16	-	92 ± 0	95 ± 3	86 ± 1	87 ± 1
8. P-G32	-	93 ± 0	95 ± 1	86 ± 1	87 ± 2
9. P-S16/E16	16	95 ± 2	98 ± 1	87 ± 2	87 ± 1
10. P-S24/E8	24	95 ± 0	98 ± 2	88 ± 1	86 ± 1
11. P-S16/G16	16	94 ± 3	95 ± 4	85 ± 2	87 ± 2
12. P-S24/G8	24	98 ± 1	99 ± 2	85 ± 3	86 ± 2
Average		**94 ± 1**	**97 ± 2**	**87 ± 2**	**88 ± 2**

In the case of single sorption, MeOH solubilities of P-S films increase with increasing SPMAK content; see solid line in Fig. 9.7(A). This is presumably due to the increase in free volume (as indicated by the water volume fraction, Fig. 9.4(A)), which introduces more regions for the polymer network to interact with the solution (1 M MeOH). Moreover, MeOH is expected to be more preferred in polymers over water as MeOH is partially hydrophobic as polymers [48]; see solid lines in Fig. 9.7(B). Similarly, MeOH solubilities of P-E and P-G films increase with increasing comonomer content. This is presumably due to the increasing hydrophobicity of the polymer with the introduction of phenyl groups and, therefore, more MeOH is expected to interact with the film. For ternary film (P-S/E and P-S/G), MeOH solubilities slightly increase with increasing SPMAK content; see solid lines in Fig. 9.7(C). This is consistent with binary films (P-S, P-E, and P-G), as the MeOH solubility increases more rapidly in P-S films than in other films.

In the case of single sorption, KOAc solubilities in P-S films decrease with increasing SPMAK content; see solid line in Fig. 9.7(F). This is partially due to the electrostatic repulsion (Donnan exclusion [20]) between bound sulfonate anions and mobile OAc^-. Similarly, KOAc solubilities of P-E and P-G films slightly decrease with increasing comonomer content in part due to the increase in hydrophobicity of the film with increasing phenyl content; see solid lines in Fig. 9.7(G,H). For ternary films, KOAc solubilities slightly decrease with increasing SPMAK content; see solid lines in Fig. 9.7(I,J). Again, this is consistent with the binary films, as the decrease in KOAc solubilities is more rapid in P-S films than in other films.

In the case of co-sorption (1 M each solute), both MeOH and KOAc solubilities increase; see dashed lines in Fig. 9.7. One contribution to this behavior is the larger difference in osmotic pressure inside the film and the external solution in co-sorption (less water in the external solution). As a result, more water in the film will be replaced by solutes (MeOH or KOAc) from the external

solution. While MeOH solubilities of P-S films increase to a similar degree with increasing comonomer content (Fig. 9.7(A)), the gap between those of P-E and P-G films in single and co-permeation becomes narrower with increasing comonomer content (Fig. 9.7(B,C)). For instance, MeOH solubilities of P-E and P-G films prepared with 0, 16, and 32 mol% of comonomers increase by 1.4, 1.2, and 1.1 times, respectively, on average. To rationalize this behavior, we conjecture hydrophilic KOAc induces a phase separation near hydrophobic phenyl groups and suppresses MeOH from further penetration near the polymer structure [50] (solute-solute-polymer interaction). We observe similar behavior in ternary films, where the gap between single and co-permeation becomes narrower with increasing phenyl content (decreasing SPMAK content); see Fig. 9.7(D,E).

In the case of co-sorption, KOAc solubilities of P-S films increase uniformly; see Fig. 9.7(F). Again, this is partially due to an increase in osmotic pressure (larger water concentration difference in binary mixture, 1 M each). In the case of phenyl-containing films (P-E, P-G, P-S/E, and P-S/G), KOAc solubilities slightly increase in co-sorption; see Fig. 9.7(G-J). Nonetheless, the differences between those solubilities measured in single and co-sorption are very close to one another. This indicates the apparent differences in KOAc permeabilities in single and co-permeation are weakly associated with sorption.

9.2.6. Single and Multi-solute Diffusivity

The diffusivity, D_i, of all films to MeOH and KOAc in single and co-diffusion are calculated using the solution-diffusion relationship ($D_i = P_i/K_i$). Calculated diffusivities are shown in Fig. 9.8; where (A-C) and (D-F) are scaled differently. Additionally, the Mackie-Meares model [51] was used to estimate the MeOH and KOAc diffusivities in these films (solid lines in Fig. 9.8), which states:

$$D_i = D_{o,i}\left(\frac{\phi_w}{2-\phi_w}\right)^2 \quad (8)$$

where D_i is the diffusivity of a membrane to solute i, ϕ_w is the water volume fraction, and $D_{0,i}$ is the solute diffusivity in pure water (1.49×10^{-5} cm^2/s for MeOH [52] and 1.52×10^{-5} cm^2/s for KOAc [26,53,54]). The model tends to fit better with salts over other small molecules as Mackie and Meares devised the model to estimate salt diffusivities [51]. As a result, KOAc diffusivities are closer to the model (Fig. 9.8(D-F)), than MeOH diffusivities (Fig. 9.8(A-C)), where similar behavior is reported elsewhere [8,14,26,55].

Generally, MeOH diffusivities in both binary and ternary films were increased with increasing SPMAK content; see red markers in Fig. 9.8(A-C). This is consistent with our previous report on comonomer-free crosslinked PEGDA films, where we observed MeOH permeabilities were decreased in co-permeation with sodium acetate (NaOAc) and the difference from the single permeation was greater as the water volume fraction of the film increases [12]. In co-diffusion, MeOH diffusivities of all films decrease; see Fig. 9.8(A-C). This is presumably due to competitive diffusion, which states the diffusional path of fast-diffusing MeOH can be obstructed by slow-diffusing KOAc [26].

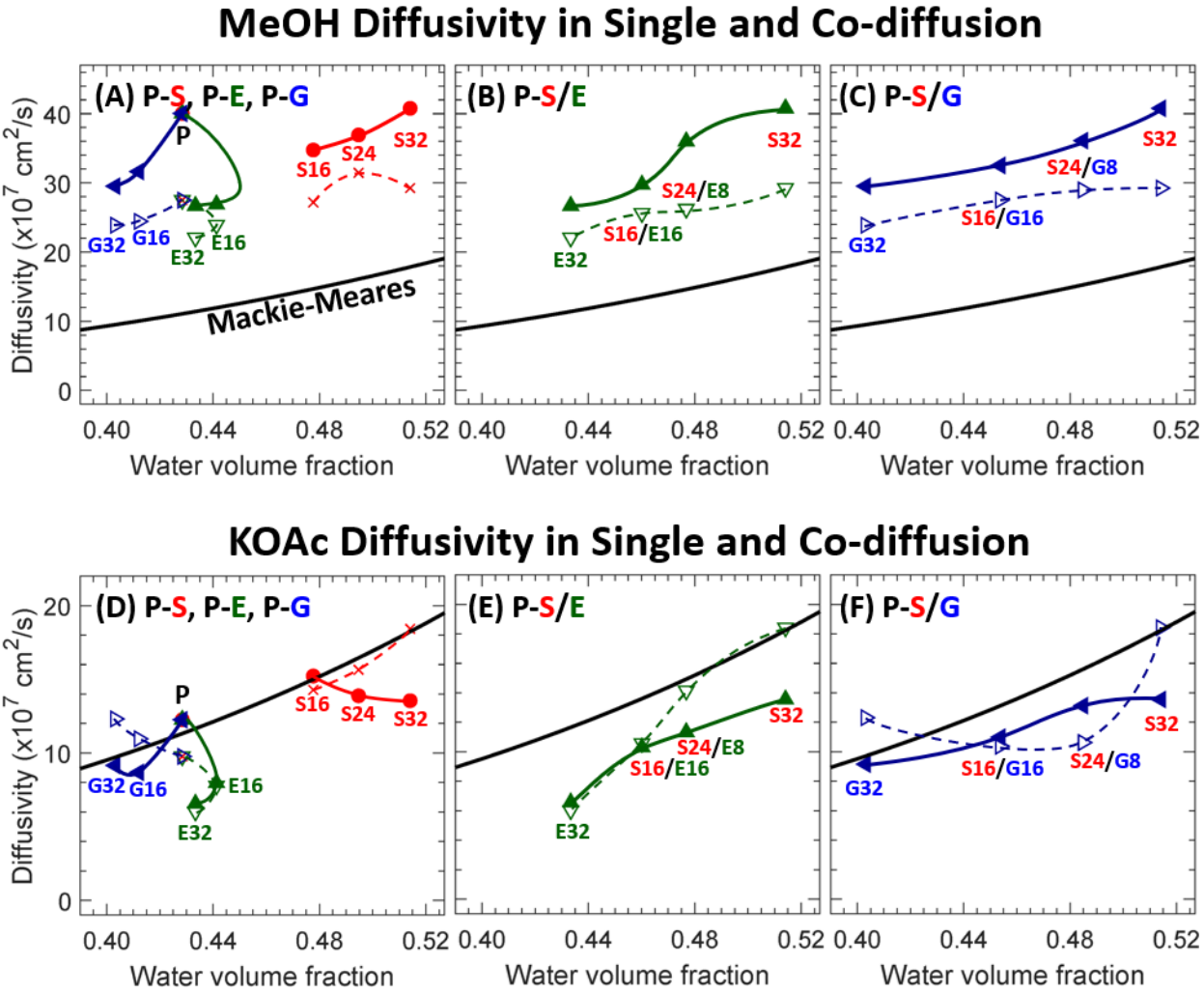

Figure 9.8. (A-C) MeOH and (D-F) KOAc diffusivities of (A,D) binary films (P-S, P-E, and P-G), (B,E) P-S/E films, and (C,F) P-S/G films. Single diffusivities are shown in solid lines with filled markers (E: ▲, G: ◀, and S: ●) and co-diffusivities are shown in dashed lines with empty markers(E: ▽, G: ▷, and S: ×). Lines are present as a guide to the eye. Mackie-Meares' fits for each solute are shown in black solid lines.

In the case of P-S films, KOAc diffusivities increase in co-diffusion with MeOH; see Fig. 9.8(D). We observed similar behavior in various CEMs (i.e. Nafion® 117 and PEGDA-AMPS) [17,18,26,35], where the diffusivities of carboxylate salts (OFm^- and OAc^-) increased in co-diffusion with an alcohol (MeOH or EtOH). To rationalize this co-transport behavior, we conjectured a charge screening behavior [24–26], which states the electrostatic repulsion (Donnan

exclusion [20]) between bound sulfonate anions and mobile carboxylate anions is suppressed by co-diffusing alcohols; see Fig. 9.1(A,D).

In co-diffusion, KOAc diffusivities of P-E films are essentially the same, when those of P-G films increase; see Fig. 9.8(D). To rationalize this behavior, we conjecture (1) more MeOH may interact with phenyl end groups on PEGPEA (n = 3) than PEA (n = 1) with a longer chain length, (2) more segmental motion will be induced in P-G by co-diffusing MeOH, and (3) increased segmental dynamics will increase the overall solute diffusivity; see Fig. 9.1(C,F). Nonetheless, more investigation on segmental dynamics must be conducted to validate these conjectures as other factors (relative permittivity [56–58], hydration number [37,59], pH, etc.) likely also play a role in this co-transport behavior.[35]

In the case of P-S/G films, both P-S24/G8 and P-S16/G16 diffusivities to KOAc in co-diffusion were slightly less than those in single diffusion; see Fig. 9.8(F). This behavior is different than that observed in P-S and P-G films, as KOAc diffusivities of both P-S32 and P-G32 films in co-diffusion with MeOH were higher than those in single diffusion by 1.36 and 1.34 times, respectively; see Fig. 9.8(F). A possible cause of this behavior is increasing steric effects between SPMAK and PEGPEA chains in co-diffusion with MeOH due to its interactions with the phenyl groups and likelihood of increased chain rotation; see Fig. 9.1(B,E). However, since PEGPEA (n = 3) are longer than PEA (n = 1), the phenyl groups (hydrophobic) in P-S/G may experience the more steric hinderance from the sulfonate groups (hydrophilic) and, consequently, the overall segmental dynamics can be rather reduced.

This potential chain-chain interaction between these comonomers might provide helpful insight to the conjectured charge screening behavior; see Fig. 9.1(A,D) [26]. Since KOAc diffusivities do not increase in P-S/G films in co-permeation with MeOH, the charge screening

behavior can be suppressed by reducing the overall segmental dynamics. Nonetheless, more investigations are needed to provide additional insights into this complex behavior and to assess the validity of our hypotheses described above. However, the physiochemical or transport roots of this behavior aside, the strategic inclusion of PEGPEA in CEMs targeting CO_2 reduction cells may be beneficial as they suppress the crossover of negatively-charged CO_2 reduction products.

9.3. Conclusion

A series of binary films (PEGDA-SPMAK (P-S), PEGDA-PEA (P-E), and PEGDA-PEGPEA (P-G)) and ternary films (P-S/E and P-S/G) films were prepared at a constant pre-polymerization water content (20 wt.%). Ionic conductivities and ion exchange capacities (IEC) of cation exchange membranes (P-S, P-S/E, and P-S/G) were measured to understand the impact of bound sulfonate anions on both binary and ternary films. Water volume fractions, storage moduli, and glass transition temperatures of all films were measured to fully understand the transport behavior within these films. Permeabilities and solubilities of all films to methanol (MeOH) and potassium acetate (KOAc) were measured in single and co-transport. Diffusivities were calculated by the solution-diffusion relationship. An interesting co-diffusive behavior was observed in P-S/G films, where KOAc diffusivities were not increased in co-diffusion with MeOH, when those of P-S and P-G films were increased by 1.35 times, on average. To rationalize this behavior, we conjecture a steric effect between sulfonated chains and PEGPEA chains might be increased in co-diffusion with MeOH and reduce the overall segmental dynamics. More investigations on PEGPEA can be helpful to further understand this multi-component transport behavior and validate the viability of introducing PEGPEA for CO_2 reduction cells.

9.4. References

[1] M.R. Singh, A.T. Bell, Design of an artificial photosynthetic system for production of alcohols in high concentration from CO 2, Energ Environ Sci. 9 (2015) 193–199. https://doi.org/10.1039/c5ee02783g.

[2] A.J. Garza, A.T. Bell, M. Head-Gordon, Mechanism of CO2 reduction at copper surfaces: pathways to C2 products, Acs Catal. 8 (2018) 1490–1499. https://doi.org/10.1021/acscatal.7b03477.

[3] D.J. Miller, F.A. Houle, Energy and Environment Series, (2018) 341–385. https://doi.org/10.1039/9781788010313-00341.

[4] A. Kusoglu, A.Z. Weber, New insights into perfluorinated sulfonic-acid ionomers, Chem Rev. 117 (2017) 987–1104. https://doi.org/10.1021/acs.chemrev.6b00159.

[5] L.M. Robeson, H.H. Hwu, J.E. McGrath, Upper bound relationship for proton exchange membranes: Empirical relationship and relevance of phase separated blends, J Membrane Sci. 302 (2007) 70–77. https://doi.org/10.1016/j.memsci.2007.06.029.

[6] G. Geise, M. Hickner, B. Logan, Ionic resistance and permselectivity tradeoffs in anion exchange membranes., Acs Appl Mater Inter. 5 (2013) 10294–301. https://doi.org/10.1021/am403207w.

[7] B.M. Carter, L. Keller, M. Wessling, D.J. Miller, Preparation and characterization of crosslinked poly(vinylimidazolium) anion exchange membranes for artificial photosynthesis, J Mater Chem A. (2019). https://doi.org/10.1039/c9ta00498j.

[8] J.M. Kim, Y. Lin, B. Hunter, B.S. Beckingham, Transport and co-transport of carboxylate ions and ethanol in anion exchange membranes, Polymers. 13 (2021) 2885. https://doi.org/10.3390/polym13172885.

[9] S.M. Dischinger, S. Gupta, B.M. Carter, D.J. Miller, Transport of neutral and charged solutes in imidazolium-functionalized poly(phenylene oxide) membranes for artificial photosynthesis, Ind Eng Chem Res. 59 (2019) 5257–5266. https://doi.org/10.1021/acs.iecr.9b05628.

[10] M. Krödel, B.M. Carter, D. Rall, J. Lohaus, M. Wessling, D.J. Miller, Rational design of ion exchange membrane material properties limits the crossover of CO2 reduction products in artificial photosynthesis devices, Acs Appl Mater Inter. 12 (2020) 12030–12042. https://doi.org/10.1021/acsami.9b21415.

[11] B.M. Dobyns, J.M. Kim, B.S. Beckingham, Multicomponent transport of methanol and sodium acetate in poly(ethylene glycol) diacrylate membranes of varied fractional free volume, Eur Polym J. 134 (2020) 109809. https://doi.org/10.1016/j.eurpolymj.2020.109809.

[12] M. Soniat, S.M. Dischinger, L. Weng, H.M. Beltran, A.Z. Weber, D.J. Miller, F.A. Houle, Toward predictive permeabilities: Experimental measurements and multiscale simulation of methanol transport in Nafion, J Polym Sci. (2021). https://doi.org/10.1002/pol.20200771.

[13] M. Galizia, D.R. Paul, B.D. Freeman, Liquid methanol sorption, diffusion and permeation in charged and uncharged polymers, Polymer. 102 (2016) 281–291. https://doi.org/10.1016/j.polymer.2016.09.010.

[14] B.M. Carter, B.M. Dobyns, B.S. Beckingham, D.J. Miller, Multicomponent transport of alcohols in an anion exchange membrane measured by in-situ ATR FTIR spectroscopy, Polymer. 123 (2017). https://doi.org/10.1016/j.polymer.2017.06.070.

[15] B.M. Dobyns, J.M. Kim, J. Li, Z. Jiang, B.S. Beckingham, Multicomponent transport of alcohols in Nafion 117 measured by in situ ATR FTIR spectroscopy, Polymer. (2020) 123046. https://doi.org/10.1016/j.polymer.2020.123046.

[16] B.S. Beckingham, N.A. Lynd, D.J. Miller, Monitoring multicomponent transport using in situ ATR FTIR spectroscopy, J Membrane Sci. 550 (2018). https://doi.org/10.1016/j.memsci.2017.12.072.

[17] J.M. Kim, B.M. Dobyns, R. Zhao, B.S. Beckingham, Multicomponent transport of methanol and acetate in a series of crosslinked PEGDA-AMPS cation exchange membranes, J Membrane Sci. (2020) 118486. https://doi.org/10.1016/j.memsci.2020.118486.

[18] J.M. Kim, B.S. Beckingham, Comonomer effects on co-permeation of methanol and acetate in cation exchange membranes, Eur Polym J. (2021) 110307. https://doi.org/10.1016/j.eurpolymj.2021.110307.

[19] J.M. Kim, B.S. Beckingham, Transport and co-transport of carboxylate ions and alcohols in cation exchange membranes, J Polym Sci. (2021). https://doi.org/10.1002/pol.20210383.

[20] H. Ju, B.D. McCloskey, A.C. Sagle, V.A. Kusuma, B.D. Freeman, Preparation and characterization of crosslinked poly(ethylene glycol) diacrylate hydrogels as fouling-resistant membrane coating materials, J Membrane Sci. 330 (2009) 180–188. https://doi.org/10.1016/j.memsci.2008.12.054.

[21] P.J. Flory, Principles of Polymer Chemistry, Cornell University Press, 1953.

[22] N. Yan, D.R. Paul, B.D. Freeman, Water and ion sorption in a series of cross-linked AMPS/PEGDA hydrogel membranes, Polymer. 146 (2018) 196–208. https://doi.org/10.1016/j.polymer.2018.05.021.

[23] K. Chang, T. Xue, G.M. Geise, Increasing salt size selectivity in low water content polymers via polymer backbone dynamics, J Membrane Sci. 552 (2018) 43–50. https://doi.org/10.1016/j.memsci.2018.01.057.

[24] E.M. Ahmed, Hydrogel: Preparation, characterization, and applications: A review, J Adv Res. 6 (2015) 105–121. https://doi.org/10.1016/j.jare.2013.07.006.

[25] H. Yasuda, C.E. Lamaze, L.D. Ikenberry, Permeability of solutes through hydrated polymer membranes. Part I. Diffusion of sodium chloride, Die Makromolekulare Chemie. 118 (1968) 19–35. https://doi.org/10.1002/macp.1968.021180102.

[26] H. Yasuda, A. Peterlin, C.K. Colton, K.A. Smith, E.W. Merrill, Permeability of solutes through hydrated polymer membranes. Part III. Theoretical background for the selectivity of dialysis membranes, Die Makromolekulare Chemie. 126 (1969) 177–186. https://doi.org/10.1002/macp.1969.021260120.

[27] G.M. Geise, L.P. Falcon, B.D. Freeman, D.R. Paul, Sodium chloride sorption in sulfonated polymers for membrane applications, J Membrane Sci. 423 (2012) 195–208. https://doi.org/10.1016/j.memsci.2012.08.014.

[28] F.G. Helfferich, Ion Exchange, Dover, 1995.

[29] A.E. Allegrezza, B.S. Parekh, P.L. Parise, E.J. Swiniarski, J.L. White, Chlorine resistant polysulfone reverse osmosis modules, Desalination. 64 (1987) 285–304. https://doi.org/10.1016/0011-9164(87)90103-2.

[30] G.M. Geise, D.R. Paul, B.D. Freeman, Fundamental water and salt transport properties of polymeric materials, Prog Polym Sci. 39 (2014) 1–42. https://doi.org/10.1016/j.progpolymsci.2013.07.001.

[31] L. Kwisnek, J. Goetz, K.P. Meyers, S.R. Heinz, J.S. Wiggins, S. Nazarenko, PEG containing thiol–ene network membranes for CO2 separation: Effect of cross-linking on thermal, mechanical, and gas transport properties, Macromolecules. 47 (2014) 3243–3253. https://doi.org/10.1021/ma5005327.

[32] A. Katzenberg, A. Angulo, A. Kusoglu, M.A. Modestino, Impacts of organic sorbates on the ionic conductivity and nanostructure of perfluorinated sulfonic-acid ionomers, Macromolecules. 54 (2021) 5187–5195. https://doi.org/10.1021/acs.macromol.1c00494.

[33] J.S. Mackie, P. Meares, The diffusion of electrolytes in a cation-exchange resin membrane I. Theoretical, Proc Royal Soc Lond Ser Math Phys Sci. 232 (1955) 498–509. https://doi.org/10.1098/rspa.1955.0234.

[34] L. Hao, D.G. Leaist, Binary mutual diffusion coefficients of aqueous alcohols. Methanol to 1-heptanol, J Chem Eng Data. 41 (1996) 210–213. https://doi.org/10.1021/je950222q.

[35] E.E. Hills, M.H. Abraham, A. Hersey, C.D. Bevan, Diffusion coefficients in ethanol and in water at 298K: Linear free energy relationships, Fluid Phase Equilibr. 303 (2011) 45–55. https://doi.org/10.1016/j.fluid.2011.01.002.

[36] P. Vany´sek, Ionic Conductivity and Diffusion at Infinite Dilution, CRC Handbook of Chemistry and Physics, 93rd Edition. (2012).

[37] E.-S. Jang, J. Kamcev, K. Kobayashi, N. Yan, R. Sujanani, T.J. Dilenschneider, H.B. Park, D.R. Paul, B.D. Freeman, Influence of water content on alkali metal chloride transport in cross-linked Poly(ethylene glycol) diacrylate.2. Ion diffusion, Polymer. 192 (2020) 122316. https://doi.org/10.1016/j.polymer.2020.122316.

[38] K. Chang, G.M. Geise, Dielectric permittivity properties of hydrated polymers: measurement and connection to ion transport properties, Ind Eng Chem Res. 59 (2019) 5205–5217. https://doi.org/10.1021/acs.iecr.9b03950.

[39] K. Chang, H. Luo, G.M. Geise, Water content, relative permittivity, and ion sorption properties of polymers for membrane desalination, J Membrane Sci. 574 (2019) 24–32. https://doi.org/10.1016/j.memsci.2018.12.048.

[40] K. Chang, H. Luo, G.M. Geise, Influence of salt concentration on hydrated polymer relative permittivity and state of water properties, Macromolecules. 54 (2021) 637–646. https://doi.org/10.1021/acs.macromol.0c02188.

[41] E.-S. Jang, J. Kamcev, K. Kobayashi, N. Yan, R. Sujanani, T.J. Dilenschneider, H.B. Park, D.R. Paul, B.D. Freeman, Influence of water content on alkali metal chloride transport in cross-linked Poly(ethylene glycol) Diacrylate.1. Ion sorption, Polymer. 178 (2019) 121554. https://doi.org/10.1016/j.polymer.2019.121554.

[42] M. Galizia, F.M. Benedetti, D.R. Paul, B.D. Freeman, Monovalent and divalent ion sorption in a cation exchange membrane based on cross-linked poly (p-styrene sulfonate-co-divinylbenzene), J Membrane Sci. 535 (2017) 132–142. https://doi.org/10.1016/j.memsci.2017.04.007.

Chapter 10

New class of IEMs for DUFCs

Reproduced from: J.M. Kim, Y. Wang, Y. Lin, J. Yoon, T. Huang, D.-J. Kim, M.L. Auad, B.S. Beckingham, Fabrication and Characterization of Cross-Linked Phenyl-Acrylate-Based Ion Exchange Membranes and Performance in a Direct Urea Fuel Cell, Ind Eng Chem Res. (2021). https://doi.org/10.1021/acs.iecr.1c02798.

10.1. Introduction

Ion exchange membranes (IEM) are hydrated, dense polymeric membranes with a charged functional group that have been applied in various applications, such as direct fuel cells (direct methanol fuel cells [1–4] and direct urea fuel cells (DUFC) [5–7]) and CO_2 reduction cells [8–12]. Major roles of IEMs in these devices are to provide ion selective transport for device operation and to minimize the crossover of charge-neutral solutes (i.e. methanol (MeOH), ethanol (EtOH), and urea), which reduce performance. While many efforts have focused on enhancing the ion selective transport through higher ionic conductivity [13–15], investigations on minimizing neutral solute crossover are relatively lacking [16–18]. Common strategies for mitigating this types of solute crossover are (1) to engineer the surface of the membrane with functional groups or chemistry that inhibit transport [9] and (2) to incorporate solid additive materials (silica nanoparticles and carbon nanotubes [19,20]) within the membrane to obstruct the transport of undesired molecules.

Previously, we prepared a series of crosslinked copolymeric ion exchange membranes (IEM) with a crosslinker, poly(ethylene glycol) diacrylate (PEGDA), a charged monomer (i.e.

AMPS (Chapter 4, 5, 7, and 8), APTA (Chapter 6), and SPMAK (Chapter 9)) and an uncharged monomer with either a hydroxyl end group (AA, HEMA, PEGMA (Chapter 7, 8)) or a phenyl end group (PEMA, PEA, and PEGPEA (Chapter 9)). Although this series of investigations provided valuable insights on understanding the impact of various pendant groups on the transport and co-transport of solutes, the applicability of these materials as crosslinked IEMs is doubtful as they must be mechanically stable (crosslinked IEMs with PEGDA are quite fragile).

Here, we introduce a class of crosslinked IEMs that are significantly enhanced in mechanical properties with relatively low water content [21]. Recently, Mredha et al. introduced a hydrogel with great mechanical properties (i.e. modulus and strength), where they prepared a series of copolymeric organogels with a crosslinker, N,N′-methylenebisacrylamide (MBAA), a hydrophobic comonomer, phenyl acrylate (PA), and a hydrophilic comonomer, acrylamide (AAm) in an organic solvent, dimethyl sulfoxide (DMSO), and converted the organogels to hydrogels by a solvent exchange from DMSO to water [21]. Here, we take inspiration from this approach to improving mechanics but vary the chemistry to prepare IEMs. In lieu of AAm we utilize an ionomer, either AMPS or methacroylcholine chloride (MACC, bearing a quaternary ammonium (QA^+)), and prepare crosslinked MBAA-PA/AMPS CEMs (briefly PA/A) and MBAA-PA/MACC (briefly PA/M). Further, we also replace PA with phenyl methacrylate (PMA/A and PMA/M) to understand the effect of the additional methyl group on the polymer backbone [22] on membrane properties. From these IEMs, we select an AEM with a low water volume fraction (PA/M prepared with 30 mol% of MBAA, briefly PA/M-30) to examine the applicability of these membranes in a fuel cell (i.e. DUFC). DUFC is an emerging type of direct fuel cell, which converts urea (from industrial wastewater and urine) to electrical power [23] with a relatively high energy density and a low operating temperature [24–26]. One of the challenges of these devices is a lack of IEMs

(either CEM [27] or AEM [7]) that minimize crossover of urea to the cathode side of the cell (especially at higher concentrations) as this crossover can suppress the overall reaction (sweeping effect). To further examine the likelihood of urea crossover, we measure urea permeability of PA/M-30. Finally, we perform similar experiments on a commercial AEM (Fumasep® FAA-3-50, briefly FAA) to validate our crosslinked IEMs as competitive with commercial IEMs for such devices.

10.2. Results and Discussion

A series of hydrogel-based cation exchange membranes, PA/A and PMA/A, and anion exchange membranes, PA/M and PMA/M, were prepared by free radical copolymerization with varying crosslinker (MBAA) content as a new class of ion exchange membranes; see 3.2.2 for synthesis, Fig. 10.1 for exemplary photos, Fig. 10.2 for chemical structures, and Table 10.1 for compositions. We characterize these IEMs for a range of physical properties relevant to their use in DUFCs (ϕ_w, IEC, σ, and Young's modulus). Based on this characterization we selected an AEM with a low water volume fraction (PA/M-30) for characterization in a direct urea fuel cell [6] and compare its performance to a selected a commercial AEM (Fumasep FAA-3-50, FAA [28]). The following sections describe and discuss the results of this investigation.

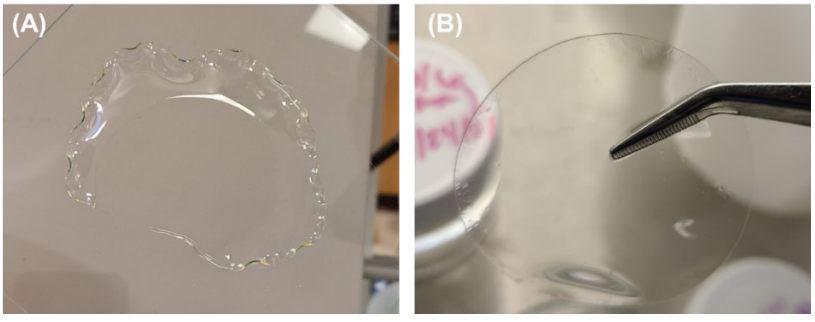

Figure 10.1. Photos of (A) organogel after polymerization and (B) hydrogel after solvent exchange from DMSO to water.

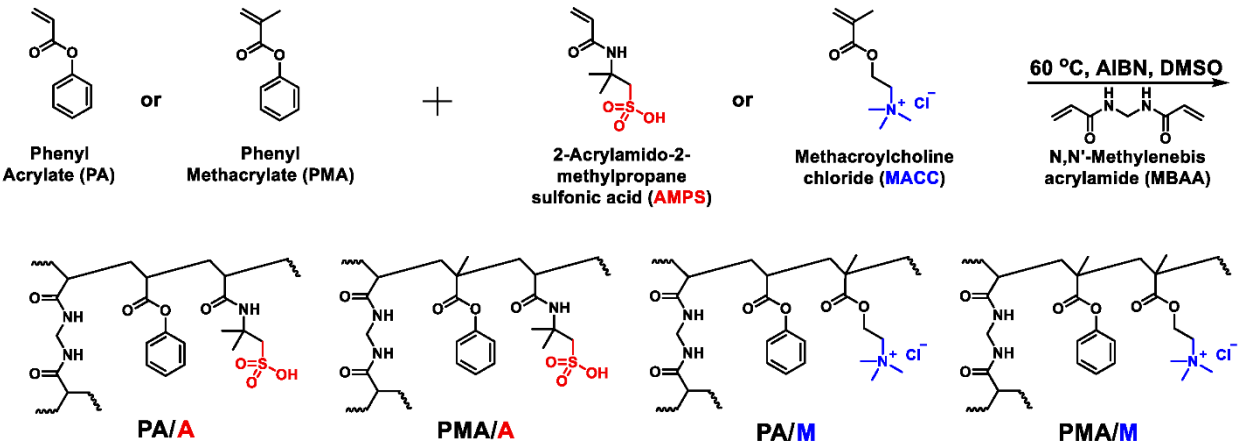

Figure 10.2. Scheme of prepared (A) PA/A, (B) PMA/A, (C) PA/M, and (D) PMA/M organogels.

Table 10.1. Membrane characteristics from pre-polymerization mixtures.
Cation Exchange Membranes

Name	MBAA[a] (mol%)	AMPS[b] (mol%)	PA or PMA (g)	AMPS (g)	AIBN (g)	MBAA (g)	DMSO (g)
PA/A-5	5	30	1.492	0.894	0.003	0.111	2.500
PA/A-10	10	30	1.428	0.856	0.003	0.212	2.500
PA/A-20	20	30	1.317	0.789	0.003	0.391	2.500
PA/A-30	30	30	1.221	0.732	0.002	0.545	2.500
PMA/A-5	5	30	1.541	0.844	0.003	0.112	2.500
PMA/A-10	10	30	1.475	0.808	0.003	0.214	2.500
PMA/A-20	20	30	1.359	0.744	0.003	0.394	2.500
PMA/A-30	30	30	1.260	0.690	0.002	0.547	2.500

Anion Exchange Membranes

Name	MBAA[a] (mol%)	MACC[c] (mol%)	PA or PMA (g)	MACC (g)	AIBN (g)	MBAA (g)	DMSO (g)	Water[d] (g)
PA/M-5	5	30	1.491	0.896	0.003	0.111	2.276	0.224
PA/M-10	10	30	1.427	0.858	0.003	0.212	2.286	0.214
PA/M-20	20	30	1.316	0.790	0.003	0.391	2.302	0.198
PA/M-30	30	30	1.220	0.733	0.002	0.544	2.317	0.183
PMA/M-5	5	30	1.540	0.845	0.003	0.112	2.289	0.211
PMA/M-10	10	30	1.474	0.809	0.003	0.214	2.298	0.202
PMA/M-20	20	30	1.358	0.745	0.003	0.394	2.314	0.186

[a]MBAA = mol of MBAA/(mol of PA or PMA + mol of AMPS or MACC) × 100 %
[b]AMPS = mol of AMPS/(mol of PA or PMA + mol of AMPS) × 100 %
[c]MACC = mol of MACC/(mol of PA or PMA + mol of MACC) × 100 %
[d]Water, from the MACC solution as 20 % of the solution is water.

10.2.1. Young's modulus and storage modulus

Tensile experiments of all films were performed in triplicate, an exemplary stress-strain curve from all films is shown in Fig. 10.3 (where (A-E) are scaled differently), and the Young's moduli are shown in Fig. 10.4 and Table 10.2.

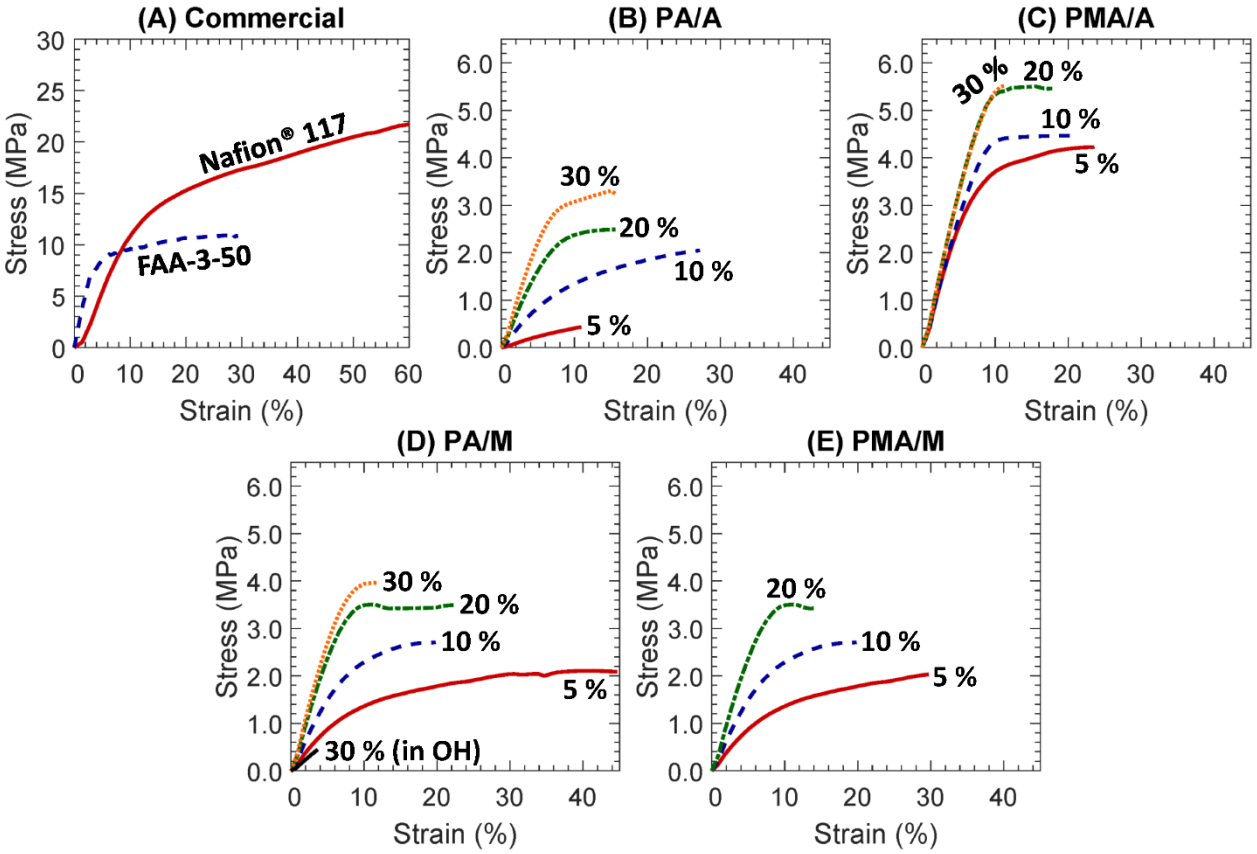

Figure 10.3. Stress-strain curves of (A) commercial CEM (Nafion® 117, red-solid) and AEM (FAA-Br, blue-dashed), (B) PA/A, (C) PMA/A, (D) PA/M, and (E) PMA/M, where the MBAA (crosslinker) contents are specified as 5 (red-solid), 10 (blue-dashed), 20 (green-dot-dashed), and 30 (orange-dotted) mol%.

Generally, commercial films show a higher toughness (both strong and ductile) over crosslinked films. A contribution to the relatively higher ductility of these commercial films is that they are thermoplastic polymers (crosslink-free) such that they can freely elongate, whereas the crosslinked films undergo irreversible damage to the film upon breaking of the internal network under strain [29]. For crosslinked IEMs, films prepared with less MBAA (crosslinker) were more

ductile than the films prepared with higher MBAA contents, as would be expected. In the case of PA/M-30, the toughness of the film was significantly decreased after ion exchange to the OH-form (PA/M-30-OH); see Fig. 10.3(D).

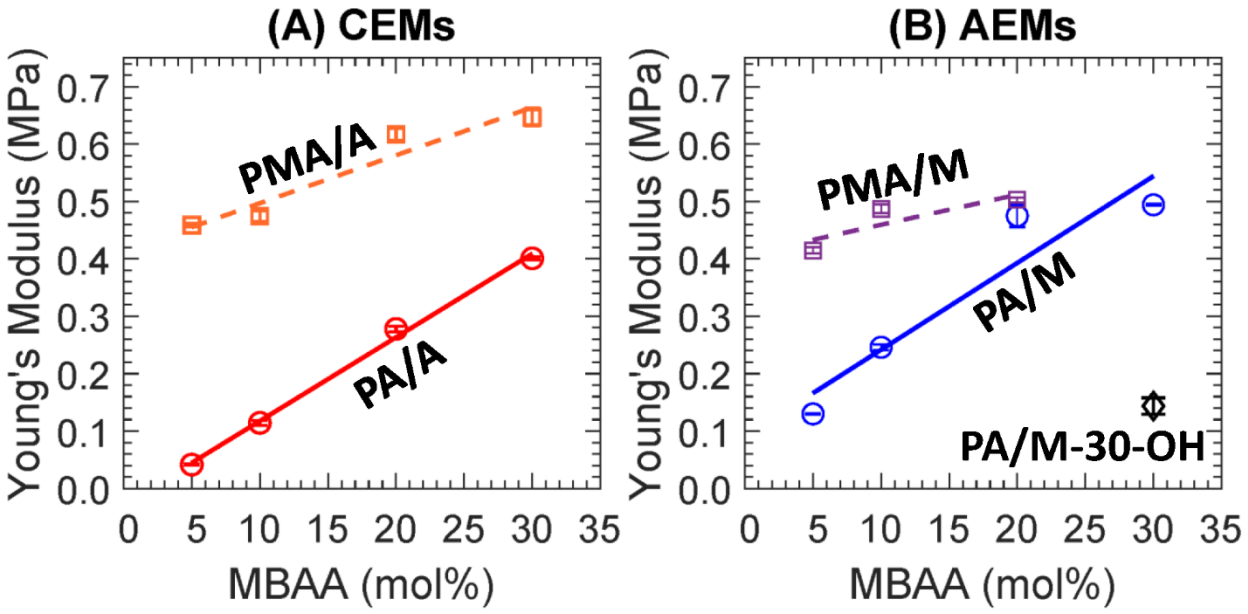

Figure 10.4. Young's modulus of (A) CEMs, PA/A (○, red, solid line) and PMA/A (□, orange, dashed line). Young's modulus of (B) AEMs, PA/M (○, blue, solid line) and PMA/M (□, purple, dashed line). Each data point is the average of 3 membranes with error bars corresponding to the standard deviation. Lines are present as a guide to the eye.

The Young's modulus within each series (PA/A, PMA/A, PA/M, or PMA/M) of membranes increases with increasing MBAA (crosslinker) content; see Fig. 10.4. This is due to the increase in the crosslink density (number of crosslinks per volume, see Table 10.2), which reduces the ductility of each film [29–31]. Moreover, the Young's moduli of PMA-containing films (PMA/A and PMA/M) are higher than those of PA-containing films (PA/A and PA/M) which can be attributed, in part, to an increase in polymer backbone rigidity from the additional methyl groups (Fig. 10.1) [22]. Again, the Young's modulus of PA/M-30-OH was less than PA/M-30 (in Cl-form); see Fig. 10.4(B). Similarly, the storage modulus of all films increased with increasing

MBAA content; see Table 10.2. This is likely due to the increase in the crosslink density (Flory's rubber elasticity relationship) with increasing MBAA content.

Table 10.2. Young's modulus, storage modulus, and estimated crosslink density of CEMs and AEMs.

Cation Exchange Membranes

Name	Young's Modulus (MPa)[a]	Storage Modulus, E' (GPa)[b]	Estimated Crosslink Density, ν_e (mmol/cm^3)	Density (g/mL)	Water Volume Fraction (v/v)
Nafion® 117	1.0 ± 0.0	-	-	1.80 ± 0.01	0.25 ± 0.00[c]
PA/A-5	0.04 ± 0.00	0.06 ± 0.04	8 ± 6	1.30 ± 0.05	0.66 ± 0.00
PA/A-10	0.11 ± 0.00	0.28 ± 0.07	38 ± 9	1.30 ± 0.03	0.49 ± 0.03
PA/A-20	0.28 ± 0.01	0.40 ± 0.13	54 ± 18	1.30 ± 0.00	0.45 ± 0.00
PA/A-30	0.40 ± 0.00	0.42 ± 0.04	57 ± 5	1.32 ± 0.03	0.46 ± 0.01
PMA/A-5	0.46 ± 0.00	0.29 ± 0.11	39 ± 15	1.25 ± 0.02	0.59 ± 0.03
PMA/A-10	0.47 ± 0.01	0.35 ± 0.07	47 ± 10	1.27 ± 0.00	0.52 ± 0.01
PMA/A-20	0.62 ± 0.01	0.43 ± 0.19	58 ± 25	1.26 ± 0.02	0.43 ± 0.00
PMA/A-30	0.65 ± 0.02	0.35 ± 0.09	47 ± 13	1.27 ± 0.01	0.41 ± 0.00

Anion Exchange Membranes

Name	Young's Modulus (MPa)[a]	Storage Modulus, E' (GPa)[b]	Estimated Crosslink Density, ν_e (mmol/cm^3)	Density (g/mL)	Water Volume Fraction (v/v)
FAA	2.0 ± 0.0	-	-	1.34 ± 0.02	0.12 ± 0.02
FAA-OH	-	-	-	1.27 ± 0.08	0.58 ± 0.06
PA/M-5	0.13 ± 0.00	0.63 ± 0.17	84 ± 23	1.23 ± 0.00	0.48 ± 0.01
PA/M-10	0.25 ± 0.00	0.46 ± 0.08	62 ± 11	1.22 ± 0.01	0.43 ± 0.01
PA/M-20	0.47 ± 0.02	1.02 ± 0.15	137 ± 20	1.23 ± 0.00	0.39 ± 0.01
PA/M-30[d]	0.49 ± 0.00	-	-	1.24 ± 0.00	0.40 ± 0.01
PA/M-30-OH[d]	0.14 ± 0.01	-	-	1.43 ± 0.02	0.67 ± 0.01
PMA/M-5	0.41 ± 0.01	0.25 ± 0.08	33 ± 10	1.20 ± 0.02	0.53 ± 0.04
PMA/M-10	0.49 ± 0.01	0.46 ± 0.11	62 ± 15	1.22 ± 0.01	0.50 ± 0.00
PMA/M-20	0.50 ± 0.00	0.40 ± 0.12	54 ± 16	1.23 ± 0.02	0.44 ± 0.00

[a]The thickness of the films was ~0.35 mm

[b]The thickness of the films was ~1 mm

[c]Literature [32]

[d]Could not prepare the film (PA/M-30) for 1 mm thickness due to phase separation.

10.2.2. Water volume fraction

The water volume fractions of all films were measured as shown in Fig. 10.5 and Table 10.2. Generally, the water volume fraction of all films decreases with increasing MBAA content. For instance, the water volume fraction of the films prepared with 30 mol% of MBAA is less than those prepared with 5, 10, and 20 mol% of MBAA by 1.33, 1.14, and 1.01 times, on average, respectively. The water volume fractions of CEMs are slightly higher than those of AEMs. This is likely due to the higher sulfonate anion hydration numbers (λ_i, H_2O/ion (i)) of sulfonate anion (λ_{Sulf}: 12-16 [33]) is higher than that of quaternary ammonium cations (λ_{QA}: 4 [34]). The difference in the water volume fraction of films prepared with PA and PMA was not apparent, where the water volume fractions of PA/A films were slightly higher than those of PMA/A films and those of PMA/M films were slightly higher than those of PA/M films; see Fig. 10.5(A,B).

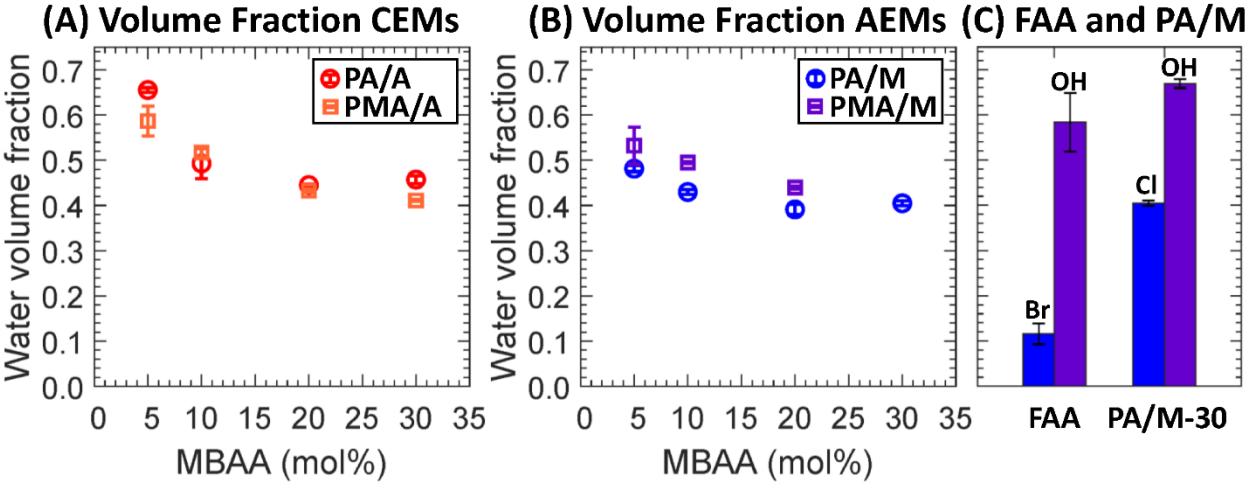

Figure 10.5. Water volume fractions of (A) CEMs, PA/A (○, red) and PMA/A (□, orange). Water volume fractions of AEMs, (B) PA/M (○, blue) and PMA/M (□, purple) and (C) FAA-Br, FAA-OH, PA/M-30-Cl, and PA/M-30-OH. Each data point is the average of 3 membranes with error bars corresponding to the standard deviation.

The water volume fraction of PA/M-30 in Cl-form (λ_{Cl} = 1 [35]) was significantly higher than that of FAA in Br-form (λ_{Br} = 1 [35]). One possible cause is the difference in the polymer structure such that FAA is more tightly structured via its poly(phenylene oxide) backbone [28]

than PA/M-30 with a crosslinked poly(phenyl acrylate-co-MACC) backbone. However, the water volume fraction of FAA is much closer to that of PA/M-30 after exchange the counterion to OH- form (λ_{OH} = 3 [35]); see Fig. 10.5(C). Two primary factors likely contribute to this behavior, the higher ion exchange capacity for FAA (IEC, 2.02 meq/g) compated to PA/M-30 (1.41 meq/g) and the higher hydration number for OH (λ_{OH} = 3 [35]) compared to the Br^- and Cl^- anions.

10.2.3. IEC and Ionic conductivity of membranes

The IEC of CEMs (PA/A and PMA/A) and AEMs (PA/M and PMA/M) were measured yielding the results shown in Fig. 10.6 and Table 10.3. IECs of each series of films decrease with increasing MBAA content, which is likely due to the decrease in the ionomer content. The measured IECs of all films were closely matched with the theoretical IECs.

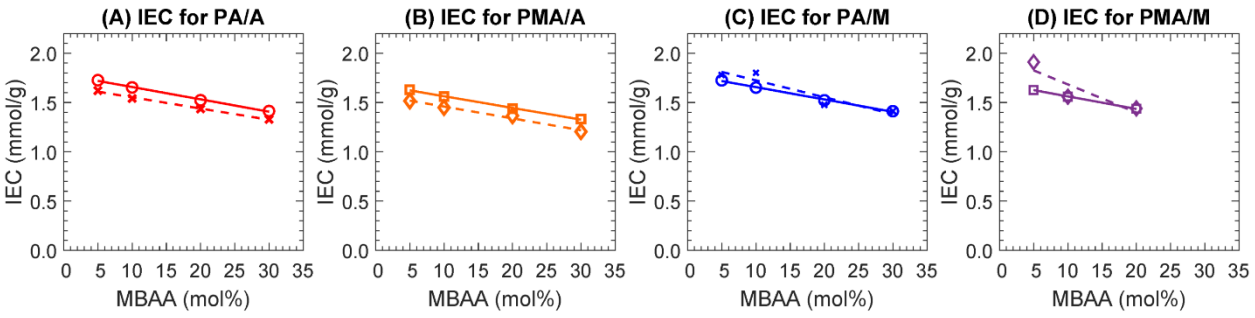

Figure 10.6. Theoretical IECs (solid lines) of (A) PA/A (red, ○) and (B) PMA/A (orange, □), (C) PA/M (○, blue) and (D) PMA/M (□, purple). Measured IECs (dashed lines) of (A) PA/A (red, ×), (B) PMA/A (orange, ◊), (C) PA/M (×, blue), and (D) PMA/M (◊, purple). Lines are present as a guide to the eye.

Table 10.3. Ionic conductivity, and ion exchange capacity of CEMs and AEMs.
Cation Exchange Membranes

Name	Conductivity (σ, mS/cm)	Theoretical IEC (meq/g dry polymer)[a]	Measured IEC (meq/g dry polymer)
Nafion® 117	78 ± 1[b]	≥0.90[c]	-
PA/A-5	91.0 ± 0.0	1.73	1.62
PA/A-10	88.1 ± 0.0	1.65	1.54
PA/A-20	65.2 ± 0.0	1.52	1.43
PA/A-30	56.4 ± 0.1	1.41	1.33
PMA/A-5	61.5 ± 0.1	1.63	1.52
PMA/A-10	53.9 ± 0.5	1.56	1.45
PMA/A-20	35.7 ± 0.2	1.44	1.37
PMA/A-30	33.5 ± 0.0	1.33	1.20

Anion Exchange Membranes

Name	Conductivity (σ, mS/cm)	Theoretical IEC (meq/g dry polymer)[a]	Measured IEC (meq/g dry polymer)
FAA	2.9 ± 0.0	2.02[c]	-
FAA-OH	16.2 ± 0.1	-	-
PA/M-5	15.6 ± 0.3	1.72	1.78
PA/M-10	14.3 ± 0.0	1.65	1.80
PA/M-20	9.1 ± 0.0	1.52	1.48
PA/M-30	6.0 ± 0.0	1.41	1.41
PA/M-30-OH	55.0 ± 0.1	-	-
PMA/M-5	19.6 ± 1.2	1.63	1.91
PMA/M-10	16.2 ± 0.2	1.56	1.56
PMA/M-20	12.7 ± 0.5	1.44	1.44

[a]Theoretical IEC = (mmol of AMPS or MACC)/(g of MBAA + g of PA or PMA + g of AMPS or MACC)
[b]Literature [32]
[c]Reported by manufacturers

The ionic conductivities of all films were measured at 25 °C as shown in Table 10.3 and Fig. 10.7; where Fig. 10.7(A-C) are scaled differently. Generally, the ionic conductivities of the AEMs were lower than the CEMs. Here, the difference in molar conductivities of the counterion plays a role, where the molar conductivity of H^+ (for PA/A and PMA/A) is 350×10^{-4} $m^2\cdot S/mol$ and that of Cl^- (for PA/M and PMA/M) 76×10^{-4} $m^2\cdot S/mol$ [36]. We observed the ionic conductivities of PA-containing CEMs (PA/A) to be higher than those of PMA-containing CEMs (PMA/A), whereas ionic conductivities of PA-containing AEMs (PA/M) are less than those of PMA-containing AEMs (PMA/M); see Fig. 10.7(A,B). This is likely related to the measured IEC (dotted lines in Fig. 10.6), where the IECs of PA/A films are higher than those of PMA/A films, when those of PA/M films are equal to or less than those of PMA/M films.

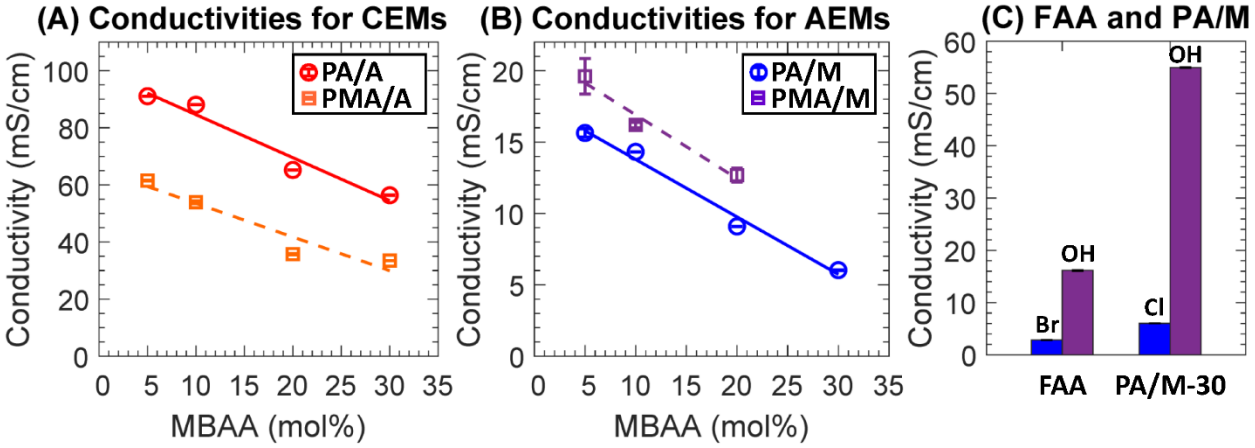

Figure 10.7. Ionic conductivities of (A) CEMs, PA/A (○, red, solid line) and PMA/A (□, orange, dashed line) and (B) AEMs, PA/M (○, blue, solid line) and PMA/M (□, purple, dashed line). Lines are present as a guide to the eye. (C) Ionic conductivities of FAA in Br^- form (blue) and OH^- form (purple) and PA/M-30 in Cl^- form (blue) and OH^- form (purple). Each data point is the average of 3 membranes with error bars corresponding to the standard deviation.

The ionic conductivities of FAA and PA/M-30 are significantly increased after the counterion conversion to OH^- form; see Fig. 10.7(C). This is due to the molar conductivity of OH^- (198×10^{-4} $m^2\cdot S/mol$) being significantly higher than those of Br^- (78×10^{-4} $m^2\cdot S/mol$) and Cl^- [36].

Another contribution is the increase in water volume fraction as the ionic conductivity of IEMs often increases with increasing the water volume fraction (upper bound relationship [37]).

10.2.4. Direct Urea Fuel Cell

Two membrane electrode assemblies (MEA), prepared with FAA-OH and PA/M-30-OH, were used in analogous fuel feeds of 1 M KOH containing 0.33 M urea and humidified air (relative humidity: 100 %) as the electron- and donor-acceptors [7]. The anode and cathode reactions in the fuel cell are as follow [5]:

Reaction 1 (Anode): $CO(NH_2)_2 + 6\ OH^- \rightarrow CO_2 + 5\ H_2O + N_2 + 6\ e^-$

Reaction 2 (Cathode): $3/2\ O_2 + 3\ H_2O + 6\ e^- \rightarrow 6\ OH^-$

The $Ni(OH)_2$ catalysts on the anode will adsorb the urea molecules, followed by urea oxidation under alkaline media. As a result of a urea oxidation reaction, six electrons flow to the cathode through the external circuit, forming a hydroxide ion (OH^-) with the humidification at cathode; see Fig. 10.8.

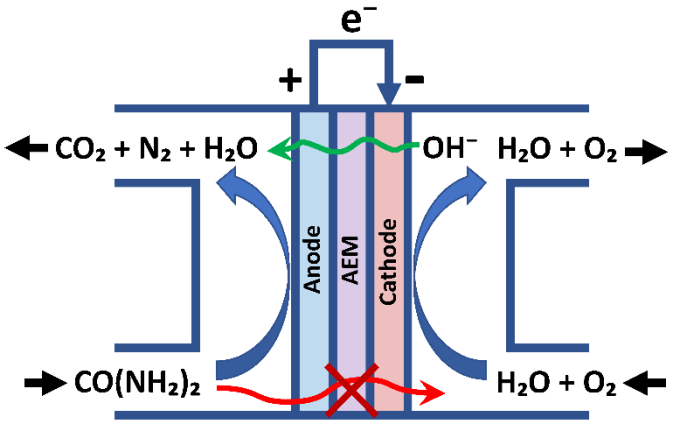

Figure 10.8. Schematic diagram of a direct urea fuel cell [5].

The relative DUFC performance of both MEAs was investigated in a DUFC utilizing a $Ni(OH)_2$/C anode and Ag/C cathode at 20 °C, as shown in Fig. 10.9(A,B). After the activation process, the

initial difference of electrical potential between the two electrodes was read as the open circuit voltage (OCV). The power output, *P*, of the fuel cell is also determined through the product of voltage, *V*, and current, *I* (*P* = *V*/*I*). The OCV and power densities were evaluated, reaching 0.89 V and 2.16 mW/cm^2 at FAA-OH and 0.89 V and 2.19 mW/cm^2 at PA/M-30-OH, respectively; see Table 10.4 and Fig. 10.9. The two prominent roles of the membrane in a DUFC are (1) restricting the urea flow from anode to cathode for improving urea oxidation efficiency and (2) transferring OH^- from the cathode to the anode in alkaline media. Critically, the obtained OCV and power density using the PA/M-30-OH membrane were comparable to those obtained for the commercially available FAA-OH membrane.

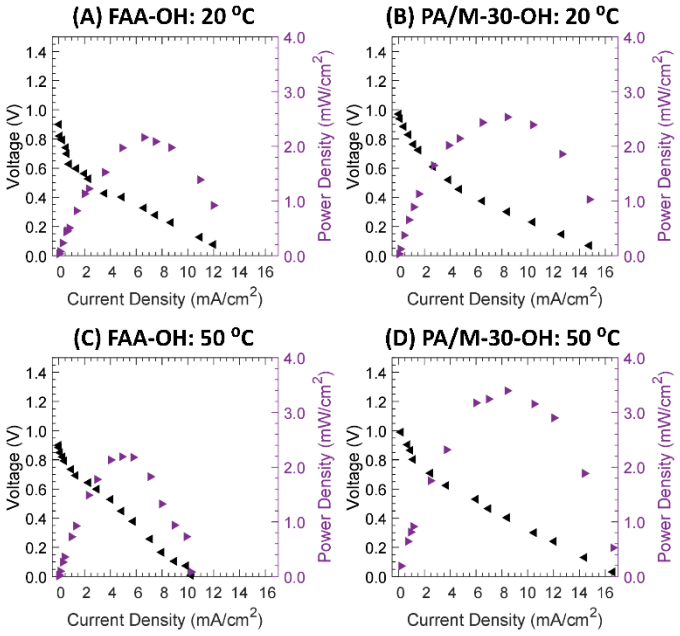

Figure 10.9. The power density and OCV, in initial voltage, of (A,C) FAA-OH and (B,D) PA/M-30-OH at (A,B) 20 and (C,D) 50 °C.

As the DUFC efficiency improves at higher working temperatures due to diminished polarization resistances, analogous tests were performed in a DUFC system at moderate elevated temperature (50 °C) under the same feed conditions, as shown in Fig. 10.9(C,D). At this elevated

temperature, FAA-OH exhibits an OCV of 0.97 V and maximum power density of 2.53 mW/cm^2 and PA/M-30-OH demonstrated an OCV of 0.99 V and a maximum power density of 3.40 mW/cm^2; see Table 10.4. These differences in operation at elevated temperature are presumably linked with the crossover of urea ($CO(NH_2)_2$) and OH^- from the anode to the cathode which diminishes the anodic reaction and interferes with the cathodic reaction [5]. In addition, AEMs undergoes the loss of ion conductivity as the OH^- ions flow is hindered by the direct contact of anode and urea molecules in the urea-based environment [38]. More details on the urea crossover will be discussed in the next section.

Table 10.4. Maximum power density and voltage at the maximum power density.

Name	Temperature (°C)	Maximum Power Density (mW/cm^2)	Voltage at the Maximum Power Density (V)
FAA-OH	20	2.16	0.327
	50	2.53	0.301
PA/M-30-OH	20	2.19	0.449
	50	3.40	0.404

10.2.5. Urea Permeability

The diffusive permeabilities of FAA-OH and PA/M-30-OH to urea at 25 and 55 °C at 1, 2, and 3 M were measured via diffusion cell experiments; see Fig. 10.10(B).

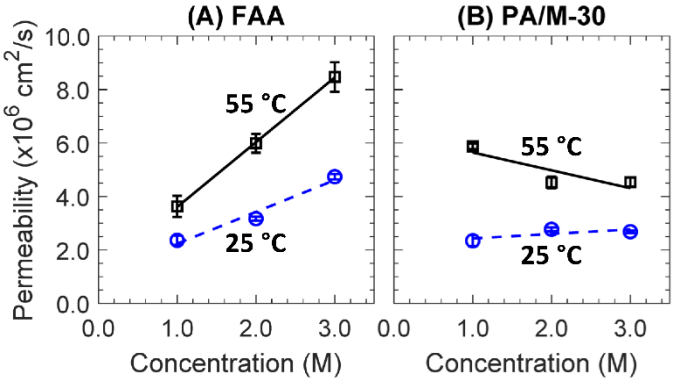

Figure 10.10. Urea permeabilities of (A) FAA-OH and (B) PA/M-30-OH at 25 °C (dashed, blue, ○) and 55 °C (solid line, black, □) at 1, 2, and 3 M of urea. Lines are present as a guide to the eye.

Generally, permeability of both FAA-OH and PA/M-30-OH to urea measured at 55 °C were higher than those measured at 25 °C by a factor of 2, on average. This is due to the increase in the diffusivity (Stokes-Einstein [39]) with temperature [40]. While PA/M-30-OH permeabilities to urea were essentially consistent under different concentrations (1, 2, and 3 M, with a slight decrease observed from 1 to 2 M at 55 °C), FAA-OH permeabilities were increased with increasing urea concentrations. This is presumably due to the solubility (dependent on the affinity between solute and polymer) of the FAA-OH to urea is a function of concentration. As a dense membrane, the permeabilities of FAA-OH can be explained by the solution-diffusion relationship (permeability = solubility × diffusivity [41,42]). Since the solute diffusivity is dependent on the free volume, we calculated the ratios between the solvated film (after 2 days in 0.33, 1, 2, and 3 M urea) and hydrated film to understand the volume changes (as the change in volume can be a proxy for the change in free volume); see Table 10.5 for values.

Table 10.5. The volumetric ratio between solvated films (Solutions: 0.33, 1, 2, and 3 M Urea) and hydrated films (V_S/V_H) measured via the photograph-caliper method at 25 °C, where the surface area of each film was measured from a digital photograph coupled with the ImageJ software and the film thickness was measured with a digital caliper by taking the average of 5 random points.

	$V_{0.33M}/V_H$	V_{1M}/V_H	V_{2M}/V_H	V_{3M}/V_H
FAA-OH	0.996 ± 0.007	1.010 ± 0.007	1.000 ± 0.000	1.014 ± 0.031
PA/M-30-OH	1.000 ± 0.006	0.995 ± 0.004	0.996 ± 0.002	1.010 ± 0.011

We observed negligible changes in film volumes under all concentrations, which indicates the change in permeability is presumably due to the changes in sorption. Further investigation on FAA-OH (such as sorption-desorption [43] and relative permittivity [44–46]) can be considered for a better understanding of this behavior. Based on the higher permeability to urea, a higher urea crossover is expected during DUFC operation with FAA-OH than with PA/M-30-OH, which is likely contributing to the lower FAA-OH power densities. Nevertheless, more investigations on the crosslinked IEMs introduced here and their chemically similar analogues is underway

(compositional optimization, other fuel tests, and further characterizations) to validate and integrate the broad applicability of this class of crosslinked IEMs.

10.3. Conclusion

A new class of crosslinked CEMs (PA/A and PMA/A) and AEMs (PA/M and PMA/M) was prepared and characterized. As the crosslinker (MBAA) content increases, Young's modulus increases and water volume fraction decreases, both desirable improvements. An AEM composition with a low water volume fraction (PA/M-30) was selected to validate the applicability of the film in a direct fuel cell (i.e. DUFC) and the performance was compared with a commercial anion exchange membrane (FAA-3-50). The power density from the DUFC prepared with PA/M-30-OH was slightly higher than that with Fumasep FAA-3-50-OH. This is likely due to a higher ionic conductivity (55 > 16 mS/cm) and presumably less urea crossover. This new class of crosslinked IEM can be a promising candidate for various energy devices upon target-specific compositional optimization.

10.4. References

[1] M. Galizia, D.R. Paul, B.D. Freeman, Liquid methanol sorption, diffusion and permeation in charged and uncharged polymers, Polymer. 102 (2016) 281–291. https://doi.org/10.1016/j.polymer.2016.09.010.

[2] A. Heinzel, V.M. Barragán, A review of the state-of-the-art of the methanol crossover in direct methanol fuel cells, J Power Sources. 84 (1999) 70–74. https://doi.org/10.1016/s0378-7753(99)00302-x.

[3] K. Matsuoka, Y. Iriyama, T. Abe, M. Matsuoka, Z. Ogumi, Alkaline direct alcohol fuel cells using an anion exchange membrane, J Power Sources. 150 (2005) 27–31. https://doi.org/10.1016/j.jpowsour.2005.02.020.

[4] D.T. Hallinan, Y.A. Elabd, Diffusion and sorption of methanol and water in Nafion using time-resolved fourier transform infrared−attenuated total reflectance spectroscopy, J Phys Chem B. 111 (2007) 13221–13230. https://doi.org/10.1021/jp075178n.

[5] E.T. Sayed, T. Eisa, H.O. Mohamed, M.A. Abdelkareem, A. Allagui, H. Alawadhi, K.-J. Chae, Direct urea fuel cells: challenges and opportunities, J Power Sources. 417 (2019) 159–175. https://doi.org/10.1016/j.jpowsour.2018.12.024.

[6] J. Yoon, Y.S. Yoon, D.-J. Kim, Silver-nanoparticle-decorated NiOOH nanorods for electrocatalytic urea sensing, Acs Appl Nano Mater. 3 (2020) 7651–7658. https://doi.org/10.1021/acsanm.0c01279.

[7] J. Yoon, D. Lee, Y.N. Lee, Y.S. Yoon, D.-J. Kim, Solid solution palladium-nickel bimetallic anode catalysts by co-sputtering for direct urea fuel cells (DUFC), J Power Sources. 431 (2019) 259–264. https://doi.org/10.1016/j.jpowsour.2019.05.059.

[8] M.R. Singh, E.L. Clark, A.T. Bell, Effects of electrolyte, catalyst, and membrane composition and operating conditions on the performance of solar-driven electrochemical reduction of carbon dioxide, Phys Chem Chem Phys. 17 (2015) 18924–18936. https://doi.org/10.1039/c5cp03283k.

[9] D.A. Salvatore, C.M. Gabardo, A. Reyes, C.P. O'Brien, S. Holdcroft, P. Pintauro, B. Bahar, M. Hickner, C. Bae, D. Sinton, E.H. Sargent, C.P. Berlinguette, Designing anion exchange membranes for CO2 electrolysers, Nat Energy. (2021) 1–10. https://doi.org/10.1038/s41560-020-00761-x.

[10] D.M. Weekes, D.A. Salvatore, A. Reyes, A. Huang, C.P. Berlinguette, Electrolytic CO2 reduction in a flow cell, Accounts Chem Res. 51 (2018) 910–918. https://doi.org/10.1021/acs.accounts.8b00010.

[11] D.J. Miller, F.A. Houle, Energy and Environment Series, (2018) 341–385. https://doi.org/10.1039/9781788010313-00341.

[12] B.S. Beckingham, N.A. Lynd, D.J. Miller, Monitoring multicomponent transport using in situ ATR FTIR spectroscopy, J Membrane Sci. 550 (2018). https://doi.org/10.1016/j.memsci.2017.12.072.

[13] Z. Yin, H. Peng, X. Wei, H. Zhou, J. Gong, M. Huai, L. Xiao, G. Wang, J. Lu, L. Zhuang, An alkaline polymer electrolyte CO 2 electrolyzer operated with pure water, Energ Environ Sci. 12 (2019) 2455–2462. https://doi.org/10.1039/c9ee01204d.

[14] Z. Liu, H. Yang, R. Kutz, R.I. Masel, CO2 electrolysis to CO and O2 at high selectivity, stability and efficiency using Sustainion membranes, J Electrochem Soc. 165 (2018) J3371–J3377. https://doi.org/10.1149/2.0501815jes.

[15] L. Li, J. Zhang, T. Jiang, X. Sun, Y. Li, X. Li, S. Yang, S. Lu, H. Wei, Y. Ding, High ion conductivity and diffusivity in the anion exchange membrane enabled by tethering with multication strings on the poly(biphenyl alkylene) backbone, Acs Appl Energy Mater. 3 (2020) 6268–6279. https://doi.org/10.1021/acsaem.0c00409.

[16] M. Krödel, B.M. Carter, D. Rall, J. Lohaus, M. Wessling, D.J. Miller, Rational design of ion exchange membrane material properties limits the crossover of CO2 reduction products in artificial photosynthesis devices, Acs Appl Mater Inter. 12 (2020) 12030–12042. https://doi.org/10.1021/acsami.9b21415.

[17] P.K. Leung, Q. Xu, T.S. Zhao, L. Zeng, C. Zhang, Preparation of silica nanocomposite anion-exchange membranes with low vanadium-ion crossover for vanadium redox flow batteries, Electrochim Acta. 105 (2013) 584–592. https://doi.org/10.1016/j.electacta.2013.04.155.

[18] J.M. Kim, B.S. Beckingham, Comonomer effects on co-permeation of methanol and acetate in cation exchange membranes, Eur Polym J. (2021) 110307. https://doi.org/10.1016/j.eurpolymj.2021.110307.

[19] L. Cui, Q. Geng, C. Gong, H. Liu, G. Zheng, G. Wang, Q. Liu, S. Wen, Novel sulfonated poly (ether ether ketone)/silica coated carbon nanotubes high-performance composite membranes for direct methanol fuel cell, Polym Advan Technol. 26 (2015) 457–464. https://doi.org/10.1002/pat.3473.

[20] Y.-H. Su, Y.-L. Liu, Y.-M. Sun, J.-Y. Lai, D.-M. Wang, Y. Gao, B. Liu, M.D. Guiver, Proton exchange membranes modified with sulfonated silica nanoparticles for direct methanol fuel cells, J Membrane Sci. 296 (2007) 21–28. https://doi.org/10.1016/j.memsci.2007.03.007.

[21] Md.T.I. Mredha, S.K. Pathak, V.T. Tran, J. Cui, I. Jeon, Hydrogels with superior mechanical properties from the synergistic effect in hydrophobic–hydrophilic copolymers, Chem Eng J. 362 (2018) 325–338. https://doi.org/10.1016/j.cej.2018.12.023.

[22] K. Chang, T. Xue, G.M. Geise, Increasing salt size selectivity in low water content polymers via polymer backbone dynamics, J Membrane Sci. 552 (2018) 43–50. https://doi.org/10.1016/j.memsci.2018.01.057.

[23] N. Senthilkumar, G.G. kumar, A. Manthiram, 3D hierarchical core–shell nanostructured arrays on carbon fibers as catalysts for direct urea fuel cells, Adv Energy Mater. 8 (2018) 1702207. https://doi.org/10.1002/aenm.201702207.

[24] N. Kakati, G. Li, P.-Y.A. Chuang, Insights into the Ni/C-Based thin-film catalyst layer design for urea oxidation reaction in a three-electrode system, Acs Appl Energy Mater. 4 (2021) 4224–4233. https://doi.org/10.1021/acsaem.1c00607.

[25] A. Modak, R. Mohan, K. Rajavelu, R. Cahan, T. Bendikov, A. Schechter, Metal–organic polymer-derived interconnected Fe–Ni alloy by carbon nanotubes as an advanced design of urea

oxidation catalysts, Acs Appl Mater Inter. 13 (2021) 8461–8473. https://doi.org/10.1021/acsami.0c22148.

[26] D. Yang, L. Yang, L. Zhong, X. Yu, L. Feng, Urea electro-oxidation efficiently catalyzed by nickel-molybdenum oxide nanorods, Electrochim Acta. 295 (2019) 524–531. https://doi.org/10.1016/j.electacta.2018.10.190.

[27] F. Guo, K. Cheng, K. Ye, G. Wang, D. Cao, Preparation of nickel-cobalt nanowire arrays anode electro-catalyst and its application in direct urea/hydrogen peroxide fuel cell, Electrochim Acta. 199 (2016) 290–296. https://doi.org/10.1016/j.electacta.2016.01.215.

[28] A.M. Barnes, B. Liu, S.K. Buratto, Humidity-dependent surface structure and hydroxide conductance of a model quaternary ammonium anion exchange membrane, Langmuir. 35 (2019) 14188–14193. https://doi.org/10.1021/acs.langmuir.9b02160.

[29] J.D. Ferry, Viscoelastic Properties of Polymers, 3rd ed., John Wiley & Sons, 1980.

[30] N. Yan, D.R. Paul, B.D. Freeman, Water and ion sorption in a series of cross-linked AMPS/PEGDA hydrogel membranes, Polymer. 146 (2018) 196–208. https://doi.org/10.1016/j.polymer.2018.05.021.

[31] A.C. Sagle, H. Ju, B.D. Freeman, M.M. Sharma, PEG-based hydrogel membrane coatings, Polymer. 50 (2009) 756–766. https://doi.org/10.1016/j.polymer.2008.12.019.

[32] J.M. Kim, B.M. Dobyns, R. Zhao, B.S. Beckingham, Multicomponent transport of methanol and acetate in a series of crosslinked PEGDA-AMPS cation exchange membranes, J Membrane Sci. (2020) 118486. https://doi.org/10.1016/j.memsci.2020.118486.

[33] A. Kusoglu, A.Z. Weber, New insights into perfluorinated sulfonic-acid ionomers, Chem Rev. 117 (2017) 987–1104. https://doi.org/10.1021/acs.chemrev.6b00159.

[34] D.R. Dekel, Review of cell performance in anion exchange membrane fuel cells, J Power Sources. 375 (2018) 158–169. https://doi.org/10.1016/j.jpowsour.2017.07.117.

[35] J.N. Israelachvili, Intermolecular and Surface Forces, 3rd ed., 2011.

[36] P. Vany´sek, Ionic Conductivity and Diffusion at Infinite Dilution, CRC Handbook of Chemistry and Physics, 93rd Edition. (2012).

[37] L.M. Robeson, H.H. Hwu, J.E. McGrath, Upper bound relationship for proton exchange membranes: Empirical relationship and relevance of phase separated blends, J Membrane Sci. 302 (2007) 70–77. https://doi.org/10.1016/j.memsci.2007.06.029.

[38] W. Xu, H. Zhang, G. Li, Z. Wu, A urine/Cr(VI) fuel cell — Electrical power from processing heavy metal and human urine, J Electroanal Chem. 764 (2016) 38–44. https://doi.org/10.1016/j.jelechem.2016.01.013.

[39] J.T. Edward, Molecular volumes and the Stokes-Einstein equation, J Chem Educ. 47 (1970) 261. https://doi.org/10.1021/ed047p261.

[40] S.P. Cadogan, G.C. Maitland, J.P.M. Trusler, Diffusion coefficients of CO2 and N2 in water at temperatures between 298.15 K and 423.15 K at pressures up to 45 MPa, J Chem Eng Data. 59 (2014) 519–525. https://doi.org/10.1021/je401008s.

[41] R.W. Baker, Membrane Technology and Applications, (2018). https://doi.org/10.1002/9781118359686.

[42] J.G. Wijmans, R.W. Baker, The solution-diffusion model: a review, J Membrane Sci. 107 (1995) 1–21. https://doi.org/10.1016/0376-7388(95)00102-i.

[43] G.M. Geise, L.P. Falcon, B.D. Freeman, D.R. Paul, Sodium chloride sorption in sulfonated polymers for membrane applications, J Membrane Sci. 423 (2012) 195–208. https://doi.org/10.1016/j.memsci.2012.08.014.

[44] K. Chang, G.M. Geise, Dielectric permittivity properties of hydrated polymers: measurement and connection to ion transport properties, Ind Eng Chem Res. 59 (2019) 5205–5217. https://doi.org/10.1021/acs.iecr.9b03950.

[45] K. Chang, H. Luo, G.M. Geise, Influence of salt concentration on hydrated polymer relative permittivity and state of water properties, Macromolecules. 54 (2021) 637–646. https://doi.org/10.1021/acs.macromol.0c02188.

[46] K. Chang, H. Luo, G.M. Geise, Water content, relative permittivity, and ion sorption properties of polymers for membrane desalination, J Membrane Sci. 574 (2019) 24–32. https://doi.org/10.1016/j.memsci.2018.12.048.

Chapter 11

Conclusion and future work

11.1. Conclusion

A series of membranes were studied (1) to provide new insights on multi-solute transport behavior in ion exchange membranes (IEM) (Chapter 4-9) and (2) to introduce a new class of IEM (Chapter 10). From the first series of investigations, we conjectured a competitive diffusion and a charge screening behavior in co-diffusion. The competitive diffusion states the diffusional path of fast-diffusing solute (i.e. alcohol) can be obstructed by slow-diffusing co-solute (i.e. carboxylate). The charge screening in co-diffusion states the electrostatic interaction (i.e. repulsion and attraction) between polymer-bound charge groups (i.e. sulfonate anions or quaternary ammonium cations) and mobile polyatomic anions (i.e. carboxylate anions) can be interfered with by co-diffusing solute (i.e. alcohol), where a possible cause is the alcohol (relatively hydrophobic) can show a higher affinity towards polymer network (relatively hydrophobic) than both water and carboxylates (relatively hydrophilic). From the second series of investigations, we introduced new crosslinked IEMs with a decent ionic conductivity, mechanical properties, and crossover minimization (i.e. urea). In my opinion, both series of investigations are at a nascent stage and I would like to provide some suggestions for future research.

11.2. Future work

11.2.1. Alcohol-Carboxylate transport in IEMs

- **Larger solutes**

In this series of investigations, relatively smaller solutes (i.e. methanol (MeOH), ethanol (EtOH), formate (OFm^-), and acetate (OAc^-)) were selected. It would be interesting to investigate larger solutes, such as 1-propanol (1-PrOH), 2-propanol (2-PrOH), 1-butanol (1-BuOH), and 2-butanol (2-BuOH) for alcohol; and propionate$^-$ (OPr^-), ethyl butyrate$^-$ (1-OBu^-), and 2-methylpropanoate$^-$ (2-OBu^-) for carboxylates; see Fig. 11.1 for structures.

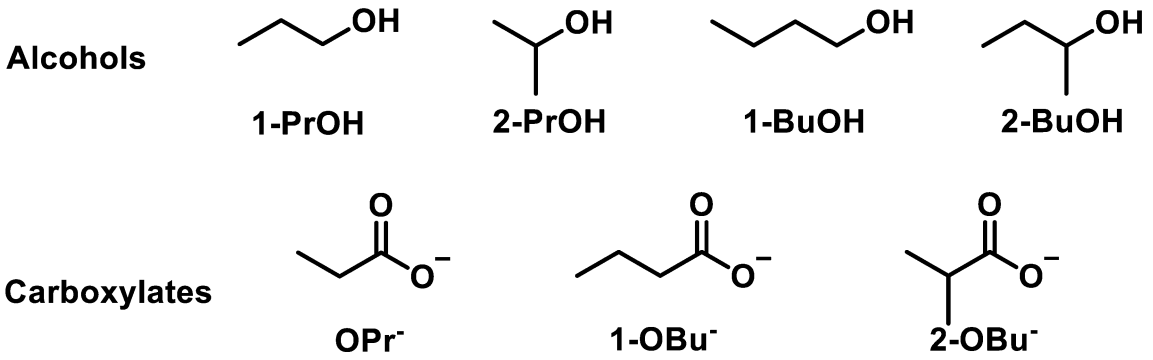

Figure 11.1. Structures of 1-propanol (1-PrOH), 2-propanol (2-PrOH), 1-butanol (1-BuOH), and 2-butanol (2-BuOH), propionate$^-$ (OPr^-), ethyl butyrate$^-$ (1-OBu^-), and 2-methylpropanoate$^-$ (2-OBu^-).

Here, the effect of the hydrophobic carbon chains of different sizes can have a significant impact on the overall transport. Following factors are some of the interactions that may affect the overall transport:

(1) Solute-Solute interactions: hydrophilic functional groups (hydroxyl (-OH) and carboxyl (-COOH)), hydrophobic functional groups (alkyl and alkyl), etc.

(2) Polymer-Solute interactions: polymer-hydroxyl, polymer-carboxyl, and polymer-alkyl.

(3) Polymer-Solvent (water) and Solute-Solvent interactions.

- **Different charge groups**

So far, the effect of sulfonate ($-SO_3^-$, for CEMs) and quaternary ammonium ($-QA^+$, for AEMs) groups on alcohol-carboxylate co-transport have been investigated. It can be interesting to investigate the effect of other charge groups (such as phosphate for CEMs and imidazolium for AEMs; see Fig. 11.2). Data from this investigation can allow a deeper understanding of the apparent co-transport behaviors in alcohol-carboxylate (i.e. charge screening by alcohol and competitive diffusion).

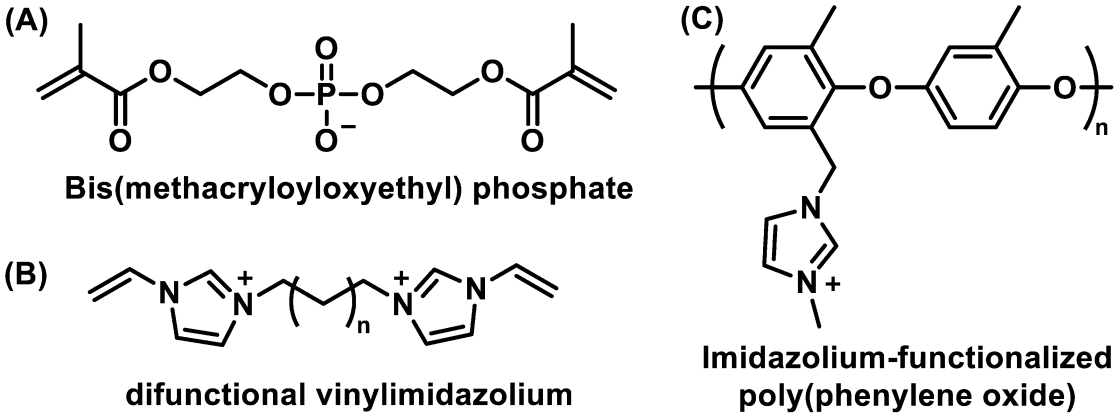

Figure 11.2. Structures of (A) bis(methacryloyloxyethyl) phosphate, (B) difunctional vinylimidazolium [1], and (C) imidazolium-functionalized poly(phenylene oxide) [2].

- **Relative permittivity (dielectric constant)**

In this study, the co-transport behaviors (i.e. competitive diffusion and charge screening by co-diffusant) has been mainly focused on diffusion (solution-diffusion theory). However, the solubilities in co-sorption must be clarified to fully conceptualize these co-transport behaviors. The measurement of relative permittivities of solvated films (after sorption in alcohol and/or carboxylate) may provide more insight. For instance, Chang et al. conjectured the relative permittivity of hydrated polymers is dependent on the hydrogen bonding between water and polymer [3]. Based on this conjecture, the hydrogen bonding

between water and polymer can be interrupted upon introduction of MeOH (as partially hydrophobic polymers tend to favor the interaction with MeOH over water). Therefore, the measured relative permittivity of the film can be lower than the expected relative permittivity. For instance, the relative permittivity of solvated films (1 M MeOH, x_{water} = 0.97) will be less than that of hydrated films as the relative permittivity of MeOH is 32 and water is 78 at 25 °C; see Figure 11.3 [4]. However, the hydrogen bonding between water and polymer can be decreased and, therefore, the relative permittivity of the solvated membrane can be further decreased.

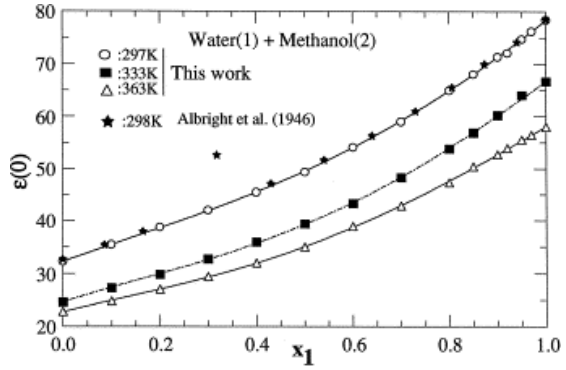

Figure 11.3. Relative permittivity of water-MeOH solution.

Furthermore, the differences and similarities of the relative permittivities of the films solvated in 1 M KOAc, 1 M MeOH, and 1 M each might provide further insights. For instance, the decrease in hydrogen bonding by MeOH can be intensified as hydrophilic KOAc takes up the bulk water region (i.e. freezable water) and pushes MeOH even closer to the polymer.

- **Competitive diffusion**

  In this study, we observed alcohol diffusivities in all films being decreased in co-diffusion with carboxylate in all films. To rationalize this behavior, we conjectured the diffusional path of fast-diffusing alcohol has been obstructed by slow-diffusing carboxylate. To validate this hypothesis, a computational transport simulation (molecular flow module, COMSOL) can be considered. Following steps are suggested, (1) water transport through a large pore, (2) MeOH, NaOAc, Water-MeOH, Water-NaOAc, and Water-MeOH-NaOAc transport through a large pore, (3) reduce the pore size and/or introduce a tight mesh-like structure to mimic the nonporous polymer structure. If MeOH diffusivity in Water-MeOH is higher than that in Water-MeOH-NaOAc, then the competitive diffusion may become a reasonable hypothesis.

- **Charge screening by co-diffusing alcohol**

  In this study, we observed the carboxylate diffusivity being increased in co-diffusion with an alcohol (either MeOH or EtOH). To rationalize this behavior, we conjectured a charge screening behavior that partially hydrophobic alcohol diffuses closer to the polymer network (also partially hydrophobic) relative to water and carboxylates (hydrophilic). To strengthen this conjecture, a differential scanning calorimetry (DSC) can be utilized to measure the freezable/non-freezable water of these polymers and measure the freezable/non-freezable solution (i.e. 1 M MeOH). For instance, if the freezable solution is greater than the freezable water, then MeOH expands the bulk region (reduces the bound water region) and, therefore, potentially diffuses closer to the polymer network.

- **Hydraulic permeability**

  We conjectured two co-diffusion behaviors, (1) competitive diffusion (slower alcohol diffusivity due to slow diffusing carboxylate) and (2) charge screening by alcohol (carboxylate diffusivity being increased in CEMs and decreased in AEMs due to the electrostatic repulsion and attraction, respectively, being interfered by co-diffusing alcohol). These conjectures were based on diffusivity acquired from diffusive permeability, which neglects the back diffusion of water due to osmotic pressure. To further investigate these conjectures, one can set up a dead-end stirred cell experiment to measure the hydraulic permeabilities of water, alcohol, and carboxylate. If the hydraulic permeability of both CEM and AEM to alcohols decreases in co-permeation with a carboxylate, then this result can still be explained with the competitive diffusion. If the hydraulic permeability of CEMs to carboxylates increases and that of AEMs to carboxylates decreases in co-permeation with an alcohol, then this result can be explained by the charge screening behavior.

- **Impact of current on diffusion**

  So far, this study has been focused on understanding the general multi-solute transport behavior in absence of electric current. To further mimic the CO_2 reduction cell, one can apply current. A suggested range of working electrode potential vs reversible hydrogen electrode is from -0.88 to -1.07 V [5], but the potential higher than -0.88 V or lower than -1.07 V can be considered to analyze the impact of electric current on the diffusion.

- **Applicability of the solution-diffusion model**

  In this study, all solute transport has been analyzed based on the solution-diffusion model. The solution-diffusion model is more applicable for a tighter polymer network, which describes the solute transport as the solute enters the free volume elements and diffuse via polymer segmental dynamics. Therefore, the solute concentration near the feed (highly concentrated) side of the membrane is higher than that near the receiver (less concentrated) side of the membrane. Another popular membrane transport model is called the pore-flow model. The pore-flow model is more applicable for a wider polymer network, which describes the spaces (free volume) within the membrane are connected as a tortuous path (much larger than the solute). As a result, the concentration within the membrane is constant. To identify which transport model is more suitable for our membranes (PEGDA-based and commercial films), one can prepare a stack of membranes, perform a diffusion cell experiment, and perform the sorption-desorption experiment over each membrane. If the solubility of the membrane gradually decreases near the receiver cell, then it indicates the transport behavior is more closely related to the solution-diffusion model. However, if the solubility of the membrane is constant over the whole film, then the transport behavior will be more closely linked with the pore-flow model.

11.2.2. Impact of comonomers in CEMs

- **More on PEGPEA**

  Among the films prepared with a phenyl-containing comonomers (PEA or PEGPEA), the most interesting co-transport behavior was observed in PEGPEA-containing films (i.e. PEGDA-SPMAK/PEGPEA). Therefore, more understanding on solute transport behavior in PEGPEA-containing films can be interesting. Firstly, varying the SPMAK-to-PEGPEA content on a narrower scale would be helpful to identify an optimum ratio between SPMAK and PEGPEA that provides the lowest carboxylate diffusivity in co-diffusion with an alcohol (crossover minimization). Moreover, extensive membrane characterization, such as measuring the freezable/non-freezable water ratio with differential scanning calorimetry (DSC) and the average mesh size with a positron annihilation lifetime spectroscopy (PALS) or transmission electron microscopy (TEM), may provide valuable insights.

- **Other comonomers**

  Besides all the monomers considered in this study, there are many more monomers to be considered that are either commercially available or easily synthesizable. Therefore, the internal structure of the crosslinked films can further be tailored with other charge-neutral comonomers. Particularly, methyl acrylate, ethyl acrylate, propyl acrylates, and butyl acrylates are suggested as they might reduce the water volume fraction and suppress the solute diffusion; Figure 11.4.

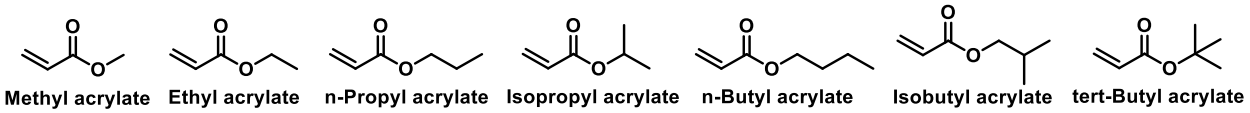

Figure 11.4. Structures of potential alkyl-based comonomers.

Moreover, these monomers can be mixed along with other comonomers (i.e. PEGPEA) to design more favorable internal structures. Additionally, computational approaches (i.e. density functional theory, DFT) can be helpful to estimate the internal structures and identify potential monomers.

11.2.3. New class of IEMs

- **Compositional optimization**

  In this project, a hydrophobic monomer (either PA or PMA, 70 mol% of the total monomer), and a charged monomer (either AMPS or MACC, 30 mol% of the total monomer), and a crosslinker (MBAA, 5 to 30 mol% of the total polymer) were used in DMSO (50 wt.% of the prepolymerization mixture). Although PA/M-30 [Phenyl acrylate (30 mol% of total monomers), MACC (70 mol% of total monomers), and MBAA (30 mol% of total polymer)] showed a decent performance, there could be a better composition for DUFCs.

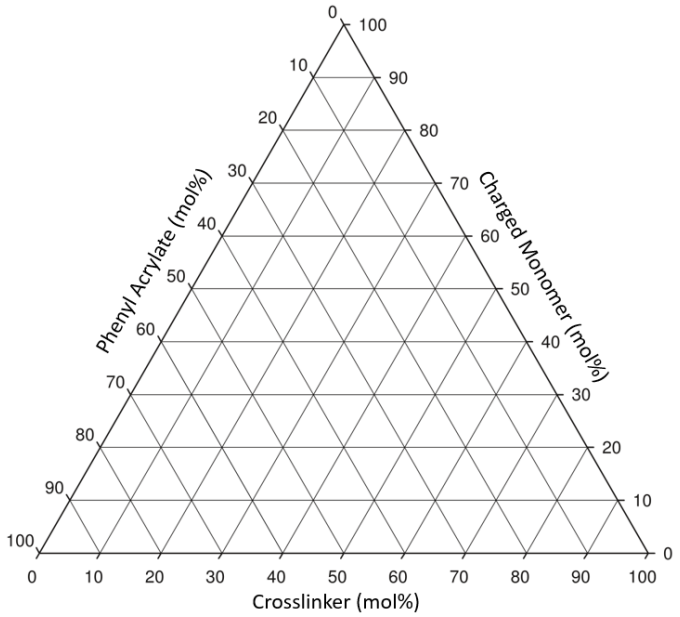

Figure 11.5. A proposed ternary diagram to analyze the miscibility of the prepolymerization mixture.

Moreover, I believe computational support (i.e. DFT) can be helpful in designing the internal structure of the membrane.

- **Other applications**

  Besides DUFC, there are many other applications that requires more selective IEMs for crossover minimization, such as direct methanol fuel cells (DMFC), PEC-CRC, and polymer electrolytes. Therefore, I would like to strongly encourage polymer/membrane scientists to consider this facile approach for designing new materials.

11.3. References

[1] B.M. Carter, L. Keller, M. Wessling, D.J. Miller, Preparation and characterization of crosslinked poly(vinylimidazolium) anion exchange membranes for artificial photosynthesis, J Mater Chem A. (2019). https://doi.org/10.1039/c9ta00498j.

[2] S.M. Dischinger, S. Gupta, B.M. Carter, D.J. Miller, Transport of Neutral and Charged Solutes in Imidazolium-Functionalized Poly(phenylene oxide) Membranes for Artificial Photosynthesis, Ind Eng Chem Res. 59 (2019) 5257–5266. https://doi.org/10.1021/acs.iecr.9b05628.

[3] K. Chang, H. Luo, G.M. Geise, Water content, relative permittivity, and ion sorption properties of polymers for membrane desalination, J Membrane Sci. 574 (2019) 24–32. https://doi.org/10.1016/j.memsci.2018.12.048.

[4] R.L. Smith, S.B. Lee, H. Komori, K. Arai, Relative permittivity and dielectric relaxation in aqueous alcohol solutions, Fluid Phase Equilibr. 144 (1998) 315–322. https://doi.org/10.1016/s0378-3812(97)00275-6.

[5] M. Krödel, B.M. Carter, D. Rall, J. Lohaus, M. Wessling, D.J. Miller, Rational Design of Ion Exchange Membrane Material Properties Limits the Crossover of CO 2 Reduction Products in Artificial Photosynthesis Devices, Acs Appl Mater Inter. 12 (2020) 12030–12042. https://doi.org/10.1021/acsami.9b21415.